

UCSF

UC San Francisco Electronic Theses and Dissertations

Title

An analysis of antisense oligonucleotide binding and efficacy

Permalink

<https://escholarship.org/uc/item/7pz6n8f0>

Author

Stull, Robert A.

Publication Date

1995

Peer reviewed|Thesis/dissertation

An Analysis of Antisense Oligonucleotide Binding and Efficacy:
Computational and Experimental Approaches

by

Robert A. Stull

B. S. Chemistry, Univ. of Akron, 1988

DISSERTATION

Submitted in partial satisfaction of the requirements for the degree of

DOCTOR OF PHILOSOPHY

in

Pharmaceutical Chemistry

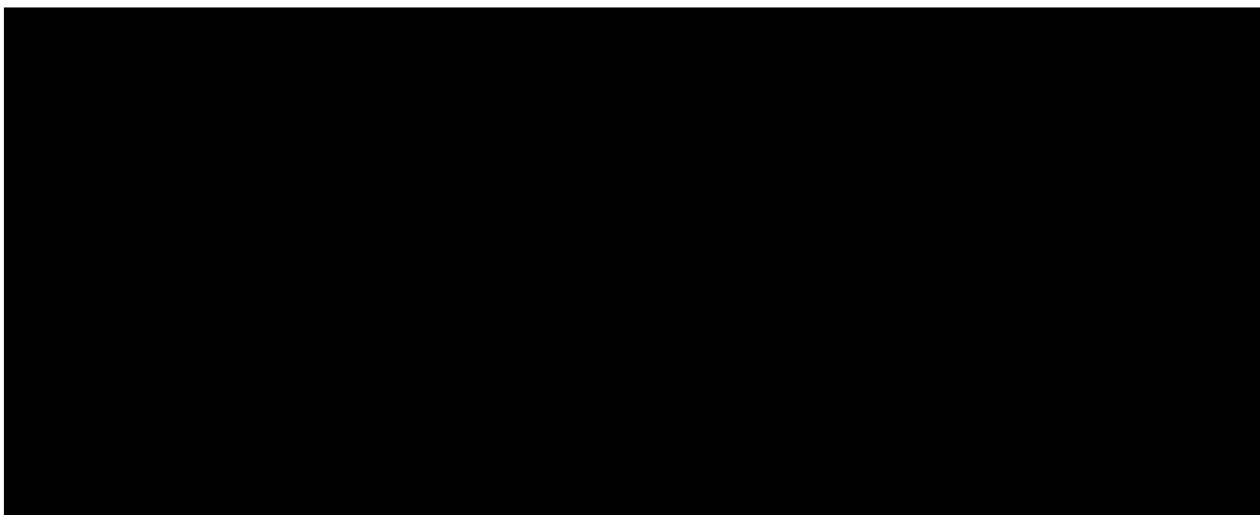
in the

GRADUATE DIVISION

of the

UNIVERSITY OF CALIFORNIA

San Francisco



Date

University Librarian

Degree Conferred:

copyright 1995
by
Robert A. Stull

To my parents, Sylvia and Dennis,
who gave me my roots, and then gave me my wings.

To S. P.
'L'anima ho milionaria' perché sono amato da te

ACKNOWLEDGMENTS

I would first like to thank my mentor, Francis C. Szoka, Jr., for his support and encouragement throughout my thesis research. Without his guidance and his model, I would not have grown into a research scientist. I thank him for both his patience, personally and professionally, during my time as a graduate student under his direction.

I would like to thank the members of my thesis committee, Dr. Frances Brodsky and Dr. Richard Shafer, and the members of my oral qualifying examination committee, Dr. Frances Brodsky, Dr. Richard Guy, Dr. Richard Shafer, Dr. Susan Hawkes, and Dr. Anthony DeFranco for their helpful comments and suggestions. I would also like to thank Dr. Ron Siegel, for graciously reading Appendix 4 and offering encouragement and helpful comments.

I wish to also acknowledge those members, faculty, staff, post-docs and graduate students in the Departments of Pharmacy and Pharmaceutical Chemistry who kindly offered friendship during my stay as a graduate student. A special thanks goes to the faculty of the Department of Pharmacy, who often went out of their way to provide advice, encouragement and support, both financial and personal, to graduate students under their care.

A special acknowledgment goes to Leslie Taylor of the Computer Graphics Facility at UCSF. Her assistance in constructing the histograms and modifying the RNA folding programs was invaluable, and her patience and endurance during that time most gratefully appreciated. I would also like to thank Dr. Chris Leamon and Dr. Wayne Hendren of Glaxo, with whom I collaborated on the studies concerning luciferase.

I must gratefully acknowledge those investigators whose kind gifts allowed me perform my research: Dr. James Larrick, Dr. Frank Lee, Dr. Patricia Olson, Dr. Robert Newton, Dr. Ueli Gebbler and especially Dr. Gerald Zon, for supplying all of the oligonucleotides used in these studies, except those used in the luciferase studies.

I would like to thank all those members of the Szoka Lab with whom I have had the great fortune of interacting with during the course of my thesis studies: Dr. June Chu, Dr. Roberta

Parente, Dr. Aeri Kim, Dr. Jean-Yves Legendre, Dr. Elias Fattel, Dr. Jean Haensler, Dr. Regine Peschka, Mr. Lee Barron, Dr. Marsha Thompson, Dr. Kathleen Meyer, and Dr. Menashe Levy. Special acknowledgments go to those post-docs and graduate students with whom I performed oligonucleotide research: Dr. Sekhar Majumdar, Dr. Osamu Moro, and Dr. Sophie Sixou. I would like to thank Mr. Gary Green and Dr. Daren Knoell, for their helpful instruction in molecular biology, and Ms. Mary Tang and Ms. Yuhong Xu, for many insightful comments concerning mathematics and personal relationships. I would like to thank Dr. Tara Wyman for graciously providing me the use of her PowerBook during the period in which I was writing my dissertation.

Several good friends were instrumental in providing emotional support as we made the journey towards our degrees: Dr. Darren Wong, and Sharon Walker (long live Besix!) and Ms. Carolyn Koo, Ms. Anne Pollack, Ms. Ann Pace and Dr. Joanna Gilbert.

I would like to thank Dr. Louis G. Ceci for his advice, wisdom and encouragement during the difficult time preceding my orals and for helpful comments on designing and coding efficient computer programs.

I would like especially to thank Ms. Tyra Wolfsberg. There are too many things to thank her for in this space, but Tyra, *je t'aime autant que j'aime mes soeurs. A grâce de toi, je me suis retrouvé. Je t'en remercie de tout mon coeur.*

Of course, I also must acknowledge the encouragement and support provided by my family—my sisters Autumn, Debra, and Lisa and their families, my grandparents Ethelyn and Aubrey, and my parents Dennis and Sylvia. They each share with me the achievement of this goal.

Finally, I must thank Mr. S. P. Giorgi. His patience and friendship often carried me through difficult times, and his presence in my life makes completion of this goal so very much more rewarding. *Festeggiamo! Io ho il dottorato e tu hai il dottore. T'amo sopra ogni cosa al mondo e sonno tutto tuo.*

AN ANALYSIS OF ANTISENSE OLIGONUCLEOTIDE BINDING AND EFFICACY:
COMPUTATIONAL AND EXPERIMENTAL APPROACHES.

BY: ROBERT A. STULL

MARCH, 1995

ABSTRACT

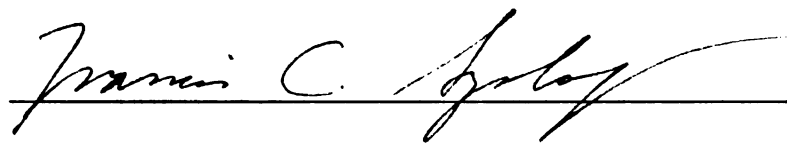
Computational and experimental strategies were employed to analyze antisense oligonucleotide (ASO) binding affinity and efficacy. Several thermodynamic-based predictive indices were developed. In a retrospective analysis, a simple duplex formation index (Dscore) was the most consistent predictor of ASO efficacy. A more detailed retrospective analysis of the *in vitro* binding of ASO to a simple hairpin loop target demonstrated that under conditions of well known RNA secondary structure, thermodynamic calculations could reasonably estimate ASO binding behavior.

An *in vitro* gel-shift binding assay was developed to empirically determine the affinity of an ASO for a structured RNA target. This assay was used to construct apparent binding isotherms for twenty-six 12-nucleotide ASO targeted to various regions of the murine TNF- α mRNA. Fourteen of these ASO did not bind the structured TNF mRNA within the assay detection limits ($K_D > 100$ nM), while twelve displayed measurable binding to the TNF mRNA (0.9 nM $\leq K_D \leq 100$ nM). Analysis of the binding behavior of longer ASO targeted to the start codon region afforded determination of ASO sequences with nanomolar apparent K_D values. The experimentally determined binding constants tended to be several orders of magnitude weaker than those computed for binding to an unstructured complement, and did not correlate with computed Dscore values. These results reflect the kinetic and thermodynamic effects of RNA structure upon ASO affinity.

Forty-five ASO targeted to luciferase mRNA were screened for apparent $K_D \leq 5$ nM. The best binding ASO from this screen was determined to have an apparent K_D value of 10 nM, and inhibited luciferase expression in a cell-free translation system ($IC_{50} = 230$ nM). Other ASO with apparent $K_D \leq 50$ nM likewise inhibited luciferase expression *in vitro* ($IC_{50} \leq 250$ nM). Thus an *in vitro* binding assay may be used to screen potential ASO compounds as an empirical

method for determining ASO sequences with strong affinities for their target RNA and therefore likely to inhibit translation.

Thesis Committee Chairman:

A handwritten signature in cursive script, reading "Francis C. Szoka, Jr.", written over a horizontal line.

Francis C. Szoka, Jr., Ph. D.

TABLE OF CONTENTS

TITLE: AN ANALYSIS OF ANTISENSE OLIGONUCLEOTIDE BINDING AFFINITY UPON ASO EFFICACY: COMPUTATIONAL AND EXPERIMENTAL APPROACHES.

PRELIMINARY PAGES

LIST OF TABLES.....	xiv
LIST OF FIGURES.....	xvi
ABBREVIATIONS.....	xix
OBJECTIVE AND HYPOTHESIS OF RESEARCH.....	1
CHAPTER ONE: <u>INTRODUCTION TO ANTISENSE OLIGONUCLEOTIDES</u>	2
I.1 NUCLEIC ACID THERAPEUTICS AND ASO.....	2
I.1.1 Information management: the central dogma of genetics.....	2
I.1.2 Nucleic acid drugs and antisense oligonucleotides.....	3
I.1.3 Mechanism of action of ASO.....	4
I.1.4 Obstacles facing application of ASOs as therapeutics.....	5
I.2 STABILITY AND DELIVERY OBSTACLES.....	10
I.2.1 Stability.....	10
I.2.2 Membrane permeability.....	12
I.3 ASO SELECTIVITY.....	14
I.3.1 ASO selectivity: Herschlag's discrimination index.....	14
I.3.2 ASO selectivity: statistical considerations.....	15
I.3.2a Statistical uniqueness	15
I.3.2b Mismatched site statistics	16
I.3.3 ASO selectivity: thermodynamics.....	17
I.3.4 ASO selectivity: kinetics.....	19
I.4 ASO AFFINITY.....	21
I.4.1 Components of affinity due to the chemical structure of the ASO.....	21
I.4.1a ASO affinity and ASO sequence	21
I.4.1b Chemical modifications to ASO and their effects upon ASO affinity	22
I.4.2 ASO affinity and RNA structure.....	24
I.4.2a Target site secondary structure	24
I.4.2b Topology of ASO binding	26
I.4.2c RNA secondary structure and hybridization kinetics	30

I.5	RATIONALE FOR RESEARCH.....	30
I.6	GENERAL STRATEGY OF THESIS RESEARCH, ORGANIZATION OF THE DISSERTATION.....	31
I.7	LIST OF PUBLICATIONS RESULTING FROM THIS RESEARCH.....	33
CHAPTER TWO: <u>PREDICTING ANTISENSE OLIGONUCLEOTIDE INHIBITORY EFFICACY: A COMPUTATIONAL APPROACH USING HISTOGRAMS AND THERMODYNAMIC INDICES</u>.....		
II.1	ABSTRACT.....	34
II.2	INTRODUCTION.....	35
II.2.1	Rationale for experiments.....	35
II.2.2	General overview of folding algorithms.....	37
II.2.2a	RNA secondary and tertiary structure prediction	37
II.2.2b	RNA folding algorithms	37
II.2.2c	Thermodynamics of RNA-RNA interactions	38
II.3	METHODS AND ALGORITHMS.....	41
II.3.1	Folding algorithms.....	41
II.3.2	Histograms.....	43
II.3.3	Energy scaled histograms.....	45
II.3.4	EWINDOW program, window-score histograms.....	46
II.3.5	Mean stacking temperature calculations.....	49
II.3.6	Statistics.....	49
II.3.7	Inhibition studies analyzed and sequences examined.....	50
II.4	RESULTS AND DISCUSSION	
II.4.1	General approach of the experiments.....	51
II.4.2	Analysis of ASO action in cell-free translation systems.....	51
II.4.2a	Rabbit reticulocyte lysates	51
II.4.2b	Wheat germ extracts	54
II.4.3	Analysis of ASO action in intact cells.....	55
II.4.3a	Predictions for human <i>c-myc</i> inhibition in HL-60 cells	55
II.4.3b	Predictions for human ICAM-1 inhibition in HUVECS and A549 cells	58
II.4.3c	Use of alternative folding algorithms	62
II.4.4	Comparison of Dscore with other physical parameters of ASO.....	62
II.4.5	Dscores– computation with RNA:RNA, DNA:DNA, and	

	RNA:DNA nearest-neighbor thermodynamic values.....	63
II.4.6	Calculation of a DifScore using LRNA to produce constrained folds..	65
II.5	CONCLUSIONS.....	66
	CHAPTER THREE: <u>SINGLE-STRANDED PHOSPHODIESTER AND PHOSPHOROTHIOATE OLIGONUCLEOTIDES BIND ACTINOMYCIN D AND INTERFERE WITH TNF-INDUCED LYSIS IN THE L929 CYTOTOXICITY ASSAY.</u>	68
III.1	ABSTRACT.....	68
III.2	INTRODUCTION.....	68
III.3	MATERIALS AND METHODS.....	70
III.3.1	Chemicals.....	70
III.3.2	Oligonucleotides.....	70
III.3.3	Cell culture.....	70
III.3.4	Initial oligonucleotide screening for anti-TNF effects.....	71
III.3.5	Production of TNF-positive supernatants.....	71
III.3.6	L929/TNF Assay.....	72
III.3.7	UV absorption spectra.....	72
III.4	RESULTS AND DISCUSSION.....	73
III.5	CONCLUSIONS.....	79
	CHAPTER FOUR: <u>DEVELOPING AN EMPIRICAL ASO BINDING ASSAY.</u>	80
IV.1	ABSTRACT.....	80
IV.2	INTRODUCTION.....	80
IV.3	MATERIALS AND METHODS.....	81
IV.3.1	Materials.....	81
IV.3.2	Oligonucleotide selection and synthesis.....	82
IV.3.3	Plasmid Construction.....	84
IV.3.4	Determination of apparent K_d values for ASO.....	85
IV.3.4a	RNA generation	85
IV.3.4b	Oligonucleotide labeling	85
IV.3.4c	Solution hybridization reactions	86
IV.3.4d	Gel electrophoresis to resolve hybridization products	86

IV.3.5	RNase H mapping of ASO binding sites.....	87
IV.4	RESULTS.....	88
IV.4.1	<i>In vitro</i> binding of ASO to a cDNA-derived TNF- α mRNA.....	88
IV.4.2	RNase H mapping of ASO binding sites.....	90
IV.4.3	Analysis of ASO binding to the start codon region.....	91
IV.4.4	Comparison of computed versus empirical affinity constants.....	93
IV.5	DISCUSSION.....	96
IV.5.1	Comments about the gel-shift binding technique.....	97
IV.5.2	Comments about the results of the gel-shift experiments.....	98
IV.5.3	Comments about the Dscores and ASO binding affinity.....	100
IV.6	CONCLUSIONS.....	101
CHAPTER FIVE: <u>WALKING ALONG THE LUCIFERASE MESSENGER RNA</u>		
<u>- EXAMINATION OF ASO BINDING AND INHIBITORY CAPACITY</u>		103
V.1	ABSTRACT.....	103
V.2	INTRODUCTION.....	103
V.3	METHODS.....	104
V.3.1	Materials.....	104
V.3.2	Oligonucleotide sequence selection and synthesis.....	104
V.3.3	<i>In vitro</i> RNA synthesis.....	106
V.3.4	Oligonucleotide labeling.....	106
V.3.5	Screening the ASO for binding to luciferase RNA: 5 nM screen.....	107
V.3.5a	Solution hybridization reactions	107
V.3.5b	Gel electrophoresis to resolve hybridization products	107
V.3.6	Measuring the binding isotherms for selected anti-luciferase ASO.....	107
V.3.7	<i>In vitro</i> translation of luciferase RNA.....	108
V.4	RESULTS.....	108

V.4.1	Gel shift screen for ASO with tight binding and potent inhibition.....	108
V.4.1a	Walking along the luciferase message	108
V.4.1b	<i>In vitro</i> translation of luciferase in the presence of the luciferase walk ASO	109
V.4.2	Start codon region saturation.....	111
V.4.3	Selected isotherms and dose-response studies.....	112
V.4.3a	ASO 393-15-PD	112
V.4.3b	Longer start region ASO	113
V.4.4	Comparison of binding data, inhibition data, and Dscores.....	115
V.5	DISCUSSION.....	117
V.6	CONCLUSIONS.....	119
CHAPTER SIX: <u>MAIN CONCLUSIONS OF THE THESIS RESEARCH</u>		120
REFERENCES.....		124
APPENDIX ONE: <u>A SIMPLE THERMODYNAMIC MODEL OF ASO SELECTIVITY</u>		150
APPENDIX TWO: <u>DSCORES PROGRAM</u>		154
AIII.1	FUNCTIONALITY OF DSCORES.....	154
AIII.2	COMMENTARY ON THE CODE.....	155
APPENDIX THREE: <u>THERMODYNAMIC VALUES FOR BASE-STACKING INTERACTIONS...</u>		167
APPENDIX FOUR: <u>EXTENDING THE THERMODYNAMIC ANALYSIS OF ASO BINDING TO INCLUDE CONCENTRATION TERMS</u>		168
AIV.1	INTRODUCTION.....	168
AIV.2	METHODS.....	172
AIV.2.1	Thermodynamics of ASO binding: generalized descriptive equations	172
AIV.2.1a	Global binding reaction	172
AIV.2.1b	Treating the binding on a local level	172
AIV.2.1c	A general comment about the local model	175
AIV.2.2	Effect of [c'] upon the binding of an ASO to its target.....	176
AIV.2.3	Estimations of [c']: establishing boundaries.....	177
AIV.2.3a	An extreme case based upon a maximally extended molecule	178
AIV.2.3b	Gaussian type behavior in a random-walk chain.....	180

AIV.2.4	Estimations of [c']: a trial spatial distribution function.....	182
AIV.2.4a	Gaussian distribution for a random-walk polymer: The Jacobson-Stockmayer derivation	182
AIV.2.4b	Correction for self-avoiding random walk polymers: The Fisher approximation to Jacobson-Stockmayer	183
AIV.2.4c	Values of l	183
AIV.2.5	Summary of methods.....	185
AIV.3	RESULTS AND DISCUSSION.....	186
AIV.3.1	The ASO:RNA system studied.....	186
AIV.3.2	Binding of 10-mer RNA ASO to their 10-mer RNA complements.....	188
AIV.3.2a	Derivation of suitable concentration-based equations	188
AIV.3.2b	Comparison of theory to experimental results	189
AIV.3.3	Binding of ASO to the 47-mer RNA hairpin: predictions from the thermodynamic indices (Dscore, Sscore, and Cscore).....	190
AIV.3.3a	Calculation of ΔG°_f for the hairpin structures	190
AIV.3.3b	Failure of the thermodynamic indices as predictors of binding behavior towards a structured target	191
AIV.3.4	Analysis of ASO binding to the structured RNA target: $\Delta\Delta G^\circ_{rxn}$ computations.....	192
AIV.3.5	Binding of the ASO to the 47-mer RNA hairpin: Estimating the effective concentration of the competitor strand, [c'].....	196
AIV.3.5a	Estimations of [c'] from RNA chain behavior models	196
AIV.3.5b	Checking the theoretical [c'] values versus a [c'] value computed from the experimental data	197
AIV.3.6	Computing $[a_0]_{50\%}$ values for each of the ASO.....	198
AIV.3.6a	Predictions for loop binding ASO	198
AIV.3.6b	Predictions for stem binding ASO	199
AIV.4	DISCUSSION.....	201
AIV.4.1	Dscores and ASO binding to 10-mer complements.....	201
AIV.4.2	Caveats about RNA structure prediction.....	202
AIV.4.3	Failure of the thermodynamic indices as predictors of ASO binding to structured targets.....	202
AIV.4.4	Comments about the ASO binding model, $\Delta\Delta G^\circ$ calculations, and predicted ASO concentrations required to produce 50% binding.....	203
AIV.4.4a	$\Delta\Delta G^\circ$ calculations	203
AIV.4.4b	Results for each of the local binding reactions	204
AIV.5	CONCLUSIONS.....	207

LIST OF TABLES

<u>Table</u>	<u>Page</u>	<u>Title/Description</u>
1-1	4	Classes of nucleic acid drugs
1-2	6	Review of ASO studies
1-3	12	Physicochemical properties of modified nucleic acids
1-4	13	Strategies to enhance cellular delivery of ASO
1-5	18	$\Delta\Delta G^\circ_{37}$ binding penalties for single mismatched DNA • RNA ASO
1-6	23	Comparative T_m values for various ASO analogs
2-1	40	Thermodynamic values used by fold algorithms and DSCORES
2-2	52	Antisense phosphodiester oligomers used in cell-free translation systems
2-3	53	Coefficients of determination (r^2) between predictive indices and reported inhibition in cell-free systems.
2-4	56	Antisense phosphodiester against human <i>c-myc</i> in HL-60 cells
2-5	57	Coefficients of determination (r^2) between predictive indices and reported inhibition: human <i>c-myc</i> in HL-60 cells
2-6	59	Antisense phosphorothioates against human ICAM-1 in HUVEC and A549 cells
2-7	61	Coefficients of determination (r^2) between predictive indices and reported inhibition: human ICAM-1 studies in cultured cells
2-8	64	Coefficients of determination (r^2) for Dscores based upon different thermodynamic data sets, and reported inhibition
2-9	65	DifScore calculations for antisense phosphorothioates against human ICAM-1
4-1	83	Anti-murine TNF- α ASO sequences used in this study
4-2	90	Apparent K_d values for anti-TNF 12-mer ASO
4-3	91	Mapping of ASO binding sites using RNase H
5-1	105	Initial 45 luciferase walk ASO used in screening studies
5-2	112	Walking around the luciferase mRNA start codon region
5-3	114	Effect of ASO length upon apparent affinity and inhibitory capacity

LIST OF TABLES (continued)

<u>Table</u>	<u>Page</u>	<u>Title/Description</u>
A3-1	167	Nearest neighbor stacking energies for base-pair duplex
A4-1	184	[c'] as a function of n, in nucleotides, and l, in angstroms
A4-2	186	Oligoribonucleotides used by Lima and colleagues (1992)
A4-3	189	Binding of 10-mer ASO to the 10-mer complements
A4-4	192	Analysis of 10-mer ASO binding to 47-mer target (16/12 structure) using thermodynamic indices
A4-5	195	Computed $\Delta\Delta G^\circ$ values as rank predictors of ASO binding
A4-6	197	Values of [c'] from models; comparison of theoretical [c'] to observed [c']
A4-7	198	Predicted [a ₀] _{50%} values for loop binding ASO
A4-8	200	Calculations of [a ₀] _{50%} for stem binding ASO

LIST OF FIGURES

Figure	Page	Title/Description
1-1	3	Flow of information within cells and points of regulation or potential regulation of expression
1-2	10	Obstacles to ASO activity and their interrelationships
1-3	11	Chemical modifications to oligonucleotides
1-4	17	Thermodynamic selectivity for ASO binding
1-5	25	Summary of Uhlenbeck's data (1971) for the binding of various tetramers and trimer ASO complementary to the tRNA ^{tyr}
1-6	27	RNA pseudoknots and pseudo half-knots
1-7	28	Minimum spatial distance between two phosphate residues in the A-form RNA:RNA helix
1-8	29	Summary of ASO binding to a model TAR element hairpin (from Ecker <i>et al.</i> , 1992)
2-1	35	Main mechanisms of antisense mediated inhibition
2-2	36	Processes which may compete with ASO binding to its target site on the mRNA
2-3	38	Features of RNA secondary structure
2-4	41	Thermodynamic indices used to evaluate competitive processes at the ASO target site
2-5	44	tRNA secondary structure and stem-frequency histogram representation of base-pairing
2-6	47	Energy-scaled histogram and window score histograms for tRNA
3-1	73	Initial observation of oligonucleotide-mediated interference in the L929 bioassay
3-2	74	Titration of protective effect correlates with titration of oligonucleotide present in the supernatant
3-3	75	Comparison of transcriptional and translational inhibitors as sensitizing agents in the L929 assay
3-4	76	Effect of different metabolic inhibitors on oligonucleotide-mediated protection of L929 cells
3-5	77	UV absorption spectra of actinomycin D and oligonucleotides in bioassay medium

LIST OF FIGURES (continued)

Figure	Page	Title/Description
4-1	82	ASO target sites along the murine TNF- α cDNA derived mRNA
4-2	84	Construction of the plasmid pCMV-TNF- α (pCMV-Ts)
4-3	89	Sample gel autoradiograph and manipulation from ASO binding experiments
4-4	92	Analysis of ASO binding to sites around the start codon
4-5	94	Plot of observed binding constants versus calculated $\Delta G^{\circ}_{duplex}$
4-6	95	Summary of TNF Dscore statistical data
5-1	110	Summary of luciferase walk experiments
5-2	111	Binding and biological properties of ASO targeted to the luciferase start codon
5-3	113	Apparent K_d , IC_{50} , and RNase-H dependence of ASO 393-15-PD activity
5-4	114	Effect of different length ASO targeted to start codon region
5-5	115	Relationships between Dscore, percent shift and percent inhibition for luciferase walk ASO
5-6	116	Relationships between Dscore, percent shift and percent inhibition for ASO targeted near the start codon of luciferase mRNA.
6-1	122	Schematic of an empirical ASO sequence selection procedure
A1-1	151	Comparative binding curves for an ASO to its matched and mismatched sites
A4-1	169	Representation of competitive RNA folding and ASO binding
A4-2	173	Thermodynamic cycle applicable to correcting for reactions not at standard state
A4-3	176	The influence of [c'] upon ASO binding
A4-4	179	The linear extended model of an RNA chain
A4-5	180	Relationship between separation distance and effective concentration (I)
A4-6	181	The Gaussian random-walk model of an RNA chain

LIST OF FIGURES (continued)

Figure	Page	Title/Description
A4-7	184	Single virtual bond representation of RNA backbone atoms
A4-8	185	Relationship between separation distance and effective concentration (II)
A4-9	187	47-mer hairpin structure targeted in ASO binding study by Lima <i>et al.</i> , 1992
A4-10	194	Predicted RNA structures adopted upon ASO binding to the target 47-mer hairpin, and their calculated free energies of formation.

ABBREVIATIONS

ASO	antisense oligonucleotide (DNA or RNA oligomer)
ATP	adenosine triphosphate
bp	base pair
CAT	chloramphenicol acetyl transferase
cpm	counts per minute
dCTP	deoxycytidine triphosphate
DEPC	diethylpyrocarbinat
DHFR	dihydrofolate reductase
DME	Dulbecco's modified Eagle's medium
dsDNA	double stranded DNA
EDTA	ethylenediaminetetraacetic acid
g. r. w.	Gaussian random-walk
HIV	human immunodeficiency virus
HUVEC	human umbilical vein endothelial cell
ICAM	intracellular adhesion molecule
j. s.	Jacobson-Stockmayer
j. s. f.	Jacobson-Stockmayer-Fisher
l. e. m.	linear extended model
LPS	bacterial lipopolysaccharide
LTR	long terminal repeat
MHC	major histocompatibility complex
MTT	(3-[4,5-dimethyl-thiazol-2-yl]-2,5-diphenyltetrazolium bromide
NP40	nonidet P-40 (octylphenoxy polyethoxy ethanol)
OD	optical density (usually at 260 nm)
PBS	phosphate buffered saline

PCR	polymerase chain reaction
PMA	phorbol 12-myristate 13-acetate
PNA	peptide nucleic acids
RSV	Rous sarcoma virus
SDS	sodium dodecylsulfate
snRNP	small nuclear ribonucleoprotein
ssDNA	single stranded DNA
SV 40	simian virus 40
TAR	trans-acting response [element]
TBE	tris-borate-ETDA electrophoresis buffer
T_m	melting temperature
TNF	tumor necrosis factor
Tris	tris(hydroxymethyl)aminomethane
UTR	untranslated region

AN ANALYSIS OF ANTISENSE OLIGONUCLEOTIDE BINDING AND EFFICACY: COMPUTATIONAL AND EXPERIMENTAL APPROACHES

BY: ROBERT A. STULL

March, 1995

The past fifteen years have seen the explosive growth of the new field of antisense oligonucleotide technology, which depends upon an oligonucleotide sequence in the antisense orientation hybridizing to a target nucleic acid sequence. Antisense oligonucleotides (ASO) hold promise both as scientific tools for studying gene function, and as therapeutics capable of offering revolutionary strategies in the treatment of inflammatory, oncogenic and viral diseases. Their appeal is the ease of their design if the sequence of the target gene is known, and the inherent specificity of nucleic acid hybridization. However, antisense oligonucleotides have not yet fully delivered upon their promise due to the stability, delivery, and affinity obstacles they must overcome within living organisms. One central yet simple barrier to the robust application of ASO is selection of antisense sequences most likely to produce biological effects.

OBJECTIVE AND HYPOTHESIS OF RESEARCH

The objective of this work is to establish methods that facilitate the selection of ASO sequences for biological testing. Even a cursory glance at the scientific literature concerning ASO suggests certain sequences are more effective than others in achieving biological effects. The fundamental hypothesis of this research is that ASO efficacy is related primarily to the affinity of the ASO for its RNA target, since hybridization of the ASO to the RNA is a prerequisite for ASO activity. ASO affinity is principally determined by the specific

sequence and the higher order structure of the RNA target. Therefore, both computational and experimental approaches were employed to evaluate the effects of these variables upon ASO affinity, and to develop strategies which might facilitate ASO sequence selection.

CHAPTER ONE: Introduction to Antisense Oligonucleotides

The goals of this chapter are threefold: first, to introduce the reader to ASO within their context as members of a broad spectrum of nucleic acid drugs; second, to state briefly the main obstacles facing application of ASO as useful biological reagents; and third, to describe in detail how these obstacles impact ASO sequence selection.

I.1 NUCLEIC ACID THERAPEUTICS AND ASO

I.1.1 Information management: the central dogma of genetics

The central dogma of genetics states that information within cells flows from DNA to proteins via mRNA molecules. Since regulating gene expression is vital to the proper functioning of the cell, the flow of information is controlled at many points (Figure 1-1). Generalized interference with this regulation would obviously be detrimental to the cell. However, modulation of specific gene expression and noting concomitant changes in cell physiology can provide critical insight into the biological function of particular genes. Specific modulation of gene expression may also be beneficial in inflammatory, neoplastic or viral disease since it would be desirable to affect only the inflammatory genes, oncogenes or viral genes without harming the normal functions of the cell (Zon, 1988).

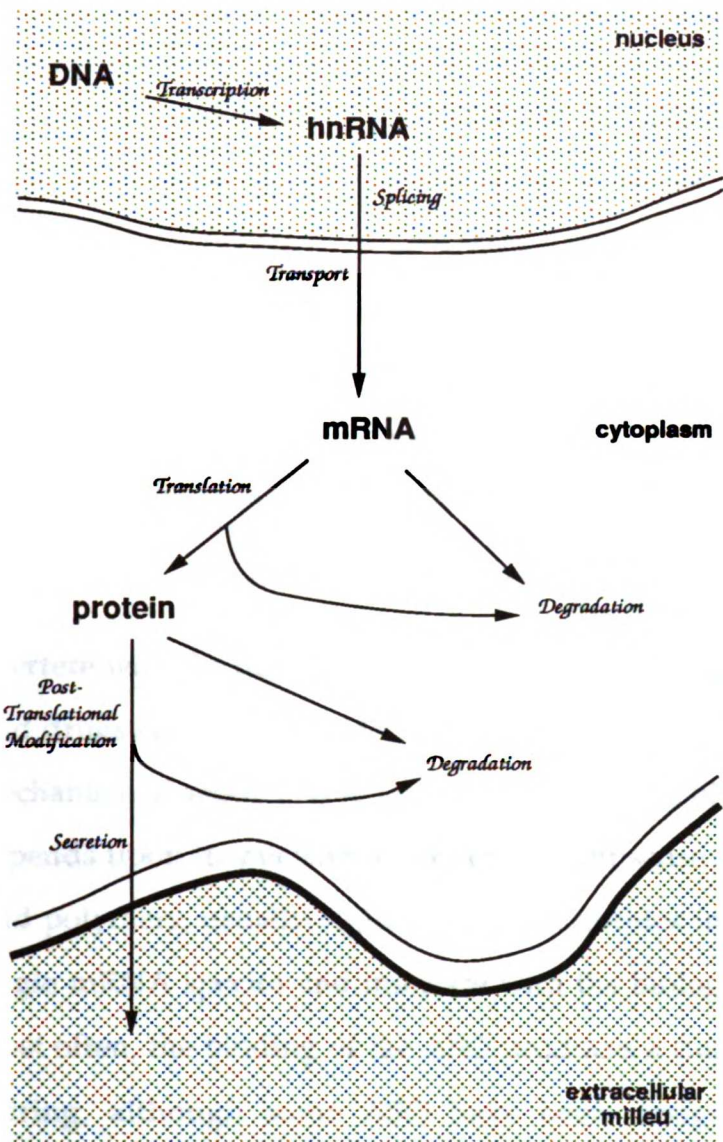


Figure 1-1: Flow of information within cells and points of potential or actual regulation of gene expression.

Information flows from the repository molecule (DNA) to a functional molecule (protein) via a template molecule (RNA). In the case of most genes, the DNA is transcribed into heteronuclear RNA (hnRNA) by RNA polymerase II. The hnRNA is then spliced, polyadenylated, and transported from the nucleus to the cytoplasm. Once in the cytoplasm, the mRNA is translated by ribosomes into a polypeptide product. The polypeptide may either be cotranslationally inserted into the endoplasmic reticulum or released into the cytoplasm. Once in the endoplasmic reticulum, a polypeptide may be glycosylated or otherwise modified through post-translational processes prior to being stored by or secreted from the cell.

A gene may be regulated by control of transcription rates and by RNA degradation versus translation rates. Alternative splicing of viral RNAs suggests that splicing may be used to regulate gene expression. Any controls upon the post-translational processing of the protein, and controlled secretion of the protein also may be considered to be points of regulation in gene expression. Finally, the half-life of the protein itself may be considered to be a point of gene regulation. It is currently unclear if transport processes or RNA degradation processes are tightly regulated points of gene expression.

I.1.2 Nucleic acid drugs and antisense oligonucleotides

The majority of currently employed pharmacologic approaches to modulation of gene function rely upon the interaction of low molecular weight chemical compounds with protein targets so as to alter the function of the protein. The past fifteen years have seen the embryogenesis of new therapeutic strategies, in which nucleic acid polymers are used to alter protein function or to

TABLE 1-1: Classes of nucleic acid drugs

	APTAMER	ANTIGENE	CATALYTIC	ANTISENSE
<i>target</i>	protein	duplex DNA	mRNA	mRNA
<i>drug type</i>	DNA/RNA	DNA/RNA	RNA	DNA/RNA
<i>mechanism</i>	<i>binding:</i> interfere with biological function of protein	<i>triplex formation:</i> block transcription or replication	<i>hybrid assembly:</i> cleavage and destruction of target RNA	<i>hybrid assembly:</i> translation arrest and/or RNase H mediated cleavage of RNA
<i>site of action</i>	intra- and/or extracellular	nucleus	nucleus and/or cytoplasm	nucleus and/or cytoplasm

interfere with the function of nucleic acids encoding the target protein. Nucleic acid drugs can be subdivided into four classes based upon their target site and mechanism of action (Table 1-1). In each case, the biological function of the drug depends upon its nucleotide sequence. Antisense oligonucleotides are nucleic acid polymers, usually eight to fifty nucleotides in length, designed to bind a single mRNA species and interfere with the biological function of the mRNA. Most often, the binding of the ASO produces a duplex via Watson-Crick base-pairing, although some ASO have been designed to form triple helical complexes upon binding (Brossalina *et al.*, 1993; Giovannageli *et al.*, 1993).

I.1.3 Mechanism of action of ASO

Antisense oligonucleotides are postulated to produce their biological effects by mechanisms which have been demonstrated or inferred from *in vitro* studies. The main mechanisms of sequence-specific inhibition include: translational arrest produced by physical occlusion of ribosome assembly or translocation (Paterson *et al.*, 1977; Boiziau *et al.*, 1991); blocking the processing

of the RNA (Cotten *et al.*, 1989); perturbation of functional secondary structures in the target RNA (Vickars *et al.*, 1991; Ecker *et al.*, 1992); and/or providing a double stranded heteroduplex substrate for endogenous RNase H enzymatic activity (Dash *et al.*, 1987; Walder and Walder, 1988). It can be inferred that multiple mechanisms occur in cells, based upon studies where one ASO down regulates target protein expression without apparent alteration in the protein-encoding mRNA levels, while another ASO down-regulates both target protein and target mRNA levels (Chiang *et al.*, 1991). Non sequence-specific inhibitory mechanisms also have been noted in viral systems, particularly for interactions of phosphorothioate ASO with viral polymerases and reverse transcriptases (reviewed by Crooke, 1991; see also Boiziau, 1992). Published reports of ASO displaying biological effects in cells are summarized in Table 1-2.

I.1.4 Obstacles facing application of ASO as therapeutics

The proposed mechanisms of ASO mediated inhibition of gene expression have as their prerequisite an intracellular RNA binding event. Therefore, antisense drugs face four major barriers to efficacy: 1) stability in serum and within cells; 2) membrane permeability/cellular delivery; 3) selectivity for their intended target and 4) high affinity for their intended target. Each of these obstacles directly impact ASO efficacy in biological systems. Strategies devised to circumvent one obstacle may also impact other obstacles (Figure 1-2). For example, chemical modifications designed to improve the stability of the ASO may alter the mechanisms whereby the ASO produces its effects, which in turn, may alter the selectivity of the ASO.

Table 1-2: Cellular studies utilizing antisense oligonucleotides (ASO)

<i>target gene</i>	<i>ASO</i>	<i>cell line</i>	<i>reference(s)</i>
<i>c-abl</i>	18 (D); v; uM	human hematopoietic progenitors	Caracciolo <i>et al.</i> , 1989
AChR	15 (D); u	neurons	Listerud <i>et al.</i> , 1991
angiotensin II	20 (D); s; uM	mesangial cells neuroblastoma cells	Cook <i>et al.</i> , 1992
annexin and phosphoglycerate kinase	20 (T); s; uM	HeLa	Kumble <i>et al.</i> , 1992
<i>bcl-2</i>	20 (D, T); s; uM	human leukemia cells human lymphoma cells	Reed <i>et al.</i> , 1990 Kitada <i>et al.</i> , 1993
<i>bcr-abl</i>	18 (T); s, c; uM 18 (D); t; uM	K562 cells leukemia blast cells	Taj <i>et al.</i> , 1990 Szczylik <i>et al.</i> , 1991
butyryl-cholinesterase	15 (T); v; uM	murine bone marrow cells	Patinkin <i>et al.</i> , 1990
casein kinase II	20 (D); s; uM 21 (D); c; uM	primary human fibroblasts; mouse neuroblastoma cells	Pepperkok <i>et al.</i> , 1991 Ulloa <i>et al.</i> , 1993
<i>cdc2</i>	18 (D); s; uM	human T-cells	Furukawa <i>et al.</i> , 1990
CFTR	23 (D); s; uM	sweat duct cells	Sorscher <i>et al.</i> , 1991
cholinesterase related cell division controller	15 (T); v; uM	murine bone marrow cells	Lapidot-Lifson <i>et al.</i> , 1992
CSF-1	15 (D); s; uM	murine monocytes	Birchenall <i>et al.</i> , 1990
EGF	15 (D); s; uM	mouse mandibular organ culture	Kronmiller <i>et al.</i> , 1991
Egr-1	15 (D); s; uM	rat cardiomyocytes	Neyes <i>et al.</i> , 1991
erythropoietin; erythropoietin receptor	18 (D); v; uM	murine bone marrow cells	Hermine <i>et al.</i> , 1991
bFGF	15 (D); v; uM 21 (D); v; uM	primary melanoma cells smooth muscle cells glioblastoma hippocampal cells	Becker <i>et al.</i> , 1989 Becker <i>et al.</i> , 1992 Vignovich and Becker, 1993 Ali <i>et al.</i> , 1993 Itoh <i>et al.</i> , 1993 Morrison 1991 Murphy <i>et al.</i> , 1992 Morrison <i>et al.</i> , 1993 Mattson <i>et al.</i> , 1993
FGFR-1	15 (D); v; uM	melanocytes and melanoma cells	Becker <i>et al.</i> , 1992 Vignovich and Becker, 1993
43 kD growth associated protein	17 (D); s; nM	primary neurons	Aigner and Caroni, 1993
<i>c-fos</i>	12 (D); s; uM 15 (T); s; uM 15(D); s; uM 18(D); s; uM 18(D); s; uM	Sertoli cells brain (<i>in vivo</i>) neurons Rat-1 fibroblasts murine pituitary cells	Norton and Skinner, 1992 Chaissan <i>et al.</i> , 1992 Lucas <i>et al.</i> , 1993 McDonnell <i>et al.</i> , 1990 Fagarasan <i>et al.</i> , 1990
GABA receptor	15 (D); c; uM	rat cerebellar granule cells	Holopainen and Wojcik, 1993
G-CSF	18 (D); s; uM	human endothelial cells	Segal <i>et al.</i> , 1992
GHF1	21 (D); s; uM	murine pituitary cells	Castrillo <i>et al.</i> , 1991
glial fibrillary acidic protein	20 (D); v; uM	primary astrocyte cultures	Yu <i>et al.</i> , 1993
glutamate receptor	24 (D); s; uM	rat hippocampus	Vanderklish <i>et al.</i> , 1992
GM-CSF	18 (D); s; uM	human endothelial cells	Segal <i>et al.</i> , 1992
growth hormone	30 (D); c; uM	rat lymphocytes	Weigent <i>et al.</i> , 1991
HOX 2.3, 3c	18 (D); s; uM	bone marrow cells	Wu <i>et al.</i> , 1992
HOX B1, B3	18 (D); s; uM 18 (T); c, uM	erythroleukemia cells embryonal carcinoma	Takeshita <i>et al.</i> , 1993 Faiella <i>et al.</i> , 1994

Table 1-2: (cont.) Cellular studies utilizing antisense oligonucleotides (ASO)

<i>target gene</i>	<i>ASO</i>	<i>cell line</i>	<i>reference(s)</i>
ICAM-1	18-20(T); v; nM 20 (D); c; mM 18-21 (T); v, nM 20(T); u, uM	HUVEC, A549 K562 cells HUVEC endothelioma cells	Chiang <i>et al.</i> , 1991 Akella and Hall, 1992 Bennett <i>et al.</i> , 1994 Stepkowski <i>et al.</i> , 1994
IL-1 α	18 (D); v; uM	HUVEC	Maier <i>et al.</i> , 1990 Garfinkel <i>et al.</i> , 1992
IL-1 β	15 (T); c; uM 18 (D); s; uM	human monocytes; murine macrophages	Manson <i>et al.</i> , 1990 Fujiwara and Grimm, 1992 Witsell and Schook, 1992
IL-1R	18 (D,T); v; uM	fibroblasts/ in vivo	Burch and Mahan, 1991
IL-2	15 (D); s; uM	murine T-cells	Harel-Bellan <i>et al.</i> , 1988b
IL-4	15 (D); s; uM 15-20 (D, T); s; uM 20 (D); c, s; uM	murine T-cells murine T-cells murine B-cells	Harel-Bellan <i>et al.</i> , 1988b Benbenou <i>et al.</i> , 1993 Louie <i>et al.</i> , 1993
IL-6	15 (D); c; uM	AIDS-KS cells, human myeloma Hairy cells	Miles <i>et al.</i> , 1990 Schwab <i>et al.</i> , 1991 Levy <i>et al.</i> , 1991 Barut <i>et al.</i> , 1993
IL-8	31 (D); c ; uM	human monocytes	Koch <i>et al.</i> , 1992
ILGF-1	27 (T); s; uM	pro B-cells	Landreth <i>et al.</i> , 1992
ILGF-1 R	18 (T); c; uM	3T3 derived cells	Porcu <i>et al.</i> , 1992
c-jun	18(D); s; uM 18(D); s; uM 24 (D); s; uM	Rat-1 fibroblasts murine pituitary cells embryonic fibroblasts	McDonnell <i>et al.</i> , 1990 Fagarasan <i>et al.</i> , 1990 Brach <i>et al.</i> , 1993
kinesin	25 (T); s	<i>in vivo</i> , rabbit	Amartunga <i>et al.</i> , 1993
c-kit	15 (D); c; uM 18 (D); s; uM	human hematopoietic cells	Catlett <i>et al.</i> , 1991 Migliaccio <i>et al.</i> , 1993
lck	19-20(D); v; uM	B-cells	Cheung and Dosch, 1991
LH receptor	21 (D); v; uM	mouse Leydig cells	West and Cooke, 1991
M2-receptor,	15 (D); c; uM	rat cerebellar granule cells	Holopainen and Wojcik, 1993
mdr	15-27(T); v; uM	MCF-7 cells	Jaroszewski <i>et al.</i> , 1990
MHC-I (H-2K)	21 (T); v; uM	murine melanoma cells	Kanbe <i>et al.</i> , 1992
c-mos	24-25 (D); v 15 (D); v	Xenopus oocytes murine oocytes	Sagata <i>et al.</i> , 1988 O'Keefe <i>et al.</i> , 1989
c-myb	18 (D); c; uM	T-cells HL-60 cells hematopoietic cells Human colon carcinoma neuroblastoma cells smooth muscle cells in vivo	Gewirtz <i>et al.</i> , 1988 Gewirtz <i>et al.</i> , 1989 Venturelli <i>et al.</i> , 1990 Anfossi <i>et al.</i> , 1989 Citro <i>et al.</i> , 1992 Valteri <i>et al.</i> , 1991 Melani <i>et al.</i> , 1991 Raschella <i>et al.</i> , 1992 Simons and Rosenberg, 1992 Ratajczak <i>et al.</i> , 1992 Simons <i>et al.</i> , 1992
c-myc	15s (D,T); v; uM	HL-60 T-cells Burkitt cells MCF-7 Colon carcinoma cells Keratinocytes smooth muscle cells mouse adipocytes	Holt <i>et al.</i> , 1988 Wickstrom <i>et al.</i> , 1988; <i>ibid.</i> 1989; Bacon and Wickstrom, 1991 Heikkila <i>et al.</i> , 1987 Harel-Bellan, <i>et al.</i> , 1988a McManaway <i>et al.</i> , 1990 Watson <i>et al.</i> , 1991 Collins <i>et al.</i> , 1991 Hashiro <i>et al.</i> , 1991 Ebbecke <i>et al.</i> , 1992 Ninomiya-Tsuji <i>et al.</i> , 1993
N-myc	15 (D); s; uM	neuroepithelioma cells	Rosolen <i>et al.</i> , 1990
myeloblastin	18 (D); c	HL-60	Bories <i>et al.</i> , 1989

Table 1-2: (cont.) Cellular studies utilizing antisense oligonucleotides (ASO)

<u>target gene</u>	<u>ASO</u>	<u>cell line</u>	<u>reference(s)</u>
myogenin	15 (D); s; uM	myoblasts	Florini and Ewton, 1990 Florini <i>et al.</i> , 1991
NCAM	24 (T); s; <uM	neuroblastoma	Perides <i>et al.</i> , 1992
NF- κ B, RelA subunit	18,21 (T)l sl uM	Jurkat T-cells	Kunsch and Rosen, 1993
NGF-I	15 (D); s; uM	T-cells	Perez-Castillo <i>et al.</i> , 1993
NGFR	18 (T); u; uM	rat kidney cells	Sariola <i>et al.</i> , 1991
p120	20-mers (T); v; <uM 15 (D); sj; >uM	3T3 cells human lymphocytes	Perlaky <i>et al.</i> , 1993 Fonagy <i>et al.</i> , 1992
PCNA	18 (D); s; uM 27 (D); c; uM 15-18 (A); s; uM 18(T); s, uM	3T3 cells CHO cells smooth muscle cells gastric cancer cells	Jaskulski <i>et al.</i> , 1988 Liu <i>et al.</i> , 1989 Speir and Epstein, 1992 Sakakura <i>et al.</i> , 1994
perforin	18 (D); s; uM	T-cells	Acha-Orbea <i>et al.</i> , 1990
peripherin	21 (D); v; < uM	rat pheochromocytoma	Troy <i>et al.</i> , 1992
phospholipase A2	20 (T); u; uM	murine macrophages	Barbour and Dennis, 1993
phospholipase A2 activating protein	25 (D); s; uM	smooth muscle , endothelial cells	Clark <i>et al.</i> , 1991
type-1 plasminogen activator inhibitor	20 (2T); v, uM	HUVEC cells aortic smooth muscle cells	Sawa <i>et al.</i> , 1994
human procollagen	18 (T); v; < uM	transfected 3T3	Colige <i>et al.</i> , 1993
progesterone receptor	18 (D); s; uM	T47D cell line in vivo (rats)	Pollio <i>et al.</i> , 1993
prohibitin	18 (D); s	fibroblasts, HeLa	Nuell <i>et al.</i> , 1991
cAMP-dependent PKC	21 (D); s; uM 15 (D); s; uM	transfected pheochromocytoma cells; mouse mammary epithelial cells	Tortola and Cho-Chung, 1990 Sheffield, 1991
PKC	15 (D); s; uM 15 (D); c; uM	rat adipocytes human bone marrow cell line	Farese <i>et al.</i> , 1991 Baxter <i>et al.</i> , 1992
	18 (D); c; uM 20 (T); v, uM	K562 cells human lung carcinoma	Murray <i>et al.</i> , 1993 Dean <i>et al.</i> , 1994
prothymosin	16-21 (D); v; uM	human myeloma cells	Sburlati <i>et al.</i> , 1991
human prorenin	16 (T); v; < uM	transfected CHO cells	Cumin <i>et al.</i> , 1993
rab3b	22 (D); v	pituitary cells	Lledo <i>et al.</i> , 1993
rab8p	15 (T); v; uM	neurons	Huber <i>et al.</i> , 1993
rac	16 (D); s; uM	B-cells	Dorseuil <i>et al.</i> , 1992
c-Ha-ras	15 (D); v; uM	3T3 cells	Daaka and Wickstrom, 1990
Ha-ras	9,10 (Dd);s; uM	bladder carcinoma cells, human mammary cells	Saison-Behmoaras <i>et al.</i> , 1991
N-ras	18 (D); s; uM	human hematopoietic progenitor cells	Skorski <i>et al.</i> , 1992
ras	11 (M); s; uM	3T3 derived cells	Brown <i>et al.</i> , 1989 Chang <i>et al.</i> , 1991
Rb-1	18 (T); s; uM 21 (T); s; uM	human embryonic lung fibroblasts hematopoietic progenitors	Hatzfeld <i>et al.</i> , 1991 Strauss <i>et al.</i> , 1992
retinoid receptor	15 (D); s; uM	human malignant keratinocytes	Cope and Wile, 1989
RFX-1/MHC expression	14-20 (T); v; uM	EBV transformed B cells	Siegroost and Mach, 1993
S100 β	15 (D); s; uM	rat glioma cells	Selinfreund <i>et al.</i> , 1990
T-cell receptor	22-23 (D); s; uM	T-cell hybridomas	Zheng <i>et al.</i> , 1989

Table 1-2 (cont.): Cellular studies utilizing antisense oligonucleotides (ASO)

<i>target gene</i>	<i>ASO</i>	<i>cell line</i>	<i>Reference(s)</i>
tau	20-25 (D); s; uM 36 (D); s; uM	primary neurons neuroblastoma cells cerebellar granule cells	Caceres and Kosik, 1990 Shea <i>et al.</i> , 1992 Pizzi <i>et al.</i> , 1993
TGF- α	23 (D); s	colon carcinoma cells	Sizeland and Burgess, 1991
TGF- β 1	16 (A); s; uM	chicken explants	Sizeland and Burgess, 1992 Potts <i>et al.</i> , 1991
TGF- β 3	21 (T); s; uM	human hematopoietic progenitors	Runyan <i>et al.</i> , 1992 Hatzfeld <i>et al.</i> , 1991
TNF- α	17 (D); s; uM	murine macrophages	Witsell and Schook, 1992
Transferrin receptor	17,30 (T); v; uM	HL-60	Ho <i>et al.</i> , 1991
troponin C	18 (D); c; uM	chicken myotubes	Thinakaran and Bag, 1990
tubulin	19-21 (D); v; uM	rat pheochromocytoma	Teichman-Weinberg <i>et al.</i> , 1988
ubiquitin	15 (D); s, c; uM	human lymphocytes	Delic <i>et al.</i> 1993
V-CAM	18-21 (T); v, nM	HUVEC	Bennett <i>et al.</i> , 1994

ASO column key: size (type); target region; concentration (e.g. 18 (D); s; uM)

Size = length of ASO in bases

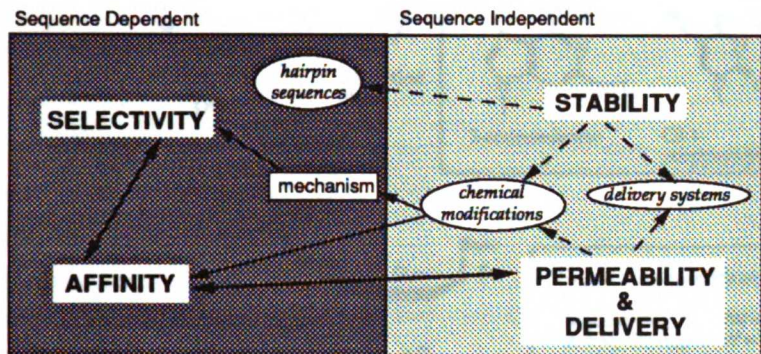
type: D= phosphodiester; T = phosphorothioate; M = methyl phosphonate;
d=derivatized (acridine, lipid, etc.); 2'T = 2'-O-methyl + thioate modification

target site: c = coding region; s = start codon region; v= various regions;

u=untranslated region; sj= splice junction; tj = translocation junction

Target gene abbreviations: AChR, acetylcholine receptor; CFTR, cystic fibrosis transmembrane regulator; CSF, colony stimulating factor; EGF, epithelial growth factor; Egr-1, early growth response gene; bFGF, basic fibroblast growth factor; FGFR, fibroblast growth factor receptor; GABA, gamma-butyric acid; G-CSF, granulocyte-colony stimulating factor; GHF-1, growth hormone factor 1; GM-CSF, granulocyte-macrophage colony stimulating factor; HOX, homeobox; ICAM, intracellular adhesion molecule; IL, interleukin; ILGF, insulin-like growth factor; ILGF-R1, insulin-like growth factor receptor type-1; LH, lutenizing hormone; *mdr*, multiple drug resistance gene; MHC, major histocompatibility complex; NCAM, neural cell adhesion molecule; NGF, nerve growth factor; NGFR, nerve growth factor receptor; PCNA, proliferating cell nuclear antigen; PKC, protein kinase C; TGF, transforming growth factor; TNF-tumor necrosis factor.

Figure 1-2: Obstacles to ASO activity and their interrelationships



The four major obstacles to ASO activity-- stability, permeability, selectivity and affinity-- can be divided into sequence dependent and sequence independent obstacles. Partial solutions to stability and delivery obstacles are shown within the ovals. Some of these solutions in turn impact the selectivity and affinity obstacles (see text for details).

I.2 Stability and delivery obstacles

Of the four obstacles mentioned above, stability and delivery obstacles do not generally impact ASO sequence selection, since all ASO regardless of their sequence face the same nucleases and membranes. Therefore, these obstacles will be discussed only briefly.

I.2.1 Stability

Phosphodiester RNA and DNA is rapidly degraded by nucleases present in serum and the cytoplasm (Wickstrom, 1986); thus stability of ASO intended for any *in vitro* or *in vivo* application is a major concern. Chemists have modified nucleic acid polymers in order to improve their stability towards nucleases. These modifications may be made to the phosphate backbone, to the conformation of the base-sugar bond, to the 2' OH of the ribofuranose ring, or to the ASO 5' or 3' termini (Figure 1-3). Many of these modifications improve ASO stability but alter other physiochemical properties of the ASO, such as ASO affinity or the ability to promote RNase H activity (Table 1-3). Several excellent

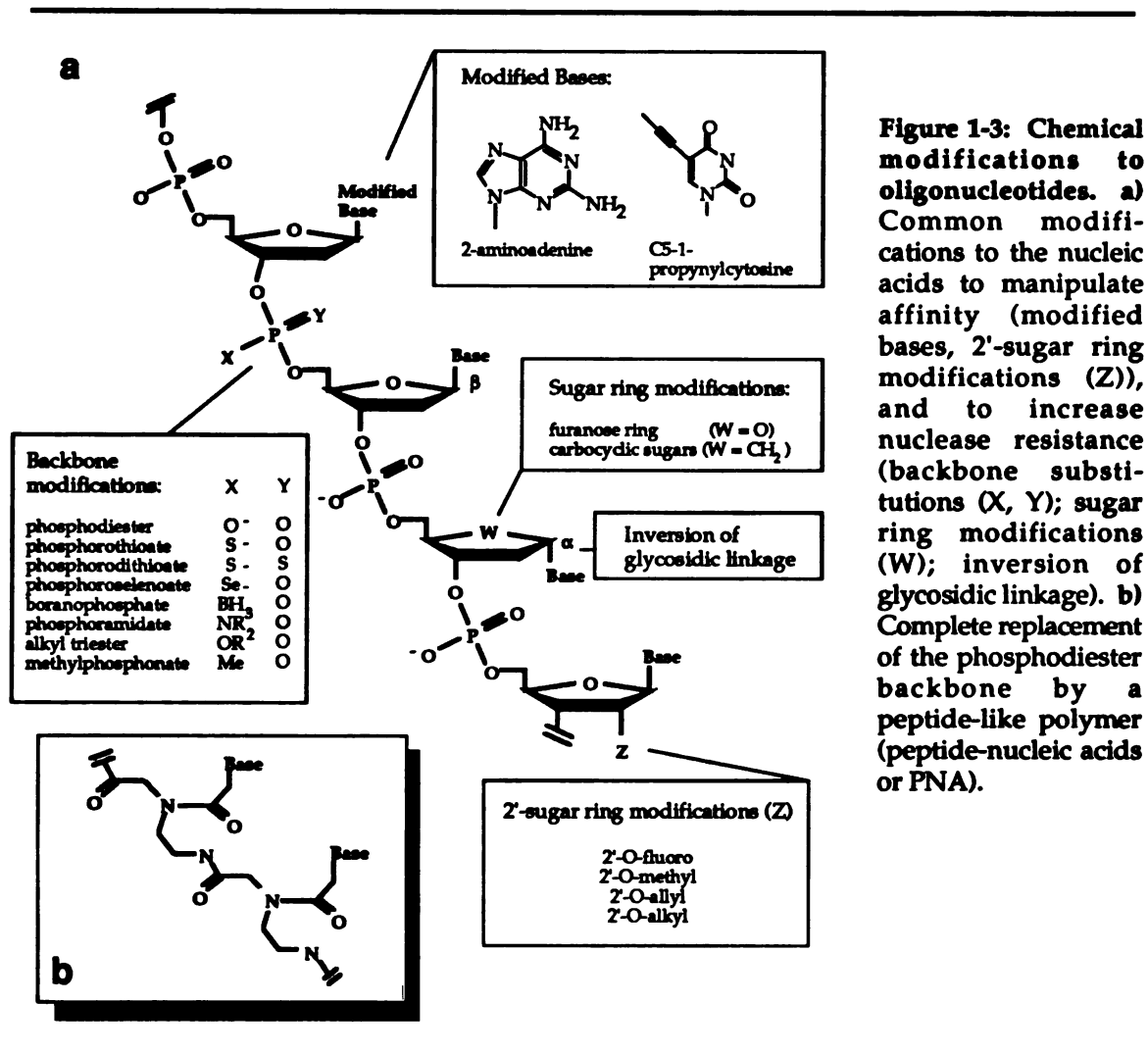


Figure 1-3: Chemical modifications to oligonucleotides. a) Common modifications to the nucleic acids to manipulate affinity (modified bases, 2'-sugar ring modifications (Z)), and to increase nuclease resistance (backbone substitutions (X, Y); sugar ring modifications (W); inversion of glycosidic linkage (W); inversion of glycosidic linkage). **b)** Complete replacement of the phosphodiester backbone by a peptide-like polymer (peptide-nucleic acids or PNA).

detailed reviews of the medicinal chemistry of ASO have been published (Uhlmann and Payman, 1990; Cook, 1991; Cook, 1993); the reader is referred to these reviews for a comprehensive analysis of the physicochemical and biological properties of modified ASO.

Tang and coworkers (1993) present an alternative strategy for stabilizing ASO towards endonucleases-- introduction of sequences into the ASO which permit formation of a stable hairpin loop near the 3' terminus. Introduction of the loop did not significantly affect the hybridization properties of several anti-

TABLE 1-3: Physiochemical properties of backbone modified nucleic acids

Nucleic Acid Compound	Charged	Chiral	T _m *	Nuclease Sensitivity	RNase H Substrate	References
phosphodiester	yes	no	-	yes	yes	
phosphorothioate	yes	yes	↓	↓	yes	Stein <i>et al.</i> , 1988a
phosphorodithioate	yes	no	↓	↓	yes	Caruthers <i>et al.</i> 1991
phosphoroselenoate	yes	yes	↓	N. R.	N. R.	Mori <i>et al.</i> , 1989a
boranophosphate	yes	yes	N. R.	↓	N. R.	Sood <i>et al.</i> , 1990
phosphoramidate	yes/n	yes	↓	↓	no	Agrawal <i>et al.</i> , 1988; 1990
	o					Froehler <i>et al.</i> 1988
alkyl triester	no	yes			N. R.	Miller <i>et al.</i> 1971; 1974
methyl phosphonate	no	yes	↓	↓	no	Miller <i>et al.</i> , 1979; 1991
peptide nucleic acid	no		↑	N. R.	no	Nielsen <i>et al.</i> , 1991

N. R. - not reported

*Measured against DNA oligomer complement

HIV (*gag*) ASO, but did increase both their efficacy in cells and their pharmacokinetic behavior and stability *in vivo*.

I.2.2 Membrane permeability

Nucleic acid polymers are large, charged macromolecules which would not be expected to readily cross cellular membranes. However, the number of studies in which ASO produce biological effects after addition directly to the culture medium of cells suggest some cytoplasmic uptake of ASO. Detailed studies of the uptake of ASO suggest that limited uptake appears to occur via a mechanism compatible with endocytosis (Loke *et al.*, 1989; Yakubov *et al.*, 1989; Chin *et al.*, 1990; Agrawal *et al.*, 1992; Bennett *et al.*, 1992). Uptake may be mediated by a 75-80 kD protein (Loke *et al.*, 1989; Yakubov *et al.*, 1989; Geselowitz and Neckers, 1992) or may occur via fluid phase endocytosis (Shoji *et al.*, 1991; Akhtar *et al.*, 1991). Several reports indicate the uptake of ASO by populations of cells is heterogeneous (Noonberg *et al.*, 1993; Nestle *et al.*, 1994),

TABLE 1-4 Strategies to enhance cellular delivery of ASO

strategy	modification	results	Reference
<i>chemical modifications</i>			
improve ASO uptake by modifying ASO lipophilicity	covalent linkage to cholesterol or thiocholesterol	improved ASO cell association, uptake, nuclear localization; some increase in non-sequence specific effects	Boutorin <i>et al.</i> , 1989; Letsinger <i>et al.</i> , 1989; Ryte <i>et al.</i> , 1992; Oberhauser and Wagner, 1992; Ing <i>et al.</i> , 1993; Kreig <i>et al.</i> , 1993
	covalent linkage to phospholipids	as above	Shea <i>et al.</i> , 1990
	covalent linkage to undecyl or dodecandiol residue	as above	Kabanov <i>et al.</i> , 1990; Saison-Behmoaras <i>et al.</i> , 1991
improve ASO uptake via conjugation to receptor ligand	covalent linkage to biotin, associate with avidin	improved uptake, but no biological characterization	Pardridge and Boado, 1991
	covalent linkage to neoglycoproteins	improved uptake, but ASO retained in vesicles	Bonfils <i>et al.</i> , 1992a,b
<i>drug delivery systems</i>			
nanoparticles associated with hydrophobic cations	electrostatic interaction with hydrophobic cations	ASO protected from degradation, no biological tests reported	Chavany <i>et al.</i> , 1992
poly-(L-lysine)	covalent linkage to ASO	enhanced cell association, uptake; potentiation of the biological effects of several antiviral ASO	Lemaitre <i>et al.</i> , 1987; Leonetti <i>et al.</i> , 1988; Stevenson and Iverson, 1989; Degols <i>et al.</i> , 1991; <i>ibid.</i> 1992
molecular conjugates with poly-(L-lysine); protein ligands	electrostatic interaction with ASO backbone; targeted via coupled ligand	improved uptake and potentiation of inhibitory effects of ASO	Leonetti <i>et al.</i> , 1990a; Wu and Wu, 1992; Bunnell <i>et al.</i> , 1992; Citro <i>et al.</i> , 1992
targeted liposomes (immunoliposomes)	encapsulation in multilamellar vesicles coupled to protein A and antibodies	substantial boost in efficacy of ASO; protection from degradation; specificity in cell targeting	Leonetti <i>et al.</i> , 1990b
non-targeted liposomes	encapsulation in liposome, pH-sensitive liposomes	enhanced efficacy of ASO relative to unencapsulated ASO	Loke <i>et al.</i> , 1988; Ropert <i>et al.</i> , 1992; 1993; Thierry <i>et al.</i> , 1992
cationic lipids (DOTMA; DOTAP)	electrostatic association between ASO and lipid head group	improved uptake and subcellular distribution	Bennett <i>et al.</i> , 1992; Vanderklish <i>et al.</i> , 1992; Colige <i>et al.</i> , 1993; Cumin <i>et al.</i> , 1992; Barbour <i>et al.</i> , 1993; Perlaky <i>et al.</i> , 1993; Yu <i>et al.</i> , 1993

and in certain cell lines, inducible (Krieg *et al.*, 1991). How ASO may escape the endosome to enter the cytoplasm is currently unknown. Studies using microinjected ASO indicate that once ASO enter the cytoplasm of living cells, they rapidly accumulate in the nucleus (Chin *et al.*, 1990, Léonetti, *et al.*, 1991). Accumulation is the result of ASO binding to various distinct nuclear sites (Clarenc *et al.*, 1993).

Two main strategies for improving cellular uptake and distribution of ASO have been reported— chemical modification of the ASO polymer, and use of drug delivery reagents to improve cellular and/or cytoplasmic delivery of the ASO (Table 1-4). In general, chemical modifications enhance cellular association of ASO, but may increase the non-sequence specific effects of these compounds or simply "trap" a larger portion of the dose in membranes or within subcellular vesicles. Drug delivery systems in general potentiate the effects of ASO, suggesting successful enhancement of cytoplasmic delivery in cell culture, but these systems have not yet afforded widespread use of ASO *in vivo*.

I.3 ASO selectivity

If a drug is to be therapeutically useful, it must display sufficient affinity for its target so as to bind a substantial fraction of its target at readily achievable biological concentrations, while maintaining selectivity. For any drug, selectivity and affinity are inherently related to the kinetics and thermodynamics of the molecular recognition processes behind the drug-macromolecule interactions. In the case of ASO, the molecular recognition processes are base-pairing. Thus the selectivity and affinity of ASO depend upon the kinetics and thermodynamics of nucleic acid oligomer-polymer base-pairing.

I.3.1 ASO selectivity: Herschlag's discrimination index

Herschlag (1991), in his discussion of ribozyme kinetics, has defined a discrimination index which is also applicable to ASO theory:

$$\text{discrimination index} = \frac{k_{\text{target}} [\text{target}]}{\sum_i k_{i,\text{mis}} [\text{target}_{i,\text{mis}}]} \quad (1-1)$$

Qualitatively, this equation reveals the selectivity of an ASO to be dependent upon the relative amounts of sequence-matched and mismatched target sites. It also indicates the selectivity of an ASO will depend upon the apparent rate constants for the processes whereby the ASO produces its biological effects at the target (k_{target}) and each of the mismatched ($k_{i,\text{mis}}$) sites. Thus ASO selectivity is a function of statistics, thermodynamics, and kinetics.

I.3.2 ASO selectivity: statistical considerations

I.3.2a Statistical uniqueness. Maximizing ASO selectivity requires a sequence length long enough to be functionally unique to the intended target, while short enough to minimize base-pair interactions at mismatched sites. The expected frequency for a given ASO sequence of length n in a genome of size N base-pairs is

$$f = 2N (0.25)^n \quad (1-2)$$

if the base distribution within the genome is considered chemically random, and each base is expected to occur with the equal frequency. Note that the $2N$ term indicates consideration of both strands of DNA. For a genome of three billion base-pairs (the approximate size of the human genome), equation 1-

2 indicates that $f \leq 1$ when $n \geq 17$. Simple revisions to account for unequal frequencies of each of the bases reveal $f \leq 1$ for $15 \leq n \leq 19$, depending upon the GC-content of the ASO sequence (von Hippel, 1979). When considering only the mRNA pool (approximately 1% of the entire genome; Lewin, 1990), $f \leq 1$ for $11 \leq n \leq 15$.

I.3.2b Mismatched site statistics. Based upon probability considerations, a 17-nucleotide sequence is likely to be statistically unique within the human genome, a 13-nucleotide sequence likely to be unique in a cellular RNA pool. However, one can intuit that many more sequences are available which differ from the specific sequence by one or a few nucleotides. For an ASO sequence of length n , the frequency of occurrence of closely related RNA target site sequences containing j mismatches at any site(s) is given by (von Hippel, 1979)

$$f = 2N (0.25)^{n-j} (0.75)^j \left\{ \frac{n!}{j!(n-j)!} \right\} \quad (1-3)$$

Equation 1-3 assumes for simplicity that each nucleotide is in equal abundance within the RNA pool. For a given ASO sequence, the number of potential mismatch sites will increase roughly one order of magnitude per every two mismatches allowed.

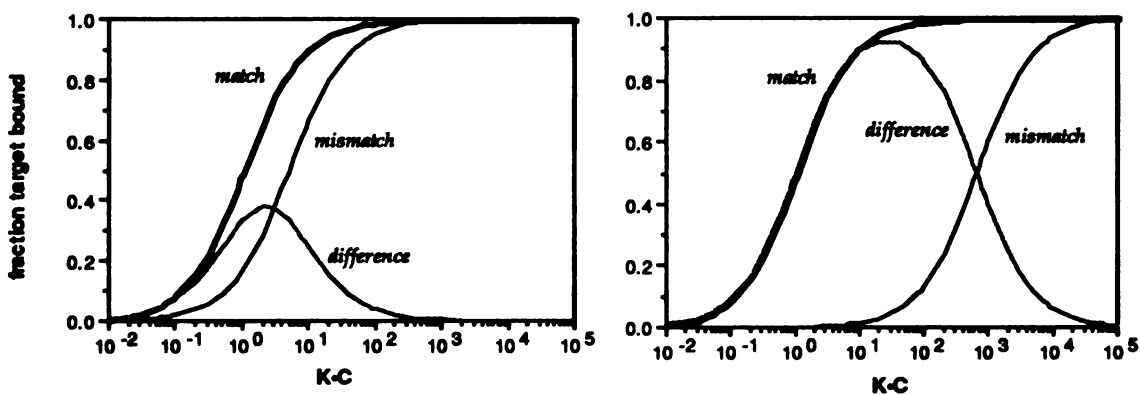
It should be noted that the expected frequencies supplied by equations 1-2 and 1-3 are rough approximations of actual sequence frequencies. First, the genome is not chemically random, since genes themselves are not chemically random. Several studies have shown that at the dinucleotide level, there are definite biases for and against certain dinucleotide sequences and their distributions within functional DNA elements (Josee *et al.*, 1961; Nussinov, 1981; Nussinov, 1984a; Nussinov 1984b; Beutler *et al.*, 1989). Similarly, certain short sequences are important signals for various components of nucleic acid

metabolism (e.g. TATA, CAAT, AUUUA, AAUAAA). More accurate models of sequence frequency have been published incorporating actual genomic dinucleotide frequencies (Han *et al.*, 1994). The simple equations presented above, however, do provide rough estimates of the frequencies of matched and mismatched target sites.

I.3.3 ASO selectivity: thermodynamics

Under equilibrium binding conditions, a simple thermodynamic model can be used to describe the relationship between ASO affinity and selectivity (Figure 1-4, after Monia *et al.*, 1992). The equilibrium binding of an ASO to a matched versus mismatched site will differ by a free energy increment $\Delta\Delta G$. If $\Delta\Delta G = 4$ kcal/mol, a selectivity optimum will occur at about $K_{eq} \cdot C = 26$, where K_{eq} is the equilibrium constant for binding, and C is the ASO concentration. At this optimum, 96% of the target site will be bound, while only 4% of the mis-

Figure 1-4: Thermodynamic selectivity for ASO binding



The fraction of target bound as a function of the concentration and affinity constant of the ASO for a matched site and a mismatched site. The left panel shows a 1 kcal/mol difference between the free energy of binding for the matched and mismatched sites; the right panel, a difference of 4 kcal/mol. Notice that as the $\Delta\Delta G$ value increases, the selectivity maximum increases, and the optima becomes less sharp. (After Monia *et al.*, 1992)

match site will be bound (assuming both sites are in equal abundance). If the free energy difference for binding is smaller, the selectivity optimum will decrease both with regard to fraction of target site bound and the $K_{eq} \cdot C$ value at which the optimum is achieved (e.g. $\Delta\Delta G^\circ = 1$ kcal/mol, then $K_{eq} \cdot C = \sim 2.25$, where 69% of the matched site is bound versus 31% of the mismatched site is bound). The relationship between $\Delta\Delta G^\circ$ and maximum selectivity is given by equation 1-4

$$\Delta\Delta G^\circ = 2RT \ln(K_{eq}C)_{\max} \quad (1-4)$$

The derivation for this equation appears in appendix 1.

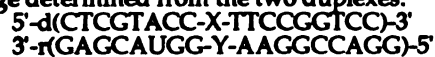
Freier (1993) has reported the influence of single mismatches upon the free energy of binding for DNA-RNA 18-mer duplexes (Table 1-5). In the case of a phosphodiester ASO binding to a point mismatched target, the free energy

Table 1-5: $\Delta\Delta G^\circ$ binding penalties for single mismatched DNA • RNA ASO (kcal/mol)^a

mismatch	DNA° RNA ^{b,c}	PS-DNA° RNA ^{c,d}	mismatch	DNA° RNA ^{b,c}	PS-DNA° RNA ^{c,d}
AA	+5.3 [74]	+2.2 [6]	GA	+5.2 [68]	+4.2 [30]
AC	+4.5 [39]	+2.3 [6]	GG	+5.2 [68]	+3.8 [22]
AG	+3.9 [24]	+2.1 [6]	GU	+5.1 [63]	+3.3 [15]
CA	+5.7 [102]	+3.2 [13]	TC	+3.4 [16]	+2.6 [8]
CC	+6.0 [130]	+3.9 [24]	TG	+1.2 [3]	+1.1 [2]
CU	+6.3 [166]	+3.8 [22]	TU	+3.7 [20]	+2.5 [8]

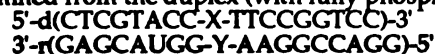
^aModified from Freier (1993)

^bAverage determined from the two duplexes:



^cSelectivity maximum (equation 1-4) shown in brackets.

^dDetermined from the duplex (with fully phosphorothioated DNA oligomer):



penalty averages about +4.5 kcal/mol; for a phosphorothioate ASO, about +3 kcal/mol. These values translate into 40 and 20 fold selectivity maxima, respectively. Although the thermodynamic values were obtained from a limited data set, this data illustrates the thermodynamic limits placed upon ASO selectivity.

1.3.4 ASO selectivity: kinetics

Herschlag's discrimination index is defined in terms of kinetics of biological effect, which may reflect the kinetics of ASO binding or the kinetics of the RNase H activity (for those ASO-RNA duplexes which are substrates for RNase H).

The affinity of an ASO will increase directly with the length of the ASO. However, the selectivity of an ASO is determined by its rates of association and disassociation to targeted and mismatched sites. For binding to an unstructured complement association rate constants for ASO will be approximately $10^8 \text{ M}^{-1} \text{ s}^{-1}$ at best, with typical k_{on} values between 10^6 and $10^7 \text{ M}^{-1} \text{ s}^{-1}$ (Riesner and Römer, 1973). For an ASO with $k_{on} = 5 \times 10^6 \text{ M}^{-1} \text{ s}^{-1}$ present at 1 nM, binding will be 90% complete in about 8 minutes. If $k_{off} = 2 \times 10^3 \text{ s}$, (i.e. $K_d = 10^{10} \text{ M}^{-1}$), virtually stoichiometric binding will occur. Increasing the affinity of the ASO by simply increasing its length will not substantially increase the rate of binding nor the extent of binding-- increases in affinity will primarily reduce the k_{off} rate for the ASO (Freier, 1993). If, at the mismatched site, the dissociation step is slower than the rate of the production of effects, the selectivity of the ASO will be decreased (Monia *et al.*, 1993).

When an ASO achieves its effects via RNase H activation, the discrimination index of an ASO will be influenced by the kinetics and substrate recognition abilities of this enzyme. It is known that RNase H is the primary

effector for ASO-mediated inhibition in *Xenopus* oocytes (Walder and Walder, 1988; Cazenave *et al.*, 1987). Woolf and coworkers (1992) attempted to experimentally address the discrimination index of ASO dependent upon RNase H activity in studies of *Xenopus* oocytes microinjected with ASO. They concluded that in *Xenopus*, as few as 10 consecutive bases of complementarity between an ASO and RNA was sufficient to allow hybridization, that RNA-ASO duplexes with internal mismatches afforded RNase H cleavage, and that any ASO longer than 10 nucleotides was likely to cause at least partial degradation of non-targeted RNAs. It is currently unclear how well these findings in RNase H- rich *Xenopus* apply to mammalian systems, but the results demonstrate mechanistic limitations to ASO selectivity.

Conversely, it is also possible that the mechanisms by which an ASO achieves its biological effects may enhance ASO selectivity. For example, consider an ASO which does not support RNase H activity but inhibits the capping reaction of its target RNA. This ASO, although binding fortuitously to the coding region of another RNA, may not produce any significant inhibition of the non-targeted gene, since ribosomes appear capable of "melting" out duplexes within the coding region of an mRNA (Liebhaber *et al.*, 1984; Shakin and Liebhaber, 1986).

Finally, it should be noted that other important kinetic factors, such as the differences in half-lives for targeted and non-targeted RNAs, will affect the apparent selectivity of the ASO. While the target molecule for an ASO is an mRNA, the desired biological effect is reduction of protein synthesis. Therefore, the half-life of the proteins encoded by targeted and non-targeted RNAs will also determine to some extent the specificity of the ASO (Hargrove *et al.*, 1990; Ramanathan *et al.*, 1993).

I.4 ASO affinity

ASO affinity is the fourth major obstacle to ASO activity. It is interrelated to the previously mentioned stability, permeability and selectivity obstacles (Figure 1-2). The affinity of an ASO must be sufficiently strong enough to permit binding to a significant fraction of the target molecules so as to achieve a measurable biological effect. Yet the affinity must not be so strong as to permit tight binding to non-targeted molecules thereby decreasing the selectivity of the ASO. Delivery obstacles impact the affinity requirements placed upon an ASO since the product of the ASO affinity constant and concentration will affect the extent of target molecules bound (Figure 1-4). Finally, while the stability of an ASO does not directly affect its affinity, chemical modifications designed to improve ASO stability may alter the binding behavior of the ASO.

While ASO affinity is generally experimentally evaluated by measurement of a T_m , affinity is a thermodynamic parameter best described by a free energy measurement of duplex formation. The thermodynamics of nucleic acid helix formation reflect hydrogen bonding, base-pair stacking, electrostatic interactions between the nucleic acid backbones, steric factors related to the conformation of the participating macromolecules, and the environment in which the hybridization is occurring (i.e. pH, ionic strength and temperature). Physiological conditions will dictate the hybridization environment for ASO used as drugs; thus the apparent affinity of an ASO drug will be a function primarily of ASO sequence and chemical composition, and of RNA structure.

I.4.1 Components of affinity due to the chemical structure of the ASO

I.4.1a ASO affinity and ASO sequence. Simple considerations of hydrogen bonding in G-C versus A-(U/T) base pairs suggest the more GC rich an ASO is, the more stable the potential ASO-mRNA duplex will be. Duplex

formation, however, shows a sequence dependence beyond that due to composition, attributable to base-pair stacking. Nearest-neighbor models have been used to interpret the effects of sequence upon the thermodynamic stability of nucleic acid helices (Freier *et al.*, 1986; Yager and von Hippel, 1991). In general, the free energy of stacking interactions follows the order purine-purine > purine-pyrimidine > pyrimidine-pyrimidine, indicating ASO sequence as well as composition will be an important component of ASO affinity.

I.4.1b Chemical modifications to ASO and their effects upon ASO affinity. Backbone modifications to ASO may alter their binding affinity in a variety of ways. Electrically neutral modifications (*e. g.* alkyl phosphate triesters, methylphosphonates) may increase ASO affinity by reducing or eliminating the electrostatic repulsion normally occurring between the polyanionic nucleic acid backbones. Large bulky substitutions at the phosphorous atom (*e. g.* some phosphoramidates) may hinder duplex formation due to steric effects. Finally, introduction of a chiral center by modifications at the phosphorus atom may destabilize the duplex, particularly if the modified group is oriented toward ["pseudoaxial"] the duplex axis (Summers *et al.*, 1986; LaPlanche *et al.*, 1986; Bower *et al.*, 1987). The magnitude of these stereospecific effects may be dependent upon the ASO sequence (Kibler-Hertzog *et al.*, 1990; *ibid.*, 1991).

Complete replacement of the phosphate backbone by a polyamide backbone produces compounds termed peptide nucleic acids (Figure 1-3b; Nielsen *et al.*, 1991; Hanvey *et al.*, 1992). Peptide nucleic acids (PNAs) display increased T_m values for DNA target sequences relative to standard phosphodiester oligonucleotides. Molecular modeling studies have suggested the exceptional stability of PNA-nucleic acid duplexes is due to interresidue hydrogen bonding along the PNA backbone (Almarsson and Bruice, 1993).

Table 1-6: Comparative T_m values for various ASO analogs^a

Sequence ^b	Analog	T_m for duplex ^c with:	
		12 mer β DNA	12-mer β -RNA
ACACCCAATTCT	β -DNA	47.6 (1) ^d	46.1 (3)
ACACCCAATTCT	β -methylphosphonate	40.3 (3)	27.4 (7)
ACACCCAATTCT	β -phosphorothioate	37.9 (7)	36.1 (6)
TCTTAACCCACA	α -DNA	42.8 (2)	43.1 (4)
TCTTAACCCACA	α -phosphorothioate	40.3 (3)	40.3 (5)
UCUUAACCCACA	α -RNA	14.3 (8)	16.5 (8)
ACACCAAUUCU	β -2'-O-methyl RNA	39.0 (5)	58.4 (1)
ACACCAAUUCU	β -2'-O-allyl RNA	35.7 (6)	54.0 (2)

^a Modified from Morvan *et al.*, 1993.

^b Targeted to the *lat* region of HIV-1, target sequence: AGAAUUGGGUGU (nts. 5357-5368); note α analogs form parallel heteroduplexes; hence their apparent sequence inversion

^c Values ± 0.5 °C as determined in 0.1M NaCl, 10 mM Na cacodylate, pH 7.0, 3 μ M each strand.

^d Ordinal ranking within the set of analogs.

Whether the high affinity and/or lack of charge increases the non-specific effects of the PNAs is not yet known. However, PNA-RNA duplexes are not substrates for RNase H (Nielsen *et al.*, 1994).

Natural ribonucleotides, due to the 2' OH group present on the ribofuranose ring, are chemically less stable than the corresponding deoxyribonucleotides. However, RNA-RNA duplexes are more thermodynamically stable than RNA-DNA duplexes (Roberts and Crothers, 1992). Therefore, a second generation of modified ASO have been designed to bind RNA tightly (although they will not trigger RNase H activity upon binding), but are chemically more stable than natural RNA. These compounds, termed "RNA mimics" (Cook, 1991), have substitutions at the 2' OH group of the ribofuranose sugar. As RNA mimics vary in their resistance to nucleases (Inoue *et al.*, 1987; Sproat *et al.*, 1989; Iribarren *et al.*, 1990; Morvan *et al.*, 1993; Kawasaki *et al.*, 1993), 2' OH modifications may be combined with backbone substitutions. These doubly modified ASO display slightly weaker affinities than

phosphodiester RNA mimics due to the backbone substitution effects described above (Monia *et al.*, 1992; Kawasaki *et al.*, 1993).

Conjugation of lipophilic groups or intercalating agents to ASO is a common strategy for improving cellular uptake, but these moieties may also alter the affinity of the ASO for its complement. Conjugation of cholesterol groups appears to alter minimally the T_m values of the ASO (Letsinger *et al.*, 1989), while intercalating groups generally increase the T_m values of ASO (Asseline *et al.*, 1984; Hélène *et al.*, 1985; Toulmé *et al.*, 1986; Thuong *et al.*, 1987; Stein *et al.*, 1988b; Mori *et al.*, 1989b).

Many modifications to the nitrogenous bases have been tested to improve the selectivity or affinity of ASO (Sanghvi, 1993). Modifications at sites other than the hydrogen bond centers may reduce the hybridization affinity of the modified ASO, probably through steric effects (see Cook, 1991). However two novel bases have been shown to enhance ASO affinity for RNA targets: 1-propynyl modified cytosine and uridine (at the C5 position, Wagner *et al.*, 1993) and 2-aminoadenine (Howard and Miles, 1984). These modified bases most likely improve the affinity through enthalpic and entropic effects (increased base-stacking and displacement of ordered water molecules from the duplex, respectively; Froehler *et al.*, 1992), or by providing additional interstrand hydrogen bonds (2-aminoadenosine).

I.4.2 ASO affinity and RNA structure

I.4.2a Target site secondary structure. The apparent affinity of the ASO will also depend upon the structure of the RNA at the binding site. Upon first consideration, when the secondary structure of the target RNA is known, avoidance of target sites participating in RNA secondary structure might appear

to be the best strategy. However, Ecker points out (1993) that targeting RNA secondary structure may be both desirable and unavoidable— desirable since disruption of mRNA secondary structure may interfere with the biological function of the RNA, and unavoidable, since large, structure-free regions of mRNA may not occur with great frequency.

Uhlenbeck (1971) studied the equilibrium binding of various trimer and tetramer oligoribonucleotides to *E. coli* tRNA^{tyr} and tRNA^{Met}. Binding was observed only to portions of loop I, the anticodon loop (loop II), loop III, and to the single-stranded region of the aminoacyl-stem (Figure 1-5). Other regions of the tRNA molecule were inaccessible for binding due to either the secondary or tertiary structure of the tRNA. Several key conclusions can be drawn from his study. First, ASO targeted to loops will vary in their binding behavior depend-

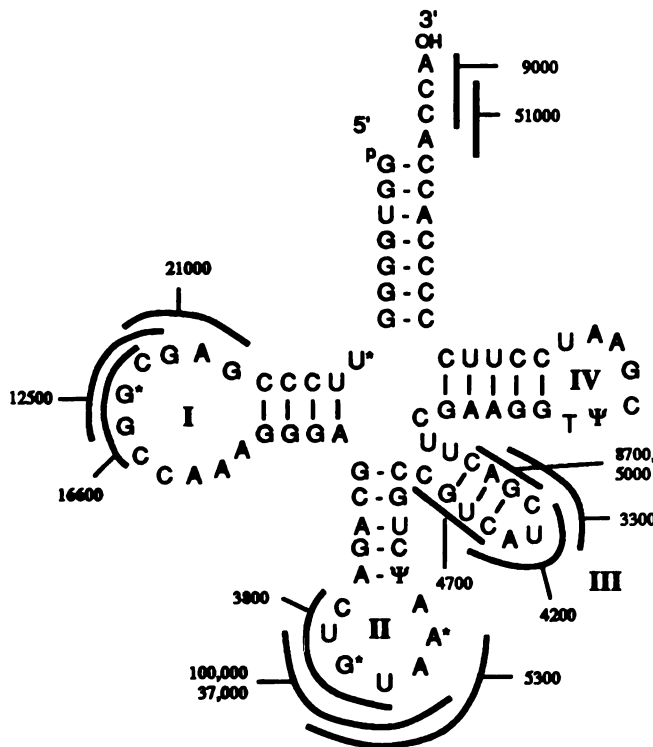
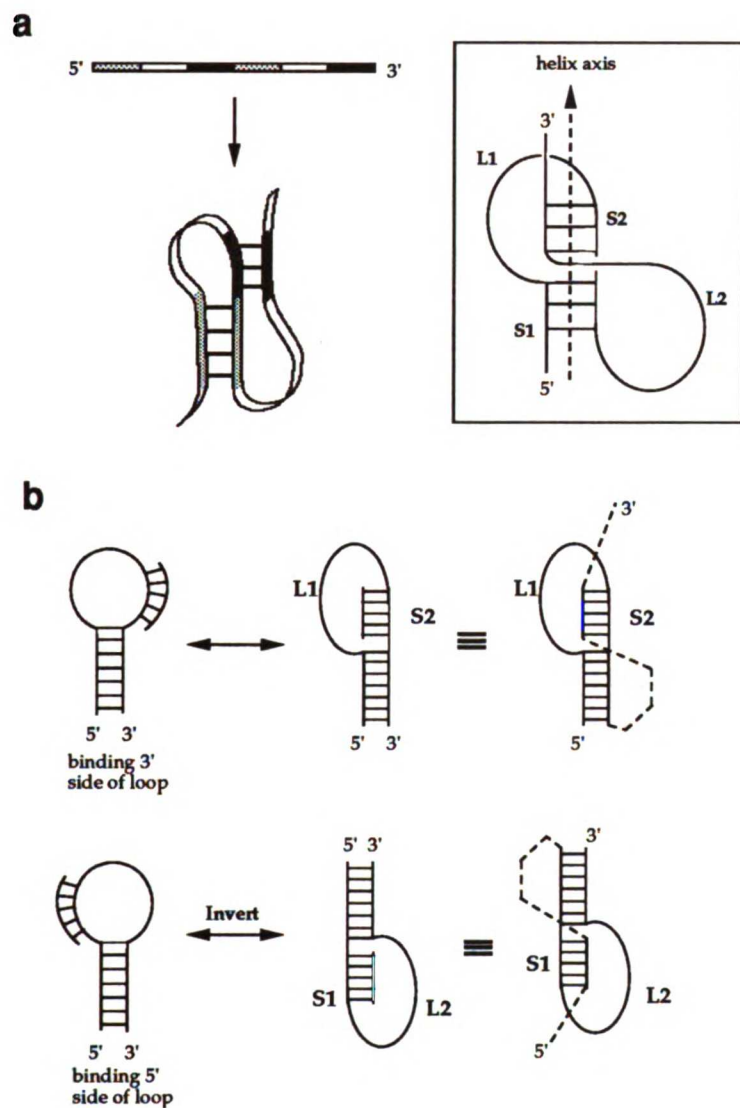


Figure 1-5: Summary of Uhlenbeck's data (1971) for the binding of various tetramers and trimer ASO complementary to tRNA^{tyr}. The binding sites for each of the oligonucleotides which bound the tRNA are denoted by bold lines; the apparent affinity constants for each are also shown. Note that no binding was observed in any strong helical region, or in loop IV; while partial binding was observed in loops I, II (the anticodon arm), and loop III. The binding of tetramers to loops I and II is asymmetric, as binding was not observed on the 3' sides of these loops. Note also that the stem in loop III affords ASO binding, as it apparently is destabilized by the 3 nucleotide hairpin loop.

ing upon the flexibility and conformation of the targeted loop. At best, the binding will be comparable to that of a single-stranded complement; at worst, the binding may be reduced significantly due to inflexibility of the loop structure. Second, subsequences in an ASO may display measurable binding, affording hybridization with single-stranded regions of the molecule. Third, ASO may successfully bind targets in helical regions, provided these helices are about as stable or weaker than potential oligomer-RNA helices. Similar conclusions can be drawn from the results of a more recent study (Kumazawa *et al.*, 1992). Lastly, oligomer binding can produce local structure changes but most likely will not alter global RNA structure. This suggests that ASO binding with intent to induce conformational changes that alter the function of the RNA is best achieved by binding at or very near the structure element to be disrupted.

I.4.2b Topology of ASO binding. Pseudoknots are stable RNA tertiary structures formed by base-pairing interactions between two hairpin loops (Pleij *et al.*, 1985) resulting in a structure containing two distinct loops, termed L1 and L2, and two helices stacked coaxially (Figure 1-6a). Binding of ASO to the 5' or 3' sides of a hairpin loop produces structures topologically equivalent to half of a pseudoknot, termed pseudo half-knots (Figure 1-6b; Ecker *et al.*, 1992).

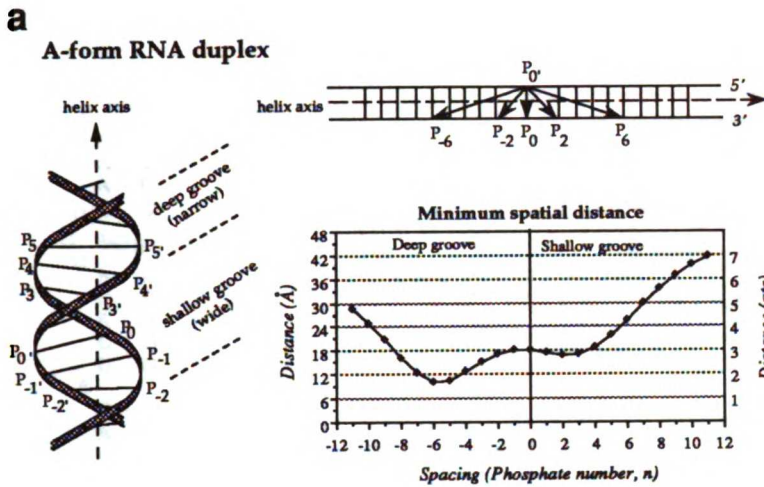
The formation of pseudo half-knots will be limited by topological constraints similar to those which restrict pseudoknot formation, namely the requirement that loop L1 and/or L2 be of a minimal size to permit pseudoknot formation (Wyatt *et al.* 1990; Pleij *et al.*, 1985). Using the spatial distances supplied by the crystallographic coordinates of the A form RNA-RNA double helix (Arnott *et al.*, 1972), the relationship between length of the coaxial stems and minimum loop closure distance for pseudoknot formation can be calculated from simple geometric distance formulas (Pleij *et al.*, 1985). This function is plotted in Figure 1-7a. Figure 1-7b relates the minimum loop closure distances



(After Ecker *et al.*, 1992)

Figure 1-6: RNA pseudoknots and pseudo half-knots. a) Representations of a pseudoknot as nested complementary regions along a linear RNA sequence, and simple secondary structural interaction of two hairpin loops. The numbering of the participating loops and stems in the pseudoknot as shown within the box. b) Schematic representation of how binding of an oligonucleotide to a hairpin loop may produce structures whose topology is similar to that of a pseudoknot. Binding of an ASO to the 3' side of the loop produces a structure equivalent to the L1 loop and S2 stem found in a pseudoknot; binding of the ASO to the 5' side of the loop produces a structure equivalent to the L2 loop and S1 stem. These structures have been termed pseudo half-knots (Ecker *et al.*, 1992) and illustrate the binding of an ASO to a "single-stranded" region may actually involve topological considerations beyond simple duplex formation. Note that the dashed lines correspond to the "missing" portions of the full pseudoknot.

calculated for pseudoknot formation to the loop closure distances (and the number of nucleotides) required for pseudo half-knot formation. The minimum distance requirements computed in Figure 1-7 may also aid in free energy computations designed to predict the binding affinity of ASO (see Discussion



(After Pleij *et al.*, 1985)

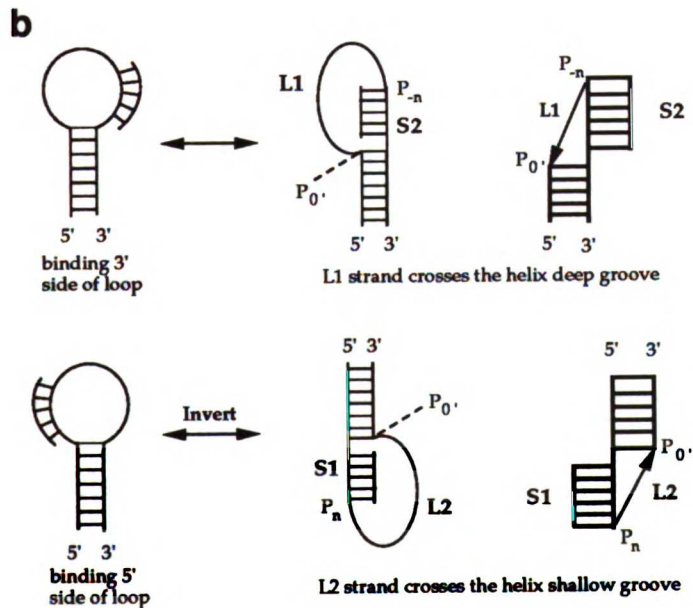
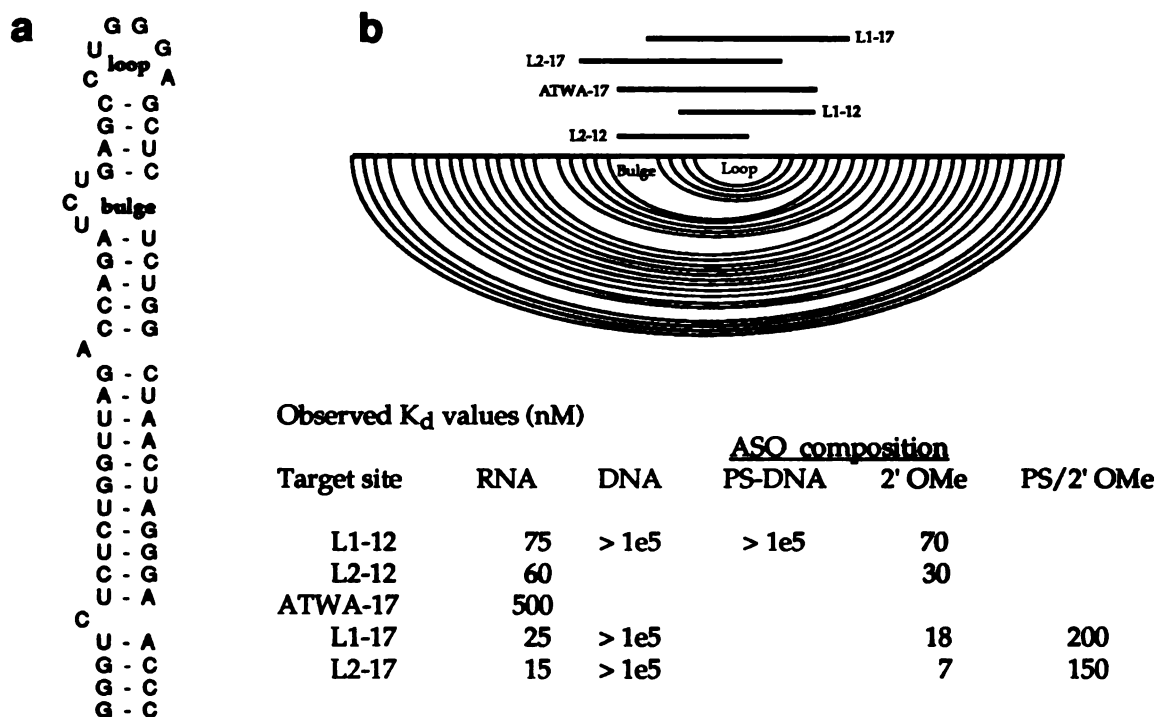


Figure 1-7 Minimum spatial distance between two phosphate residues in the A-form RNA-RNA double helix. a) The minimum spatial distance between two phosphate atoms (P_0') and (P_n) was computed from simple distance formulas based upon the crystallographic coordinates of the A-form RNA double helix (Arnott *et al.*, 1972). The shortest distance between the two phosphates located on complementary base paired residues (P_0 and P_0') is approximately 17Å (due to the tilt of the base pairs), while distances required to span the deep or shallow grooves of the RNA double helix depend upon the polarity and periodicity of the double helix. The horizontal grid in the graph represents the average nucleotide monomer length in a single-stranded RNA polymer (~6.1Å; Olson, 1975), and indicates the number of nucleotides required to span the computed distances. **b)** Application of the computed distances to pseudoknot loop closure. Formation of a pseudo half-knot by ASO binding requires the loops (L1 or L2) to be of minimum length in order to allow ASO binding. The length requirement may or may not require reorganization of the original hairpin loop.

section of Appendix 4).

The distances computed in Figure 1-7 assume the coaxial stacking of pseudoknot or pseudo half-knot stems will maintain the A-form of the RNA

Figure 1-8: Summary of the results of Ecker *et al.*, 1992 concerning binding of ASO to TAR



a) Structure of model TAR RNA hairpin as confirmed by enzymatic mapping. **b)** CIRCLES representation of TAR hairpin and ASO binding sites. Circular lines connect base-paired nucleotides in the TAR hairpin. The tabular data summarizes the binding properties of various ASO to the structured TAR hairpin. RNA indicates oligoribonucleotides; DNA, phosphodiester oligodeoxyribonucleotides; PS-DNA, phosphorothioate oligodeoxyribonucleotides; 2' OMe- 2'O-methyl RNA analogs; PS/2' OMe, 2'O-methyl RNA analogs with phosphorothioate substituted backbones

double helix. Therefore the free energy of ASO binding to form a pseudo half-knot structure is equal to the free energy of the ASO-mRNA duplex. In contrast, ASO targeted to bind the entire loop region of a hairpin cannot form pseudo half-knots and consequently will require some disruption of the hairpin stem with a corresponding thermodynamic "cost". This topological consideration explains the results of Ecker and colleagues (1992), in which the ASO targeted to either side of the TAR hairpin loop displayed stronger binding affinities than did the ASO intended to bind the loop completely (Figure 1-8). Enzymatic

mapping of the ASO-TAR RNA complexes provided confirmation of pseudo half-knot formation for four of the ASO, and also revealed that the ASO intended to bind the entire loop (ATWA-17) actually bound as a mixed population of pseudo half-knotted structures.

I.4.2c RNA structure and hybridization kinetics. RNA structure will also affect hybridization kinetics. Lima and coworkers (1992) analyzed the binding of six decamer oligoribonucleotides to a model hairpin loop derived from the c-Ha-*ras* RNA sequence. They observed "asymmetric" binding of various loop-targeted ASO (i.e. binding affinities varied according to the region of the loop targeted). The asymmetry was much more pronounced than what would be expected simply by target sequence differences ($> 10^6$ fold difference in the apparent affinity constants versus a 5-fold difference in expected affinity constant simply from ASO sequence), and was attributed to a defined single-stranded loop structure unexpected from simple secondary structure models. The structure inherent to the loop resulted in large differences in association rates for the ASO; hence RNA structure can place kinetic limitations upon ASO binding.

I.5 RATIONALE FOR RESEARCH

Simplicity of drug design is the greatest intellectual appeal of ASO compounds; one takes a known RNA sequence and synthesizes the corresponding antisense macromolecules. However, each of the four obstacles to ASO activity discussed above complicate the process of obtaining a useful therapeutic. Furthermore, the foregoing analysis of ASO affinity and selectivity suggests that the efficacy of ASO will be strongly dependent upon the ASO sequence selected. This makes it important to understand the relationship of

ASO sequence and affinity with ASO effect. The thermodynamic basis for the relationship of oligonucleotide affinity to oligonucleotide sequence and base composition has been explored in some detail (Freier *et al.*, 1986; Yager and von Hippel, 1991), affording reasonable estimation of the thermodynamics of duplex formation for two unstructured oligonucleotides. But RNA structure will strongly effect the kinetics and thermodynamics of ASO binding. Although many cases of ASO-mediated inhibition of gene expression appear in the literature, only a handful of reports have directly addressed the relationships between ASO sequence selection, RNA structure, and ASO affinity. It is the purpose of this work to investigate how well predictions of RNA structure can be used in the *a priori* design of ASO, and to develop methods which allow prescreening of the binding behavior of ASO *in vitro* as a tool to restricting the empirical testing of ASO sequences for biological effect.

I.6 GENERAL STRATEGY OF THESIS RESEARCH, ORGANIZATION OF THE DISSERTATION

The strategy of the research was to first develop thermodynamic-based indices of ASO binding behavior (and therefore presumably ASO efficacy) which incorporate considerations of RNA structure. The predictive ability of these indices was then tested by retrospective analysis of published reports of biologically active ASO (Chapter 2) and by a retrospective analysis of the binding behavior of ASO targeted to a model hairpin loop (Appendix 4). It was found that unless RNA secondary structure at the target site is known, the thermodynamic predictions were limited due to the uncertainties associated with the computer predicted RNA foldings.

Experimental techniques were developed for directly measuring the apparent affinity of ASO (12 to 20-mers) for a 1400 nucleotide murine tumor

necrosis factor- α RNA target (Chapter 4). These techniques were applied to screen a panel of ASO targeted to the firefly luciferase reporter gene, both for nanomolar binding affinities and for inhibitory properties in cell-free translation systems (Chapter 5). It was found that an *in vitro* binding assay could be used to screen for ASO which bound with apparent $K_d \sim 5$ nM. ASO sequences which bound with apparent $K_d \sim 5$ nM strongly inhibited luciferase expression in an *in vitro* translation assay, suggesting these ASO possess the potential for inhibiting luciferase expression in cells and *in vivo*..

I.7 LIST OF PUBLICATIONS RESULTING FROM THIS RESEARCH

1. Stull, R. A., Taylor, L. A., and Szoka, F. C., Jr. (1992). Predicting antisense oligonucleotide inhibitory efficacy: A computational approach using histograms and thermodynamic indices. *Nucleic Acids Res.* 20:3501-3508.

2. Stull, R. A., Zon, G., and Szoka, F. C., Jr. (1993). Single-stranded phosphodiester and phosphorothioate oligonucleotides bind actinomycin D and interfere with TNF-induced lysis in the L929 cytotoxicity assay. *Antisense Res Devel* 3:295-300.

3. Stull, R. A. and Szoka, F. C., Jr. (1995). Antigene, ribozyme and aptamer nucleic acid drugs: progress and prospects. *Pharmaceut. Res.* 12:1-19.

4. Stull R. A., Leamon, C. P., Hendren, R. W., and Szoka, F. C., Jr. (1995). Luciferase message walk (I): Screening for nanomolar antisense oligonucleotide binders by a gel-shift technique. *Manuscript in preparation.*

5. Leamon, C. P., Stull, R. A., Szoka, F. C., Jr., and Hendren, R. A. (1995). Luciferase message walk (II): Evaluation of antisense oligonucleotide efficacy in cell-free and cellular assays. *Manuscript in preparation.*

CHAPTER TWO: Predicting Antisense Oligonucleotide Inhibitory Efficacy: A Computational Approach Using Histograms and Thermodynamic Indices

IL1 ABSTRACT

Antisense oligonucleotides (ASO) are designed to bind to a specific mRNA and selectively suppress its translation. To facilitate selection of optimal ASO targets, we have developed three thermodynamic indices to evaluate putative structural complexes important in ASO action. These indices are: a duplex score (Dscore), which estimates the $\Delta G^{\circ}_{formation}$ of the ASO:mRNA target sequence duplex; a secondary structure score (Sscore), which estimates the strength of predicted local mRNA secondary structures at the ASO target site; and a competition score (Cscore), which is the difference between the Dscore and the Sscore. We also present three histograms to display graphically comparisons between different regions of the mRNA. In these histograms, the index value is positioned above the first nucleotide in a sliding window over which the index is computed.

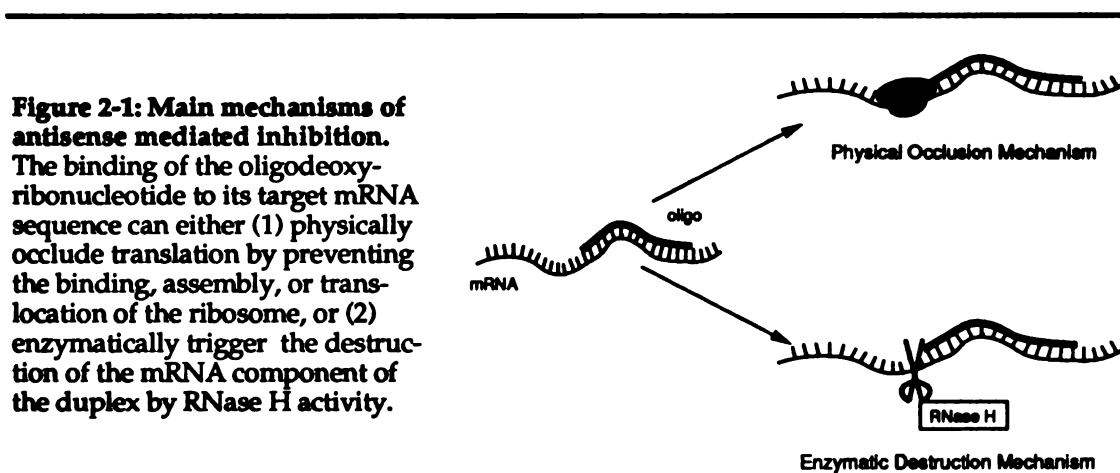
The indices are compared to the inhibition reported in five studies of ASO-mediated suppression of gene expression. The Dscore is the most consistent predictor of ASO efficacy in four of the five studies (r^2 from 0.44 to 0.99), while the results of the fifth study could not be predicted by any thermodynamic or physical index. Thus the Dscores and their histogram may prove useful in selection of ASO targets.

II.2 INTRODUCTION

II.2.1 Rationale for experiments

One obstacle to applying ASO for therapeutic purposes is selection of the most effective target sequences from the many available on a given mRNA. For example, a 1500 nucleotide mRNA sequence affords 1486 potentially different 15-mer ASO target sites. Many experiments have shown that certain ASO are more effective than others in suppressing gene expression. A rational method for determining those ASO sequences most likely to produce strong inhibition of gene expression would streamline the empirical approaches currently used to select ASO.

The efficacy of sequence specific inhibition by an ASO will depend, in part, upon its mechanism of action (Figure 2-1). These mechanisms include blocking ribosomal binding to and translocation along the mRNA, blocking the binding of regulatory proteins to the mRNA, and providing a double stranded heteroduplex substrate for RNase H enzymatic activity. In each mechanism, the oligomer must hybridize with the mRNA in order to effect inhibition. We therefore hypothesized that ASO efficacy is primarily related to the ability of the oligomer to hybridize with its mRNA target sequence,



and that analysis of factors influencing ASO hybridization would allow prediction of ASO efficacy.

Binding of the ASO to its mRNA target is a competitive process (Figure 2-2); at its binding site, the ASO competes with proteins or ribosomal binding (external competition) and with mRNA secondary structure (internal competition). A reasonable first approach to predicting the hybridization capacity and hence the efficacy of an ASO involves computations of the thermodynamic stability of each of the complexes formed by the competing processes. The binding energies for each of the many proteins and ribosomal structures that interact with the RNA are not currently known. Therefore, there is not much information available to evaluate the external competitive factors in ASO-mRNA interactions. However, the internal competition can be analyzed using computer algo-

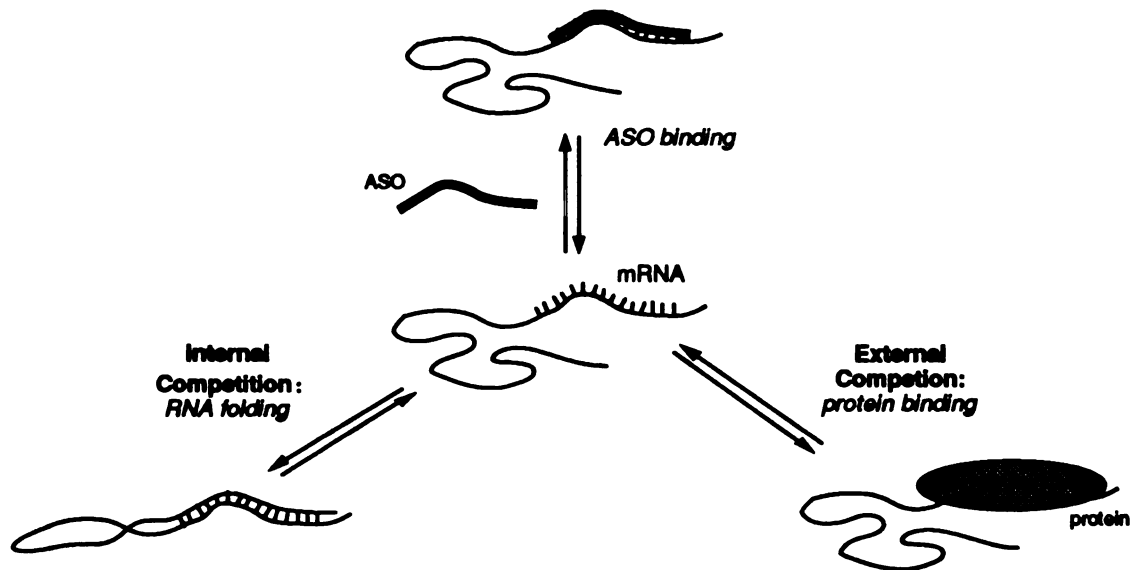


Figure 2-2: Processes which may compete with ASO binding to its target site on the mRNA. The target site of the ASO may also be a site of protein binding (external competition) or the target site may participate in RNA secondary structure formation (internal competition).

rithms that estimate the thermodynamics of mRNA secondary structure (for review, see Zuker, 1989b). By extension, these algorithms also afford analysis of ASO:mRNA duplex formation.

II.2.2 General overview of folding algorithms

II.2.2a RNA secondary and tertiary structure prediction. A major tenet of molecular biology is that functional properties of a macromolecule are intimately related to the structure of that macromolecule. Two outstanding paradigms for this tenet are the duplex structure of DNA (Watson and Crick, 1952) and the three dimensional shape of tRNA (Suddath *et al.*, 1974; Robertus *et al.*, 1974). Prediction of RNA tertiary structure is major goal of molecular biology, but the relationship between primary sequence and tertiary structure is currently not well understood. A reasonable starting point has therefore been to attempt predictions of RNA secondary structure, since it is thought that secondary structure interactions are the major contributor to the total free energy of RNA structure formation (Wyatt *et al.*, 1990).

II.2.2b RNA folding algorithms. Nearly all algorithms that predict RNA secondary structure subscribe to two fundamental hypotheses (Tinoco *et al.*, 1973; Tinoco *et al.*, 1971). First, a given RNA in solution is hypothesized to fold in such a fashion as to minimize the free-energy of the solution. Second, the free energies of all RNA secondary substructures (*i. e.* helices, loops, hairpins) are considered additive. Generally, folding algorithms also assume a nearest-neighbor model for interaction energies (Borer *et al.*, 1974). This model states the major contributions to secondary structure energetics are base-pairing and stacking energies between a given base-pair and its immediate, adjacent nucleotide neighbors. It is considered a

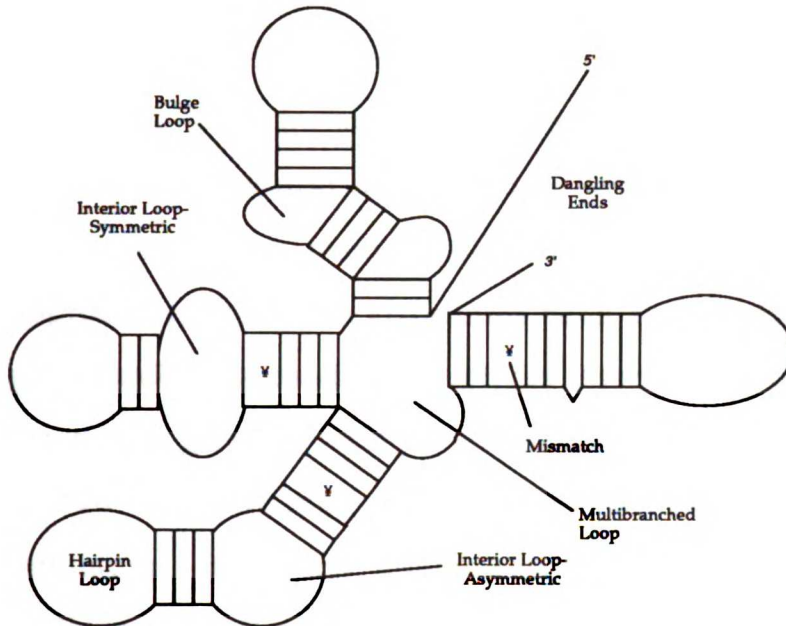


Figure 2-3: Features of RNA secondary structure. A single-stranded RNA molecule is capable of folding back upon itself to form helical structures containing standard Watson-Crick base-pairs as well as guanine-uridine base-pairs. The result is structure containing a variety of helices, stems, loops, bulges, and even mismatches.

reasonable approximation since base-stacking and base-pairing interactions are short range interactions.

II.2.2c Thermodynamics of RNA-RNA interactions. With the above hypotheses and model as guides, computation of $\Delta G^{\circ}_{formation}$ for RNA global secondary structure is straightforward provided the $\Delta G^{\circ}_{formation}$ for various RNA secondary structure motifs are known. Values for the $\Delta G^{\circ}_{formation}$ of base-pair stacking, formation of dangling ends and penalties for base-mismatches have been derived from melting curves obtained from short RNA duplexes (Table 2-1; Freier *et al.*, 1986; Salser, 1977). Loop-destabilization energies have some empirical basis, but have been derived mainly from theoretical considerations (Jacobson and Stockmeyer, 1950; Jaeger *et al.*, 1989). Consequently, in the absence of phylogenetic data or experimentally deduced structural information, one can fold a known mRNA sequence using only thermodynamic principles. However, most

algorithms make provisions to accommodate information derived from RNA structural mapping studies or from phylogeny in an attempt to increase confidence in the predicted foldings.

Due to an incomplete understanding of all the factors driving RNA folding, and because many phylogenetically or experimentally elucidated structures differ from those predicted by simple minimum energy approaches, prediction algorithms have been designed to generate multiple global mRNA secondary structures (Martinez, 1988; Zuker, 1989a). These algorithms generate multiple structures on the possibility that the functional mRNA molecule may not fold into its absolute equilibrium free-energy minimum. It is fairly intuitive that similar sequences may have optimal foldings of similar free energies, but it is less intuitive, yet quite true, that foldings of similar energies may differ widely in their structure.

In this chapter, two histograms are developed which conveniently summarize the output from RNA folding algorithms. Three indices are also described to predict the efficacy of an ASO in suppressing gene expression (Figure 2-4). The first index (S[tructure]score) is based upon the predicted secondary structure of the mRNA target region, and is dependent upon the RNA folding program used to predict RNA secondary structure. The second index (D[uplex]score) is based upon the duplex formation energy of the ASO and the mRNA target region, and is calculated from the thermodynamic values listed in Table 2-1. The third index (C[ompetition]score) combines secondary structure predictions and the duplex formation energy. The usefulness of these indices was tested by comparing the predicted efficacy of the ASO to the results obtained in five published studies of ASO-mediated inhibition of gene expression (Maher and Dolnick, 1987; Goodchild *et al.*, 1988; Cazenave *et al.*, 1987; Bacon and Wickstrom, 1991; Chiang *et al.*, 1991).

TABLE 2-1: Thermodynamic values used by fold algorithms and DSCORES

I. Nearest Neighbor Stacking Energies for Base Pair Doubles
 ΔG° (kcal/mol) in 1M NaCl, 37°C (from Freier *et al.*, 1986)

		3' Base Pair					
		AU	UA	CG	GC	GU	UG
5' B a s e P a i r	A U	-0.9	-0.9	-2.1	-1.7	-0.5	-0.7
	U A	-1.1	-0.9	-2.3	-1.8	-0.7	-0.5
	C G	-1.8	-1.7	-2.9	-2.0	-1.5	-1.5
	G C	-2.3	-2.1	-3.4	-2.9	-1.3	-1.9
	G U	-0.5	-0.7	-1.9	-1.5	-0.5	-0.5
	U G	-0.7	-0.5	-1.3	-1.5	-0.6	-0.5

II. Loop destabilization energies
 ΔG° (kcal/mol) in 1M NaCl, 37°C (from Jaeger *et al.*, 1989)

Size (n)	Internal	Bulge	Hairpin
1	-	+3.9	-
2	+4.1	+3.1	-
3	+4.5	+3.5	+4.5
4	+4.9	+4.2	+5.5
5	+5.3	+4.8	+4.9
6	+5.7	+5.0	+5.1
7	+5.9	+5.2	+5.2
8	+6.0	+5.3	+5.5

Extrapolations beyond $n = 8$:

$$\Delta G^\circ(n) = \Delta G^\circ(n_{\max}) + 1.75 RT \ln\left(\frac{n}{n_{\max}}\right)$$

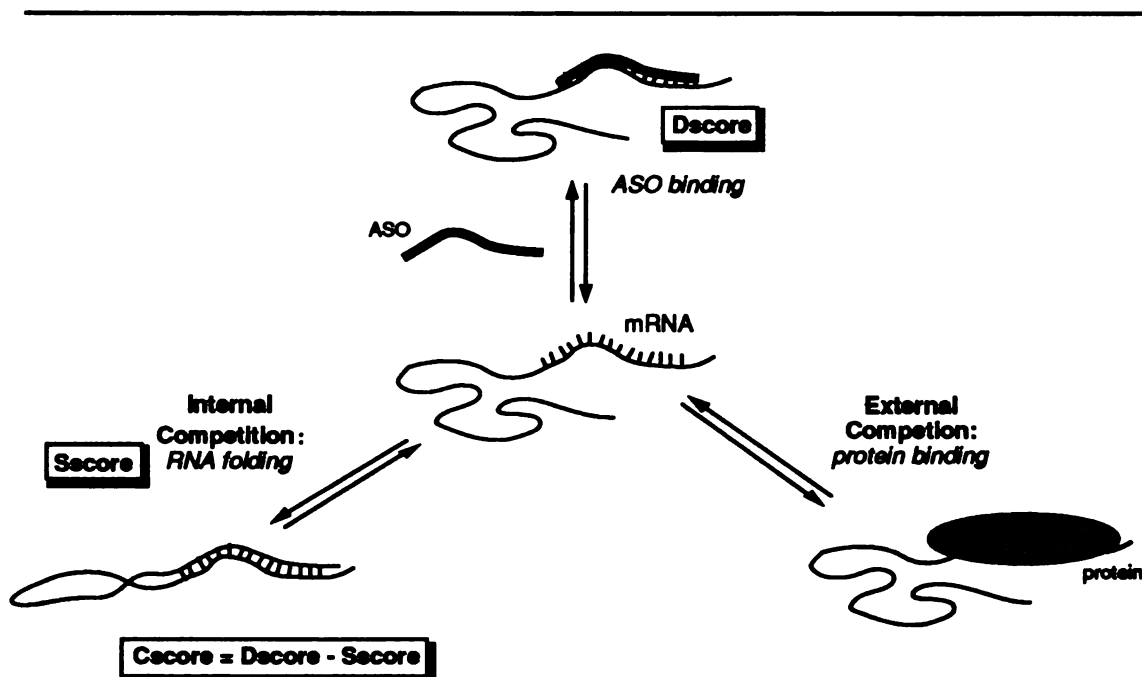


Figure 2-4: Thermodynamic indices used to evaluate competitive processes at the ASO target site. A *Dscore* is the thermodynamic index developed to evaluate the free energy of formation of the ASO:mRNA duplex. The thermodynamics of secondary structure formation at the ASO target site is assessed by means of the *Sscore*. A *Cscore* represents the competition, on a thermodynamic level, between ASO:mRNA duplex formation and possible secondary structures formed at the ASO target site.

Of these three indices, the *Dscores* most consistently possess a statistically significant correlation with inhibition in published results.

II.3 METHODS AND ALGORITHMS

II.3.1 Folding Algorithms

The MONTE CARLO mRNA folding algorithm has been described previously (Martinez, 1984; Martinez, 1988). Briefly, this algorithm hypothesizes a folding pathway in which RNA helical regions (stems) with the largest free energies form first. A pool of additional stems that are compatible with the existing structure is next generated. One stem from this pool is then selected based upon a weighted probability function, where the

stem with the largest equilibrium constant of formation (*i. e.* largest free-energy of formation) is the stem most likely to be selected. Thus, the algorithm mimics a folding pathway governed by thermodynamic laws and kinetic assumptions, but allows for some variation in predicted structures due to the probability function. It should be noted that MONTE CARLO generally does not produce RNA structures with the equilibrium global minimum free-energy for the given RNA sequence. Instead, the overall strategy is to fold a given sequence numerous times and thereby obtain a population of predicted RNA structures. All MONTE CARLO folding sets were composed of ten foldings of the particular RNA sequence being examined.

Other folding algorithms were also employed to determine their effect upon the structure based (Sscore, Cscore) indices. DYNPRO, the Martinez implementation of the Zuker optimal folding algorithm (Martinez, 1988; Zuker and Stiegler, 1981) was used to fold smaller RNA subsequences. DYNPRO first generates an energy matrix of all possible local secondary structures for a given sequence, then traces back through the matrix to assemble a single structure with the equilibrium global minimum free-energy for the given RNA sequence.

The free-energy values (ΔG°) used by MONTE CARLO and DYNPRO have been updated to those determined at 37°C, in 1M NaCl (Table 2-1, from Freier *et al.*, 1986; Jaeger, *et al.*, 1989). In addition, the equation employed by Jaeger and coworkers for extrapolating the length dependence of loop destabilization energies (Table 2-1) has been included in the calculations. However, neither their calculations for terminal unpaired nucleotides and mismatches, nor their bonus energies for stable "tetraloop" sequences, nor their linear approximation for multibranched loops have been included. G-

U pairing is the only non-Watson-Crick base pairing accommodated by these algorithms. Due to hardware limitations, sequences folded by MONTE CARLO were generally less than 3300 nucleotides, while sequences folded by DYNPRO were less than 800 nucleotides.

LRNA, an implementation of the Zuker suboptimal folding algorithm (Zuker, 1989a), was also used to generate several predicted RNA structures at or near the equilibrium global minimum free-energy for the given RNA sequence. An added feature of the LRNA program is the capacity to fold a RNA sequence constraining specified nucleotides to remain single-stranded. This feature was used to calculate DifScores (see below). LRNA incorporates the free-energy values determined at 37°C, and all aspects of the Jaeger loop model and bonus energies mentioned previously. Again, due to hardware limitations, sequences folded by LRNA were less than or equal to 600 nucleotides.

II.3.2 Histograms

To facilitate interpretation of the multiple structures generated by MONTE CARLO, we chose to summarize these folding sets in various histograms. In general, sequence information is plotted along the abscissa of the histogram, while numerical scores are plotted along the ordinate. Three types of histograms were generated. The first histogram, a stem frequency histogram (Figure 2-5b), displays the incidence of stem membership for a particular nucleotide within the multiple foldings of the folding set. This approach is similar to the P-num and S-num plots described by Jaeger and coworkers (1989).

In the stem frequency histogram, stem membership for a particular nucleotide is the result of either base-pairing or participation in an interior

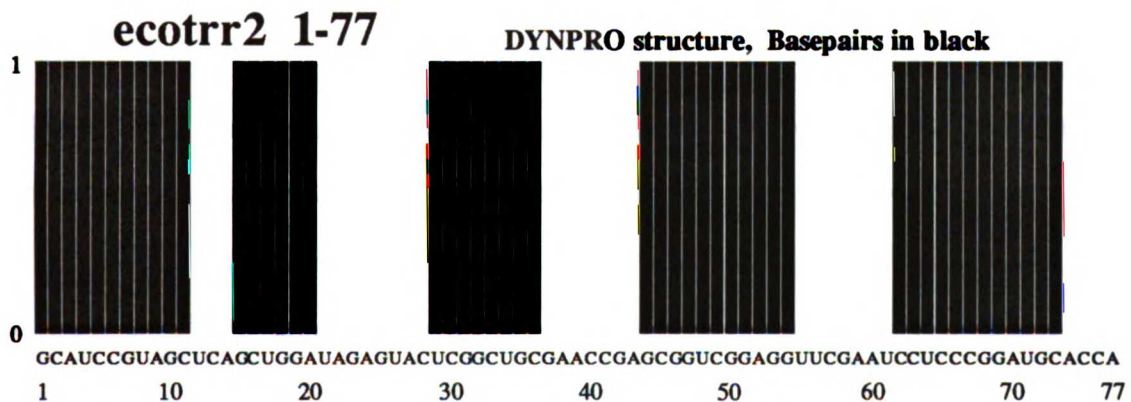
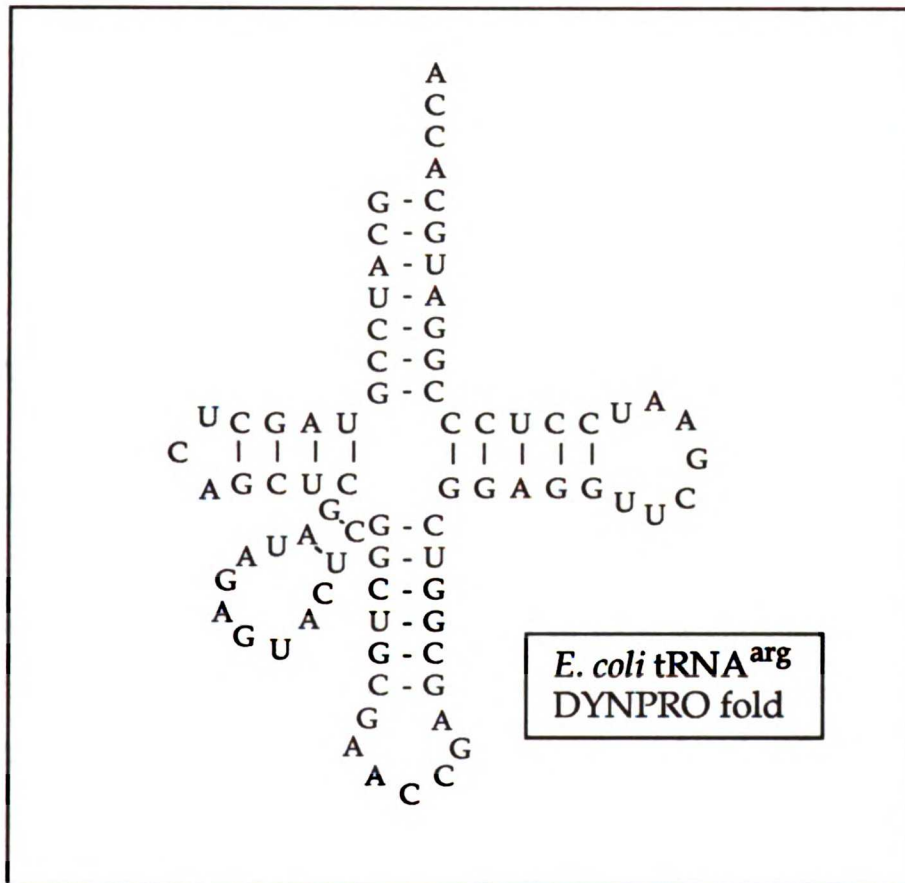


Figure 2-5: Predicted tRNA structure and stem-frequency histogram representation of predicted structure. Top panel) DYNPRO supplied predicted structure for *E. coli* tRNA^{arg} sequence, with aspects of secondary structure noted. Bottom panel) Stem frequency histogram representation of predicted structure shown in the top panel. Note that DYNPRO supplies a single predicted structure, hence the maximum histogram value is 1.

or bulge loop. Black shading on the histogram represents the base-paired case; gray shading, the bulge loop or interior loop case. Nucleotides predicted to exist outside of stems (*i. e.* within hairpin or bifurcation loops) have no shading.

II.3.3 Energy Scaled Histograms

A disadvantage of the stem frequency histogram is its all-or-nothing scoring. It ignores the relative strength of the local secondary structure in which the nucleotide appears and the overall stability of the global structure of which the local structure is a part. Therefore, we devised a second histogram in which the relative stabilities of local secondary structures are redistributed among nucleotides participating in the local structure.

According to the principle of additivity, the free-energy of stem formation, ΔG_{stem} , is defined by

$$\Delta G_{stem} = \Sigma \Delta G_{helical\ regions} + \Sigma \Delta G_{bulges} + \Delta G_{hairpin\ loop} \quad (2-1)$$

This energy can be redistributed equally among the base-paired nucleotides (helical regions) by defining an energy redistribution function, E_3 , as:

$$E_3 = \Delta G_{stem} / B \quad (2-2)$$

where the free-energy of stem formation is divided by the number of *base-paired* nucleotides, B , appearing in the helical regions. The resulting E_3 value is then assigned (as an $E_{3,N}$ score) to each nucleotide in the stem that is base-paired. All base-paired nucleotides in the same stem receive equal $E_{3,N}$

values, while those nucleotides appearing in hairpin, bulge, bifurcation or interior loops receive $E_{3,N}$ scores equal to zero.

The MONTE CARLO algorithm generates a folding set of n foldings for a given mRNA sequence; hence each nucleotide will receive n $E_{3,N}$ scores. These $E_{3,N}$ scores are weighted to produce $WE_{3,N}$ scores by the function

$$\overline{WE_{3,N}} = \frac{\sum_{i=1}^n (E_{3,N_i}) e^{-\left(\frac{\Delta G_{global,i} - \Delta G_{global,min}}{RT}\right)}}{n} \quad (2-3)$$

The exponential term is a Boltzmann factor designed to weight the $E_{3,N}$ scores from a given global mRNA folding, i , relative to the other n global foldings in the folding set. $\Delta G_{global,i}$ is the free-energy of formation for the global mRNA structure produced by folding i , while $\Delta G_{global,min}$ is the free-energy of formation for the most stable global mRNA structure in the folding set. The weighted scores are summed and then normalized by dividing by n , to produce a single, energy-weighted, composite global mRNA structure. The result of these computations is to attach structural energies to individual nucleotides (equation 2-2), and to weight these energies according to the strength of the local structure and the stability of the global structure of which the local structure is a part (equation 2-3).

An energy scaled histogram (Figure 2-6a) is generated when the normalized $WE_{3,N}$ scores are plotted versus the sequence of the mRNA.

II.3.4 EWINDOW program, window-score histograms.

A windowing program, EWINDOW, is used to calculate a duplex

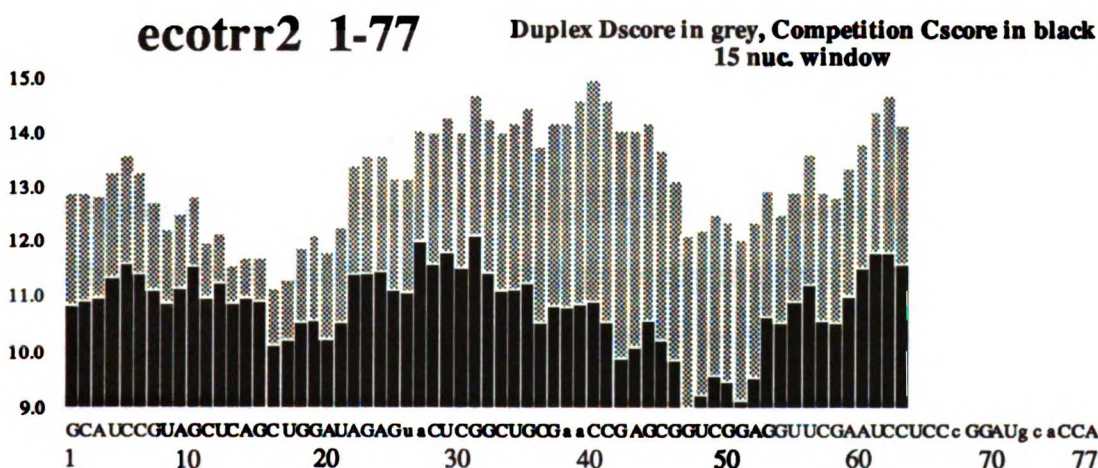
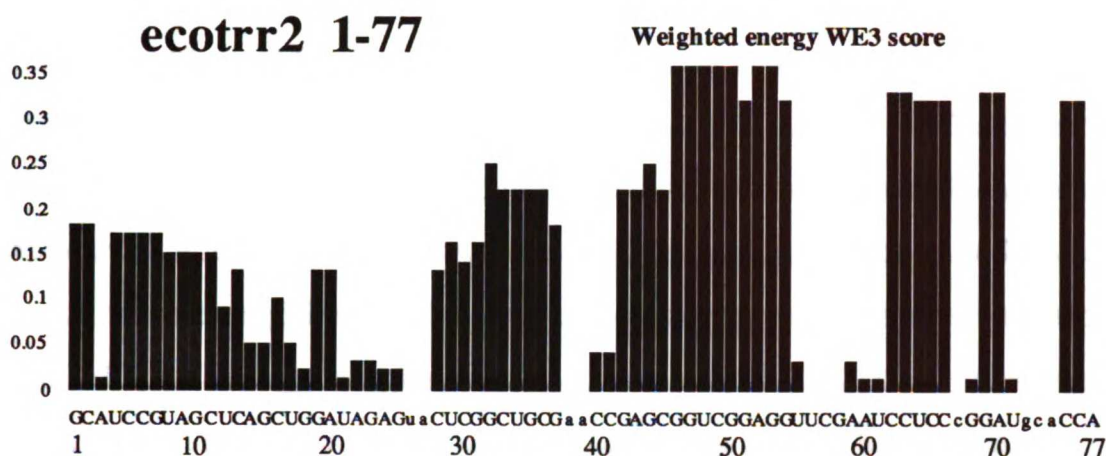


Figure 2-6: Alternate histogram representations of RNA secondary structures. Top panel) Energy scaled histogram. Base-paired nucleotides are assigned energy scores based upon the distribution functions described in the text. The histogram was produced by GENHISTO using data supplied by the MONTE CARLO algorithm for *E. coli* tRNA^{arg} sequence depicted in Figure 2-5. **Bottom panel) Windowing histogram.** This histogram displays the Dscore and Cscore for each window of m nucleotides across the RNA sequence. The Score can likewise be deduced from the histogram. In this figure, $m = 15$. The scores for each window are attached to the first nucleotide appearing in the window, and the sequence appearing in the window can be deduced by reading the next $m-1$ nucleotides downstream. For example, the last bar on the right represents the indices for the sequence CUCCCGGAUGCACCA. Dscores, Cscores and Scores were computed by EWINDO using source files produced by the MONTE CARLO folding algorithm. The histogram was generated by GENHISTO using output files produced by EWINDO.

formation score (Dscore), a competition score (Cscore), and a secondary structure score (Sscore) for each window of length m across the mRNA sequence.

The Dscore is based upon the $\Delta G^\circ_{duplex\ formation}$ of a perfectly matched duplex between an RNA oligomer of length m and the mRNA sequence appearing within the window. The $\Delta G^\circ_{duplex\ formation}$ is computed using the same nearest neighbor model thermodynamic parameters used to calculate the mRNA folding energies, and includes a helix initiation penalty of 3.4 kcal/mole (Freier *et al.*, 1986). $\Delta G^\circ_{duplex\ formation}$ is related to the Dscore by

$$Dscore = \frac{\Delta G^\circ_{duplex\ formation}}{2} = \frac{\Delta G^\circ_{init} + \Sigma \Delta G^\circ_{stack}}{2} \quad (2-4)$$

This equation is analogous to equation 2-2, and represents the special case of distributing the formation energy of a perfectly matched duplex (no bulges or loops) over all the participating nucleotides and then summing the values for one strand of the duplex (*i. e.* the ASO nucleotides).

The secondary structures found for the mRNA sequence present within a given window can be quantified by a Sscore, which is a summing of the normalized $WE_{3,N}$ scores for each nucleotide within the window. A Cscore can be defined

$$Cscore = Dscore - \sum_{j=1}^m (\overline{WE_{3,N}})_j = Dscore - Sscore \quad (2-5)$$

The Cscore is a rough approximation of the thermodynamics of competition between the formation of an ASO-mRNA duplex and the formation of mRNA secondary structure at the ASO target site.

A window-score histogram is obtained by plotting the Dscore and Cscore for each window across the mRNA sequence (Figure 2-6b). Dscores appear as gray bars, while Cscores appear in black. Both scores for each window are attached to the first nucleotide of the window sequence, so that the complete window sequence can be deduced by reading the next $m-1$ nucleotides downstream. Tabular Cscore data files are also generated for user reference. In addition, a Macintosh compatible version of EWINDOW, called DSCORES, was created. DSCORES analyzes an RNA sequence and computes Dscores for each window. It does not generate Sscores or Cscores, nor does it produce histograms. The complete program and documentation for DSCORES appears in Appendix 2.

II.3.5 Mean Stacking Temperature Calculations.

A mean stacking temperature (MST) score was calculated (Gotoh and Tagashira, 1981; McGraw *et al.*, 1990) and tested as a predictive index. Like the Dscore, the MST score is an sequence based estimator of duplex stability. However, it is computed for DNA:DNA duplex rather than a RNA:RNA duplex.

II.3.6 Statistics.

Correlations between reported experimental inhibition and predicted inhibition using a specific prediction index (*i. e.* Dscore, Cscore, Sscore) were determined by fitting the data using a least-squares method provided by a statistical analysis software package. All results are reported as coefficients of determination (r^2). P values were computed using $t = r \sqrt{(n-2) / \sqrt{(1-r^2)}}$. A correlation was rejected as being statistically insignificant if the P value was greater than 0.05.

II.3.7 Inhibition Studies Analyzed and Sequences Examined.

We examined five studies of ASO-mediated suppression of gene expression. The four genes targeted in these five studies were: (1) human dihydrofolate reductase (DHFR; Maher and Dolnick, 1987); (2) rabbit β -globin (Goodchild *et al.*, 1988; Cazenave *et al.*, 1987); (3) human *c-myc* (Bacon and Wickstrom, 1991); (4) and human intracellular adhesion molecule-1 (ICAM-1; Chiang *et al.*, 1991; C. F. Bennett, personal communication). The GenBank™ data base (Bilofsky and Burks, 1988) supplied the human genomic dihydrofolate reductase sequence (accession number X00855; Yang *et al.*, 1984; Chen *et al.*, 1984), the rabbit genomic β -globin sequence (J00659; Baralle, 1977; Efstratiadis *et al.*, 1977; Proudfoot, 1977), the human genomic *c-myc* sequence (J00120; Colby *et al.*, 1983; Gazin *et al.*, 1984), and the human ICAM-1 cDNA sequence (M24283; Tomassini *et al.* ,1989; Degitz *et al.*,1991). Each sequence was trimmed to account for mRNA transcript cap sites when known; genomic DNA sequences were also converted into cDNA sequences by removal of intron sequences.

II.4 RESULTS AND DISCUSSION

II.4.1 General approach of experiments

To test if the thermodynamic indices developed above are useful predictors of ASO efficacy, we examined published studies of ASO-mediated inhibition of gene expression and compared the computed indices to the reported inhibition achieved with different ASO. We analyzed studies carried out both in cell-free translation systems and in cultured cells. Cell-free systems afford the simplest analysis of ASO mechanism and effect, since issues of ASO transport and stability are not necessarily involved in ASO efficacy. Analysis of ASO efficacy in cultured cells may be confounded by transport and stability variables, but obviously provides a more realistic application for the indices.

II.4.2 Analysis of ASO action in Cell-free Translation Systems

II.4.2a Rabbit reticulocyte lysates The first study we examined involved the human dihydrofolate reductase (DHFR) gene. In this study by Maher and Dolnick (1987), mRNA isolated from a methotrexate-resistant, DHFR gene-amplified cell line was translated in rabbit reticulocyte lysate in the presence of nine different phosphodiester oligonucleotides (Table 2-2).

Table 2-3 shows that the correlations for the indices based upon duplex formation (Dscore; $r^2 = 0.740$ ($P < 0.005$)) and upon competition between duplex formation and mRNA secondary structure present at the target site (Cscore; $r^2 = 0.808$ ($P < 0.001$)) are both significant. We found no significant correlation between predicted secondary structure (Score) provided by Martinez's MONTE CARLO program and reported inhibition. This was to be expected since the DHFR mRNA in these experiments was first heated to

TABLE 2-2: Antisense phosphodiester oligomers used in cell-free translation systems

Oligo Name	Oligo Length	Oligo Sequence (5' to 3')	Target Site on mRNA	Dscore	Cscore ^a	Inhibition (%)
Human DHFR (Maher and Dolnick, 1987)						
A20	20	GCTCAAAGTTTGGCGGAAAT	5' UTR ^b	-16.35	-14.22	74
B14	14	CTCCGAGCCCGCTC	5' UTR	-14.05	-11.65	40
B16	16	OCTCCGAGCCCGCTCG	5' UTR	-16.50	-13.85	48
B18	18	ACCTCCGAGCCCGCTCGT	5' UTR	-18.60	-15.72	71
B20	20	GACCTCCGAGCCCGCTCGTT	5' UTR	-20.20	-17.16	72
C14	14	AGCAGCGGGAGGAC	5' UTR	-13.85	-12.43	28
C20	20	CATGACAGCAGCCGGAGGAC	start	-19.20	-17.21	80
D11	11	CGGAACCAACC	coding	-8.95	-8.35	75
D20	20	TGCAGTTTAGCGAACCAACC	coding	-16.65	-15.64	23
Rabbit β-globin Goodchild <i>et al.</i> (1988)						
β 1	20	GCAAGTAAACACACAGTTGTGT	5' UTR	-14.85	-11.41	23
β 2	20	CAGATGCACCAATTCTGTCTG	start	-16.30	-12.75	61
β 3	20	GGTAGACAACACAGCAGCCT	coding	-18.90	-14.45	18
β 4	20	TTGTTTATAACAGCAATTGC	coding	-14.00	-9.88	43
β 5	22	CAGTTGTGTCAAAGCAAGTGT	cap	-16.60	-15.63	67
β 6	23	TTTTGGGGATTGCAAGTAAACA	5' UTR	-17.65	-13.86	47
β 7	25	CAGTTGTGTCAAAGCAAGTGTCCC ^c	cap	-16.60	-15.63	75
β 8	48	(β 6 + β 7)	cap	-39.80	-34.20	89
Cazenave <i>et al.</i> (1987)						
17 Glo [3-19]	17	TTGTGTCAAAGCAAGT	cap	-11.85	-11.12	85
17 Glo [51-67]	17	GACAGATGCCACCAATTC	start	-13.65	-10.97	95
11 Glo	11	TTGTGTCTGT	start	-7.10	-4.79	75
17 Glo [113-129]	17	CACCAACTTCTTCCACA	coding	-13.30	-10.60	95

^aFrom foldings using MONTE CARLO

^bUntranslated region.

^cCap nucleotides complementary to the underlined nucleotides

TABLE 2-3: Coefficients of determination (r^2) between predictive indices and reported inhibition in cell-free systems

<u>Index</u>		<u>Human DHFR</u> (Maher and Dolnick, 1987)		<u>Rabbit β-globin</u>	
		All Targets @ 200 μ M (n = 9) ^b	Ribosome Competitors ^a @ 200 μ M (n = 4) ^b	Goodchild study (1988) @ 5.2 μ M (n = 6) ^{b,d}	Cazenave study (1987) @ 6 μ M (n = 4) ^c
duplex	Dscore	0.740 (P < 0.005)	0.962 (P < 0.002)	0.015 (N. S.)	0.933 (P < 0.05)
mRNA 2° structure	Sscore	0.181 (N. S.)	0.573 (N. S.)	0.499 (N. S.)	0.129 (N. S.)
competition	Cscore	0.808 (P < 0.001)	0.948 (P < 0.05)	0.098 (N. S.)	0.710 (N. S.)
	Length	0.943 (P < 0.001)	0.990 (P < 0.01)	0.215 (N. S.)	0.758 (N. S.)

^aThose ASO targets where protein or ribosomal binding occurs (e. g. A20, C20, D11, D20; Table 2-2).

^bPerformed in rabbit reticulocyte cell-free translation system.

^cTranslation performed in wheat germ extracts.

^dStructural analyses do not include cap nucleotides. Therefore the binding sites for $\beta 5$ and $\beta 7$ (Table 2-2) are identical, and the reported inhibition for this target was considered 71% (average of $\beta 5$ and $\beta 7$).

65°C to eliminate secondary structure, and therefore suggests the correlations observed for the Cscores merely reflect the contribution of the Dscore to the Cscore. Using the length as a predictive index of ASO efficacy produces the best correlation with experimental results ($r^2 = 0.943$ ($P < 0.001$)). Weaker but significant correlations were observed between length and reported inhibition for experiments at 100 μ M ($r^2 = 0.403$ ($P < 0.05$)) and 50 μ M ($r^2 = 0.702$ ($P < 0.005$)) oligomer concentration. Dscores, Cscores, and Sscores did not correlate with inhibition at these lower concentrations (data not shown).

Rabbit reticulocyte lysates have variable, but generally very low levels of RNase H activity (Minshull and Hunt, 1986; Walder and Walder, 1988).

This suggests that ASO used in this system act primarily through a RNase H independent (*i. e.* physical occlusion) mechanism. One might expect that ASO targeted to regions of the mRNA at which the ribosomal subunits bind (e.g. within approximately the first fifteen nucleotides downstream of the m⁷G cap (Lawson *et al.*, 1986)) or adjacent to or across the AUG translation initiation codon (Shakin and Liebhaber, 1986)) might therefore be more effective inhibitors of gene expression than ASO targeted elsewhere along the mRNA. A subgroup of ASO in the Maher and Dolnick study can be classified as "ribosome competitors" (e.g. A20, C14, C20, D11, D20). For the ribosome competing ASO, length correlates best with reported inhibition ($r^2 = 0.990$ ($P < 0.01$)). The correlations for the Dscores ($r^2 = 0.962$ ($P < 0.02$)) and Cscores ($r^2 = 0.948$ ($P < 0.05$)) are also excellent.

We also examined the results of ASO-mediated inhibition of translation of rabbit β -globin mRNA in rabbit reticulocyte lysates. These studies by Goodchild and coworkers (1988) used eight different phosphodiester ASO targeted to the globin mRNA. When examining ASO $\beta 1 - \beta 8$ at 5.2 μ M concentration, we found no significant correlations between observed inhibition and any predictive indices (Table 2-3).

The results of the study by Goodchild and colleagues clearly suggest that in rabbit reticulocyte lysates, ASO targeted to the cap site or the start codon work better than those targeted to other regions of the mRNA (Table 2-2). However, when analyzing ASO $\beta 2, \beta 5, \beta 7$ and $\beta 8$, no significant correlations were obtained between inhibition and Dscore, Cscore, Score or length (data not shown).

II.4.2b Wheat Germ Extracts Cazenave and colleagues (1987) used an 11-mer and three 17-mer ASO targeted to rabbit β -globin mRNA in a wheat

germ cell-free translation system (Table 2-2). At 6 μM oligomer concentration, Dscores correlate very well with reported inhibition ($r^2 = 0.933$ ($P < 0.05$); Table 2-3). Wheat germ extracts contain significant amounts of RNase H activity, and RNase H mediated processes are likely to be the major mode by which ASO produce inhibition in this cell-free translation system (Minshull and Hunt, 1986). Any region of the mRNA accessible to the ASO should allow duplex formation, and thereby permit RNase H to degrade the mRNA. More energetically favored duplexes should render the mRNA more sensitive to RNase H, and therefore result in greater inhibitions. The strong correlation between inhibition and Dscores for all targets in the wheat germ system is consistent with RNase H mediated ASO inhibition. For the same ASO experiments, the Cscores, Sscores, and ASO length do not correlate with reported inhibition (Table 2-3).

For experiments with oligomer concentrations below 6 μM , no significant correlations were obtained between reported inhibitions of β -globin translation and any of the predictive indices (data not shown).

II.4.3 Analysis of ASO action in Intact Cells

II.4.3a Predictions for human *c-myc* inhibition in HL-60 cells. Bacon and Wickstrom (1991) selected multiple ASO targets located between the 5' cap site and the tenth codon in the coding sequence of human *c-myc* mRNA (Table 2-4). They tested phosphodiester ASO at 10 μM against these targets when attempting to suppress the *c-myc* gene in cultured HL-60 cells. Since a genomic *c-myc* sequence was available and because ASO presumably may bind to either hnRNA or mRNA within the cells, we folded both unspliced and spliced *c-myc* sequences. All reported inhibition values were adjusted prior to calculating correlation coefficients to account for non-sequence

TABLE 2-4: Antisense phosphodiesterase inhibitors against human *c-myc* in HL-60 cells (Bacon and Wickstrom, 1991)

Oligo Name	Oligo Length	Oligo Sequence	Target Site ^a	Dscore	MONTE CARLO		Inhibition (%) ^b
					Cscore ^a	DYNPRO Cscore ^a	
E ^c	15	CTCGCATTATAAAGG	orf(?) ^{d,e,f}	N D	N D	N D	-258
F	15	GCACAGCTCGGGGT	cap ^e	-15.25	-11.15	-11.31	38
G	15	CCGGCGGTGGCGCC	5' UTR ^{e,h}	-17.05	-11.72	-11.98	35
H	15	GCCCCGAAACCCGGC	5' UTR ^e	-14.50	-12.46	-12.57	16
I	15	CGCCCGGCTCTTCCA	5' UTR	-14.85	-8.91	-9.18	8
J	15	TGGGCCAGAGCCGAA	5' UTR	-14.75	-13.59	-13.64	21
K	15	GTGTTGTAAGTTCCA	5' UTR	-10.55	-9.31	-9.36	11
L	15	GAGGCTGCTGTTTT	splice	-12.50	-7.18	-7.81	23
M	15	GGGGCATCGTCGGG	start	-15.20	-13.60	-13.69	15
N	12	GTTGAGGGGCAT	start	-10.10	-9.98	-9.99	6
O	15	AACGTTGAGGGGCAT	start	-12.60	-12.39	-12.39	17
Q	15	CTCAAGTCGCATGAG	control ^l	N D	N D	N D	(52) ^k
R	18	GCTAACGTTGAGGGGCAT	start	-15.70	-14.32	-14.40	28
S	15	CCTGTTGGTGAAGCT	coding	-12.30	-8.55	-8.72	0

^aSpliced P1 transcript.

^bSpecific inhibition calculated by subtracting out inhibition due to oligomer Q.

^cNot included in correlation data since oligomer was stimulatory.

^dTarget site does not appear in the P1 transcripts.

^eTarget site does not appear in the P2 transcripts.

^fUntranslated region.

^gOligomer was stimulatory.

^hWithin cap-sensitive region (Shakin and Liebhaber, 1986).

ⁱControl oligomer with sequence/composition derived from scrambling oligomer O sequence.

^kFactor referred to in note b.

specific inhibition (e. g. oligomer Q ; Table 2-4). Since oligomer E produced a stimulation of *c-myc* p65 expression (Table 2-4), it was not included in any of the best fit correlation calculations.

When considering all the possible ASO targets on the spliced (sP1) or unspliced (usP1) transcripts, only the Dscores have statistically significant correlations to reported inhibition (Table 2-5). The coefficient of determination for the targets on the usP1 transcript ($r^2 = 0.497$ ($P < 0.02$)) is slightly better than that for the ASO targets on the sP1 transcript ($r^2 = 0.437$ ($P < 0.05$)). However, this improvement simply reflects elimination of oligomer L from the usP1 correlation data set. We excluded oligomer L

TABLE 2-5: Coefficients of determination (r^2) between predictive indices and reported inhibition: human *c-myc* in HL-60 cells (Bacon and Wickstrom, 1991)

		<u>MONTE CARLO</u>		<u>DYNPRO</u>
		sP1 @ 10 μ M (n = 12)	usP1 @ 10 μ M (n = 11) ^a	sP1 @ 10 μ M (n = 12)
duplex	Dscore	0.437 (P < 0.05)	0.497 (P < 0.02)	
mRNA 2° structure	Sscore	0.061 (N. S.)	0.032 (N. S.)	0.060 (N. S.)
competition	Cscore	0.155 (N. S.)	0.327 (N. S.)	0.183 (N. S.)
<u>Ribosome Binding Competitors^c (n = 6)</u>				
duplex	Dscore	0.665 (P < 0.05)	0.665 (P < 0.05)	
mRNA 2° structure	Sscore	0.735 (P < 0.05)	0.878 (P < 0.01)	0.746 (P < 0.05)
competition	Cscore	0.022 (N. S.)	0.292 (N. S.)	0.039 (N. S.)

^aIndicates data for oligomer L was not included in these correlations.

^bThose ASO targets where protein or ribosomal binding occurs (e. g. F, G, M, N, O, R; Table 2-4).

because it is capable of partial binding to two distinct sites on the usP1 transcript, and we were uncertain how partial binding would affect computation of Dscores. Indices incorporating secondary structure considerations (Cscores, Sscores) do not correlate to reported inhibition when examining the ASO targets on either transcript.

When examining the ribosome competitor set of ASO (*e. g.* oligomers F, G, M, N, O, and R; Table 2-5), Dscore correlations to the reported specific inhibition improve ($r^2 = 0.665$ ($P < 0.05$), Table 2-5). The correlations between Sscore and reported inhibition are also significant for both transcripts (sP1, $r^2 = 0.735$ ($P < 0.05$); usP1, $r^2 = 0.878$ ($P < 0.01$)). However, the Sscore correlations are negative (increasingly strong secondary structures correlated to increasingly efficacious ASO). The anomalous behavior of the Sscores compensates for the correlations obtained with the Dscores, and explains why the Cscores are such poor indicators of ASO efficacy for this subset of ASO (sP1, $r^2 = 0.022$; usP1, $r^2 = 0.292$).

Transcripts from other c-myc promoters. The *c-myc* gene also contains two other promoters, termed P0 (Bentley and Groudine, 1986) and P2 (Battey *et al.*, 1983). The results obtained for both the spliced and unspliced transcripts originating from the P0 promoter were similar to those obtained for the corresponding transcripts from the P1 promoter (data not shown). In the case of the spliced and unspliced transcripts originating from the P2 promoter, there was no statistically significant correlation obtained between any of the three indices and reported inhibition. It should be noted that the targets for ASO F, G, and H do not appear on the P2 transcripts (Table 2-4).

II.4.3b Predictions for human ICAM-1 inhibition in HUVECs and A549 cells. Chiang and colleagues (1991) examined the effects of multiple

TABLE 2-6: Antisense phosphorothioates against human ICAM-1 in HUVEC and A549 cells (Chiang *et al.*, 1991)

Oligo Name	Oligo Length	Sequence	Target Site	Dscore	Cscore ^h	<u>Inhibition (%)</u> ^a HUVEC	A549
ISIS 1930	20	GGGCGGTGATCCTTATAGC	5' UTR ^{b,c}	N D ^d	N D ^d	0	0
ISIS 1571	20 ^b	GAGGAGCTCAGCGTCGACTG ^e	5' UTR	N D ^d	N D ^d	0	0
ISIS 1931	19	CATAGCGAGCTGAGGTIG	start AUG	-16.50	-14.67	45	50
ISIS 1570	18	TGGGAGCCATAGCGAGGC	start AUG	-17.85	-15.56	55	45
ISIS 1934	20	TGCCCATCAGGGCAGTTTGA	coding	-18.40	-13.79	10	30
ISIS 1574	18	CGATGGGCAGTGGGAAAG	coding	-15.90	-10.70	30	0
ISIS 1938	20	CCTGTCCCGGATAGGTTCA	3' UTR	-18.50	-12.52	45	50
ISIS 1939	20	CCCCACCACTTCCCTCTC	3' UTR	-20.25	-10.86	75	70
ISIS 2302	20	GCCCAAGCTGGCATCCGTC	3' UTR	-19.75	-17.29	75	70
ISIS 1572	20	GACACTCAATAAGCTGGT	3' UTR	-14.35	-8.16	5	30
ISIS 1573	18	GAGGCTGAGGTGGAGGA	3' UTR	-18.10	-14.98	42	5
ISIS 1940	20	TTGAGAAAGCTTTAATAACT	poly(A)	-12.35	-12.35	0	0
ISIS 1821	18	CATGGCCGGCCCGCGGG	control ^f	N D	N D	(45) ^g	(20) ^g

^aFor HUVECs, specific inhibition at 0.06 μ M oligomer; for A549 cells, inhibition at 0.8 μ M oligomer.

^bAccording to sequence of Tomassini *et al.*(1989) (see text).

^cUntranslated region.

^dNot determined(see text).

^eLength of hybrid may only be the underlined nucleotides (see text).

^fOligo targeted to 5-lipoxygenase mRNA (control ASO).

^gConsidered non-specific inhibition, and subtracted from remaining oligomers

^hCscores from MONTE CARLO algorithm

phosphorothioate ASO upon cytokine induced expression of ICAM-1 in human umbilical vein endothelial cells (HUVEC) and in human lung carcinoma cells (A549). They selected targets located across the entire mRNA sequence (Table 2-6) and tested each ASO over a range of concentrations in both cell lines. For computing the correlations, we used the percent of inhibition occurring at the midpoint of each range of concentrations (*i. e.* 0.06 μ M in HUVECs and 0.8 μ M in A549 cells). These inhibition values are shown in Table 2-6. Each value was adjusted to eliminate a non-sequence specific inhibition of ICAM-1 reported for a control oligonucleotide (*e. g.* ISIS 1821; Table 2-6) prior to calculating correlation coefficients.

Chiang and colleagues selected their ASO targets using a published ICAM-1 cDNA sequence whose cap site had not been determined (Tomassini *et al.*, 1989). Subsequently, the cap-site was mapped for human ICAM-1 transcripts isolated from cytokine-stimulated epithelial cells (Degitz *et al.*, 1991). This mapping study suggests that the target for ISIS 1930 lies upstream of the ICAM-1 transcriptional initiation site and therefore would not be found on the ICAM-1 mRNA sequence. The study also suggests that the target site for ISIS 1571 spans the cap site, and therefore would consist of 9 nucleotides rather than 20 (Table 2-6). We were uncertain how this partial binding would affect the activity of ISIS 1571, and presumed ISIS 1930 would not be able to produce any effects through an antisense mechanism. Consequently, we did not include inhibition data for either ASO in our correlations.

For all 10 ASO targets in both cell lines, the Dscores showed statistically significant correlations to specific inhibition ($r^2 = 0.658$ ($P < 0.005$) for HUVECs; $r^2 = 0.489$ ($P < 0.02$) for A549s). No statistically significant correlations could be drawn between the Sscores or Cscores and observed

TABLE 2-7: Coefficients of determination (r^2) for predictive indices and reported inhibition: human ICAM-1 studies in cultured cells (Chiang *et al.*, 1991)

<u>index</u>		<u>HUVECs</u>	<u>A549 cells</u>
		All Targets (n = 10)	
duplex	Dscore	0.658 (P < 0.005)	0.489 (P < 0.05)
mRNA 2° structure	Sscore	0.075 (N. S.)	0.133 (N. S.)
competition	Cscore	0.237 (N. S.)	0.208 (N. S.)
All 20-mer Targets (n = 5)			
duplex	Dscore	0.699 (P < 0.05)	0.820 (P < 0.02)
mRNA 2° structure	Sscore	0.169 (N. S.)	0.346 (N. S.)
competition	Cscore	0.188 (N. S.)	0.101 (N. S.)

inhibition in either HUVECs or A549 cells (Table 2-7).

To control for possible length dependent effects upon ASO uptake and therefore ASO inhibition, we also examined only the 20-mer ASO used in the ICAM studies. The correlations between Dscore and observed inhibition were significant in both cell lines ($r^2 = 0.699$ (P < 0.05) for HUVECs; $r^2 = 0.820$ (P < 0.02) for A549s), while Cscores and Sscores for this subgroup did not correlate with reported inhibition in either cell line. This result suggests that the Dscores are best used to compare ASO of identical length in the absence of information concerning intracellular concentrations of ASO.

II.4.3c Use of alternative folding algorithms. We also used DYNPRO, Martinez's implementation of the Zuker optimal folding algorithm (Zuker and Steigler, 1981) to fold a 610 nucleotide fragment of the *c-myc* sP1 transcript. This sequence contained all twelve ASO binding sites we considered in our analyses. However, no significant improvements in the correlations between Sscores or Cscores and reported inhibition were observed (Table 2-5). Used of DYNPRO to fold nine, staggered and overlapping 600 nucleotide fragments of the ICAM-1 transcript likewise did not produce improvements in the correlation between Sscores or Cscores and reported inhibition (data not shown). Thus use of a different folding algorithm did not improve the predictive values of the indices incorporating secondary structure considerations.

II.4.4 Comparison of Dscore with other physical parameters of ASO

Often, the melting temperature of a DNA duplex is estimated by a simple "two plus four" rule based upon the GC content of the oligomer. Simple GC compositional analysis (expressed as percent of ASO nucleotides that are G or C) did not correlate with reported inhibition for any of the cell free-systems, nor for the entire set or any subset of the *c-myc* ASO (data not shown). For the ICAM-1 experiments, a moderate correlation was observed between ASO GC content and specific inhibition in HUVECs ($r^2 = 0.694$ ($P < 0.005$)), while no significant correlation was observed for the data from the A549 cells ($r^2 = 0.230$). Therefore, except in the case of the HUVECs, the simple "two plus four" rule of thumb for computing the T_m of the duplex did not appear to be a useful predictor of inhibition. This result illustrates the importance of ASO sequence rather than composition when predicting the efficacy of the ASO.

The ICAM-1 inhibition studies included information concerning the measured T_m values for duplexes between the phosphorothioate ASO and complementary phosphodiester ASO (data not shown). While the experimentally determined T_m 's correlate with observed inhibition as well as our Dscores for the HUVEC system ($r^2 = 0.692$ ($P < 0.02$)), there was no correlation between measured T_m 's and the specific inhibition in A549 cells ($r^2 = 0.171$).

II.4.5 Dscores-- computation with RNA:RNA, DNA:DNA, and RNA:DNA nearest-neighbor doublet thermodynamic values

Dscores, as developed above, are based upon experimentally derived thermodynamic data for the free-energy of formation of RNA:RNA duplexes. However, all of the studies examined above involve DNA ASO binding to mRNA targets. Thus, we also compared DSCORE values calculated from thermodynamic values for DNA:DNA and RNA:DNA nearest-neighbor doublets to reported inhibition (Table 2-8).

McGraw and colleagues (1990) published a program that computes a Mean Stacking Temperature (MST) for a DNA-DNA duplex, based upon thermodynamic values obtained from work by Gotoh and Tagashira (1981). A second set of thermodynamic values for DNA:DNA nearest-neighbor doublets was used to calculate a DNA-based Dscore ($Dscore_{DNA:DNA}$; Yager and von Hippel, 1991). Yager and von Hippel derived their DNA:DNA thermodynamic values at 37°C by adjusting previously published values determined experimentally at 25°C, 1M NaCl (Breslauer *et al.*, 1986). Although little data has been published concerning the direct determination of nearest-neighbor stacking energies for RNA:DNA duplex formation, Yager and von Hippel (1991) have computed an approximate data set for

TABLE 2-8: Coefficients of determination (r^2) for Dscores based upon different thermodynamic data sets, and reported inhibition

	Dscore	MST	Dscore _{DNA:DNA}	Dscore _{RNA:DNA}
<i>c-myc</i> / HL-60 cells				
(Bacon and Wickstrom, 1991)				
(n = 11)	0.497 (<i>P</i> < 0.05)	0.268 (N. S.)	0.308 (N. S.)	0.403 (<i>P</i> < 0.05)
ICAM-1				
(Chiang <i>et al.</i> , 1991)				
(n = 10)				
HUVECs	0.658 (<i>P</i> < 0.005)	0.640 (<i>P</i> < 0.01)	0.610 (<i>P</i> < 0.01)	0.655 (<i>P</i> < 0.005)
A549 cells	0.489 (<i>P</i> < 0.05)	0.243 (N. S.)	0.501 (<i>P</i> < 0.05)	0.535 (<i>P</i> < 0.02)
^aNot significant				

RNA:DNA hybrids based upon existing experimental data. This data set was used to compute a Dscore based upon RNA:DNA duplex formation (Dscore_{RNA:DNA}).

The results summarized in Table 2-8 indicate the predictive ability of the Dscore index is not affected significantly by the choice of RNA:RNA or RNA:DNA thermodynamic data sets, since the standard Dscores, computed from RNA:RNA thermodynamic values, appear to predict inhibition as well as the Dscores computed from estimated RNA:DNA thermodynamic values. However, Dscores computed from DNA:DNA thermodynamic values worsen the predictive ability of the Dscore, and the MST index does not appear to predict inhibition at all. These results may reflect the fact that the ASO-mRNA duplex adopts a conformation closer to the A form of ribonucleic acid helices, rather than the B form of DNA helices (Wang *et al.*,

1982; Hall and McLaughlin, 1991). As better RNA:DNA thermodynamic values become available, they can easily be incorporated into the DSCORES program.

II.4.6 Calculation of a DifScore using LRNA to produce constrained folds

One final approach to analyzing the ICAM data was employed. Zuker's suboptimal folding algorithm, LRNA, was used to fold four subfragments of the ICAM-1 mRNA (Table 2-9). Each subfragment was folded to generate the structure with the minimum equilibrium global free-

TABLE 2-9: DifScore calculations for antisense phosphorothioates against human ICAM-1 (Chiang *et al.*, 1991)

Oligo	Length	$\Delta G^{\circ}_{f,opt}{}^b$	$\Delta G^{\circ}_{duplex}$	$\Delta G^{\circ}_{f,cons}{}^c$	DifScore	Inhibition (%) ^a	
						HUVEC	A549
icam 1.0 (fragment of ICAM-1 mRNA, nts 1-600)							
ISIS 1931	19	-182.6	-33.0	-175.6	-26.0	45	50
ISIS 1570	18	-182.6	-35.8	-172.6	-25.8	55	45
ISIS 1934	20	-182.6	-36.8	-167.6	-21.9	10	30
icam 3.0 (fragment of ICAM mRNA, nts 1200-1800)							
ISIS 1574	18	-162.5	-31.8	-149.7	-19.2	30	0
ISIS 1938	20	-162.5	-37.0	-152.4	-27.1	45	50
icam 4.0 (fragment of ICAM-1 mRNA, nts 1801-2400)							
ISIS 1939	20	-123.5	-40.6	-108.6	-25.7	75	70
ISIS 2302	20	-123.5	-39.6	-113.7	-29.8	75	70
ISIS 1572	20	-123.5	-28.8	-114.5	-19.8	5	30
icam 5.0 (fragment of ICAM-1 mRNA, terminal 572 nts)							
ISIS 1573	18	-128.3	-36.2	-123.1	-31.0	42	5
ISIS 1940	20	-128.3	-24.8	-127.1	-23.6	0	0

^aFor HUVECS, specific inhibition at 0.06 μ M ASO; for A549 cells, inhibition at 0.8 μ M oligomer

^b $\Delta G^{\circ}_{f,optimal}$, supplied by Zuker suboptimal LRNA program; units kcal/mol

^c $\Delta G^{\circ}_{f,constrained}$; calculated by keeping the ASO target site single-stranded while allowing the rest of the RNA sequence to fold; units kcal/mol.

energy (optimal folding). Then each subsequence was folded again to obtain a constrained folding, in which the target sites of the various ASO on the RNA were forced to remain single stranded. A DifScore was then generated according to the relation

$$DifScore = \left(\Delta G_{f,constrained}^{\circ} + \Delta G_{duplex\ formation}^{\circ} \right) - \Delta G_{f,optimal}^{\circ} \quad (2-6)$$

Like the Cscore, the DifScore is a measure of the favorability of ASO-mRNA duplex formation relative to the formation of a native RNA structure. However, unlike the Cscore, the DifScore attempts to account for changes in the global structure of the RNA due to ASO binding, rather than only considering perturbations to a local secondary structure. Comparison of DifScores to reported inhibition in the ICAM studies reveals no statistically significant correlations in the A549 cells ($r^2 = 0.145$). However, in the case of the HUVEC cells a weak, but statistically significant correlation, was obtained ($r^2 = 0.424$ ($P < 0.05$)).

II.5 CONCLUSIONS

Our results suggest Dscores are the most consistently useful indicators of ASO efficacy. Other physical parameters of the oligonucleotides (T_m , GC content, length) were unable to predict ASO efficacy in a consistent fashion. Comparison of the strong correlations obtained between Dscores and ASO inhibition in cell free systems to the weaker correlations observed in cell systems suggests other variables besides hybridization thermodynamics affect ASO efficacy. Therefore, the Dscores displayed as histograms along the target mRNA sequence permit rapid determination of the ASO likely to produce

strong inhibition based solely upon hybridization thermodynamics. This strategy of using Dscores to select ASO sequences may work best when comparing ASO targets that overlap a specific mRNA region (i. e. determining the best 15-mer spanning the start codon) An added advantage of the Dscore is that it can be calculated by a quick and simple sequence analysis algorithm, and therefore is not computationally expensive.

Why doesn't predicted mRNA structure correlate with ASO efficacy?

Certainly the binding of an ASO is important to inhibition, even when crudely assessed by a Dscore. However, the lack of consistent significant correlations between inhibition and indices which incorporate considerations of mRNA secondary structure (Sscore, Cscore or DifScore) suggests the structure prediction algorithms we used may not be reliable enough for this type of analysis, and therefore it is unreasonable to expect a strong correlation with experimental results observed in cells. It is also true that the role of tertiary mRNA structure and mRNA binding proteins in ASO hybridization are not addressed by the folding algorithms or by our thermodynamic analysis. In the absence of known, mapped RNA structures, it cannot be determined if the predicted structures are accurate for the four mRNA targets analyzed in this chapter. It is also possible that better thermodynamic predictions could be obtained if the concentrations of reactants and products are included in the thermodynamic analysis, although this approach is hindered by the lack of knowledge concerning intracellular and intracompartamental concentrations of oligonucleotides in complex biological systems. Our attempts to deal with these issues of RNA structure and concentrations are addressed in Appendix 4.

CHAPTER THREE: Single-stranded Phosphodiester and Phosphorothioate Oligonucleotides Bind Actinomycin D and Interfere with TNF-Induced Lysis in the L929 Cytotoxicity Assay.

III.1 ABSTRACT

Antisense oligonucleotides may prove useful tools to elucidate the biological functions of cytokines and to address regulatory control of cytokine expression. The functional activity of cytokines generally is determined by biological assays, and a standard biological assay for TNF-activity measures the cytotoxic effect of TNF upon actinomycin D-sensitized L929 cells (Matthews and Neale, 1987). We observed that phosphorothioate and phosphodiester oligonucleotides, at concentrations > 100 nM in supernatants tested in this bioassay, prevented TNF-induced lysis of L929 cells. This "protective" effect was due to an interaction of the single-stranded oligonucleotides with actinomycin D as demonstrated by UV spectra of an actinomycin D/oligonucleotide solutions. Substitution of cycloheximide for actinomycin D in the L929 assay eliminated the "protective" effect of the oligonucleotide. Our results reinforce the importance of controlling for non-specific effects of oligonucleotides, particularly when a functional assay for protein activity is used to screen for antisense-mediated reductions in target protein expression.

III.2 INTRODUCTION

Antisense oligodeoxyribonucleotides have become widely used tools to elucidate gene product function in cell culture. An attractive set of targets

for oligonucleotide-mediated inhibition are the inflammatory mediator cytokines, interleukin-1 (IL-1), interleukin-6 (IL-6), and tumor necrosis factor-alpha (TNF- α). These cytokines, like many cytokines in general, show great redundancy of function. Each participates in complex inductive and suppressive interactions with other cytokines. *In vitro* studies using recombinant cytokines and monoclonal antibodies have allowed some dissection of these induction and suppression interactions. Antisense oligonucleotides promise to be useful tools, both as reagents for investigating fundamental regulation properties of the inflammatory mediators and as potential therapeutics in the variety of pathological states associated with overexpression of these proteins (*e.g.* septic shock, wasting syndromes, rheumatoid arthritis).

Investigators use a variety of biological assays to assess the activity of cytokines (Mosmann and Fong, 1989). For instance, TNF bioactivity can be measured by examining its cytotoxic effects upon tumor cell lines. Although the exact mechanisms of TNF-mediated cell killing have not been elucidated, various studies have shown that the biological action of TNF is related to both second messenger pathways initiated by TNF binding and that internalization of TNF is required for cell death (reviewed by Larrick and Wright, 1990). Inhibitors of lysosomal enzymes and cytoskeletal-disrupting agents decrease TNF-cytotoxic activity, while inhibitors of transcription and translation enhance the cytotoxic effect of TNF (Kull and Cuatrecasas, 1981; Ruff and Gifford, 1981). A common assay for TNF bioactivity measures TNF-induced lysis of actinomycin D-sensitized murine L929 tumor cells (Ruff and Gifford, 1981; Matthews and Neale, 1987).

While screening multiple antisense oligonucleotides for their inhibitory properties on TNF expression, we discovered that the presence of

oligonucleotides in test supernatant negated the biological activity of TNF in the L929 assay. Further experiments indicated this negation of activity was not due to a reduction in TNF expression nor due to interference with TNF binding, but the result of interactions of the single-stranded oligonucleotides with actinomycin D.

III.3 MATERIALS AND METHODS

III.3.1 Chemicals

All cell culture reagents (media, serum) were supplied by the UCSF Cell Culture facility. Pentosan polysulfate, actinomycin D, cycloheximide and (3-[4,5-dimethyl-thiazol-2-yl]-2,5-diphenyltetrazolium bromide) (MTT) were purchased from Sigma (St. Louis, MO). Bacterial lipopolysaccharide (LPS), derived from *Salmonella minnesota* R595, was purchased from List Biological Laboratories (Campbell, CA). Recombinant murine TNF- α was purchased from Genzyme (Cambridge, MA).

III.3.2 Oligonucleotides

All phosphorothioate and phosphodiester oligonucleotides were supplied by Lynx Therapeutics (Foster City, CA). The sequences for each oligonucleotide used are: TNF1, 5'-GCTTCTGTGCTCATGGTCT-3'; REV, 5'-TCGTCGCTGTCTCCGCTTCTTCCTGCCA-3'; IL-1 α 2C, 5'-CCTCTCTATGCTTATCAGTC-3'; TNF2, 5'-GGCCAGGTGGGCGTTGGCGC-3'. Concentrations of oligonucleotide stock solutions in water were determined using 1 O.D. (A_{260}) = 33 μ g/mL oligonucleotide.

III.3.3 Cell culture

A murine macrophage-like cell line, RAW 264.7, was used to supply

TNF-positive supernatants. RAW 264.7 cells were grown in DME H-16 medium, supplemented with 10% fetal calf serum which had been heat inactivated at 56°C for 30 minutes (hiFCS). L929 cells, an adherent murine tumor cell line, were propagated in T175 flasks (Fisher, Santa Clara, CA) using RPMI-1640 medium supplemented with 0.025M HEPES, 5% hiFCS, and 50 μ M β -mercaptoethanol. All cells were grown at 37°C, in a humidified incubator containing 5% CO₂

III.3.4 Initial oligonucleotide screening for anti-TNF effects

RAW 264.7 cells (2×10^5) in growth medium were plated into each well of a 24-well culture plate (Costar). Cells were allowed to rest overnight, washed once with warm PBS, and then 10 μ M oligonucleotide was added in 200 μ L of bioassay medium (RPMI-1640 containing 0.025M HEPES and 4% hiFCS). After a 4 hour pre-incubation with the oligonucleotide, LPS was added to each well to a final concentration of 1 μ g/mL. Supernatants were harvested 24 hours after LPS addition.

III.3.5 Production of TNF-positive supernatants

RAW 264.7 cells (2×10^7) were seeded in 100 mm culture dishes (Costar, Cambridge MA) and allowed to settle overnight prior to addition of 1 μ g/mL LPS. Supernatants (10 mL) were collected 96 hours after LPS addition, concentrated 20-fold using Amicon 8010 concentration device with a YM10 filter (molecular weight cutoff 10,000), sterile filtered through a 0.22 μ m Millex-GV syringe top filter (Millipore, Bedford, MA), and stored at -80°C until use in the L929/TNF biological assay.

III.3.6 L929/TNF Assay

L929 cells (4×10^4) in bioassay medium were plated into each well of a 96-well culture plate (Costar) and allowed to grow 22 hours to form a confluent monolayer. Plating medium was removed from the monolayers just prior to addition of test supernatants. Test supernatants (50 μ L) containing TNF and oligonucleotide or TNF and pentosan polysulfate were serially diluted (each dilution 1:2) across 10 dilutions. Bioassay medium (50 μ L) containing either 1.6 mM actinomycin D or 8 μ M cycloheximide was then added to each of the serially diluted samples, and the resulting solutions transferred to the L929 plates. After a 20 hour incubation at 37°C, cell viability was determined using the MTT colorimetric assay (Mosmann, 1983). In this method, 10 μ L of MTT dissolved in PBS (5 mg/mL) was added to each well, and the plates incubated for 4 hours at 37°C. Isopropanol/ 0.04 N HCl developer solution (150 μ L) was added to each well, the solutions thoroughly mixed, and the plates read on Dynatech ELISA plate reader. Absorbances were expressed as a ratio of the absorbances at 570 and 630 nm, and converted into percent cell survival using the following equation:

$$\text{percent survival} = \frac{(Abs_{\text{observed}} - Abs_{\text{background}})}{(Abs_{\text{maximum}} - Abs_{\text{background}})} \times 100 \quad (3-1)$$

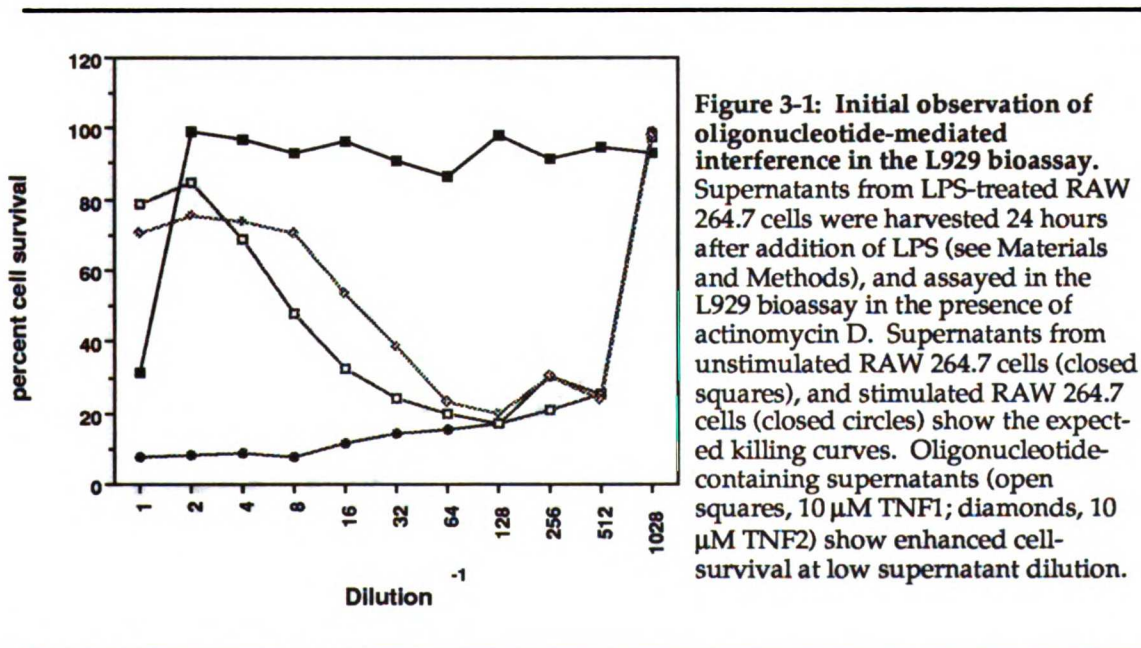
III.3.7 UV Absorption Spectra

UV spectra were obtained using a Hewlett Packard 8452A diode array UV-visible spectrophotometer (Palo Alto, CA). Actinomycin D was diluted in bioassay medium (pH 7.4) to the indicated concentrations, as determined from $\epsilon_{440} = 21900 \text{ L mol}^{-1} \text{ cm}^{-1}$ for aqueous solutions. For the actinomycin D / single-stranded oligonucleotide solution, both species were diluted in

bioassay medium and allowed to incubate at room temperature for 30 minutes prior to taking the spectra. Actinomycin D incubation with PPS, nucleotide cocktail and duplex phosphorothioate DNA was performed similarly.

III.4 RESULTS AND DISCUSSION

While testing anti-TNF phosphorothioate oligonucleotides for TNF-inhibitory activity, we observed that oligonucleotide-containing culture supernatants protected L929 cells from TNF-induced lysis (Figure 3-1). As the test supernatants were serially diluted, the protective effect was diminished. Supernatant from LPS-treated RAW 264.7 cells cultured in the absence of oligonucleotide produced the expected killing curve due to TNF-activity. Addition of TNF1 or TNF2 oligonucleotides to the TNF-positive supernatants prior to dilution negated the TNF-killing effects. These results



suggested the oligonucleotides were interfering with the events necessary for TNF-induced killing of the target cells.

Subsequent experiments revealed two other phosphorothioate oligonucleotides, IL-1 α 2C and REV, prevented TNF from killing the L929 cells, while a polyanionic heparin analog, pentosan polysulfate, did not (data not shown). This result suggested the protection of L929 cells by the phosphorothioates was not due to the polyanionic nature of the oligonucleotides, and the protection was not unique to the anti-TNF oligonucleotides. The protection of L929 cells from TNF-induced lysis could be titrated with respect to the amount of oligonucleotide present in test samples (Figure 3-2). Cell-derived TNF-positive supernatants were spiked with varying concentrations of REV phosphorothioate oligomer (10, 5, 2.5, and 0.2 μ M) prior to dilution. As the initial concentration of oligomer was reduced from 10 to 0.2 μ M, the protective effect was diminished at successively earlier serial dilutions. This result further confirmed that the

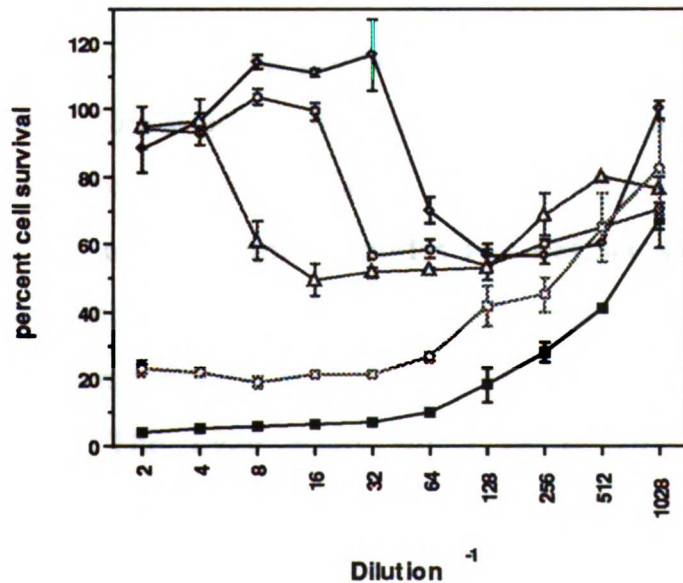


Figure 3-2: Titration of protective effect correlates with titration of oligonucleotide present in the supernatant. TNF-positive supernatants were spiked with varying concentrations of REV phosphorothioate oligonucleotide, serially diluted, and assayed in the presence of actinomycin D.

Open diamonds- 10 μ M oligomer; open circles- 5 μ M oligomer; open triangles- 2.5 μ M oligomer; open squares- 0.2 μ M oligomer; closed squares- no oligomer present in test supernatants. n = 3 for each point, error bars not visible are smaller than the diameter of the symbol

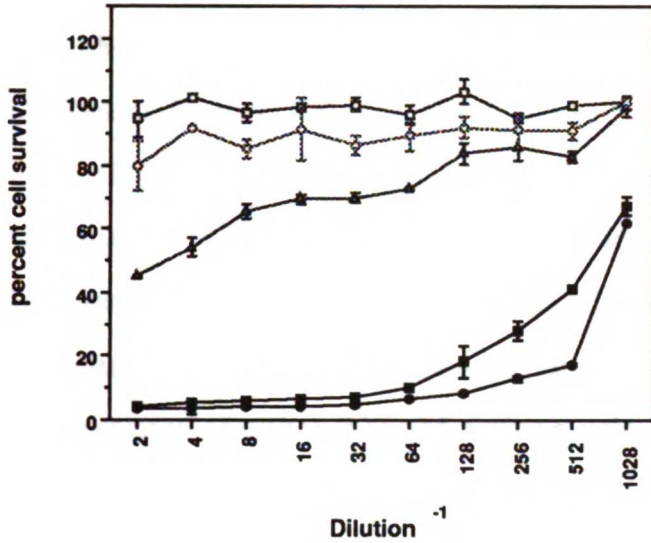


Figure 3-3: Comparison of transcriptional and translational inhibitors as sensitizing agents in the L929 assay. TNF-positive supernatants from RAW 264.7 cells were tested in the L929 bioassay in the absence of any sensitizer (open triangles), or in the presence of actinomycin D (800 nM, closed squares) or cycloheximide (4 μ M, closed circles). The cytotoxicity of the sensitizers on L929 cells in the absence of TNF was also examined (open squares- actinomycin D, 800 nM; open circles- cycloheximide, 4 μ M). n = 3 for each point. Error bars not visible are smaller than the diameter of each symbol.

oligonucleotides were responsible for protecting the L929 cells from TNF-induced lysis.

To control for oligonucleotide interactions with other components present in the supernatants obtained from LPS-treated RAW 264.7 cells, we examined the effect of the REV phosphorothioate oligomer when mixed with recombinant murine TNF- α . While the recombinant TNF- α displayed the normal killing profile, samples in which recombinant TNF- α was mixed with 10 μ M REV phosphorothioate oligomer prior to dilution showed no cytotoxic activity (data not shown). Therefore, we concluded the protective effect of the oligonucleotides was not necessarily due to an interaction with an undefined component present in the LPS-treated RAW 264.7 cell supernatants.

The L929 assay for TNF activity, as performed in the above experiments, employs 800 nM (1 μ g/mL) actinomycin D to sensitize the L929 cells to the lytic effect of TNF (Figure 3-3). Although actinomycin D is used most frequently as a sensitizing agent, other inhibitors of transcription or

translation can be used (Ruff and Gifford, 1981). Use of either actinomycin D (800 nM) or cycloheximide (4 μ M) allows detection of 250-fold less TNF in the L929 assay (Figure 3-3).

To examine if the protective effect of the phosphorothioate oligonucleotides was due to an interaction with actinomycin D, cell-derived TNF-positive supernatants were mixed with 10 μ M REV phosphorothioate oligonucleotide, the resulting solutions serially diluted, and then assayed in the presence of either 800 nM actinomycin D or 4 μ M cycloheximide (Figure 3-4a).

The oligonucleotide/TNF supernatants used in conjunction with actinomycin D showed no cell killing effects at dilutions lower than 1:32. The same supernatants used in conjunction with 4 μ M cycloheximide showed a killing profile identical to the TNF-positive supernatants tested in

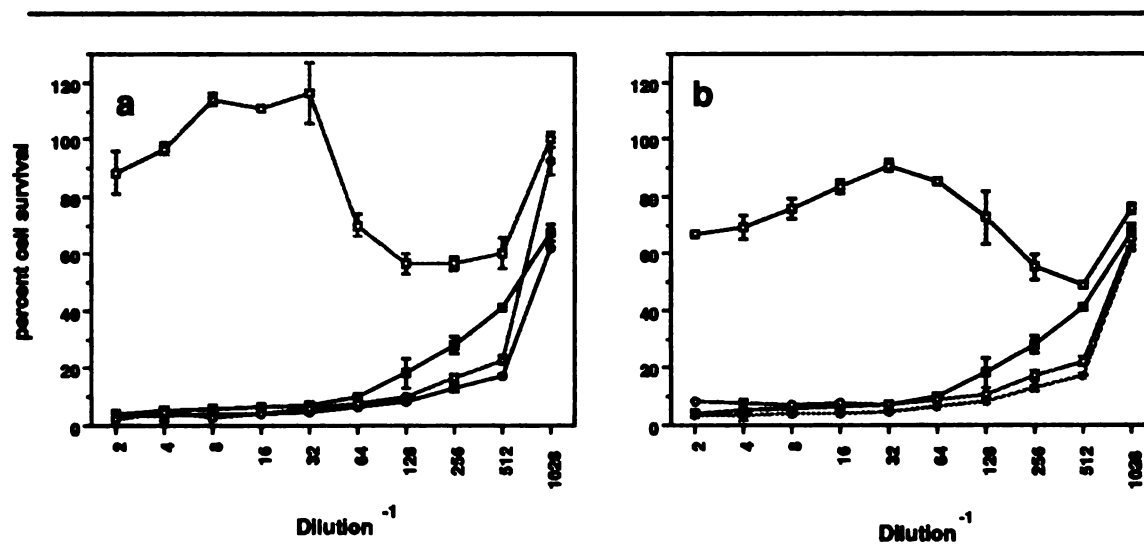


Figure 3-4: Effect of different metabolic inhibitors on oligonucleotide-mediated protection of L929 cells. For each point, n = 3; error bars not visible are smaller than the diameter of the symbol. 4a) TNF-positive supernatants were mixed in bioassay medium with (open symbols) or without (closed symbols) 10 μ M REV phosphorothioate oligonucleotide, diluted, and assayed in the presence of 800 nM actinomycin D (squares) or 4 μ M cycloheximide (circles). 4b) TNF-positive supernatants were mixed in bioassay medium with (open symbols) or without (closed symbols) 10 μ M REV phosphodiester oligonucleotide, diluted, and assayed in the presence of 800 nM actinomycin D (squares) or 4 μ M cycloheximide (circles).

the absence of oligonucleotide (Figure 3-4a). These results suggested the oligonucleotide was interacting with actinomycin D and preventing it from sensitizing the L929 cells to TNF-induced lysis. It can also be seen that 4 μM cycloheximide renders the L929 cells slightly more sensitive to TNF than does 800 nM actinomycin D (compare dilutions 1:128, 1:256 and 1:512 in Figures 3-3, 3-4a). REV phosphodiester oligonucleotide displayed similar behavior (Figure 3-4b), as did duplex phosphorothioate oligonucleotides (data not shown).

To further confirm that interactions were taking place between the oligonucleotides and actinomycin D, the UV absorption spectra for actinomycin D alone and actinomycin D in the presence of varying amounts of REV phosphorothioate oligonucleotide were obtained (Figure 3-5a). Addition of increasing amounts of REV oligonucleotide (0, 0.7, 1.75 μM) to 17.5 μM actinomycin D results in a decrease of the actinomycin D absorbance

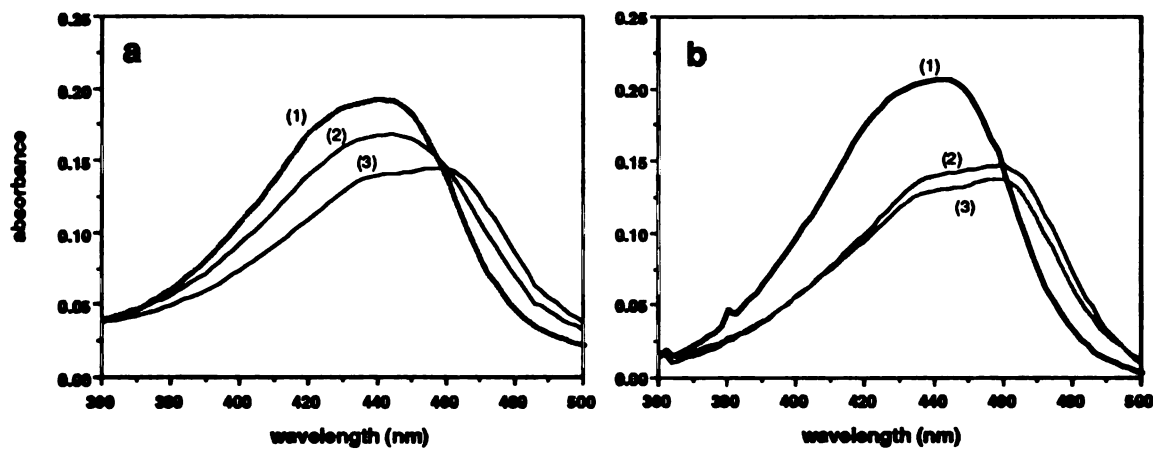


Figure 3-5: UV absorption spectra of actinomycin D and oligonucleotides in bioassay medium, pH 7.4 (see Materials and Methods). 5a) The absorbance spectrum of 17.5 μM free actinomycin D (1) and 17.5 μM actinomycin D in the presence of 0.7 μM (2) and 1.75 μM (3) REV phosphorothioate oligonucleotide. 5b) The absorbance spectrum of 20 μM free actinomycin D (1) and 20 μM actinomycin D in the presence of 20 μM REV phosphodiester oligonucleotide (2) or 20 μM REV phosphorothioate oligonucleotide (3).

maximum at 440 nm, and a shift in the absorbance maximum from 440 nm to 460 nm. Both results are suggestive of a physical interaction between actinomycin D and the single-stranded oligonucleotide (Zhou *et al.*, 1989).

Absorption spectra of 20 μM actinomycin D alone and 20 μM actinomycin D in the presence of equimolar concentrations of single-stranded REV phosphorothioate or phosphodiester oligonucleotides were obtained (Figure 3-5b), indicating this phenomenon was not unique to the phosphorothioate oligonucleotides. Similar spectra were obtained when PBS rather than bioassay medium is used as the solvent (data not shown). Duplex phosphorothioate DNA at 20 μM , produced by annealing the REV-phosphorothioate oligonucleotide to its phosphorothioate complement, resulted in a spectrum with a similar decrease in absorbance at 440 nm and a shift in the absorbance maximum from 440 nm to 460 nm (data not shown). Incubation of 20 μM actinomycin D with 20 μM of a nucleotide cocktail composed of the phosphodiester nucleotides in the same molar ratios as the intact REV phosphodiester oligonucleotide, or with 20 μM PPS, showed no decrease or hypochromic shift in the absorbance maximum of actinomycin D (data not shown).

Actinomycin D is known to intercalate into double-stranded nucleic acid duplexes (Kamitori and Takusagawa, 1992). One previous study has shown actinomycin D can bind to single-stranded phosphodiester oligonucleotides with dissociation constants of 50-900 nM (Wadkins and Jovin, 1991). This is consistent with the concentrations of actinomycin D in the L929 assay (800 nM). It is likely that the binding of actinomycin D to the single-stranded REV oligonucleotides is not due to intercalation into an existing secondary structure in the oligonucleotide. The single-stranded REV

phosphorothioate oligonucleotide displays no secondary structure as determined by UV analysis of melting curves obtained over the range of 10-80°C (S. Sixou, personal communication).

III.5 CONCLUSIONS

Our results demonstrate the importance of testing how oligonucleotides affect biological assays used to measure protein function and activity. Had the concentrations of oligonucleotides present in our supernatants been higher, we might not have seen the dilution of the L929 protective effect (i.e. dilution of the actinomycin D-binding oligonucleotides) and erroneously attributed the L929 protection to reductions in TNF bioactivity or a non-sequence specific blockade of TNF binding to and internalization by L929 cells. In this specific example, our results indicate that cycloheximide should be used in place of actinomycin D in the L929 cytotoxicity assay if oligonucleotides are present in the test samples.

CHAPTER FOUR: Developing An Empirical ASO Binding Assay.

IV.1 ABSTRACT

The apparent dissociation constants for thirty-two phosphodiester and five phosphorothioate ASO targeted to murine tumor necrosis factor-alpha (TNF- α) mRNA were determined using a gel-shift binding assay. In this assay, ^{32}P -labeled oligonucleotides are hybridized in solution to a structured RNA transcript generated *in vitro*. Free ASO is resolved from bound ASO on a two-phase polyacrylamide gel. Excision of the gel slices containing free and bound ASO, followed by Cerenkov counting of the slices, affords construction of apparent binding isotherms for each ASO. Apparent dissociation constants for anti-TNF ASO varied from $> 100 \mu\text{M}$ to $0.4 \mu\text{M}$. Observed binding affinity did not correlate directly with the computed binding constants for ASO hybridization to an unstructured complement (Dscores), demonstrating the effects of RNA secondary structure upon ASO binding. Slight differences in RNA target site position resulted in significant differences in apparent affinity, particularly for shorter (12-mer) ASO. This binding assay provides an empirical means for selecting ASO sequences possessing high affinity for their target RNA, sequences which are suitable for experimentation in cell culture and *in vivo*.

IV.2 INTRODUCTION

An ASO must bind its intended target RNA species as a prerequisite to effecting inhibition of gene expression via an antisense mechanism. Although designing ASO is procedurally simple given primary sequence data and Watson-Crick base-pairing rules, no comparable *a priori*

understanding of the relationship between RNA structure and ASO affinity currently exists. It is clear that the binding of an ASO is guided by thermodynamic and kinetic constraints (Monia *et al.*, 1992; Freier, 1993), some of which are imposed by RNA structure (Uhlenbeck, 1971; Lima *et al.*, 1992; Eckers *et al.*, 1992). To date, computational methods of predicting RNA structure have had at best, limited success; any purely computational method of predicting ASO binding and efficacy which incorporates RNA structure prediction is limited to the confidence which can be placed in the predicted RNA structures (Stull *et al.*, 1992).

Given the lack of predictive approaches, and the limited data base of RNAs whose secondary structures are well known, it would be useful to develop experimental techniques for measuring apparent binding constants of various ASO for their intended mRNA target. Such techniques would afford means to select ASO sequences known to bind their target prior to cellular studies. The techniques would also provide a larger data base of information which may permit development of new strategies for predicting ASO binding and efficacy. The studies detailed in this chapter utilize a gel-shift technique developed to determine empirically the apparent binding affinity of ASO for their structured mRNA target. The model system selected involved an mRNA derived from a murine TNF- α cDNA.

IV.3 MATERIALS AND METHODS

IV.3.1 Materials

Plasmid pUC-9-mTNF- α was kindly supplied by Dr. Patricia Olson of Chiron Corp. (Emeryville, CA). Acrylamide-methylene bis acrylamide (pre-mixed, 29:1) was purchased from Boehringer Mannheim (Indianapolis, IN).

Murine TNF- α cDNA derived RNA transcript

~ 1400 nucleotides

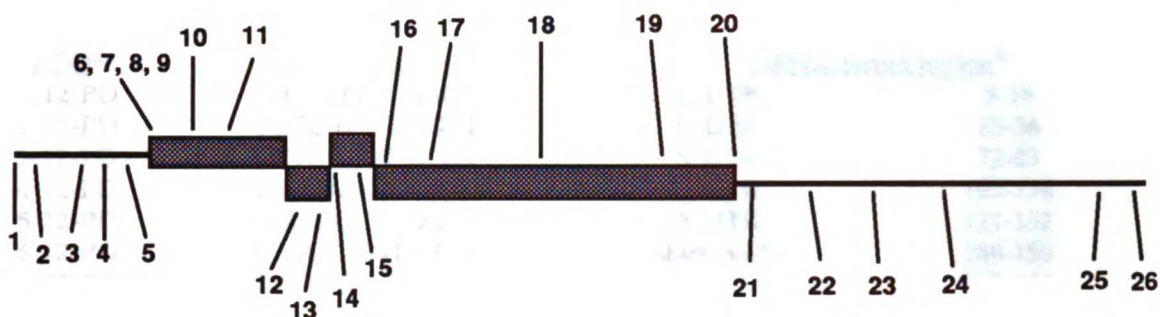


Figure 4-1: ASO target sites along the murine TNF- α cDNA derived mRNA.

X-OMAT™ AR film for autoradiography was purchased from Kodak (Rochester, NY). All other chemicals were purchased from Sigma (St. Louis, MO.)

IV.3.2 Oligonucleotide sequence selection and synthesis

A murine TNF- α cDNA sequence was derived from a TNF- α cDNA sequence (Caput *et al.*, 1986) retrieved from GenBank™ (Bilofsky and Burks, 1988). Thirty-three phosphodiester and five phosphorothioate oligonucleotide sequences were selected from the cDNA sequence (Figure 4-1; Table 4-1). All oligonucleotides were synthesized by Lynx Therapeutics (Hayward, CA) and supplied as lyophilized sodium salts. ASO were resuspended in DEPC-treated pyrogen-free water to a final concentration of 1 mM, as determined by UV absorption spectroscopy using sequence based extinction coefficients for each oligonucleotide calculated according to published techniques (Borer, 1974). Oligonucleotides are named in the following manner: site number-length-backbone type (e. g. 7-12-PD), where

Table 4-1: Anti-murine TNF- α ASO sequences used in this study.

<u>ASO^a</u>	<u>Oligo Sequence</u>	<u>mRNA target region^b</u>	
1-12-PD	TCCT CGCT GAGG	5' UTR	8-19
2-12-PD	TCCC TCCT GGCT	5' UTR	25-36
3-12-PD	CTTG CTTT TCTG	5' UTR	72-83
4-12-PD	GTGA AAGG GACA	5' UTR	103-114
5-12-PD	GGCG CCTT GGCG	5' UTR	121-132
6-12-PD	CATG GTGT CTTT	start AUG	148-159
6-12-PT	CATG GTGT CTTT	start AUG	148-159
7-12-PD	CTCA TGGT GTCT	start AUG	150-161
8-12-PD	GTGC TCAT GGIG	start AUG	153-164
8-12-PT	GTGC TCAT GGIG	start AUG	153-164
8u-16-PD	GTGC TCAT GGIG TCTT	start AUG	149-164
8s-16-PD	CTGT GCTC ATGG TGTC	start AUG	151-166
8s-16-PT	CTGT GCTC ATGG TGTC	start AUG	151-166
8d-16-PD	TTCT GTGC TCAT GGIG	start AUG	153-168
8u-20-PD	GTGC TCAT GGIG TCTT TTGT	start AUG	144-163
8s-20-PD	TTCT GTGC TCAT GGIG TCTT	start AUG	149-168
8s-20-PT	TTCT GTGC TCAT GGIG TCTT	start AUG	149-168
8d-20-PD	TGCT TTCT GTGC TCAT GGIG	start AUG	153-172
9-12-PD	TTCT GTGC TCAT	start AUG	157-168
9-12-PT	TTCT GTGC TCAT	start AUG	157-168
10-12-PD	CCCA TCTT TTGG	coding, exon #1	210-221
11-12-PD	GGCA CCGC CTGG	coding, exon #1	236-247
12-12-PD	TAGA ACTG ATGA	coding, exon #2	365-376
13-12-PD	TGTG AGGG TCTG	coding, exon #2	382-393
14-12-PD	TGAT CTGA GTGT	splice jxn; exons 2-3	391-410
15-12-PD	GCTT GTCA CTCG	coding, exon #3	416-427
16-12-PD	GTTG GCCA GGAG	coding, exon #4	499-510
17-12-PD	AGTA GACA AGGT	coding, exon #4	560-571
18-12-PD	GGGC AGGG GCTC	coding, exon #4	684-695
19-12-PD	AAAG TCTA AGTA	coding, exon #4	811-822
20-12-PD	CCTT CACA GAGC	stop codon	856-867
21-12-PD	CTGG GTAG AGAA	3' UTR	885-896
22-12-PD	TAGA CAAT AAAG	3' UTR	925-936
23-12-PD	AGCT CTGA GCAC	3' UTR	1004-1015
24-12-PD	TTTG AGTC CTTG	3' UTR	1086-1097
25-12-PD	GGGG GGCT GGCT	3' UTR	1268-1279
26-12-PD	TAAA TAAT AAAT	3' UTR Poly A	1302-1313

^aName of ASO indicates site, length, backbone: (i.e. 7-12-PD: site 7, 12-mer, diester)

PD= phosphodiester, PT = phosphorothioate.

^bIndicates position on cDNA sequence (Caput *et al.*, 1986)

PD is phosphodiester, and PT is phosphorothioate.

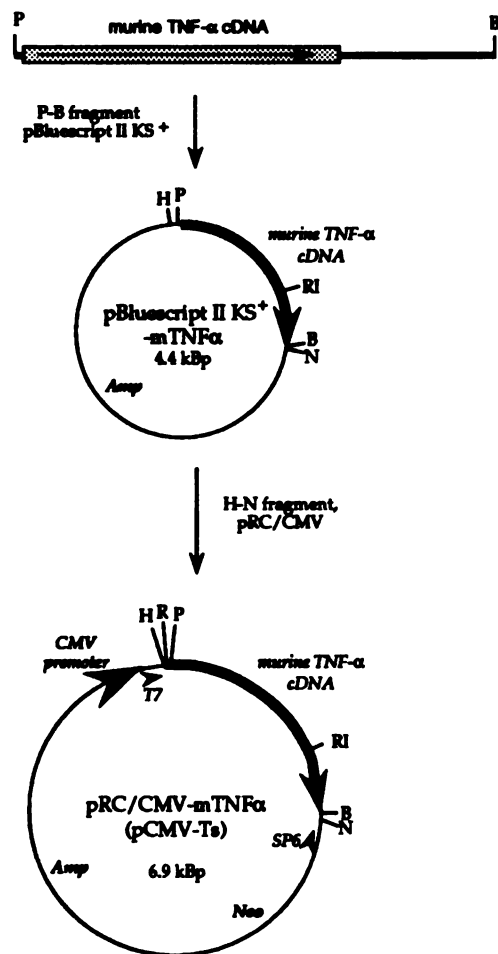


Figure 4-2: Construction of plasmid pCMV-TNF- α (pCMV-Ts) A murine TNF- α cDNA was recovered from plasmid pUC-9-TNF- α as a 1.4 kB, Pst I - Bam HI flanked fragment. This fragment was directionally subcloned into the pBluescript/KS⁺ plasmid to generate pBluescript/KS⁺-mTNF- α . Recovery of the TNF- α cDNA from pBluescript/KS⁺-TNF- α as a Hind III - Not I flanked fragment allowed directional subcloning into the mammalian expression vector pRC/CMV, generating plasmid pCMV-TNF- α (pCMV-Ts). pCMV-Ts was determined to be the desired construct by nested restriction digest mapping and by sequencing across the ligation junctions. Sense TNF- α RNA transcripts were generated *in vitro* from pCMV-Ts using bacteriophage T7 and a template linearized downstream of the cDNA at an Xba I site. Antisense TNF- α RNA was generated *in vitro* from pCMV-Ts using bacteriophage SP6 and a template linearized upstream of the cDNA at a Hind III site.

Restriction site key: B, Bam HI; H, Hind III; N, Not I; P, Pst I; RI, Eco RI.

IV.3.3 Plasmid Construction.

The cDNA encoding murine tumor necrosis factor- α (TNF- α ; Caput *et al.*, 1986) was provided by the ~1.4 kB Pst I - Bam HI fragment of plasmid pUC-9-TNF- α (Fig. 4-2). This cDNA sequence includes all of the 5' UTR, protein coding sequence, and the majority (minus the terminal 293 nucleotides) of the 3' UTR from native murine TNF- α mRNA (Semon *et al.*, 1987)

The Pst I - Bam HI flanked murine TNF- α cDNA fragment of pUC-9-TNF- α was directionally cloned into pBluescript II /KS⁺ (Stratagene; La Jolla,

CA) to produce pBluescript/KS⁺-mTNF- α . The TNF- α cDNA was then recovered from pBluescript/KS⁺-mTNF- α as a Hind III - Not I flanked fragment and directionally subcloned into the eukaryotic expression vector pRc/CMV (InVitrogen; San Diego, CA) to create plasmid pCMV-Ts. Nested restriction digests and sequencing across the ligation junctions confirmed that pCMV-Ts was the desired construct (data not shown). With pCMV-Ts as template, sense murine TNF- α RNA can be generated by bacteriophage T7 RNA polymerase, while antisense TNF- α RNA can be generated by bacteriophage SP6 RNA polymerase (Figure 4-2).

IV.3.4 Determination of apparent K_d values for ASO.

IV.3.4a RNA generation. Plasmid pCMV-Ts was linearized with Xba I to provide template for sense RNA generation, while pCMV-Ts plasmid linearized with Hind III afforded template for antisense RNA generation. Uncapped RNA transcripts were produced *in vitro* using a MEGAscript™ RNA synthesis kit (Ambion). All reactions were assembled according to manufacturer's instructions using 3 μ g of linearized DNA template. After DNase I treatment to degrade the template, RNA was recovered from the reaction by standard phenol:chloroform:isoamyl extraction followed by two rounds of precipitation from ethanol in the presence of 2.5M ammonium acetate. Precipitated RNA was resuspended in DEPC-treated water, and aliquots subjected to UV absorption spectroscopy for quantitation. Transcripts were judged to be full length by electrophoretic analysis on formaldehyde-1% agarose gels (Sambrook *et al.*, 1989). RNA was stored in DEPC-water at -20°C prior to use (typically 3-5 days maximum).

IV.3.4b Oligonucleotide labeling. ASO were 5' end-labeled using T4 polynucleotide kinase (GIBCO-BRL; Gaithersburg, MD) and [γ ³²P]-ATP (sp.

act. 6000 Ci/mmol; NEN-DuPont; Boston, MA) according to established protocols (Ausubel *et al.*, 1989). The final oligonucleotide specific activity was approximately 3000 Ci/mmol. Labeled oligonucleotides were purified from unincorporated radioactivity by gel electrophoresis on 22% native polyacrylamide gels run in 44 mM tris-borate, 1 mM EDTA (0.5X TBE). The position of the labeled oligonucleotide band was identified by autoradiography, a gel slice excised, and the oligonucleotide eluted into DEPC-treated water by overnight incubation in a shaker water bath at 37°C.

IV.3.4c Solution hybridization reactions. Hybridization reactions were performed in 0.5 mL screw cap eppendorf tubes (reaction volume 20 μ L). 1 fmol of ASO (~ 6600 cpm) was added to solutions containing RNA (1 fmol - 100 pmol) in hybridization buffer (100 mM NaCl, 10 mM phosphate, pH 7.0; 0.1 mM EDTA). Reactions were incubated for 16 hours in a 37°C water bath. Two drops of mineral oil (Sigma; St. Louis, MO) were placed on the surface of the aqueous layer to prevent evaporation during the incubation.

IV.3.4d Gel electrophoresis to resolve hybridization products. At the end of the hybridization reaction, 4 μ L of loading buffer (15% Ficoll, 0.25% bromophenol blue, 0.25% xylene cyanole FF) was added to the reaction mixture and the entire reaction volume loaded onto a two layer native polyacrylamide gel (top layer 4.5%, bottom layer 20%). Gels were run at 4°C, 75V, for 4 hours in 44 mM Tris-borate, 1 mM EDTA (0.5X TBE). Following electrophoresis, gels were wrapped in Saran, and the positions of the free and bound ASO bands were determined by autoradiography. Bands were excised from the gel, and the radioactivity quantitated by Cerenkov counting. Binding curves for each ASO were constructed using the following equation:

$$\text{fraction bound} = \frac{cpm_{\text{bound}}}{(cpm_{\text{bound}} + cpm_{\text{free}})} \quad (4-1)$$

In all cases, the sum of the cpm terms in the denominator was within 10% of the total counts loaded onto the gel. Provided the RNA is in molar excess of the ASO, apparent K_d values can be determined from the concentration of RNA for which the fraction bound equals 0.5. This assay affords determination of K_d values between 0.5 fM and ~ 10 μ M.

IV.3.5 RNase H mapping of ASO binding sites

Uniformly 32 P labeled sense TNF- α mRNA (sp. act. $\sim 2 \times 10^5$ cpm/pmol) was generated from the Xba I linearized pCMV-Ts template using the MEGAscript™ kit and a tracer amount of 32 P-CTP (800 Ci/mmol; NEN-DuPont). Hybridization reactions were assembled (20 μ L total volume) using 500 fmol of labeled RNA and 500 nmol of oligonucleotide in RNase H buffer (20 mM Tris-HCl (pH 7.2), 9 mM MgCl₂, 100 mM KCl, 5 μ g/mL BSA), and allowed to incubate 16 hours at 37°C. Recombinant *E. coli* RNase H (Promega) was added (1.5 U) and the incubation continued for 1 hour at 37°C. RNase loading cocktail was added (final concentration- 80% formamide, 2 mM EDTA, 0.05% bromophenol blue, 0.05% xylene cyanole FF) and the digestion products resolved by denaturing PAGE (4.5% acrylamide/ 8M urea) followed by autoradiography. Fragment relative mobilities were calculated, and apparent sizes determined from a plot of the relative mobilities of known RNA fragment standards (RNA century markers, Ambion).

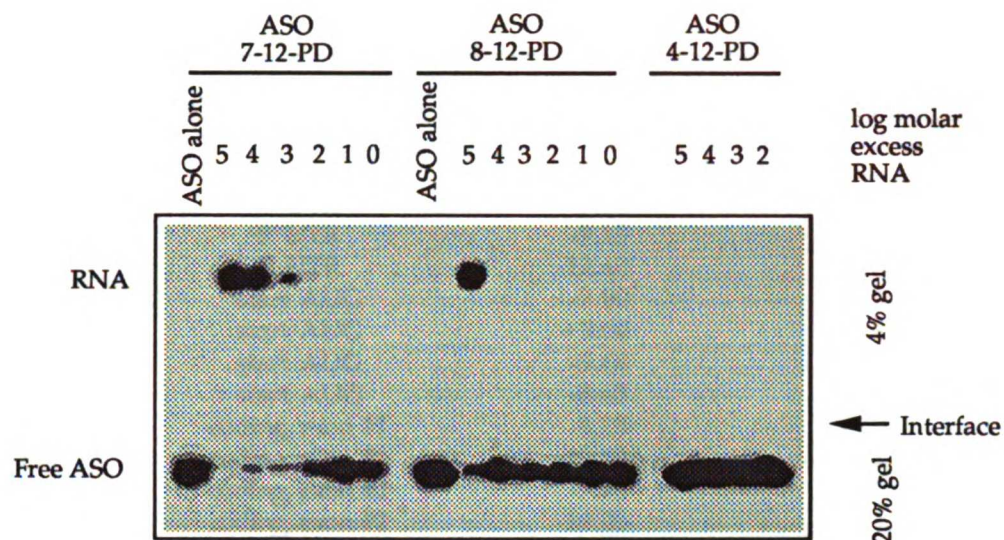
IV.4 RESULTS

IV.4.1 *In vitro* binding of ASO to a cDNA-derived TNF- α mRNA.

As a first approximation of the binding behavior of ASO within a cellular environment, a solution hybridization technique for measuring the apparent dissociation constants of various ASO was developed. In this technique, the *in vitro* binding of the ASO was measured under near physiological conditions while allowing the target RNA to retain higher order structure. Binding of the ASO to the target mRNA was detected using a gel retention assay. Free ASO was separated from bound ASO on a two-phase, low ionic strength polyacrylamide gel system. The binding reactions were performed using a constant amount of ^{32}P 5'-end labeled ASO incubated in the presence of increasing amounts of target RNA. It was thus expected that any free ASO would migrate to the bottom of the gel, while "bound" ASO would co-localize with the RNA band. Figure 4-3a shows the results of a typical hybridization experiment. It can be seen that free ASO is resolved from bound ASO in each of the hybridization reactions where binding occurs.

Excision of the radioactive bands from the acrylamide gel, followed by Cerenkov counting of the bands, allowed quantitation of amounts of ASO migrating in the free and bound bands. This data was then converted into an apparent binding isotherm using equation 4-1 (see Figure 4-3b). Best fit lines to data points in the log-linear regions of the generated isotherms (see Figure 4-3b) were then constructed in order to extract apparent K_d values. The apparent binding constants for each of the 12-mer ASO are listed in Table 4-2. Control binding experiments performed using labeled ASO and a 10^5 molar excess of antisense TNF- α RNA afforded no apparent binding (data not shown).

a



b

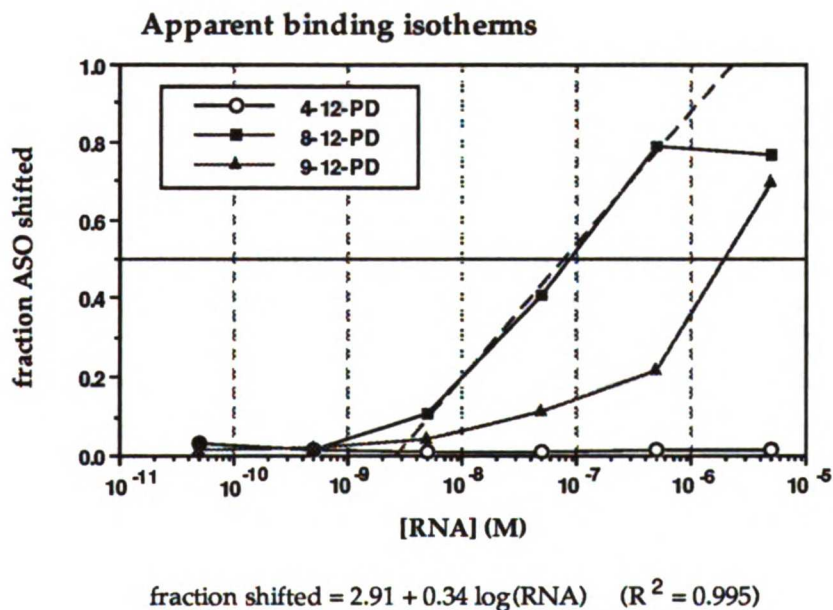


Figure 4-3: Sample autoradiograph and data manipulation from ASO binding experiments. Panel a) Three ASOs were hybridized to the sense TNF- α mRNA derived from pCMV-Ts, and the reactions resolved on the two phase polyacrylamide gel system described in the Methods section. Overnight exposure of the gel produced the autoradiograph shown. Note that ASO 4-12-PD did not bind the sense RNA over the concentrations tested in this assay. Panel b) Bound and free ASO, once located using the autoradiograph, were excised from the gel and counted by Cerenkov counting. Data thus obtained were converted into fraction ASO shifted, and plotted as shown. K_d values were determined by a best fit equation (i.e. least squares fit; denoted by dashed line) to the data points located in the log-linear portion of the apparent binding isotherm (Shown here for ASO 8-12-PD).

Table 4-2: Apparent K_d values for anti-TNF 12-mer ASO

ASO	mRNA target region	Dscore	apparent K_d (μM)
1-12-PD	5' UTR	-10.80	> 10
2-12-PD	5' UTR	-11.55	> 10
3-12-PD	5' UTR	-7.30	> 10
4-12-PD	5' UTR	-9.15	>10
5-12-PD	5' UTR	-12.40	0.5
6-12-PD	start AUG	-7.90	3.0
7-12-PD	start AUG	-9.00	4.0
8-12-PD	start AUG	-9.60	0.09
9-12-PD	start AUG	-8.65	2.0
10-12-PD	coding, exon #1	-8.25	> 10
11-12-PD	coding, exon #1	-12.20	1.6
12-12-PD	coding, exon #2	-7.75	> 10
13-12-PD	coding, exon #2	-10.00	1.5
14-12-PD	splice jxn; exons 2-3	-8.70	9.4
15-12-PD	coding, exon #3	-9.35	6.0
16-12-PD	coding, exon #4	-10.50	4.7
17-12-PD	coding, exon #4	-8.50	> 10
18-12-PD	coding, exon #4	-12.70	2.7
19-12-PD	coding, exon #4	-6.55	> 10
20-12-PD	stop codon	-9.60	> 10
21-12-PD	3' UTR	-9.00	> 10
22-12-PD	3' UTR	-6.00	> 10
23-12-PD	3' UTR	-10.25	> 10
24-12-PD	3' UTR	-7.95	> 10
25-12-PD	3' UTR	-13.00	0.15
26-12-PD	3' UTR Poly A	-3.55	> 10

IV.4.2 RNase H mapping of ASO binding sites.

In order to map where the ASO were binding the mRNA, and to detect any secondary sites of partial or weaker binding, the unlabeled ASO previously shown to bind the TNF- α mRNA were incubated with uniformly radiolabeled TNF- α RNA and subsequently cleaved by RNase H. Cleavage produced fragments from which the ASO binding site could be determined. Table 4-3 shows the results of this experiment. It can be seen that the size of the observed cleavage fragments agrees quite well with the size of the expected cleavage products. Characterization of the apparent binding iso-

Table 4-3: Mapping of ASO binding sites using RNase H

<u>ASO</u>	<u>expected fragment</u>	<u>measured fragment</u>
5-12-PD	181	178 ± 3
6-12-PD	208	208 ± 3
8-12-PD	213	214 ± 3
9-12-PD	217	218 ± 3
11-12-PD	295	296 ± 4
13-12-PD	442	442 ± 7
14-12-PD	451	449 ± 7
15-12-PD	476	477 ± 8
18-12-PD	744	748 ± 18

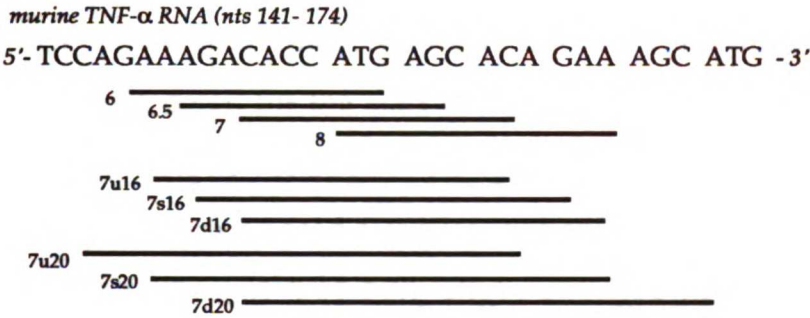
therm for ASO 8-12-PD in the both the hybridization buffer (100 mM NaCl, 10 mM phosphate, pH 7.0; 0.1 mM EDTA) and the RNase H buffer (20 mM Tris-HCl (pH 7.2), 9 mM MgCl₂, 100 mM KCl, 5 µg/mL BSA) indicated no difference in the measured apparent K_d value (data not shown).

IV.4.3 Analysis of ASO binding to the start codon region.

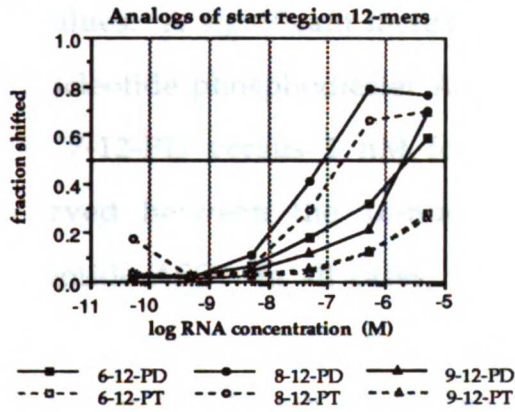
The results of the 12-nucleotide ASO studies suggested the region around the start codon was amenable to binding of ASO, although slight differences in RNA target site position produced significant changes in apparent binding affinity (compare the apparent K_d values for ASO 6-12-PD, 8-12-PD, and 9-12-PD). In order to further characterize this region of the RNA, longer ASO complementary to this region were synthesized (Fig. 4-4). Two phosphodiester ASO (8u-16-PD, 8u-20-PD) were designed to bind the RNA slightly *upstream* of the site for ASO 8-12-PD. Two other phosphodiester ASO (8s-16-PD, 8s-20-PD) were designed to span the target site of ASO 8-12-PD, while two other ASO (8d-16-PD, 8d-20-PD) were designed to bind slightly *downstream* of the site originally bound by ASO 8-12-PD.

Figure 4-4: ASO targeted to start codon region

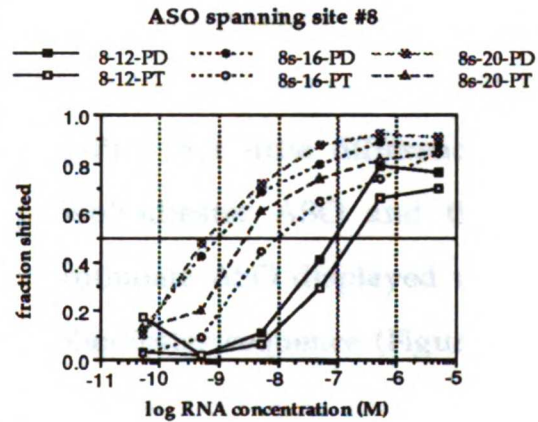
a



b



c



ASO	Oligonucleotide Sequence	RNA binding site	Dscore	diester apparent K_d (nM)	thioate (nM)
6-12	CATG GTGT CTTT	148-159	-7.90	3000	> 5000
7-12	CTCA TGGT GTCT	150-161	-9.00	4000	
8-12	GTGC TCAT GGTG	153-164	-9.60	90	200
9-12	TTCT GTGC TCAT	157-168	-8.65	2000	> 5000
8u-16	GTGC TCAT GGTG TCIT	149-164	-13.10	0.7	
8s-16	CTGT GCTC ATGG TGTC	151-166	-13.55	1	30
8d-16	TTCT GTGC TCAT GGTG	153-168	-12.30	0.8	
8u-20	GTGC TCAT GGTG TCIT TTGT	144-163	-16.00	0.7	
8s-20	TTCT GTGC TCAT GGTG TCIT	149-168	-16.45	0.8	4
8d-20	TGCT TTCT GTGC TCAT GGTG	153-172	-16.85	0.4	

Panel a) Schematic of ASO binding sites. Panel b) Apparent binding isotherms for 12-mer phosphodiester (solid line) and phosphorothioate (dashed line) ASO. Panel c) Apparent binding isotherms for different length (12-, 16-, and 20-mer) ASO spanning target site 8.

Additionally, five phosphorothioate ASO analogs targeted to the same region were synthesized (*i.e.* 6-12-PT, 8-12-PT, 9-12-PT, 8s-16-PT, and 8s-20-PT). In this fashion, the effects upon apparent binding affinity due to slight changes in position and changes due to backbone modifications could be examined in more detail for the start codon region.

Whereas slight changes in position for the 12-nucleotide phosphodiester ASO produced significant changes in apparent K_d values (e. g. 6-12-PD, 8-12-PD, and 9-12-PD), slight changes in position for the 16-nucleotide and 20-nucleotide ASO did not significantly alter their apparent K_d values. A significant increase in affinity was noted when comparing the 12-nucleotide phosphodiester ASO to the 16-nucleotide ASO (e. g. 90 nM for ASO 7-12-PD versus 1 nM for ASO 7s-16-PD), but little difference was observed between the 16-nucleotide phosphodiester ASO and the 20-nucleotide ASO. In all cases, the phosphorothioate ASO displayed weaker affinities than did the corresponding phosphodiester sequence (Figure 4-4). Increasing the length of the phosphorothioate ASO also increased the apparent affinity (e. g. 200 nM for ASO 7-12-PT, 30 nM for ASO 7s-16-PT, and 4 nM for ASO 7s-20-PT).

IV.4.4 Comparison of computed versus empirical affinity constants.

No significant direct correlations were obtained between the computed ΔG°_{duplex} values and the observed apparent binding constants of the twenty five ASO tested (Figure 4-5). ASO with calculated Dscore > -7.75 kcal/mol did not display measurable binding, while those ASO with calculated Dscore < -11.5 kcal/mol did bind. The behavior of ASO with calculated Dscore values between these limits, however, was unpredictable.

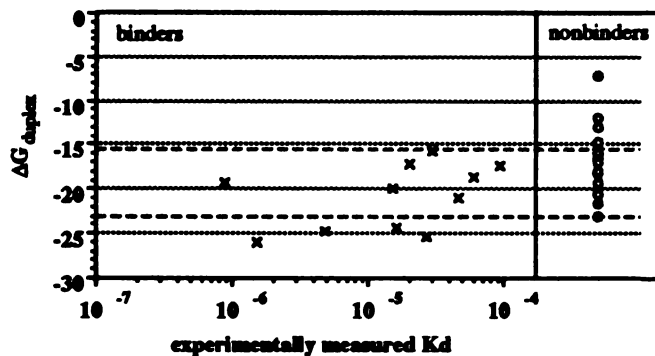


Figure 4-5: Plot of observed binding constants versus calculated $\Delta G^\circ_{\text{duplex}}$. (Note that $\Delta G^\circ_{\text{duplex}} = 2 * \text{Dscore}$). No simple correlations were observed. Examination of binders and nonbinders suggests a possible cutoff of -15.5 kcal/mol required for binding (top dashed line) and a cutoff of -23 kcal/mol to assure binding.

Figure 4-6 shows the binding data presented together with Dscore distribution and frequency information for the TNF- α message. The majority of 12-mer ASO which bound the mRNA were targeted to sites located in the coding region, while those ASO targeted to sites in the 5' UTR or 3' UTR tended not to bind (Fig 4-6, panels a and b). The ability of an ASO to bind the mRNA did not correlate with its Dscore (Fig 4-5), nor with local Dscore minima (Fig 4-6c). While the frequency of the Dscore distribution across the TNF mRNA is approximately bell-shaped, no correlations between Dscore frequency (a crude approximation of sequence complexity) and binding are apparent (Fig 4-6, panels d and e).

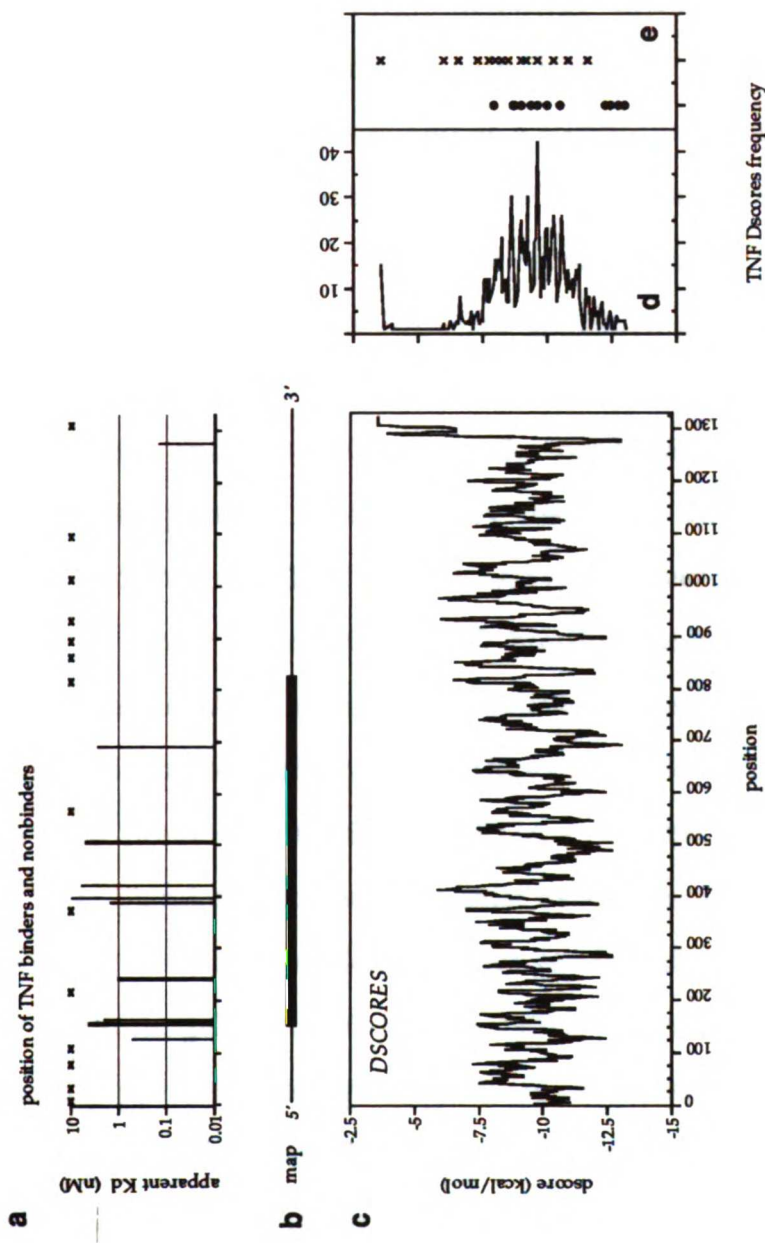


Figure 4-6: Summary of TNF Dscores statistical data. Panel a) Map of ASO binding values versus binding site location. Bar graphs indicate apparent K_d values of ASO which bound; crossed symbols indicate those ASO which did not bind within the limits of the assay. **Panel b)** Schematic map of TNF mRNA. The wide line indicates the coding region of the mRNA. **Panel c)** Dscores profile across the TNF mRNA as a function of position. Note that the minima indicate better Dscore values. **Panel d)** Frequency histogram of Dscore values for the TNF mRNA. **Panel e)** Plot of ASO binders (closed circles) and non-binders (crossed symbols) relative to the frequency histogram.

IV.5 DISCUSSION

These studies were performed in order to determine empirically the apparent affinity of ASO for an RNA target during solution hybridization at near physiological conditions. Various techniques have been employed previously to measure oligonucleotide affinity. Equilibrium dialysis measurements of oligonucleotide binding to structured RNA were performed over twenty years ago as a technique for mapping RNA structure (Eisinger *et al.*, 1970; Högenhauer, 1970; Lewis and Doty, 1970; Uhlenbeck *et al.*, 1970; Uhlenbeck, 1971). Such measurements are perhaps the most rigorous biophysical technique for measuring ligand affinity constants, although processing of large numbers of samples may be difficult. Hybridization and dissociation rates for ASO binding to a 540 nucleotide CAT RNA transcript were measured by means of an RNase-H cleavage assay (Young and Wagner, 1991). That assay, however, relies upon an enzymatic activity in order to measure ASO binding, and therefore is a less direct measurement of ASO affinity. Gel shift assays are routinely used to measure nucleic acid-protein interactions (Revzin, 1989; Lim *et al.*, 1991) and have been used previously to measure RNA structural features (Bhattacharyya *et al.*, 1990). Standardized methods exist by which quantitative parameters such as binding constants, stoichiometries of reactions and cooperativity can be extracted from gel shift data (Carey, 1991). Therefore this technique should be broadly applicable to quantitatively measuring other macromolecular interactions. Indeed, a gel shift assay forms the basis of a study analyzed in detail in Appendix 4 (Lima *et al.*, 1992). Lima and coworkers examined the solution binding of 10-mer ASO to a 47-mer target RNA. A similar solution hybridization technique followed by a gel-shift analysis was reported by Kumazawa and colleagues (1992) while they were developing a purification

scheme for selected tRNA molecules. To date, however, no direct measurements of oligonucleotide affinity constants for solution binding to a structured, full length mRNA have been reported.

IV.5.1 Comments about the gel-shift binding technique.

Due to the size of the target (~1400 ribonucleotides), ASO binding was not expected to significantly alter the migration properties of the RNA. However, a substantial shift in the mobility of the ASO upon binding was expected, provided the two species could be simultaneously resolved. An early report whereby radioactively labeled 4S, 5S, 18S and 28S RNA species from HeLa cells were simultaneously resolved and quantitated suggested a discontinuous acrylamide gel system (3.5%/10%) would afford the required resolution (Zylber and Penman, 1971). In our binding studies, a top layer of 4.5% acrylamide was used to resolve the ASO comigrating with the RNA band, while a bottom layer of 20% acrylamide permitted resolution of free ASO. All gels were run at 4°C and under low salt conditions (0.5X TBE) so as to minimize large changes in salt concentrations which might perturb the binding equilibrium during the gel separation step. Such perturbations would be visible on the autoradiographs as smeared bands between the free ASO and bound ASO bands; in no cases was such a result observed.

In order to approximate ASO binding within cells, solution hybridizations were carried out in phosphate buffer, at neutral pH, 37°C and near physiological ionic strength. The RNA target for ASO binding was transcribed *in vitro* from a TNF- α cDNA construct originally isolated from LPS stimulated RAW 264.7 cells (Caput *et al.*, 1986). Hybridizations were performed for 24 hours so as to allow equilibrium, or an approach to equilibrium, to be established. It is unlikely that ASO which do not display

equilibrium binding to their intended target within this time frame would be useful as biological reagents.

Although an *in vitro* transcribed RNA may not adopt conformations similar to the RNA conformation adopted within cells, one study of 16S RNA has suggested that the secondary structure of the "naked" RNA is a reasonable approximation to that observed in the protein (30S) associated RNA (Moazed *et al.*, 1986). The main caveat with extrapolation of *in vitro* ASO binding to hybridization occurring within the cells is the possibility of occlusion of ASO target regions by RNA binding proteins.

The isotherms from the binding assay, as performed in the limit of RNA excess, do not discriminate single site ASO binding affinities from aggregate site binding affinities, nor do they demonstrate the measured binding constant for the ASO reflects complete hybridization to its intended target site. Aggregate site binding appears unlikely based upon the results of the RNase H mapping studies, where the observed cleavage fragment sizes agreed quite well with the expected fragment sizes. Analysis of the TNF- α mRNA did not reveal continuous homologies of greater than six nucleotides at sites other than the putative target site for each of the ASO sequences, also suggesting that ASO duplex formation at multiple target sites was improbable at best, and unlikely to significantly affect the measured binding constant at worst. Finally, binding experiments using the antisense RNA transcript suggested significant non-specific binding was not occurring over the range of RNA concentrations tested (data not shown).

IV.5.2 Comments about the results of the gel-shift experiments.

The data above demonstrate that phosphorothioate ASO display weaker binding affinities than corresponding phosphodiester ASO. This is to

be expected since it is known that phosphorothioate ASO display decreased T_m and $\Delta G^{\circ}_{binding}$ values relative to their phosphodiester counterparts when hybridizing to complementary oligonucleotides (LaPlanche *et al.*, 1986; Eckers *et al.*, 1992; Freier, 1993). The decrease in apparent affinity of phosphorothioates is likely due to the introduction of a chiral center at each modified phosphorus atom, with consequent effects upon ASO backbone conformation and charge density. When binding to the mRNA, the decrease in affinity observed for the phosphorothioates did not appear to correlate uniformly with the number of modifications (i. e. the length of the ASO), suggesting ASO-specific effects both due to the ASO sequence and possibly to the structure of the RNA at the target site.

It is interesting to note that the majority of ASO which did not show binding to the RNA in our assay were generally targeted to the UTRs of the mRNA, consistent with the notion that these regions may contain relatively strong secondary structures involved in regulation of RNA metabolism. The limited number of secondary structures which have been mapped on various mRNAs generally appear in the RNA UTRs (e.g. the iron response element (IRE) of transferrin and ferritin mRNAs and the TAR element of the HIV-1 RNA transcripts). Similarly, the majority of intermediate binders were targeted to the coding region of the RNA which has been proposed to lack strong stable secondary structures since such structures would block ribosome translocation (Kozak, 1989). The three ASO which bound with the highest affinities bound to diverse regions of the RNA, indicating local relatively accessible regions of the RNA. Closer examination of ASO binding to one of the "hot spots" (i.e. start codon) then afforded determination of phosphodiester and phosphorothioate ASO displaying approximately nanomolar binding constants.

IV.5.3 Comments about the Dscores and ASO binding affinity.

The ASO binding constants determined using the gel-shift technique clearly demonstrate the influence of RNA structure upon ASO hybridization. Target site structure appeared to have a "leveling" effect upon the binding of 12-nucleotide ASO 6-12-PD, 8-12-PD and 9-12-PD, which were all targeted to the start codon region of the TNF RNA-- predicted binding constants differed by a factor of 500, while observed binding constants differed by a factor of 30. Still, such large variations in apparent binding affinity were the result of only minor differences in position along the target RNA. Furthermore, the changes in binding affinity due to slight differences in position appeared to decrease as the length of the ASO increased.

The measured apparent binding constants of ASO directed toward a structured RNA were generally several orders of magnitude weaker than those predicted from the $\Delta G^{\circ}_{duplex}$ values. For example, ASO 8-12-PD is calculated to have a Dscore of -9.60 kcal/mol, or a $\Delta G^{\circ}_{duplex} = -19.2$ kcal/mol. Using the relationship $\Delta G = -RT \ln K_{eq}$, this is equivalent to a $K_d = 29$ fM. The observed apparent K_d for ASO 8-12-PD was measured to be 90 nM, six orders of magnitude weaker than the calculated value. Simple computations using the Dscore to calculate K_d values for ASO binding to unstructured complementary oligonucleotides are in good agreement with experimentally determined K_d values (see Appendix 4, Table A4-3), suggesting the Dscores are valid predictors of binding behavior for hybridization between two complementary unstructured oligonucleotides. The large difference between calculated and observed K_d values of ASO binding to structured RNA then may be attributable to either of the following: partial binding of the ASO to its target, or the influence of RNA structure upon the kinetics of ASO binding.

It is possible that certain ASO were undergoing only partial binding to their intended target site (Ecker *et al.*, 1992). An observed affinity thus measured would not be expected to correlate with a predicted affinity for the entire 12-mer, and detection of such partially bound ASO complexes would require alternate experimental strategies. It is more likely, however, that the large discrepancy illustrated above for ASO 8-12-PD indicates the influence of RNA secondary structure upon ASO binding kinetics. Unstructured oligonucleotides display association rates typically between 10^6 and 10^7 $M^{-1} s^{-1}$ (Riesner and Roemer, 1973), while ASO association rates for binding to known RNA structures range between 10^1 and 10^8 $M^{-1} s^{-1}$ (Freier, 1993). Dissociation rates for ASO are relatively insensitive to target structure, being primarily a function of ASO length and sequence (Freier, 1993). With such a large range in association rates possible, RNA structure will clearly alter the binding behavior of ASO relative to hybridization to an unstructured complement. Thus the Dscore calculations represent the upper limit to apparent K_d values; more often than not, RNA structure will significantly lower the apparent K_d value. Thus any binding computation which does not account for RNA structure will fare poorly as predictive index.

IV.6 CONCLUSIONS

Although antisense oligonucleotides allow facile design of potential therapeutic compounds, rational design of biologically useful ASO remains an elusive goal. In our attempts to devise predictive indices of ASO behavior, we were lead to the conclusion that RNA structure was the ultimate obstacle to ASO effect. The experiments reported in this chapter demonstrate that RNA secondary structure clearly is a formidable obstacle to ASO binding. Our inability to consistently predict binding behavior of ASO

in the absence of structural knowledge of the target RNA suggests that the utility of the Dscores is quite limited. The gel-shift technique developed herein may afford means for empirically locating local regions of the RNA target which are accessible for ASO binding, and thus provide ASO "lead compounds" for further testing. However, by its very nature, the screening technique admits that empirical methods are still the only viable pathways to useful ASO compounds.

Each of the 12-mer ASO tested in the gel-shift assay was screened in biological assays for its ability to inhibit TNF expression. No discernible inhibitory effects were observed for any of the 12-mer ASO in a LPS-stimulated murine macrophage-like cell line (unpublished results). Likewise, the lack of strong *in vitro* expression of TNF protein using a two cell-free translation systems precluded further characterization of these ASO for biological effects. Therefore, the gel-shift technique was used to screen ASO targeted to the firefly luciferase gene. The luciferase data is presented in Chapter 5.

CHAPTER FIVE: Luciferase Messenger Walk-- Evaluation of Antisense Efficacy in a Cell-free Assay

V.1 ABSTRACT

Forty-five 15-nucleotide ASO were evaluated for their ability to solution hybridize to luciferase mRNA under conditions approximating those within cells. The gel-shift assay developed in chapter 4 was used in a screen the ASO for those which bound with an apparent $K_d \leq 5$ nM. Several ASO sequences so screened possessed K_d values slightly weaker than 5 nM. Each of the forty-five ASO were also evaluated for biological efficacy in a rabbit reticulocyte lysate cell-free translation assay. The best binding ASO sequence, 393-15-PD, possessed an apparent $K_d \sim 10$ nM, and showed an $IC_{50} \sim 230$ nM. Several other 15-base ASO targeted toward the start codon region bound in the gel shift assay. Increases in the length of ASO targeted toward this region did not produce substantial changes in the binding properties or biological efficacy of the ASO. Correlations between Dscores and binding behavior or biological efficacy were poor, except when confined to localized regions of the mRNA. The results demonstrate an empirical screening assay for ASO with nanomolar binding constants is successful in isolating biologically effective ASO sequences which may not otherwise have been selected and tested in experimental studies.

V.2 INTRODUCTION

The studies presented in the previous chapters have suggested RNA structure influences the binding behavior of an ASO, and that computational approaches to predicting ASO binding are severely limited in the absence of reliable RNA structural information. An empirical assay for determining apparent ASO binding was developed and presented in chapter 4. This assay

affords a means of screening a panel of ASO targeted to various regions of a target RNA (i.e. a "walk" along the mRNA), in order to determine which ASO sequences which will bind their target. The studies presented in this chapter examine the relationship between apparent ASO binding and biological effect. A sensitive reporter gene, firefly luciferase, was used as the target mRNA in these studies, while biological effects of ASO were evaluated in a cell-free rabbit reticulocyte lysate translation system.

V.3 METHODS

V.3.1 Materials

Plasmid pT3/T7-luc was purchased from Clontech (Palo Alto, CA). Acrylamide-methylene bis acrylamide (premixed, 29:1) was purchased from Boehringer Mannheim (Indianapolis, IN). X-OMAT™ AR film for autoradiography was purchased from Kodak (Rochester, NY). All other chemicals were purchased from Sigma (St. Louis, MO).

V.3.2 Oligonucleotide sequence selection and synthesis

A genomic firefly luciferase sequence (accession number M15077; DeWet *et al.*, 1987) was retrieved from GenBank™ (Bilofsky and Burks, 1988) and trimmed to correspond to the cDNA sequence. This cDNA sequence was then analyzed using the DSCORES program (Chapter 2; Appendix 3). Forty-five 15-mer antisense oligonucleotide sequences targeted to sites along the cDNA encoded mRNA were selected (Table 5-1). All oligonucleotides were synthesized as phosphodiester by Oligos Etc. (Wilsonville, OR), and supplied as lyophilized sodium salts. ASO were resuspended in DEPC-treated pyrogen-free water to a final concentration of 1 mM, as determined by UV absorption spectroscopy using extinction coefficients for each oligonucleotide calculated

Table 5-1: Initial 45 luciferase walk ASO used in screening studies

ASO	Name ^a	ASO sequence (5' -> 3')	position ^b	shift ^c	inhibition ^d	Dscore
1	13-15-PD	ATGTCACTGCGAGCG	13-27	5.4	10.0	-12.95
2	39-16-PD	CATTTTACCAACAGTA	39-54	2.7	20.5	-9.80
3	40-15-PD	CATTTTACCAACAGT	40-54	2.6	28.0	-9.25
4	41-15-PD	CCATTTTACCAACAG	41-55	7.8	42.1	-9.65
5	42-15-PD	TCCATTTTACCAACA	42-56	4.4	31.2	-9.95
6	43-15-PD	TTCCATTTACCAAC	43-57	3.0	37.6	-9.50
7	44-15-PD	CTTCCATTTTACCAA	44-58	4.5	43.2	-9.30
8	46-15-PD	GTCTTCCATTTTACC	46-60	38.0	85.8	-10.15
9	47-15-PD	CGTCTCCATTTTAC	47-61	28.0	81.4	-9.70
10	48-15-PD	GCGTCTTCCATTTTA	48-62	26.9	87.4	-10.35
11	52-15-PD	TTTGGCGTCTTCCAT	52-66	35.9	83.2	-11.70
12	64-15-PD	TTTCTTTATGTTTTT	64-78	1.3	48.8	-6.85
13	79-15-PD	GAATGGCGCCGGGCC	79-93	6.6	6.8	-15.60
14	206-15-PD	GTATTCGCGTACGT	206-220	16.9	77.0	-11.80
15	248-15-PD	ATATCGTTTCATAGC	248-262	1.3	71.5	-9.45
16	249-15-PD	CATATCGTTTCATAG	249-263	1.2	62.9	-8.65
17	250-15-PD	CCATATCGTTTCATC	250-264	1.4	64.9	-9.25
18	308-15-PD	CATAAAGAATTGAAG	308-322	1.0	7.6	-7.80
19	393-15-PD	TCATACTGTTGAGCA	393-407	42.2	88.6	-11.15
20	413-15-PD	TACGGTAGGCTGCGA	413-427	5.6	59.9	-13.55
21	518-15-PD	TCCCTGGTAATCCGT	518-532	20.4	94.1	-12.70
22	672-15-PD	GCGGAAGGGCCACAC	672-686	16.6	61.7	-14.85
23	697-15-PD	GAGAATCTGACGCAG	697-711	14.2	78.0	-11.90
24	799-15-PD	CGAGTGTAGTAAACA	799-813	1.2	55.2	-10.15
25	839-15-PD	CTATACATTAAGACT	839-853	3.0	97.2	-8.60
26	868-15-PD	GGGATCGTAAAAACA	868-882	1.8	58.6	-10.30
27	875-15-PD	TCCTGAAGGGATCGT	875-889	2.2	36.5	-12.81
28	897-15-PD	CAACGCACTTTGAAT	897-911	5.1	93.2	-10.05
29	967-16-PD	CGTGTA AATTAGATAAAT	967-982	1.8	94.0	-9.55
30	980-15-PD	GAAGCAATTTTCGTGT	980-994	3.6	92.1	-10.30
31	993-15-PD	AGGTGCGCCCCCAGA	993-1007	9.8	78.9	-15.65
32	1084-15-PD	ATAGCTGATGTAGTC	1084-1098	1.3	69.7	-10.75
33	1104-15-PD	CCCCCTCGGGTGTA	1104-1118	13.7	56.8	-14.00
34	1126-15-PD	CCGACCGCGCCCGGT	1126-1140	7.0	48.3	-16.20
35	1198-15-PD	CTCTGATTAACGCC	1198-1212	4.2	64.3	-11.75
36	1337-15-PD	GAAGAAGTGTTCGTC	1337-1351	3.5	93.2	-11.00
37	1373-15-PD	TTTGATTTAATTA	1373-1387	1.0	24.0	-5.95
38	1393-15-PD	GCGGGGGCCACCTGA	1393-1407	10.0	67.0	-16.25
39	1400-15-PD	CAATTCAGCGGGGC	1400-1414	7.7	66.3	-13.65
40	1415-15-PD	GTAACAATATCGATTC	1415-1430	4.0	96.8	-9.55
41	1418-16-PD	GTTGTAACAATATCGA	1418-1433	3.4	96.0	-9.90
42	1419-16-PD	GTTGTAACAATATCG	1419-1434	3.8	96.3	-8.75
43	1466-15-PD	GTCATCGTCGGGAAG	1466-1480	1.8	64.8	-12.55
44	1632-15-PD	ACTCCTCCGCGCAAC	1632-1646	10.0	87.6	-14.05
45	1712-15-PD	TGGCCTTTATGAGGA	1712-1726	3.1	80.0	-12.05

^aName indicates position along mRNA-length-ASO type (PD= phosphodiester)

^bIndicates position along mRNA (De Wet *et al.*, 1987)

^cPercent shift in 5 nM gel-shift screening assay (see Methods, Results)

^dPercent inhibition in cell-free transcription-translation assay, ASO at 1 μ M

according to published techniques (Borer, 1974).

V.3.3 *In vitro* RNA synthesis

Uncapped, full length luciferase RNA was produced from Xho I linearized pT7/T3-luc plasmid using a MEGAscript™ *in vitro* RNA synthesis kit (Ambion; Austin, TX). All reactions were assembled according to manufacturer's instructions using 1.5 µg of linearized DNA template. After DNase I treatment to degrade the template, RNA was recovered from the reaction by standard phenol:chloroform:isoamyl extraction followed by two rounds of precipitation from ethanol in the presence of 2.5M ammonium acetate. Precipitated RNA was resuspended in DEPC-treated water, and aliquots subjected to UV absorption spectroscopy for quantitation. Transcripts were judged to be full length by electrophoretic analysis on formaldehyde-1% agarose gels (Sambrook *et al.*, 1989). RNA was stored in DEPC-water at -20°C prior to use (typically 3-5 days maximum).

V.3.4 Oligonucleotide labeling

Oligonucleotides were 5' end-labeled using T4 polynucleotide kinase (GIBCO-BRL; Gaithersburg, MD) and [γ 32 P]-ATP (sp. act. 6000 Ci/mmol; NEN-DuPont; Boston, MA) according to established protocols (Ausubel *et al.*, 1989). The final oligonucleotide specific activity was approximately 3000 Ci/mmol. Labeled oligonucleotides were purified from unincorporated radioactivity by gel electrophoresis on 22% native polyacrylamide gels run in 44 mM tris-borate, 1 mM EDTA (0.5X TBE). The position of the labeled oligonucleotide band was identified by autoradiography, a gel slice excised, and the oligonucleotide eluted into DEPC-treated water by overnight incubation in a water bath at 37°C.

V.3.5 Screening the ASO for binding to luciferase RNA: 5 nM screen

V.3.5a Solution hybridization reactions. Hybridization reactions were performed in 0.5 mL screw cap eppendorf tubes (reaction volume 20 μ L). 1 fmol of ASO (~ 6600 cpm) was added to 100 fmol of RNA in hybridization buffer (100 mM NaCl, 10 mM phosphate, pH 7.0; 0.1 mM EDTA). Reactions were incubated for 16 hours in a 37°C water bath. Two drops of mineral oil (Sigma; St. Louis, MO) were placed on the surface of the aqueous layer to prevent evaporation during the incubation.

V.3.5b Gel electrophoresis to resolve hybridization products. At the end of the hybridization reaction, 4 μ L of loading buffer (15% Ficoll, 0.25% bromophenol blue, 0.25% xylene cyanole FF) was added to the reaction mixture and the entire reaction volume loaded onto a two layer native polyacrylamide gel (top layer 4.5%, bottom layer 20%). Gels were run at 4°C, 75V, for 4 hours in 44 mM Tris-borate, 1 mM EDTA (0.5X TBE). Following electrophoresis, gels were wrapped in Saran, and the positions of the free and bound ASO bands were determined by autoradiography. Bands were excised from the gel, and the radioactivity quantitated by Cerenkov counting. The fraction bound was calculated according to the equation:

$$\text{fraction bound} = \frac{cpm_{\text{bound}}}{(cpm_{\text{bound}} + cpm_{\text{free}})} \quad (5-1)$$

In all cases, the sum of the cpm terms in the denominator was within 10% of the total counts loaded onto the gel. At the ratio of ASO to RNA in this assay (50 pM ASO: 5 nM RNA), a fraction bound = 0.5 corresponds to an apparent K_d of 5 nM.

V.3.6 Measuring the binding isotherms for selected anti-luciferase ASO.

Solution hybridization reactions were performed as described above,

using 1 fmol of ASO added to solutions containing RNA (1 fmol - 10 pmol) in hybridization buffer. After 16 hour incubation, reactions were resolved on the two layer gel-system, the location of the free and bound ASO species determined by autoradiography, and gel-slices counted as described above. Data was analyzed using equation 5-1, and isotherms constructed as described previously (Chapter 4). Apparent K_d values possess an error \pm factor of 2.

V.3.7 *In vitro* translation of luciferase RNA.

Luciferase protein was generated *in vitro* using either the TnT rabbit reticulocyte lysate coupled transcription-translation kit (Promega; Madison WI) or a Retic Lysate IVT™ kit (Ambion). Reactions were assembled (25 μ L total volume) according to manufacturers' instructions, spiked with *E. coli* RNase H (Promega), ASO, and indicated amounts of luciferase plasmid (T3/T7-luc) or uncapped luciferase mRNA. Luciferase activity was determined directly from a 10 μ L aliquot of the translation reaction. The sample to be assayed was added to 100 μ L of luciferase assay reagent (20 mM tricine, 1.07 mM $(\text{MgCO}_3)_4\text{Mg}(\text{OH})_{2.5}\cdot\text{H}_2\text{O}$, 2.67 mM MgSO_4 , 0.1 mM EDTA, 33.3 mM DTT, 270 μ M coenzyme A, 470 μ M luciferin, 530 μ M ATP; final pH 7.8). Relative light units of luciferase activity were measured on a Opticompt luminometer (MGM instruments; Hamden, CT), and converted into percent inhibition relative to a control reaction lacking ASO. In the translation assays, only full length luciferase protein is functionally active (Promega Technical Guide).

V.4 RESULTS

V.4.1 Gel-shift screen for ASO with tight binding and potent inhibition

V.4.1a Walking along the luciferase message. As an initial screen for satisfactory binding, forty-five 15-base phosphodiester ASO were synthesized

that were complementary to various regions of the luciferase mRNA. By “walking” along the message at approximately 80-100 base intervals, it was expected that some of the ASO would be targeted to regions of the mRNA possessing minimal structure, and therefore be capable of binding. Several areas of the mRNA, particularly the start codon region, were selected for shorter steps in the binding walk. It was anticipated that a biologically useful ASO would require an apparent $K_d \leq 50$ nM; therefore, a 5 nM cut-off was established for the initial screening condition.

Figure 5-1 shows the results of the 5 nM gel-shift screening assay. It can be seen that several ASO displayed fractions bound > 0.25 (e.g. ASO 46-15-PD; 47-15-PD; 48-15-PD; 393-15-PD). Background for this assay is a fraction bound ~ 0.05 , based upon the binding of an anti-TNF- α ASO sequence not-complementary to luciferase (data not shown). No ASO screened in this experiment produced a fraction bound ≥ 0.5 , indicating none of the ASO tested possessed an apparent $K_d \leq 5$ nM. Sequence 393-15-PD possessed the best binding profile of the ASO screened, with a fraction bound ~ 0.43 . Other local hot spots determined by gel shift included ASO targeted near the start codon (46-15-PD, 47-15-PD, 48-15-PD, 52-15-PD), a sequence in exon two (206-15-PD), and several sequences in exon three (518-15-PD, 672-15-PD, and 697-15-PD).

V.4.1b *In vitro* translation of luciferase in the presence of the luciferase walk ASO. In order to evaluate the relationship between the gel-shift binding screen and biological activity of the anti-luciferase ASO, each of the forty-five ASO screened for binding was tested for its capacity to inhibit luciferase expression in coupled transcription-translation cell-free assay. In these reactions, 0.5 μ g of luciferase plasmid DNA was transcribed using T3 bacteriophage polymerase, and translated in rabbit reticulocyte lysates spiked with exogenous *E. coli* RNase H and ASO to a final concentration of 1 μ M. Data

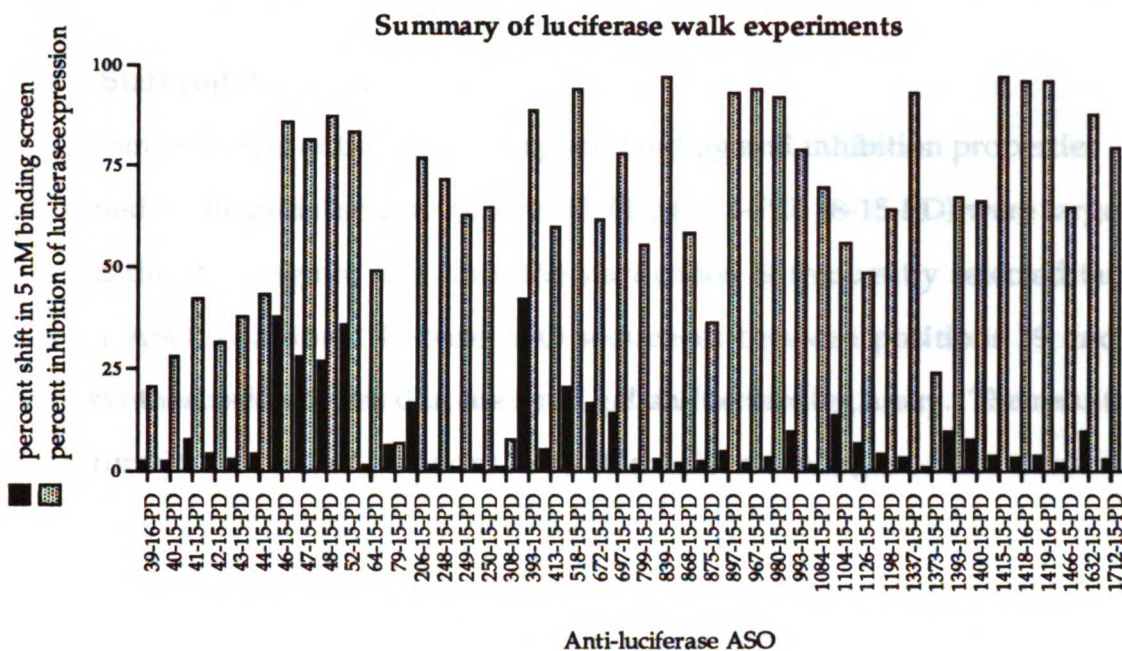


Figure 5-1: Summary of luciferase walk experiments. The fraction of ASO bound in the 5 nM binding screen assay is denoted by the black bars. Note that a fraction bound = 0.5 is equivalent to a $K_d = 5$ nM. The percent inhibition attributable to each ASO in the translation assay is denoted by the gray bars. In this assay, 0.5 μ g of DNA template is added to a coupled transcription-translation reaction incubated at 30°C for 90 minutes in the presence of 1 μ M ASO and 2 U RNase H.

from one such experiment is presented in Figure 5-1. All ASO which displayed fractions bound > 0.1 in the binding assay inhibited luciferase expression $> 60\%$ (e.g. ASO targeted to sites 46, 47, 48, 52, 206, 393, 518, 672, 697, 993, 1104, 1393, and 1632). Likewise, several ASO which did not bind in the gel-shift assay inhibited luciferase expression $< 40\%$ (e. g. ASO 39-13-PD, 40-14-PD, 42-15-PD, 43-15-PD, 79-15-PD, 308-15-PD, 875-15-PD, and 1373-15-PD). However, at 1 μ M concentration, many ASO which did not bind in the gel-shift assay displayed significant inhibition of luciferase expression *in vitro*, some $> 90\%$ (e. g. ASO 897-15-PD, 967-15-PD, 980-15-PD, 1337-15-PD, 1415-15-PD, 1418-15-PD, and 1419-15-PD). This suggests a saturation of the system at these relatively high

V.4.2 Start codon region saturation

Since several of the ASO with good binding and inhibition properties identified in the initial screens (e.g. 46-15-PD; 47-15-PD; 48-15-PD) were targeted toward the start region, and since the start codon is frequently selected target site for ASO, additional 15-base ASO sequences between positions 39 and 58 were synthesized and tested in the 5 nM gel-shift screening assay. The results of the saturation screen for positions 39 to 58 are shown in Figure 5-2a. An abrupt change in apparent binding affinity between positions 43 and 45 is noticeable, suggesting a change in the RNA secondary structure near the start codon (located at position 52).

Figure 5-2: Binding and biological properties of ASO targeted to the luciferase start codon. Panel a) Results of binding 5 nM gel-shift assay for 15-base ASO. **Panel b)** Results of translation inhibition studies with several of the 15-mer ASO in the start region. Reaction conditions: 6.4 nM RNA, 75 μM ASO, 1 U RNase H, 30°C for 90 min. Note that start codon is at position 52.

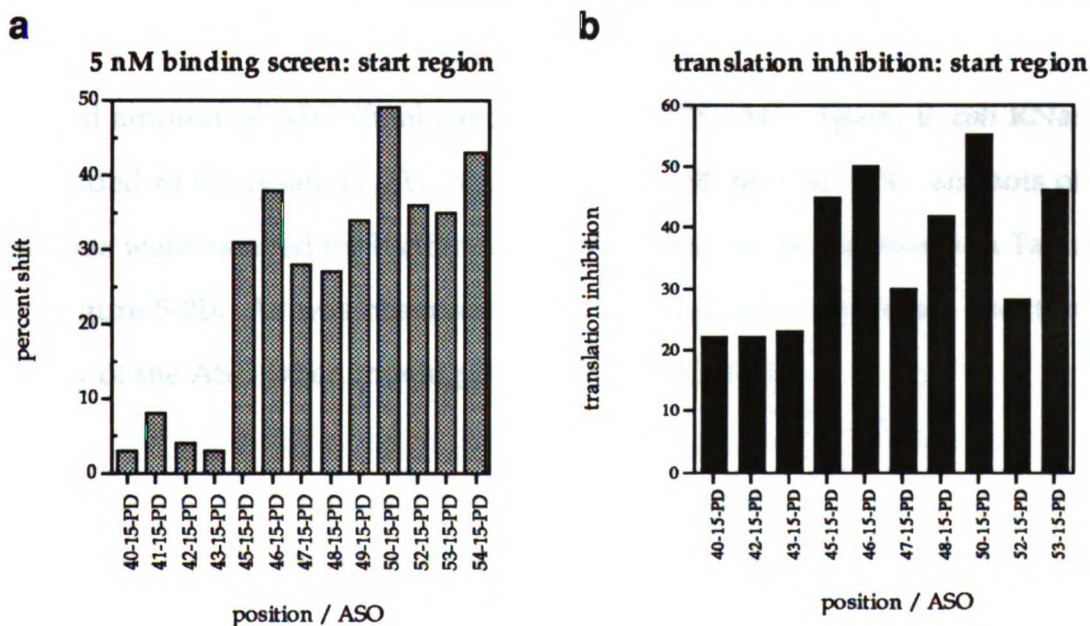


Table 5-2: Walking around the luciferase mRNA start codon region

<u>ASO</u>	<u>Sequence</u> (5' -> 3')	<u>position</u>	<u>percent bound at</u> <u>5 nM</u>	<u>percent luciferase inhibition^a</u>
40-15-PD	CATTTTACCAACAGT	40-54	2.6	22
42-15-PD	TCCATTTTACCAACA	42-56	4.4	22
43-15-PD	TTCCATTTACCAAC	43-57	3.0	23
45-15-PD	TCTTCCATTTTACCA	45-59	31	45
46-15-PD	GTCTTCCATTTTACC	46-60	38	50
47-15-PD	CGTCTCCATTTTAC	47-61	28	30
48-15-PD	GCGTCTTCCATTTTA	48-62	27	42
50-15-PD	TGGCGTCTTCCATTT	50-64	49	55
52-15-PD	TTTGGCGTCTTCCAT	52-66	36	28
53-15-PD	TTTTGGCGTCTTCCA	53-67	35	46

^aReaction conditions: $V_t = 25 \mu\text{L}$; 6.4 nM RNA, 75 nM ASO, 1 U Rnase H; rabbit reticulocyte lysate (Ambion), 30°C, 90 min.

Several of these ASO were tested for biological effects in a rabbit reticulocyte lysate translation assay. Unlike the initial inhibition screen, in which 1 μM ASO was added to 0.5 μg of DNA template in a coupled transcription-translation assay, these reactions were performed using a defined amount of uncapped luciferase RNA (final concentration of 6.4 nM) and a reduced amount of ASO (final concentration of 75 nM). Again, *E. coli* RNase H was added to the lysate (1.0 U/reaction). After 90 min. at 30°C, aliquots of the reactions were assayed for luciferase activity. The results are shown in Table 5-2 and Figure 5-2b. As was observed in the binding assay, there is a boost in the activity of the ASO when moving from position 43 to 45.

V.4.3 Selected isotherms and dose-response studies

V.4.3a ASO 393-15-PD. The best binding ASO from the initial screen, ASO 393-15-PD, was selected for further analyses in the binding and translation

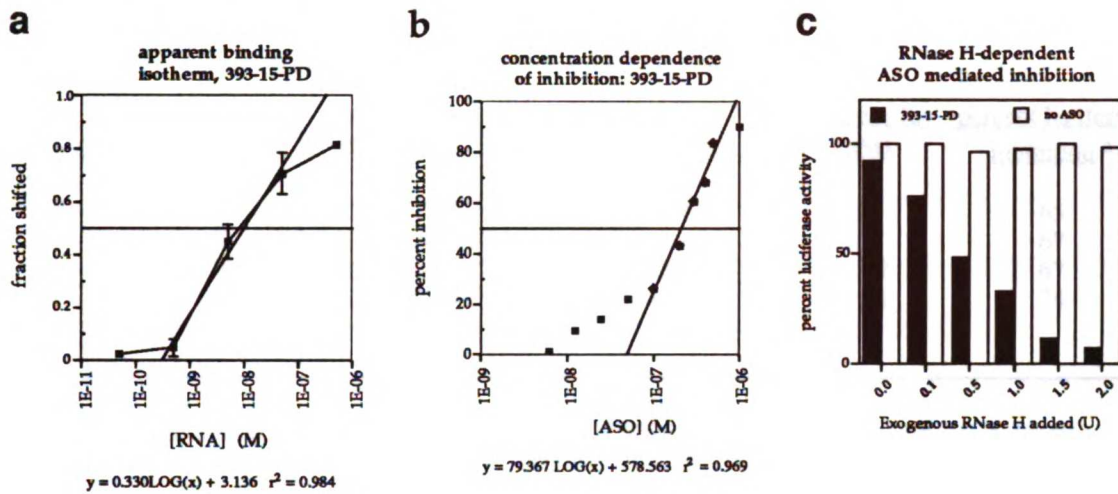


Figure 5-3: Apparent K_d , IC_{50} , and RNase-H dependence of ASO 393-15-PD activity. The apparent K_d for ASO 393-15-PD was measured to be ~10nM (panel a). This ASO inhibited luciferase expression (0.5 μ g plasmid, 2U Rnase-H) at about 230 nM (panel b). Inhibition was largely RNase-H dependent (panel c).

inhibition assays. A binding isotherm for this ASO was generated (Figure 5-3a), and its dose-response profile determined in the translation inhibition assay (Figure 5-3b). The apparent K_d of 393-15-PD was determined to be 10 nM from the measured binding isotherm. In the cell-free translation assay, this ASO inhibited luciferase expression in a dose-dependent fashion, with an IC_{50} of about 230 nM in the coupled transcription-translation assay. This inhibition was dependent upon both the amount of ASO present, and upon the amount of RNase H added to the rabbit reticulocyte assay (Figure 5-3c). It can be seen that at 1 μ M ASO, about 7% inhibition of luciferase expression is observed in the absence of exogenously added RNase H. As reticulocyte lysates are generally devoid of RNase H activity (Minshull and Hunt, 1986; Walder and Walder, 1988), this 7% inhibition is due to a non-RNase H specific mode of inhibition.

V.4.3.b Longer start region ASO. As many ASO tested in the region of

Table 5-3: Effect of ASO length upon apparent affinity and inhibitory capacity

ASO	Sequence (5' -> 3')	position	apparent K_d (nM)	percent luciferase inhibition ^a
49-14-PD	GCGTCTCCATTTT	49-62	25	65
49-16-PD	TGGCGTCTCCATTTT	49-64	13	67
48-17-PD	TGGCGTCTCCATTTTA	48-64	3.2	67
47-19-PD	TTGGCGTCTCCATTTTAC	47-65	2.1	74

^aReaction conditions: 6.4 nM RNA, 75 nM ASO, 1 U RNase H, rabbit reticulocyte lysate, 90 min at 30 °C

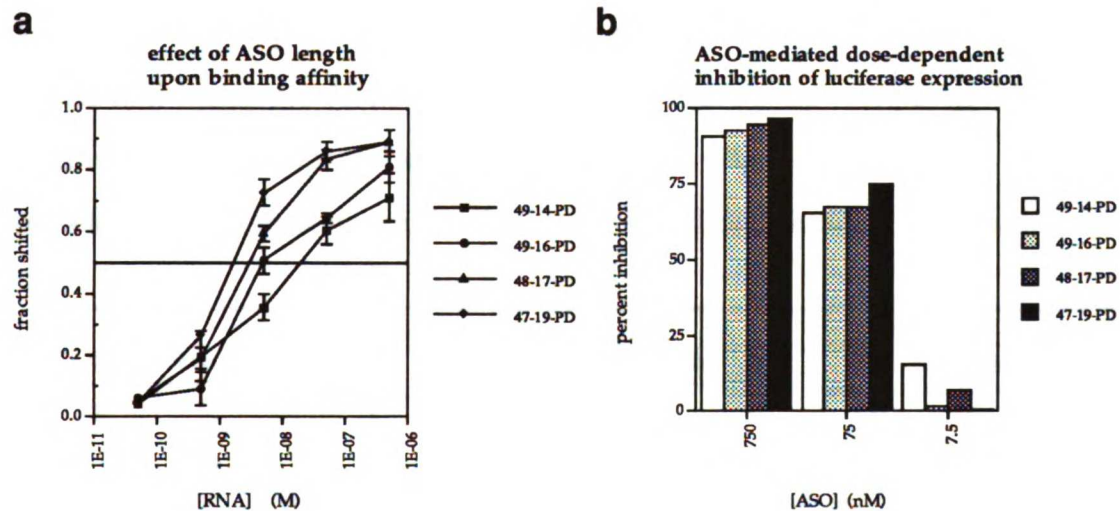


Figure 5-4: Effect of different length ASO targeted to start codon region. Panel a) Apparent isotherms for ASO ranging in length from 14 to 19 bases. Apparent K_d values are reported in Table 5-3. **Panel b)** Dose dependent inhibition of the ASO, where each shows an IC_{50} of ~40 nM. Reaction conditions: 6.4 nM RNA, 1 U RNase H, and indicated concentrations of ASO.

the start codon displayed good binding and inhibition properties, several longer ASO targeted to span the start codon were synthesized in order to investigate the effects of length upon ASO affinity and inhibition capacity (Table 5-3; Figure 5-4). Binding isotherms for these ASO were constructed, and their ability to

inhibit luciferase expression was evaluated in the rabbit reticulocyte lysate translation system in the presence of a defined amount of RNA.

In general, as the length of the ASO increased, so did its apparent binding affinity, ranging from 25 nM to 2 nM. However, the improvement in apparent K_d was at best only an order of magnitude, despite varying the length of the ASO from 14 to 19 bases. Each of the ASO also inhibited luciferase expression in a dose-dependent fashion, with IC_{50} values of approximately 40 nM.

V.4.4 Comparison of binding data, inhibition data, and Dscores

Figure 5-5 shows the correlations between Dscores, fraction bound in the 5 nM screen, and percent inhibition in the translation assay. When considering all the anti-luciferase ASO, it can be seen that there is no correlation between the Dscore and the biological efficacy of the ASO (Fig 5-5b), nor does any simple correlation emerge between the Dscore and fraction bound in the binding assay

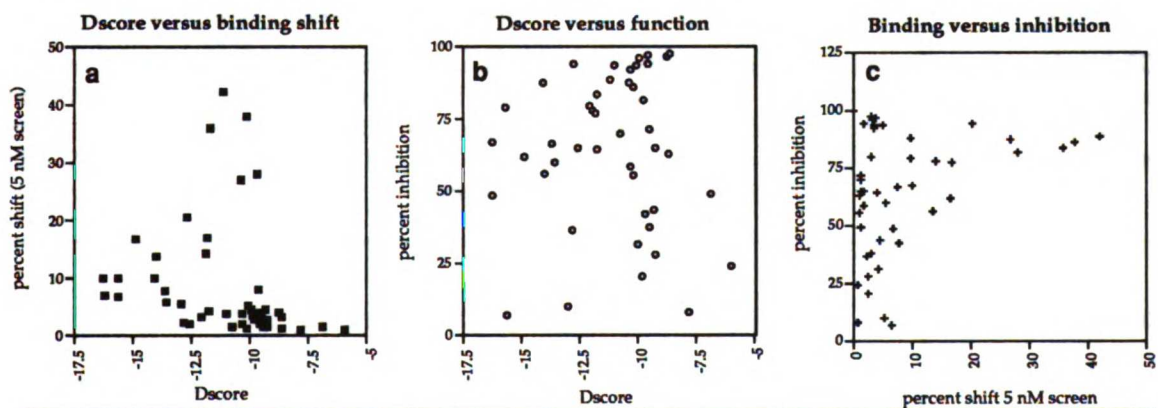
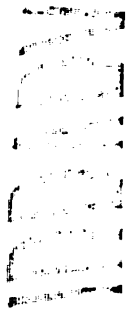
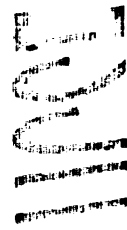


Figure 5-5: Scattergrams for relationships between Dscore, binding data, and inhibition data. No simple linear correlations exist between Dscore and the binding data (panel a), Dscore and the inhibition data (panel b) or binding and inhibition data (panel c). However, it appears that the best binding ASO possess intermediate Dscores (panel a), and that all ASO determined to bind in the gel-shift assay do inhibit luciferase expression (panel c), while all ASO that inhibit luciferase expression did not necessarily bind in the gel-shift assay (panel c).



10c



10c

(Figure 5-5a). It is intriguing to note that the best binding ASO tend to appear in the middle of the range of Dscore values tested. When comparing ASO binding behavior in the screen to functional activity (Fig 5-5c), it is apparent all ASO which bound inhibit luciferase expression. However, as many of the ASO which did not bind in the screen also inhibited expression of luciferase at 1 μ M, no simple correlation emerges.

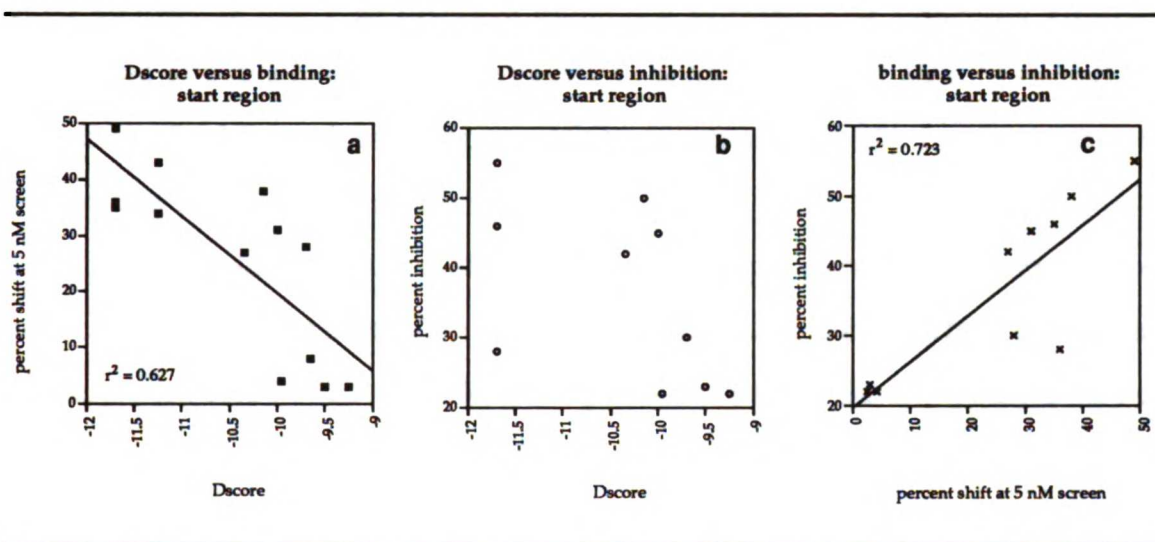


Figure 5-6: Relationships between Dscore, binding data, and inhibition data for ASO targeted to the start codon region of the luciferase mRNA. Dscores correlate with observed binding ($r^2 = 0.627$, $P < 0.002$; panel a) and observed binding correlated with inhibition ($r^2=0.723$, $P < 0.002$; panel c) for ASO targeted to the start codon region. No correlation was observed between Dscore and inhibition for these ASO (panel b).

Examination of the relationships between Dscore, fraction bound, and percent inhibition at a more local level are shown in Figure 5-6. This data is for the 15-base ASO targeted to the start region of the luciferase mRNA. A moderate correlation exists between the Dscore and fraction bound (Fig 5-6a; $r^2 = 0.627$ ($P < 0.002$)). No statistically significant correlation exists between the Dscore and the percent inhibition (Fig 5-6b), while the measured fraction bound does correlate with the percent inhibition for those ten ASO where both prop-

10
11
12
13
14
15
16
17
18
19
20
21
22
23
24
25
26
27
28
29
30
31
32
33
34
35
36
37
38
39
40
41
42
43
44
45
46
47
48
49
50
51
52
53
54
55
56
57
58
59
60
61
62
63
64
65
66
67
68
69
70
71
72
73
74
75
76
77
78
79
80
81
82
83
84
85
86
87
88
89
90
91
92
93
94
95
96
97
98
99
100

101
102
103
104
105
106
107
108
109
110
111
112
113
114
115
116
117
118
119
120
121
122
123
124
125
126
127
128
129
130
131
132
133
134
135
136
137
138
139
140
141
142
143
144
145
146
147
148
149
150
151
152
153
154
155
156
157
158
159
160
161
162
163
164
165
166
167
168
169
170
171
172
173
174
175
176
177
178
179
180
181
182
183
184
185
186
187
188
189
190
191
192
193
194
195
196
197
198
199
200

erties were determined (Fig 5-6c; $r^2 = 0.723$ ($P < 0.002$)).

V.5 DISCUSSION

ASO hybridization to mRNA is a prerequisite to an antisense effect. As numerous ASO sequences are available for a given target mRNA, a screening assay based upon ASO hybridization seems a rational strategy for determining ASO sequences likely to produce biological effects. The screening strategy presented above allows the investigator to select a defined affinity cut-off (in this case, 5 nM), and to compare ASO sequences directly *in vitro* prior to embarking upon cellular and *in vivo* studies.

The message walk, gel-shift binding technique permitted determination of local RNA regions accessible to ASO binding. All the ASO which bound the luciferase mRNA inhibited luciferase expression *in vitro*. Similarly, the extent of ASO binding to overlapping sites in the start region correlated well with ASO biological activity. Experimentally determined isotherms for ASO 393-15-PD correlated with a dose-dependent, RNase-H dependent inhibition of luciferase expression *in vitro* (apparent $K_d \sim 10$ nM versus $IC_{50} \sim 230$ nM).

The unpredictable effects of RNA structure upon ASO binding are clearly indicated in the experiments above. Computational methods for predicting ASO affinity generally did not correlate with ASO binding or activity. However, Dscores did correlate with observed binding for the various ASO targeted to the start codon region. This may reflect that these ASO are all binding to the same local RNA secondary structure. If this were the case, the thermodynamic "penalty" due to RNA structural effects would be similar for each of the ASO tested, so that differences in apparent binding affinity would be primarily due to differences in ASO sequence. Hence an indicator of ASO affinity due to ASO sequence (i.e. Dscore) would adequately predict ASO binding behavior.

However, previous studies (Lima *et al.*, 1992) and the work presented in Chapter 4 indicate slight position differences for ASO targeted to hairpin loops may produce profound effects upon ASO affinity. Thus, as has been concluded in the previous chapters, the Dscore is severely limited in its utility as an *a priori* predictor of ASO binding and efficacy.

The lack of significant length-related changes in ASO binding affinity and efficacy for ASO targeted near the start codon is also consistent with RNA structural effects. This result is suggestive of partial binding of the longer ASO to their target sites due to binding topology (Ecker *et al.*, 1992). In the absence of detailed knowledge of the local RNA secondary and tertiary structure, however, this hypothesis is speculative.

One unexpected effect observed in the initial message walk screen was the large number of ASO which did not display significant binding in the gel-shift assay, yet inhibited expression of luciferase in the coupled transcription-translation assay. This may reflect a non-antisense mediated inhibition of transcription or translation (i. e. triplex, aptamer or non-specific suppression) by the ASO at relatively high concentrations tested in the inhibition screen. The relationship between binding and inhibition is more clearly demonstrated in the start region walk, which was performed using lower concentrations of ASO in a direct translation reaction (i.e. a known amount of RNA titrated directly into the reaction).

Preliminary data indicate that ASO 46-15-PD and 393-15-PD inhibit luciferase expression at approximately 200 nM when delivered with cationic lipids to cells in culture, while ASO 308-15-PD, 839-15-PD, and 1415-15-PD do not inhibit luciferase expression in cells at 200 nM (C. Leamon, personal communication). It is intriguing that those ASO displaying biological effects in cells were those which bound and inhibited expression in the *in vitro* assays,

while those that did not inhibit expression in cells did not bind in the gel-shift assay.

V.6 CONCLUSIONS

The data presented above demonstrate that an empirical gel-shift assay of ASO binding is useful technique for determining ASO sequences capable of inhibiting target gene expression *in vitro*. Preliminary data from cellular systems suggests that the *in vitro* binding behavior of the ASO is a good indicator of biological activity in cells. Therefore, an *in vitro* binding approach may provide the foundation for combinatorial screening strategies designed to elucidate efficacious ASO sequences prior to extensive testing in cells and *in vivo*.

CHAPTER SIX: Main Conclusions of the Thesis Research

The goal of the thesis research was to examine directly the relationship between ASO binding and activity, with the aim of developing methods which might facilitate the selection of ASO sequences likely to produce strong inhibition of target gene expression. The main conclusions derived from these studies using both computational and empirical approaches are summarized below.

Computational approaches to predicting ASO efficacy.

- *Structure prediction algorithms are limited in their utility for predicting ASO binding and efficacy.* The results of the studies presented in Chapter 2 and Appendix 4 clearly demonstrate the weaknesses of current RNA structure prediction algorithms in predicting RNA structure from primary sequence. Even a simple hairpin structure was not correctly predicted by the best of the RNA structure prediction algorithms (Appendix 4). Since it is known RNA structure significantly impacts ASO binding (Chapter 1), thermodynamic calculations based upon predicted structures are only as reliable as the predicted structure is itself.

- *If the RNA structure is known, thermodynamic calculations are reasonable predictors of ASO binding behavior.* A first approach to computing ASO binding behavior to a known RNA structure was developed (Appendix 4). While the models and approach are rather simplistic, the results demonstrate that thermodynamic calculations can reasonably predict ASO binding behavior, once structure and topological considerations are incorporated into the calculations.

- *Dscores may help guide ASO selection, but are not absolute predictors of ASO efficacy.* The Dscore index does provide a guide for estimating one aspect of the thermodynamics of ASO binding, namely a duplex formation potential for two

complementary, unstructured nucleic acid strands. As such, the Dscore may be used to compare the relative merits and faults of a given ASO, based upon its sequence (as opposed to a T_m computed simply by GC/AT content). However, by definition, the Dscore cannot account for the kinetic and thermodynamic effects of RNA structure; thus it cannot be used as a sole predictor of ASO binding behavior (Chapters 2, 4, 5).

Experimental approaches to determining ASO binding and efficacy

The limitations of computational approaches indicated a more empirical technique would be required in order to quantify the relationship between ASO binding and ASO activity. One such technique is the *in vitro* binding assay, developed in Chapter 4. This technique permits the investigator to screen a panel of ASO for sequences displaying strong binding *in vitro*.

- *Relationship between observed binding behavior and observed inhibitory behavior.* The panel of anti-luciferase ASO screened for binding and biological effects demonstrated that ASO determined to bind in the 5 nM screening assay tended to be strong inhibitors in the cell-free translation assay. However, several ASO determined to have apparent K_d values substantially greater than 5 nM (and therefore showed little binding in the 5 nM screening assay) likewise substantially inhibited luciferase expression *in vitro*. Subsequent testing of these ASO suggested they were not inhibiting luciferase expression in cells. This may reflect a non-specific inhibition or an as yet to be elucidated artifact in the cell-free translation system. The results presented in Chapter 3 concerning ASO artifacts in a TNF biological assay are indicative of some of the unexpected problems which may arise when using ASO in biological assays.

- *Further comments about the gel-shift binding technique.* Although the gel-shift binding assay was initially presented as a technique for determining

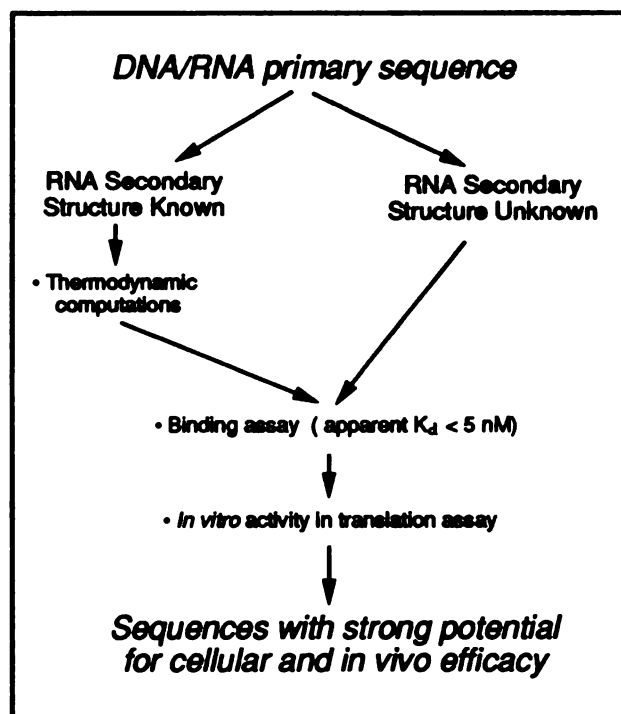
apparent binding isotherms, its utility as a screening tool was demonstrated in Chapter 5. Several ASO sequences determined in this screen to display apparent K_d values near 5 nM were shown to inhibit luciferase expression *in vitro* (Chapter 5). Some of these sequences have been shown to produce inhibitory effects in cells at about 200 nM (C. Leamon, personal communication).

Using *in vitro* techniques to facilitate ASO sequence selection

The work presented in this dissertation demonstrates that while computational predictions of ASO efficacy are still in their infancy, empirical *in vitro* binding and translation assays can be used to determine ASO sequences which will bind their target mRNA and inhibit its expression.

The empirical strategy for ASO sequence selection is summarized in Figure 6-1. Preliminary experiments performed while developing the binding assay demonstrated binding could be detected when the labeled anti-TNF ASO were screened in groups (data not presented). This result suggests that a combinatorial strategy of

Figure 6-1: Schematic of an empirical ASO sequence selection procedure



simultaneously screening multiple sequences for ASO which bind with $K_d \leq 5$ nM may also be feasible. The relatively small amounts of ASO required for the binding assay (a few picomoles) expand the number of sequences an

REFERENCES

- ACHA-ORBEA, H., SCARPELLINO, L., HERTIG, S., DUPUIS, M., and TSCHOPP, J. (1990). Inhibition of lymphocyte mediated cytotoxicity by perforin antisense oligonucleotides. *EMBO J.* 9:3815-3819.
- AGRAWAL, S., GOODCHILD, J., CIVEIRA, M. P., THORNTON, A. H., SARIN, P. S., and ZAMECNIK, P. C. (1988). Oligodeoxynucleoside phosphoramidates and phosphorothioates as inhibitors of human immunodeficiency virus. *Proc. Natl. Acad. Sci. (USA)* 85:7079-7083.
- AGRAWAL, S., MAYRAND, S. H., ZAMECNIK, P. C., and PEDERSON, T. (1990). Site-specific excision from RNA by RNase H and mixed-phosphate-backbone oligodeoxynucleotides. *Proc. Natl. Acad. Sci. (USA)* 87:1401-1405.
- AGRAWAL, S., SARIN, P. S., ZAMECNIK, M., and ZAMECNIK, P. C. (1992). "Cellular uptake and anti-HIV activity of oligonucleotides and their analogs". In *Gene Regulation: Biology of Antisense RNA and DNA*. Erickson, R. P., and Izant, J. G., eds. (Raven Press, New York, 1992). pp. 273-283.
- AIGNER, L. and CARONI, P. (1993). Depletion of 43-kD growth-associated protein in primary sensory neurons leads to diminished formation and spreading of growth cones. *J. Cell. Biol.* 123:417-429.
- AKELLA, R. and HALL, R. E. (1992). Expression of the adhesion molecules ICAM-1 and ICAM-2 on tumor cell lines does not correlate with their susceptibility to natural killer cell-mediated cytotoxicity: evidence for additional ligands for effector cell $\beta 2$ integrins. *Eur. J. Immunol.* 22:1069-1074.
- AKHTAR, S., BASU, S., WICKSTROM, E., and JULIANO, R. J. (1991). Interactions of antisense DNA oligonucleotide analogs with phospholipid membranes (liposomes). *Nucleic Acids Res.* 19:5551-5559.
- ALI, S., DAVIS, M. G., BECKER, M. W., and DORN, G. W. II (1993). Thromboxane A₂ stimulates vascular smooth muscle hypertrophy by up-regulating the synthesis and release of endogenous basic fibroblast growth factor. *J. Biol. Chem.* 268:17397-17403.
- ALMARSSON, Ö. and BRUICE, T. C. (1993). Peptide nucleic acid (PNA) conformation and polymorphism in PNA-DNA and PNA-RNA hybrids. *Proc. Natl. Acad. Sci. (USA)* 90:9542-9546.
- AMARATUNGA, A., MORIN, P. J., KOSIK, K. S., and FINE, R. E. (1993). Inhibition of kinesin synthesis and rapid anterograde axonal transport *in vivo* by an antisense oligonucleotide. *J. Biol. Chem.* 268:17427-17430.
- ANFOSSI, G., GEWIRTZ, A. M., and CALABRETTA, B. (1989). An oligomer complementary to *c-myc*-encoded mRNA inhibits proliferation of human myeloid leukemia cell lines. *Proc. Natl. Acad. Sci. (USA)* 86:3379-3383.
- ARNOTT, S., HUDKINS, D. W. L., and DOVER, S. D. (1972). Optimized parameters for RNA double helices. *Biochem. Biophys. Res. Commun.* 48:1392-1399.
- ASSELIN, U., DELARUE, M., LANCELOT, G., TOULMÉ, F., THUONG, N. Y., MONTENAY-GARESTIER, T., and HÉLÈNE, C. (1984). Nucleic acid-binding molecules with high affinity

and base sequence specificity: Intercalating agents covalently linked to oligodeoxynucleotides. *Proc. Natl. Acad. Sci. (USA)* 81:3297-3301.

AUSUBEL, F. M., BRENT, R., KINGSTON, R. E., MOORE, D. D., SEIDMAN, J. G., SMITH, J. A., and STRUHL, K. (1989). *Current protocols in molecular biology*, John Wiley, New York.

BACON, T.A. and WICKSTROM, E. (1991). Walking along human *c-myc* mRNA with antisense oligodeoxynucleotides: Maximum efficacy at the 5' cap region. *Oncogene Res.* 6:13-19.

BARALLE, F.E. (1977). Complete nucleotide sequence of the 5' noncoding region of rabbit β -globin mRNA. *Cell* 10:549-558.

BARBOUR, S. E. and DENNIS, E. A. (1993). Antisense inhibition of group II phospholipase blocks the production of prostaglandin E₂ by p388D1 cells. *J. Biol. Chem.* 268:21875-21882.

BARUT, B., CHAUHAN, D., UCHIYAMA, H., and ANDERSON, K. C. (1993). Interleukin-6 functions as an intracellular growth factor in Hairy cell leukemia *in vitro*. *J. Clin. Invest.* 92:2346-2353.

BATTEY, J., MOULDING, C., TAUB, R., MURPHY, W., STEWART, T., POTTER, H., LENOIR, G., and LEDER, P. (1983). The human *c-myc* oncogene: Structural consequences of translocation into the IgH locus in Burkitt lymphoma. *Cell* 34:779-787.

BAXTER, G. T., MILLER, D. L., KUO, R. C., WADA, H. G., and OWICKI, J. C. (1992). PKC ϵ is involved in granulocyte-macrophage colony-stimulating factor signal transduction: Evidence from microphysiometry and antisense oligonucleotide experiments. *Biochemistry* 31:10950-10954.

BECKER, D., MEIER, C. B., and HERLYN, M. (1989). Proliferation of human malignant melanomas is inhibited by antisense oligodeoxynucleotides targeted against basic fibroblast growth factor. *EMBO J.* 8:3685-3691.

BECKER, D., LEE, P. L., RODECK, U., and HERLYN, M. (1992). Inhibition of the fibroblast growth factor receptor 1 (FGFR-1) gene in human melanocytes and malignant melanomas leads to inhibition of proliferation and signs indicative of differentiation. *Oncogene* 7:2303-2313.

BENBERNOU, N., MATSIOTA-BERNARD, P., and GUENIUNOU, M. (1993) Antisense oligonucleotides to interleukin-4 regulate IgE and IgG2a production by spleen cells from *Nippostrongylus brasiliensis*-infected rats. *Eur. J. Immunol.* 23:659-663.

BENNETT, C. F., CHIANG, M-Y., CHAN, H., SHOEMAKER, J. E. E., and MIRABELLI, C. K. (1992). Cationic lipids enhance cellular uptake and activity of phosphorothioate antisense oligonucleotides. *Molecular Pharmacol.* 41:1023-1033.

BENNETT, C. F., CONDON, T. P., GRIMM, S., CHAN, H., CHIANG, M-Y. (1994). Inhibition of endothelial cell adhesion molecule expression with antisense oligonucleotides. *J. Immunol.* 152:3530-3540

BENTLEY, D.L. and GROUDINE, M. (1986). Novel promoter upstream of the human *c-myc* gene and regulation of *c-myc* expression in B-cell lymphomas. *Mol. Cell. Biol.* 6:3481-3489.

BEUTLER, E., GELBART, T., HAN, J., KOZIOL, J. A., and BEUTLER, B. (1989). Evolution of the genome and the genetic code: Selection at the dinucleotide level by methylation and polyribonucleotide cleavage. *Proc. Natl. Acad. Sci. (USA)*. 86:192-196.

BHATTACHARYYA, A., MURCHIE, A. I. H., and LILLEY, D. M.. (1990). RNA bulges and the helical periodicity of double-stranded RNA. *Nature (London)* 343:484-487.

BILOFSKY, H.S. and BURKS, C. (1988). The GenBank genetic sequence data bank. *Nucleic Acids Res.* 16:1861-1864.

BIRCHENALL-ROBERTS, M. C., FERRER, C., FERRIS, D., FALK, L. A., KASPER, J., WHITE, G., and RUSCETTI, F. W. (1990). Inhibition of murine monocyte proliferation by a colony stimulating factor-1 antisense oligodeoxynucleotide. *J. Immunol* 145: 3290-3296.

BOIZIAU, C., KURFURST, R., CAZENAVE, C., ROIG, V., THUONG, N. T., and TOULMÉ, J. J. (1991). Inhibition of translation by antisense oligonucleotides via an RNase-H independent mechanism. *Nucleic Acids Res.* 19:1113-1119.

BOIZIAU, C., THUONG, N. T., and TOULMÉ, J. J. (1992). Mechanisms of the inhibition of reverse transcription by antisense oligonucleotides. *Proc. Natl. Acad. Sci. (USA)*. 89:768-772.

BONFILS, E., DEPIERREUX, C., MIDOUX, P., THUONG, N. T., MONSIGNY, M. and ROCHE, A. C. (1992a). Drug targeting: Synthesis and endocytosis of oligonucleotide-neoglycoprotein conjugates. *Nucleic Acids Res.* 20:4621-4629.

BONFILS, E., MENDES, C., ROCHE, A. C., MONSIGNY, M., and MIDOUX, P. (1992b). Uptake by macrophages of biotinylated oligo- α -deoxythymidylate by using mannosylated streptavidin. *Bioconjugate Chemistry* 3:277- 284.

BORER, P. N. (1976). "Optical properties of nucleic acids, absorption, and circular dichroism spectra." In: *Handbook of Biochemistry and Molecular Biology*" Fasman, G., ed. (CRC Press, Cleveland). pp 589.

BORER, P. N., DENGLER, B., TINOCO, I., and UHLENBECK, O. C. (1974). Stability of ribonucleic acid double-stranded helices. *J. Mol. Biol.* 86:843-853.

BORIES, D., RAYNAL, M-C., SOLOMON, D. H., DARZYNKIEWICS, Z., and CAYRE, Y. E. (1989) Down-regulation of a serine protease, myeloblastin, causes growth arrest and differentiation of promyelocytic leukemia cells. *Cell* 59:959-968.

BOUTORIN, A. S., GUSKOVA, L. V., IVANOVA, E. M., KOBETZ, N. D., ZARYTOVA, V. F., RYTE, A. S., YURCHENKO, L. V., and VLASSOV, V. V. (1989). Synthesis of alkylating oligonucleotide derivatives containing cholesterol or phenazinium residues at their 3' terminus and their interaction with DNA within mammalian cells. *FEBS Lett.* 254:129-132.

BOWER, M., SUMMERS, M. F., POWELL, C., SHINOZUKA, K., REGAN, J. B., ZON, G., and W. D. WILSON (1987). Oligodeoxyribonucleoside methylphosphonates. NMR and UV spectroscopic studies of R_p - R_p and S_p - S_p methylphosphonate (Me) modified duplexes of [d[GGAATTCC]]₂. *Nucleic Acids Res.* 15:4915-4930.

BRACH, M. A., GRUSS, H-J, SOTT, C., and HERRMANN, F. (1993). The mitogenic response to tumor necrosis factor alpha requires c-jun/AP1. *Mol. Cell. Biol.* 13:4284-4290.

UJWI LILIMMI

1
2
3
4
5
6
7
8
9
10
11
12
13
14
15
16
17
18
19
20
21
22
23
24
25
26
27
28
29
30
31
32
33
34
35
36
37
38
39
40
41
42
43
44
45
46
47
48
49
50
51
52
53
54
55
56
57
58
59
60
61
62
63
64
65
66
67
68
69
70
71
72
73
74
75
76
77
78
79
80
81
82
83
84
85
86
87
88
89
90
91
92
93
94
95
96
97
98
99
100

101
102
103
104
105
106
107
108
109
110
111
112
113
114
115
116
117
118
119
120
121
122
123
124
125
126
127
128
129
130
131
132
133
134
135
136
137
138
139
140
141
142
143
144
145
146
147
148
149
150
151
152
153
154
155
156
157
158
159
160
161
162
163
164
165
166
167
168
169
170
171
172
173
174
175
176
177
178
179
180
181
182
183
184
185
186
187
188
189
190
191
192
193
194
195
196
197
198
199
200

- BRESLAUER, K. J., FRANK, R., BLOCKER, H., and MARKY, L. A. (1986). Predicting DNA duplex stability from the base sequence. *Proc. Natl. Acad. Sci. (USA)* 83:3746-3750.
- BROSSALINA, E., PASCOLO, E., and TOULMÉ, J. J. (1993). The binding of an antisense oligonucleotide to a hairpin structure via triplex formation inhibits chemical and biological reactions. *Nucleic Acids Res.* 21:5616-5622.
- BROWN, D., YU, Z., MILLER, P., BLAKE, K., WEI, C., KUNG, H-F., BLACK, R. J., TS'O, P. O. P., and CHANG, E. H. (1989) Modulation of *ras* expression by anti-sense, nonionic deoxyoligonucleotide analogs. *Oncogene Res.* 4:243-252.
- BUNNELL, B. A., ASKARI, F. K., and WILSON, J. M. (1992). Targeted delivery of antisense oligonucleotides by molecular conjugates. *Somatic Cell Mol. Genetics.* 18:559-569.
- BURCH, R. M. and MAHAN, L. C. (1991). Oligonucleotides antisense to the interleukin 1 receptor mRNA block the effects of interleukin 1 in cultured murine and human fibroblasts and in mice. *J. Clin. Invest.* 88:1190-1196.
- CACERES, A. and KOSIK, K. S. (1990). Inhibition of neurite polarity by tau antisense oligonucleotides in primary cerebellar neurons. *Nature (London)* 343:461-463.
- CAPUT, D., BEUTLER, B., HARTOG, K., THAYER, R., BROWN-SHIMER, S., and CERAMI, A. (1986). Identification of a common nucleotide sequence in the 3'-untranslated region of the mRNA molecules specifying inflammatory mediators. *Proc. Natl. Acad. Sci. (USA)*. 83:1690-1674.
- CARACCILO, D., VALTERI, M., VENTURELLI, D., PESCHLE, C., GERWITZ, A. M. and CALABRETTA, B. (1989). Lineage specific requirements of *c-abl* function in normal hematopoiesis. *Science* 295:1107-1110.
- CARYE, J. (1991). Gel Retardation. *Methods. Enzymol.* 208:103-117.
- CARUTHERS, M. H., BEATON, G., CUMMINS, L., DELLINGER, D., GRAFF, D., MA, Y-X., MARSHALL, W. S., SASMOR, H., SHANKLAND, P., WU, J. V., and YAU, E. K. (1991). Chemical and biochemical studies with dithioate DNA. *Nucleosides and Nucleotides.* 10:47-59.
- CASTRILLO, J-L., THEILL, L. E., and KARIN, M. (1991). Function of the homeodomain protein GHF1 in pituitary cell proliferation. *Science* 253:197-199.
- CATLETT, J. P., LEFTWICH, J. A., WESTIN, E. H., GRANT, S., and HUFF, T. F. (1991). *c-kit* expression by CD34⁺ bone marrow progenitors and inhibition of response to recombinant human interleukin-3 following exposure to *c-kit* antisense oligonucleotides. *Blood* 78:3186-3191.
- CAZENAVE, C., CHEVRIER, M., THUONG, N. T., and HÉLÈNE, C. (1987). Rate of degradation of [α]- and [β]-oligodeoxynucleotides in *Xenopus* oocytes. Implications for anti-messenger strategies. *Nucleic Acids Res.* 15:10507-10521.
- CAZENAVE, C., LOREAU, N., THUONG, N.T., TOULMÉ, J.J. and HÉLÈNE, C. (1987). Enzymatic amplification of translation inhibition of rabbit β-globin mRNA mediated by anti-messenger oligodeoxynucleotides covalently linked to intercalating agents. *Nucleic Acids Res.* 15:4717-4736.

LIVIGNI

- CHAIASSON, B. J., HOOPER, M. J., MURPHY, P. R., and ROBERTSON, H. A. (1992). Antisense oligonucleotide eliminates *in vivo* expression of *c-fos* in mammalian brain. *Eur. J. Pharmacol.* 227:451-453.
- CHANG, E. H., MILLE, P. S., CUSHMAN, C., DEVADAS, K., PIROLLO, K. F., TS'O, P. O. P., and YU, Z. H. (1991). Antisense inhibition of *ras* p21 expression that is sensitive to a point mutation. *Biochemistry* 30:8283-8286.
- CHAVANY, C., Le DOAN, T., COUVREUR, P., PUISIEUX, F., and HÉLÈNE, C. (1992). Polyalkylcyanoacrylate nanoparticles as polymeric carriers for antisense oligonucleotides. *Pharmaceut. Res.* 9:441-449.
- CHEN, M.-J., SHIMADA, T., MOULTON, A.D., CLINE, A., HUMPHRIES, R.K., MAIZEL, J., and NIENHUIS, A.W. (1984). The functional human dihydrofolate reductase gene. *J. Biol. Chem.* 259:3933-3943.
- CHEUNG, R. K. and DOSCH, H-M. (1991). The tyrosine kinase *lck* is critically involved in the growth transformation of human B lymphocytes. *J. Biol. Chem.* 266:8667-8670.
- CHIANG, M.-Y., CHAN, H., ZOUNES, M.A., FREIER, S.M., LIMA, W.F., and BENNETT, C.F. (1991). Antisense oligonucleotides inhibit intracellular adhesion molecule 1 expression by two distinct mechanisms. *J. Biol. Chem.* 266:18162-18171.
- CHIN, D. J., GREEN, G. A., ZON, G., SZOKA, F. C. Jr., and STRAUBINGER, R. A. (1990) Rapid nuclear accumulation of injected oligodeoxynucleotides. *The New Biologist* 2:1091-1100.
- CITRO G, PERROTTI D, CUCCO C, D'AGNANO I, SACCHI A, ZUPI G, and CALABRETTA B. (1992). Inhibition of leukemia cell proliferation by receptor-mediated uptake of *c-myc* antisense oligodeoxynucleotides. *Proc. Nat. Acad. Sci. (USA)* 15:7031-7035.
- CLARENC, J. P., LEBLEU, B., and LÉONETTI, J. P. (1993). Characterization of the nuclear binding sites of oligodeoxyribonucleotides and their analogues. *J. Biol. Chem.* 268:5600-5604.
- CLARK, M. A., ÖZGÜR, L. E., CONWAY, T. M., DISPOTO, J., CROOKE, S. T., and BOMALASKI, J. S. (1991). Cloning of a phospholipase A2-activating protein. *Proc. Natl. Acad. Sci. (USA)* 88:5418-5422.
- COLBY, W.W., CHEN, E.Y., SMITH, D.H. and LEVINSON, A. (1983). Identification and nucleotide sequence of a human locus homologous to the *v-myc* oncogene of avian myelocytomatosis virus MC29. *Nature (London)* 301:722-725.
- COLLINS, J. F., HERMAN, P., SCHUCH, C., and BAGBY, G. C. (1991). *c-myc* antisense oligonucleotides inhibit the colony-forming capacity of Colo 320 colonic carcinoma cells. *J. Clin. Invest.* 89:1523-1527.
- COLIGE, A., SOKOLOV, B. P., NUGENT, P., BASERGA, R., and PROCKOP, D. J. (1993). Use of an antisense oligonucleotide to inhibit expression of a mutated human procollagen gene (COL1A1) in transfected mouse 3T3 cells. *Biochemistry* 32:7-11.
- COOK, J. L., CHE, L., BHANDARU, S., BAKRIS, G. L., and RE, R. N. (1992). The use of oligonucleotides to establish autocrine angiotensin growth effects in human neuroblastoma and mesangial cells. *Antisense Res. and Devel.* 2:199-210.

COOK, P. D. (1991). Medicinal chemistry of antisense oligonucleotides- future opportunities. *Anti-Cancer Drug Design*. 6:585-607.

COOK, P. D. (1993). Medicinal chemistry strategies for antisense research. In *Antisense Research and Applications* Crooke, S. T., and Lebleu, B., eds. (CRC Press, Boca Raton) pp. 149-187.

COPE, F. and WILLE, J. (1989). Retinoid receptor antisense DNAs inhibit alkaline phosphatase induction and clonogenicity in malignant keratinocytes. *Proc. Natl. Acad. Sci. (USA)* 86:5590-5594 .

COTTEN, M. and BIRNSTEIL, M. L. (1989). Ribozyme mediated destruction of RNA *in vivo*. *EMBO J.* 8:3861-3866.

CROOKE, R. M. (1991). *In vitro* toxicology and pharmacokinetics of antisense oligonucleotides. *Anti-Cancer Drug Design* 6:609-646.

CUMIN, F., ASSELBERGS, F., LARTIGOT, M., and FELDER, E. (1993). Modulation of human prorenin gene expression by antisense oligonucleotides in transfected CHO cells. *Eur. J. Biochem.* 212:347-354.

DAKKA, Y. and WICKSTROM, E. (1990). Target dependence of antisense oligonucleotide inhibition of c-Ha-ras p21 expression and focus formation in T24-transformed NIH3T3 cells. *Oncogene Res.* 5:267-275.

DASH, P., LOTAN, I., KNAPP, M., KANDEL, E. R., and GOELET, P. (1987). Selective elimination of mRNAs *in vivo*: Complementary oligodeoxynucleotides promote RNA degradation by an RNase H-like activity. *Proc. Natl. Acad. Sci. (USA)* 84:7896-7900.

DEAN, N. M., MCKAY, R., CONDON, T. P., and Bennett, C. F. (1994). Inhibition of protein kinase C-alpha expression in human A549 cells by antisense oligonucleotides inhibits induction of intercellular adhesion molecule 1 (ICAM-1) mRNA by phorbol esters. *J. Biol. Chem.* 269:16416-16424.

DEGITZ, K., LIAN-JIE, L. and CAUGHMAN, S.W. (1991). Cloning and characterization of the 5' transcriptional regulatory region of the human intracellular adhesion molecule 1 gene. *J. Biol. Chem.* 266:14024-14030.

DEGOLS, G., LÉONETTI, J-P., MECHTI, N., and LEBLEU, B. (1991). Antiproliferative effect of antisense oligonucleotides directed to the RNA of *c-myc* oncogene. *Nucleic Acids Res.* 19:945-948.

DEGOLS, G., LÉONETTI, J-P., MILHAUD, P., MECHTI, N., and LEBLEU, B. (1992). Antisense inhibitors of HIV: Problems and perspectives. *Antiviral Res.* 17:279-287.

DELIC, J., MORANGE, M., and MAGDELENAT, H. (1993) Ubiquitin pathway involvement in human lymphocyte γ -irradiation -induced apoptosis. *Mol. Cell. Biol.* 13:4875-4883.

DeWET, J. R., WOOD, K. V., DeLUCA, M., HELSINKI, D. R., and SUBRAMANI, S. (1987). Firefly luciferase gene: structure and expression in mammalian cells. *Mol. Cell. Biol.* 7:725-737.

DORSEUIL, O., VAZQUES, A., LANG, P., BERTOGLIO, J., GACON, G., and LECA, G. (1992). Inhibition of superoxide production in B lymphocytes by *Rac* antisense oligonucleotides. *J. Biol. Chem.* 267:20540-20542.

EBBECKE, M., UNTERBERG, C., BUCHWALD, A., STÖHR, S., and WIEGAND, V. (1992). Antiproliferative effects of a c-myc antisense oligonucleotide on human arterial smooth muscle cells. *Basic Res. Cardiol.* 87:585-591

ECKER, D. J. (1993). "Strategies for invasion of RNA secondary structure." In *Antisense Research and Applications*. Crooke, S. T., and LeBleu, B., eds. (CRC Press, Boca Raton) pp. 387-400.

ECKER, D. J., VICKERS, T. A., BRUCE, T. W., FREIER, S. M., JENISON, R. D., MANOHARAN, M., and ZOUNES, M. (1992). Pseudo-half knot formation with RNA. *Science* 257:958-961.

EISINGER, J., FEUER, B., and YAMANE, T. (1970). Luminescence and binding studies of tRNA^{Phe}. *Proc. Natl. Acad. Sci. (USA)*. 65:638-644.

EFSTRATIADIS, A., KAFATOS, F.C. and MANIATIS, T. (1977). The primary structure of rabbit β -globin mRNA as determined from cloned DNA. *Cell* 10:571-585.

FAGARASAN, M. O., AIELLO, F., MUEGGE, K., DURUM, S., and AXELROD, J. (1990). Interleukin 1 induced β -endorphin secretion via *Fos* and *Jun* in AtT-20 pituitary cells. *Proc. Natl. Acad. Sci. (USA)* 87:7871-7874.

FAIELLA, A., ZAPPAVIGNA, V., MAVILIO, F., and BONCINELLI, E. (1994). Inhibition of retinoic acid-induced activation of 3' human HOXB genes by antisense oligonucleotides affects sequential activation of genes located upstream in the four HOX clusters. *Proc. Natl. Acad. Sci. (USA)*. 91:5335-5339.

FARESE, R. V., STABDAERT, M. L., ISHIZUKA, T., YU, B., HERNANDEZ, H., WALDRON, C., WATSON, J., FARESE, J. P., COOPER, D. R., and WICKSTROM, E. (1991). Antisense DNA downregulated protein kinase C isozymes (β and α) and insulin-stimulated 2-deoxyglucose uptake in rat adipocytes. *Antisense Res. and Devel.* 1:35-42.

FISHER, M. E. (1966). Effect of excluded volume on phase transitions in biopolymers. *J. Chem. Phys.* 45:1469-1473.

FLORINI, J. R. and EWTON, D. Z. (1990) Highly specific inhibition of IGF-1-stimulated differentiation by an antisense oligodeoxyribonucleotide to myogenin mRNA. *J. Biol. Chem.* 265:13435-13437.

FLORINI, J. R., EWTON, D. Z., and ROOF, S. L. (1991). Insulin-like growth factor-1 stimulated terminal myogenic differentiation by induction of myogenin gene expression. *Mol. Endo.* 5:718-724

FLORY, P. J. and SEMLYEN, J. A. (1966). Macrocyclization equilibrium constants and the statistical configuration of poly(dimethylsiloxane) chains. *J. Amer. Chem. Soc.* 88:3209-3212.

FLORY, P. J., SUTTER, U. W., and MUTTER, M. (1976). Macrocyclization equilibria. 1. Theory. *J. Amer. Chem. Soc.* 98:5733-5739.

UNIVERSITY OF MICHIGAN

FONAGY, A., SWIDERSKI, C., DUNN, M., and FREEMAN, J. W. (1992). Antisense mediated specific inhibition of p120 protein expression prevents G1 to S phase transition. *Cancer Res.* 52:5250-5256.

FREIER, S.M., KIERZEK, R., JAEGER, J.A., SUGIMOTO, N., CARUTHERS, M.H., NEILSON, T., and TURNER, D.H. (1986). Improved free-energy parameters for predictions of RNA duplex stability. *Proc. Natl. Acad. Sci. (USA)* 83:9373-9388.

FREIER, S. M. (1993). "Hybridization: Considerations affecting antisense drugs". In *Antisense Research and Applications*. Crooke, S. T., and LeBleu, B., eds. (CRC Press, Boca Raton) pp. 67-82.

FROEHLER, B., NG, P., and MATTEUCCI, M. (1988). Phosphoramidate analogues of DNA: Synthesis and thermal stability of heteroduplexes. *Nucleic Acids Res.* 16:4831-4839.

FROEHLER, B., WADWANI, S., TERHORST, T. J., and GERRARD, S. R. (1992). Oligodeoxynucleotides containing C-5 propyne analogs of 2'-deoxyuridine and 2'-deoxycytidine. *Tetrahedron Lett.* 33:5307-5310.

FUJIWARA, T. and GRIMM, E. A. (1992). Specific inhibition of interleukin 1 β gene expression by an antisense oligonucleotide: obligatory role of interleukin 1 in the generation of lymphokine-activated killer cells. *Cancer Res.* 52:4954-4959.

FURUKAWA, Y., PIWNICA-WORMS, H., ERNST, T. J., KANAKURA, Y., and GRIFFIN, J. D. (1990). *cdc2* gene expression at the G₁ to S transition in human T lymphocytes. *Science* 250:805-808.

GARFINKEL, S., HAINES, D. S., BROWN, S., WESSENDORF, J., GILLESPIE, D. H., and MACIAG, T. (1992). Interleukin-1 α mediates an alternative pathway for the antiproliferative action of poly(I \cdot C) on human endothelial cells. *J. Biol. Chem.* 267:24375-24378.

GAZIN, C., DUPONT DE DINECHIN, S., HAMPE, A., MASSON J.-M., MARINT, P., STEHELIN, D., and GALIBERT, F. (1984). Nucleotide sequence of the human *c-myc* locus: provocative open reading frame within the first exon. *EMBO J* 3:383-387.

GEWIRTZ, A. M. and CALABRETTA, B. (1988). A *c-myb* antisense oligodeoxynucleotide inhibits normal human hematopoiesis in vitro. *Science* 242:1303-1306.

GEWIRTZ, A. M., ANFOSSI, G., VENTURELLI, D., VALPREDA, S., SIMS, R., and CALABRETTA, B. (1989). G₁/S transition in normal human T-lymphocytes requires the nuclear protein encoded by *c-myb*. *Science* 245:180-183.

GESELOWITZ, D. A. and NECKERS, L. M. (1992). Analysis of oligonucleotide binding, internalization, and intracellular trafficking utilizing a novel radiolabeled crosslinker. *Antisense Res. Devel.* 2:17-25.

GIOVANNANGELI, C., THUONG, N. T., and HÉLÈNE, C. (1993). Oligonucleotide clamps arrest DNA synthesis on a single-stranded DNA target. *Proc. Natl. Acad. Sci. (USA)* 90:10013-10017.

UNIVERSITY OF TORONTO

GOODCHILD, J., CARROLL, E., and GREENBERG, J.R. (1988). Inhibition of rabbit β -globin synthesis by complementary oligonucleotides: Identification of mRNA sites sensitive to inhibition. *Arch. Biochem. Biophys.* 263:401-409.

GOTOH, O. AND TAGASHIRA, Y. (1981). Stabilities of nearest-neighbor doublets in double-helical DNA determined by fitting calculated melting profiles to observed profiles. *Biopolymers* 20:1033-1042.

HALL, K. B. and McLAUGHLIN, L. W. (1991). Thermodynamic and structural properties of pentamer DNA•DNA, RNA•RNA, and DNA•RNA duplexes of identical sequence. *Biochemistry* 30:10606-10613.

HAN J., ZHU Z., HSU, C., and FINLEY, W. H. (1994) Selection of antisense oligonucleotides on the basis of genomic frequency of the target sequence. *Antisense Res. and Devel.* 4:53-65.

HANVEY, J. C., PEFFER, N. J., BISI, J. E., THOMSON, S. A., CADILLA, R., JOSEY, J. A., RICCA, D. J., HASSMAN, F., BONHAM, M. A., AU, K. G., CARTER, S. G., BRUCKENSTEIN, D. A., BOYD, A. L., NOBLE, S. A., and BABISS, L. E. (1992). Antisense and antigene properties of peptide nucleic acids. *Science* 258:1481-1485.

HAREL-BELLAN, A., FERRIS, D. K., VINCOUR, M., HOLT, J. T., and FARRAR, W. L. (1988a). Specific inhibition of *c-myc* protein biosynthesis using an antisense synthetic deoxyoligonucleotide in human T-lymphocytes. *J. Immunol.* 140:2431-2435.

HAREL-BELLAN, A., DURUM, S., MUEGGE, K., ABBAS, A. K., and FARRAR, W. L. (1988b). Specific inhibition of lymphokine biosynthesis and autocrine growth using antisense oligonucleotides in Th1 and Th2 helper T-cells. *J. Exp. Med.* 168:2309-2318.

HARGROVE J. L., HULSEY M. G., SCHMIDT F. H., and BEALE E. G. (1990) A computer program for modeling the kinetics of gene expression. *BioTechniques* 6:654-659.

HASHIRO, M., MATSUMOTO, K., OKUMURA, H., HASHIMOTO, K., and YOSHIKAWA, K. (1991). Growth inhibition of human keratinocytes by antisense *c-myc* oligomer is not coupled to induction of differentiation. *Biochem. Biophys. Res. Commun.* 174:287-292.

HATZFELD, J., LI, M-L., BROEN, E. L., SOOKEDO, H., LEVESQUE, J-P., O'TOOLE, T., GURNEY, C., CLARK, S. C., and HATZFELD, A. (1991). Release of early human hematopoietic progenitors from quiescence by antisense transforming growth factor β 1 or Rb oligonucleotides. *J. Exp. Med.* 174:925-929.

HEIKKILA, R., SCHWAB, G., WICKSTROM, E., LOKE, S.L., PLUZNICK, D.V., WATT, R., and NECKERS, L.M. (1987). A *c-myc* antisense oligodeoxynucleotide inhibits entry into S phase but not progress from G_0 to G_1 . *Nature (London)* 328:445-449.

HÉLÈNE, C., MONTENAY-GARESTIER, T., SAISON, T., TAKASUGI, M., TOULMÉ, J. J., ASSELINE, U., LANCELOT, G., MAURIZOT, J. C., TOULMÉ, F., and THUONG, N. Y. (1985). Oligodeoxynucleotides covalently linked to intercalating agents: a new class of gene regulatory substances. *Biochimie* 67:777-783.

HERMINE, O., BERU, N., PECH, N., and GOLDWASSER, E. (1991). An autocrine role for erythropoietin in mouse hematopoietic cell differentiation. *Blood* 78:2253-2260.

UNIVERSITY OF MICHIGAN

HERSCHLAG, D. (1991). Implications of ribozyme kinetics for targeting the cleavage of specific RNA molecules *in vivo*: More isn't always better. *Proc. Natl. Acad. Sci. (USA)* 88:6921-6925.

HO, P. T. C., ISHIGURO, K., WICKSTROM, E., and SARTORELLI, A. C. (1991). Non-sequence specific inhibition of transferrin receptor expression in HL-60 leukemia cells by phosphorothioate oligodeoxynucleotides. *Antisense Res. and Devel.* 1:329-342.

HÖGENAUER, G. (1970). The stability of a codon transfer RNA complex. *Eur. J. Biochem.* 12:527-532.

HOLOPAINEN, I. and WOJCIK, W. J. (1993). A specific antisense oligodeoxynucleotide to mRNAs encoding receptors with seven transmembrane spanning regions decreases muscarinic m₂ and (gamma)-aminobutyric acid receptors in rat cerebellar granule cells. *J. Pharmacol. Exp. Therapeutics* 264:423-430

HOLT, J. T., REDNER, R. L., and NIENHUIS, A. W. (1988). An oligomer complementary to *c-myc* mRNA inhibits proliferation of HL-60 promyelocytic cells and induces differentiation. *Mol. and Cell. Biol.* 8:963-973.

HOWARD, F. B. and MILES, H. T. (1984). 2NH₂A•T helices in the ribo- and dexoyribonucleotide series. Structural and energetic consequences of 2NH₂A substitution. *Biochemistry* 23:6723-6731.

HUBER, L. A., de HOOP, M. J., DUPREE, P., ZERIAL, M., SIMONS, K., and DOTTI, C. (1993). Protein transport to the dendritic plasma membrane of cultured neurons is regulated by rab8p. *J. Cell. Biol.* 123:47-55.

INOUE, H., HAYASE, Y., IMURA, A., IWAI, S., MIURA, K., and OHTSUKA, E. (1987). Synthesis and hybridization studies on two complementary nona(2'-O-methyl)ribonucleotides. *Nucleic Acids Res.* 15:6131-6148.

IRIBARREN, A. M., SPROAT, B. S., NEUNER, P., SULSTON, I., RYDER, U., and LAMOND, A. I. (1990). 2'-O-alkyl oligoribonucleotides as antisense probes. *Proc. Natl. Acad. Sci. (USA)* 87:7747-7751.

ITOH, H., MUKOYAMA, M., PRATT, R. E., and DZAU, V. J. (1993). Multiple autocrine growth factors modulate vascular smooth muscle cell growth response to angiotensin II. *J. Clin. Invest.* 91:2268-2274.

JACOBSON, H. and STOCKMAYER, W. H. (1950). Intramolecular reaction in polycondensations. I. Theory of linear systems. *J. Chem. Phys.* 18:1600-1606.

JAEGER, J.A., TURNER, D.H. and ZUKER, M. (1989). Improved predictions of secondary structures for RNA. *Proc. Natl. Acad. Sci. (USA)* 86:7706-7710.

JAROSZEWSKI, J. W., KAPLAN, O., SYI, J-L., SCGESTED, M., FAUSTINO, P. J., and COHEN, J. S. (1990). Concerning antisense inhibition of the multiple drug resistance gene. *Cancer Commun.* 2:287-294.

JASKUSKI, D., de REIL, J. K., MERCER, W. E., CALABRETTA, B., and BASERGA, R. (1988). Inhibition of cell proliferation by antisense oligodeoxynucleotides to PCNA cyclin. *Science* 240:1544-1546.

1. The first part of the document is a list of names and addresses of the members of the committee. The names are listed in alphabetical order, and the addresses are given in full. The list includes the names of the members of the committee, the names of the members of the sub-committee, and the names of the members of the advisory committee. The addresses are given in full, including the street, city, and state.

2. The second part of the document is a list of the names and addresses of the members of the committee. The names are listed in alphabetical order, and the addresses are given in full. The list includes the names of the members of the committee, the names of the members of the sub-committee, and the names of the members of the advisory committee. The addresses are given in full, including the street, city, and state.

JOSEE, J., KAISER, A. D., and KORNBERG, A. (1961). Enzymatic synthesis of deoxyribonucleic acid: VIII. Frequencies of nearest neighbor base sequences in deoxyribonucleic acid. *J. Biol. Chem.* 236:864-875.

KABANOV, A. V., VINOGRADOV, S. V., OVCHARENKO, A. V., KRIVONOS, A. V., MELIK-NUBAROV, N. S., KISELEV, V. I., and SEVERIN, E. S. (1990). A new class of antivirals: Antisense oligonucleotides combined with a hydrophobic substituent effectively inhibit influenza virus reproduction and synthesis of virus-specific proteins in MDCK cells. *FEBS Lett.* 259:327-330.

KAMITORI, S. and TAKUSAGAWA, F. (1992). Crystal structure of the 2:1 complex between d(GAAGCTTC) and the anticancer drug Actinomycin D. *J. Mol. Biol.* 225:445-456.

KANBE, M., ARITA, D., SATOH, T., YOKOYAMA, A., MURAKAWA, Y., KIKUCHI, H., and KANAMARU, R. (1992). Influence on metastasis of the reduction of major histocompatibility complex (MHC) class I gene with an antisense oligonucleotide. *Anti-Cancer Drug Design* 7:341-350

KAWASAKI, A. M., CASPER, M. D., FREIER, S. M., LESNIK, E. A., ZOUNES, M. C., CUMMINS, L. L., GONZALEZ, C., and COOK, P. D. (1993). Uniformly modified 2' deoxy-2'-fluoro phosphorothioate oligonucleotides as nuclease-resistant antisense compounds with high affinity and specificity for RNA targets. *J. Med. Chem.* 36:831-841.

KIBLER-HERTZOG, L., KELL, B., ZON, G., SHINOZUKA, K., MIZAN, S., and WILSON, W. D. (1990). Sequence dependent effects in methylphosphonate deoxyribonucleotide double and triple helical complexes. *Nucleic Acids Res.* 18:3545-3555.

KIBLER-HERTZOG, L., ZON, G., UZNANSKI, B., WHITTIER, G., and WILSON, W. D. (1991). Duplex stabilities of phosphorothioate, methylphosphonate, and RNA analogs of two DNA 14-mers. *Nucleic Acids Res.* 19:2979-2986.

KITADA, S., MIYASHITA, T., TANAKA, S., and REED, J. C. (1993). Investigations of antisense oligonucleotides targeted against *bcl-2* RNAs. *Antisense Res. and Devel.* 3:157-169.

KOCH, A. E., POLVERINI, P. J., KUNKEL, S. L., HARLOW, L. A., DIPIETRO, L. A., ELNER, V. M., ELNER, S. G., and STRIETER, R. M. (1992). Interleukin-8 as a macrophage-derived mediator of angiogenesis. *Science* 258:1798-1801.

KOZAK, M. (1989). Circumstances and mechanisms of inhibition of translation by secondary structure in eukaryotic mRNAs. *Mol. Cell. Biol.* 9:5134-5142.

KRIEG, A. M., GMELIG-MEYLING, F., GOURLEY, M. F., KISCH, W. J., CHRISEY, L. A., and STEINBERG, A. D. (1991). Uptake of oligodeoxyribonucleotides by lymphoid cells is heterogenous and inducible. *Antisense Res. and Develop.* 1:161-171.

KREIG, A. M., TONKINSON, J., MATSON, S., ZHAO, Q., SAXON, M., ZHANG, L-M., BHANJA, U., YAKUBOC, L., and STEIN, C. A. (1993). Modification of antisense phosphodiester oligonucleotides by a 5' cholesterol moiety increases cellular association and improves efficacy. *Proc. Natl. Acad. Sci. (USA)* 90:1048-1052.

KRONMILLER, J. E., UPHOLT, W. B., and KOLLAR, E. J. (1991). EGF antisense oligodeoxynucleotides block murine odontogenesis *in vitro*. *Develop. Biol.* 147:485-488.

KULL, F. C. Jr. and CUATRECASAS, P. (1981). Possible requirement of internalization in the mechanism of *in vitro* cytotoxicity in tumor necrosis serum. *Cancer Res.* 41:4885-4890.

KUMAZAWA, Y., YOKOGAWA, T., TSURUI, H., MIURA, K., and WATANABE, K. (1992). Effect of the higher order structure of tRNAs on the stability of hybrids with oligodeoxyribonucleotides: separation of tRNA by an efficient solution hybridization. *Nucleic Acids Res.* 20:2223-2232.

KUMBLE, K. D., IVERSEN, P. L., and VISHWANATHA, J. K. (1992). The role of primer recognition proteins in DNA replication: inhibition of cellular proliferation by antisense oligodeoxyribonucleotides. *J. Cell Science* 101:35-41.

KUNSCH, C. and ROSEN, C. A. (1993). NF- κ B subunit-specific regulation of the interleukin-9 promoter. *Mol. Cell. Biol.* 13:6137-6146.

LANDRETH, K. S., NARAYANAN, R., and DORSHKIND, K. (1992). Insulin-like growth factor-I regulated pro-B cell differentiation. *Blood* 80:1207-1212

LAPIDOT-LIFSON, Y., PATINKIN, D., PRODY, C. A., EHRlich, G., SEIDMAN, S., BEN-AZIZ, R., BENSELER, F., ECKSTEIN, F., ZAKUT, H., and SOREQ, H. (1992). Cloning and antisense oligodeoxynucleotide inhibition of a human homolog of *cdc2* required in hematopoiesis. *Proc. Natl. Acad. Sci. (USA)*. 89:579-583.

LaPLANCHE, L. A., JAMES, T. J., POWELL, C., WILSON, W. D., UZNANSKI, B., STEC, W. J., SUMMERS, M. F., and ZON, G. (1986). Phosphorothioate-modified oligodeoxyribonucleotides. III. NMR and UV spectroscopic studies of the *R_p-R_p*, *S_p-S_p*, and *R_p-S_p* duplexes, [d[GG₃AATTCC]]₂, derived from diastomeric *O*-ethyl phosphonates. *Nucleic Acids Res.* 14:9081-9093.

LARRICK, J. W. and WRIGHT, S. C. (1990). Cytotoxic mechanism of tumour necrosis factor- α . *FASEB Journal.* 4:3215-3223.

LAWSON, T.G., RAY, B.K., DODDS, J.T., GRIFO, J.A., ABRAMSON, R.D., MERRICK, W.C., BETCH, D.F., WEITH, H.L., and THACH, R.E. (1986). Influence of 5' proximal secondary structure on the translational efficiency of eukaryotic mRNAs and on their interaction with initiation factors. *J. Biol. Chem.* 261:13979-13989.

LEMAÎTRE, M., BAYARD, B., and LEBLEU, B. (1987). Specific antiviral activity of a poly(L-lysine)-conjugated oligodeoxyribonucleotide sequence complementary to vesicular stomatitis virus N protein mRNA initiation site. *Proc. Natl. Acad. Sci. (USA)*. 84:648-652.

LÉONETTI, J. P., RAYNER, B., LEMAÎTRE, M., GAGNOR, C., MILHAUD, P. G., IMBACH, J-L., and LEBLEU, B. (1988). Antiviral activity of conjugates between poly(L-lysine) and synthetic oligodeoxyribonucleotides. *Gene* 72:323-332.

LÉONETTI, J. P., DEGOLS, G., and LEBLEU, B. (1990a). Biological activity of oligonucleotide-poly-(L-lysine) conjugates: Mechanism of cell uptake. *Bioconjugate Chem.* 1:149-153.

LÉONETTI, J. P., MACHY, P., DEGOLS, G., LEBLEU, B., and LESSERMAN, L. (1990b). Antibody-targeted liposomes containing oligodeoxyribonucleotides complementary to viral RNA selectively inhibit viral replication. *Proc. Natl. Acad. Sci. (USA)*. 87:2448-2451.

- LÉONETTI, J. P., MECHTI, N., DEGOLS, G., GAGNOR, C., and LEBLEU, B. (1991). Intracellular distribution of microinjected antisense oligonucleotides. *Proc. Natl. Acad. Sci. (USA)*. 88:2702-2706.
- LETSINGER, R. L., ZHANG, G., SUN, D. K., IKEUCHI, T., and SARIN, P. S. (1989). Cholesteryl-conjugated oligonucleotides: Synthesis, properties, and activity as inhibitors of replication of human immunodeficiency virus in cell culture. *Proc. Natl. Acad. Sci. (USA)* 86:6553-6556.
- LEVY, Y., TSAPIS, A., and BROUET J-C. (1991). Interleukin-6 antisense oligonucleotides inhibit the growth of human myeloma cell lines. *J. Clin Invest.* 88:696-699.
- LEWIN, B. (1990). Chapter 24: "A continuum of sequences includes structural genes". In *Genes IV* (Oxford University Press, New York). p. 475.
- LEWIS, J. B. and DOTY, P. (1970). Derivation of the secondary structure of 5S RNA from its binding of complementary oligonucleotides. *Nature (London)* 225:510-512.
- LIEBHABER, S. A., CASH, F. E., SHAKIN, S. H. (1984). Translationally associated helix-destabilizing activity in rabbit reticulocyte lysate. *J. Biol. Chem.* 259:15597-15602.
- LIM, W. A., SAUER, R. T. and LANDER, A. D. (1991). Analysis of DNA-protein interactions by affinity coelectrophoresis. *Methods Enzymol.* 208:196-211.
- LIMA, W. F., MONIA, B. P., ECKER, D. J., and FREIER, S. M. (1992). Implication of RNA structure on antisense oligonucleotide hybridization kinetics. *Biochemistry* 31:12055-12061.
- LISTERUD, M., BRUSSAARD, A. B., DEVAY, P., COLMAN, D. R., and ROLE, L. W. (1991). Functional contribution of neuronal AChR subunits revealed by antisense oligonucleotides. *Science* 254:1518-1521.
- LIU, Y-C, MARRACCINO, R. L., KENG, P. C., BAMBARA, R. A., LORD, E. M., CHOU, W-G., and ZAIN, S. B. (1989). Requirement for proliferating cell nuclear antigen expression during stages of the Chinese Hamster Ovary cell cycle. *Biochemistry* 28:2967-2974.
- LLEDO, P-M., VERNIER, P., VINCENT, J-D., MASON, W. T., and ZOREC, R. (1993). Inhibition of Rab3b expression attenuates Ca²⁺-dependent exocytosis in rat anterior pituitary cells. *Nature (London)* 364:540-544.
- LOKE, S. L., STEIN, C., ZHANG, X. H., AVIGAN, M., COHEN, J. S., and NECKERS, L. M. (1988). Delivery of *c-myc* antisense phosphorothioate oligodeoxynucleotides to hemopoietic cells in culture by liposome fusion: Specific reduction in *c-myc* protein expression correlated with inhibition of cell growth and DNA synthesis. *Cur. Top. Microbiol. Immunol.* 141:282-289.
- LOKE, S. L., STEIN, C. A., ZHANG, X. H., MORI, K., NAKANISHI, M., SUBASINGHE, C., COHEN, J. S., and NECKERS, L. M. (1989). Characterization of oligonucleotide transport into living cells. *Proc. Natl. Acad. Sci. (USA)*. 86:3474-3478.
- LOUIE, S. W., RAMIREZ, L. M., KREIG, A. M., MALISZEWSKI, C. R., and BISHOP, G. A. (1993). Endogenous secretion of IL-4 maintains growth and Thy-1 expression of a transformed B cell clone. *J. Immunol.* 150:399-406.

1. The first part of the document is a list of names and addresses of the members of the committee. The names are listed in alphabetical order, and the addresses are given in full. The list includes the names of the members of the committee, the names of the members of the sub-committee, and the names of the members of the advisory committee. The addresses are given in full, including the street, city, and state.

2. The second part of the document is a list of the names and addresses of the members of the committee. The names are listed in alphabetical order, and the addresses are given in full. The list includes the names of the members of the committee, the names of the members of the sub-committee, and the names of the members of the advisory committee. The addresses are given in full, including the street, city, and state.

1. The first part of the document is a list of names and addresses of the members of the committee. The names are listed in alphabetical order, and the addresses are given in full. The list includes the names of the members of the committee, the names of the members of the sub-committee, and the names of the members of the advisory committee. The addresses are given in full, including the street, city, and state.

2. The second part of the document is a list of the names and addresses of the members of the committee. The names are listed in alphabetical order, and the addresses are given in full. The list includes the names of the members of the committee, the names of the members of the sub-committee, and the names of the members of the advisory committee. The addresses are given in full, including the street, city, and state.

THE UNIVERSITY OF CHICAGO
LIBRARY
540 EAST 57TH STREET
CHICAGO, ILL. 60637
TEL: 773-936-3700
WWW.CHICAGO.EDU

© 2008 THE UNIVERSITY OF CHICAGO

ALL RIGHTS RESERVED
NO PART OF THIS PUBLICATION
MAY BE REPRODUCED OR
TRANSMITTED IN ANY FORM
OR BY ANY MEANS, ELECTRONIC
OR MECHANICAL, INCLUDING
PHOTOCOPYING, RECORDING, OR
BY ANY INFORMATION STORAGE
AND RETRIEVAL SYSTEM, WITHOUT
PERMISSION IN WRITING FROM
THE UNIVERSITY OF CHICAGO
PRESS

- that blocks DNA synthesis in normal fibroblasts and HeLa cells. *Mol. Cell. Biol.* 11:1372-1381.
- NUSSINOV, R. (1981). Nearest neighbor nucleotide patterns: Structural and biological implications. *J. Biol. Chem.* 256:8458-8462
- NUSSINOV, R. (1984a). Strong doublet preferences in nucleotide sequences and DNA geometry. *J. Mol. Evol.* 20:111-119.
- NUSSINOV, R. (1984b). Doublet frequencies in evolutionary distinct groups. *Nucleic Acids Res.* 12:1749-1763.
- OBERHAUSER, B. and WAGNER, E. (1992). Effective incorporation of 2'-O-methyl-oligoribonucleotides and enhanced cell association through modification with thiocholesterol. *Nucleic Acids Res.* 20:533-538.
- O'KEFFE, S. J., WOLFES, H., KIESSLING, A. A., and COOPER, G. M. (1989). Microinjection of antisense *c-mos* oligonucleotides prevents meiosis II in the maturing mouse egg. *Proc. Natl. Acad. Sci. (USA)*. 86:7038-7042.
- OLSON, W. K. (1975). Configurational statistics of polynucleotide chains. A single virtual bond treatment. *Macromolecules* 8:272-275.
- PARDRIDGE, W. M. and BOADO, R. J. (1991). Enhanced cellular uptake of biotinylated antisense oligonucleotide or peptide mediated by avidin, a cationic protein. *FEBS Lett.* 288:30-32.
- PATINKIN, D., SEIDMAN, S., ECKSTEIN, F., BENSELER, F., ZAKUT, H., and SOREQ, H. (1990). Manipulation of cholinesterase gene expression modulate murine megakaryocytopoiesis *in vitro*. *Mol. Cell. Biol.* 10:6046-6050.
- PATTERSON, B. M., ROBERTS, B. E., and KUFF, E. L. (1977). Structural gene identification and mapping by DNA•mRNA hybrid-arrested cell-free translation. *Proc. Natl. Acad. Sci. (USA)* 74:4370-4374.
- PEPPERKOK, R., LORENZ, P., JAKOBI, R., ANSORGE, W., and PYERIN, W. (1991). Cell growth stimulation by EGF: inhibition through antisense-oligodeoxynucleotides demonstrates important role of casein kinase II. *Experimental Cell Biol.* 197:245-253.
- PEREZ-CASTILLO, A., PIPAÓN, C., GARCÍA, I., and ALEMANY, S. (1993). NGFI-A gene expression is necessary for T-lymphocyte proliferation. *J. Biol. Chem.* 268:19445-19450.
- PERIDES, G., SAFRAN, R. M., REUGER, D. C., and CHARNESSE, M. E. (1992) Induction of the neural cell adhesion molecule and neuronal aggregation by osteogenic protein 1. *Proc. Natl. Acad. Sci. (USA)* 89:10326-10330
- PERLAKY, L., SAIJO, Y., BUSCH, R. K., BENNETT, C. F., MIRABELLI, C. K., CROOKE, S.T., and BUSCH H. (1993). Growth inhibition of human tumor cell lines by antisense oligonucleotides designed to inhibit p120 expression. *Anti-Cancer Drug Design.* 8:3-14.
- PIZZI, M., VALERIO, A., RIBOLA, M., SPANO, P. F., and MEMO, M. (1993). A tau antisense oligonucleotide decreases neuron sensitivity to excitotoxic injury. *NeuroReport* 4:823-826.

1. The first part of the document is a list of names and addresses of the members of the committee. The names are listed in alphabetical order, and the addresses are listed below each name. The list includes names such as Mr. John A. Smith, Mr. James B. Jones, and Mrs. Mary C. White.

2. The second part of the document is a list of the names and addresses of the members of the committee who have been appointed to the various sub-committees. The names are listed in alphabetical order, and the addresses are listed below each name.

3. The third part of the document is a list of the names and addresses of the members of the committee who have been appointed to the various sub-committees. The names are listed in alphabetical order, and the addresses are listed below each name.

- PLEIJ, C. W., RIETVELD, K., and BOSCH, L. (1985). A new principle of RNA folding based on pseudoknotting. *Nucleic Acids Res.* 13:1717-1731.
- POLLIO, G., XUE, P., ZANISI, M., NICOLIN, A., and MAGGI, A. (1993). Antisense oligonucleotide blocks progesterone-induced lordosis behavior in ovariectomized rats. *Molecular Brain Res.* 19:135-139.
- PORCU, P., FERBER, A., PIETRZOWSKI, Z., ROBERTS, C., ADAMO, M., LeROITH, D., and BASERGA, R. (1992). The growth-stimulatory effect of simian virus 40 T antigen requires the interaction of insulin-like growth factor 1 with its receptor. *Mol. Cell. Biol.* 12:5069-5077.
- POTTS, J. D., DAGLE, J. M., WALDER, J. A., WEEKS, D. L., and RUNYAN, R. B. (1991). Epithelial-mesenchymal transformation of embryonic cardiac endothelial cells is inhibited by a modified antisense oligodeoxynucleotide to transforming growth factor β 3. *Proc. Natl. Acad. Sci. USA* 88:1516-1520.
- PROUDFOOT, N.J. (1977). Complete 3' noncoding region sequences of rabbit and human β -globin messenger RNAs. *Cell* 10:559-570.
- RAMANATHAN M., MACGREGOR R. D., and HUNT C.A. (1993). Predictions of effect for intracellular antisense oligodeoxyribonucleotides from a kinetic model. *Antisense Res. and Devel.* 3:3-18.
- RASCHELLA, G., NEGRONI, A., SKORSKI, T., PUCCI, S., NIEBROWSKA-SKORSKA, M., ROMEO, A., and CALABRETTA, B. (1992). Inhibition of proliferation by *c-myc* antisense RNA and oligodeoxynucleotides in transformed neuroecodermal cell lines. *Cancer Res.* 52:4221-4226.
- RATAJCZAK, M. Z., KANT, J. A., LUGER, S. M., HIJYA, H., ZHANG, J., ZON, G., and GEWIRTS, A. M. (1992). *In vivo* treatment of human leukemia in a scid mouse model with *c-myc* antisense oligodeoxynucleotides. *Proc. Natl. Acad. Sci. (USA)* 89:11823-11827.
- REDDY, E. P. (1983). Nucleotide sequence analysis of the T24 human bladder carcinoma oncogene. *Science* 220:1061-1063.
- REED, J. C., STEIN, C., SUBASINGHE, C., HALDAR, S., CROCE, C. M., YUM, S., and COHEN, J. (1990). Antisense-mediated inhibition of BCL2 protooncogene expression and leukemic cell growth and survival: Comparisons of phosphodiester and phosphorothioate oligodeoxynucleotides. *Cancer Res.* 50:6565-6570.
- REVZIN, A. (1989). Gel electrophoresis assays for DNA-protein interactions. *BioTechniques* 7:346-355.
- RIESNER, D. and RÖMER, R. (1973). Chapter 15: "In *Physico-Chemical Properties of Nucleic Acids*" vol 2. Duchesne, J., ed (Academic Press, London) pp. 237-318.
- ROBERTS, R. W. and CROTHERS, D. M. (1992). Stability and properties of double and triple helices: Dramatic effects of RNA or DNA backbone composition. *Science* 258:1463-1446.
- ROBERTUS, J. D., LADNER, J. E., FINCH, J. T., RHODES, D., BROWN, R. S., CLARK, B. F. C., and KLUG, A. (1973). Structure of yeast phenylalanine tRNA at 3Å resolution. *Nature (London)* 250:546-551.

THE UNIVERSITY OF CHICAGO
DIVISION OF THE PHYSICAL SCIENCES
DEPARTMENT OF CHEMISTRY
5708 SOUTH ELLIS AVENUE
CHICAGO, ILLINOIS 60637
TEL: 773-936-5000
WWW.CHEM.UCHICAGO.EDU

1998
1999
2000
2001
2002
2003
2004
2005
2006
2007
2008
2009
2010
2011
2012
2013
2014
2015
2016
2017
2018
2019
2020
2021
2022
2023
2024
2025
2026
2027
2028
2029
2030
2031
2032
2033
2034
2035
2036
2037
2038
2039
2040
2041
2042
2043
2044
2045
2046
2047
2048
2049
2050

ROPERT, C., LAVIGNON, M., DUBERNET, C., COUVREUE, P., and MALVY, C. (1992). Oligonucleotides encapsulated in pH sensitive liposomes are efficient toward friend retrovirus. *Biochem. Biophys. Res. Commun.* 183:879-885.

ROPERT, C., MALVY, C., and COUVREUR, P. (1993). Inhibition of the friend retrovirus by antisense oligonucleotides encapsulated in liposomes: Mechanism of action. *Pharmaceutical Res.* 10:1427-1433.

RUFF, M. R. and GIFFORD, G. E. (1981). Rabbit tumor necrosis factor: Mechanism of action. *Infection and Immunity* 31:380-385.

RUNYAN, R. B., POTTS, J. D., and WEEKS, D. L. (1992). TGF-(beta)3-mediated tissue interaction during embryonic heart development. *Molec. Reproduction and Develop.* 32:152-159.

RYTE, A. S., KARAMYSHEV, V. N., NECHAEVA, M. V., GUSKOVA, Z. V., IVANOVA, E. M., ZARYTOVA, V. F., and VLASSOV, V. V. (1992). Interaction of cholesterol-conjugated alkylating oligonucleotide derivative with cellular biopolymers. *FEBS Lett.* 2:124-126.

SAGATA, N., OSKARSSON, M., COPELAND, T., BRUMBAUGH, J., and VANDEWOUDE, G. F. (1988). Function of *c-mos*-proto-oncogene product in meiotic maturation in *Xenopus* oocytes. *Nature (London)* 335:519-525.

SAISON-BEHMOARAS, T., TOCQUÉ, B., REY, I., CHASSIGNOL, M., THUONG, N. T., and HÉLÈNE, C. (1991). Short modified antisense oligonucleotides directed against *Ha-ras* point mutation induce selective cleavage of the mRNA and inhibit T24 cells proliferation. *EMBO J.* 10:1111-1118.

SAKAKURA, C., HAGIWARA, A., TSUJIMOTO, H., OZAKI, K., SAKAKIBARA, T., OYAMA, T., OGAKI, M., and TAKAHASHI, T. (1994). Inhibition of gastric cancer cell proliferation by antisense oligonucleotides targeting the messenger RNA encoding proliferating cell nuclear antigen. *British J. Cancer* 70:1060-1066.

SALSER, W. (1977). Globin mRNA sequences: Analysis of base pairing and evolutionary implications. *Cold Spring Harbor Symp. Quant. Biol.* 42:985-1002.

SAMBROOK, J., FRITSCH, E. F., and MANIATIS, T. (1989). *Molecular cloning: A laboratory manual*. 2nd ed. Cold Spring Harbor Laboratory Press.

SANGHVI, Y. S. (1993). "Heterocyclic base modifications in nucleic acids and their applications in antisense oligonucleotides". In *Antisense Research and Applications* Crooke, S. T., and Lebleu, B., eds. (CRC Press, Boca Raton) pp. 273-288.

SARIOLA, H., SAARMA, M., SAINIO, K., ARUMÄE, U., PALGI, J., VAAHTOKARI, A., THESLEFF, I., and KARAVANOV, A. (1991). Dependence of kidney morphogenesis on the expression of nerve growth factor receptor. *Science.* 254:571-573.

SAWA, H., SOBEL, B. E., and FUJII, S. (1994). Inhibition of type-1 plasminogen activator inhibitor production by antisense oligonucleotides in human vascular endothelial and smooth muscle cells. *J. Biol. Chem.* 152:3530-3540.

SBURLATI, A. R., MANROW, R. E., and BERGER S. L. (1991). Prothymosin a antisense oligomers inhibit myeloma cell division. *Proc. Natl. Acad. Sci. (USA)* 88:253-257.

1. The first part of the document discusses the importance of maintaining accurate records of all transactions. It emphasizes that proper record-keeping is essential for the integrity of the financial system and for the ability to detect and prevent fraud.

2. The second part of the document outlines the specific requirements for record-keeping, including the need for clear, legible entries and the requirement to retain records for a minimum of seven years. It also discusses the importance of regular audits and the role of internal controls in ensuring the accuracy of the records.

SCHWAB, G., SIEGALL, C. B., AARDEN, L. A., NECKERS, L. M., and NORDAN, R. P. (1991) Characterization of an interleukin-6-mediated autocrine growth loop in the human multiple myeloma cell line, U266. *Blood* 77:587-593.

SEGAL, G. M., SMITH, T. D., HEINRICH, M. C., EY, F. S., and BAGBY, G. C. Jr. (1992). Specific repression of granulocyte-macrophage and granulocyte colony stimulating factor gene expression in interleukin-1 stimulated endothelial cells with antisense oligonucleotides. *Blood* 80:609-616.

SELINFREUND, R. H., BARGER, S. W., WELSH, M. J., and van ELDIK, L. J. (1990). Antisense inhibition of glial S100 β production results in alterations in cell morphology, cytoskeletal organization, and cell proliferation. *J. Cell. Biol.* 111:2021-2028.

SEMON, D., KAWASHIMA, E., JONGENEEL, C. V., SHAKOV, A. N., and NEDOSPASOV, S. A. (1987). Nucleotide sequence of the murine TNF locus, including the TNF-alpha (tumor necrosis factor) and TNF-beta (lymphotoxin) genes. *Nucleic Acids Res.* 15:9083-9084.

SHAKIN, S. H. and LIEBHABER, S. A. (1986). Destabilization of messenger RNA/complementary DNA duplexes by the elongating 80S ribosome. *J. Biol. Chem.* 261:16081-16025.

SHAKIN-ESHELMAN, S.H., and LIEBHABER, S.A. (1986). Influence of duplexes 3' to the mRNA initiation codon on influencing the efficiency of monosome formation. *J. Biol. Chem.* 261:16018-16025.

SHEA, R. G., MARSTERS, J. C., and BISCOGOFBERGER, N. (1990). Synthesis, hybridization properties and antiviral activity of lipid-oligodeoxynucleotide conjugates. *Nucleic Acids Res.* 18:3777-3783.

SHEA, T. B., BEERMANN, M. L., NIXON, R. A., and FISCHER, I. (1992). Microtubule-associated protein tau is required for axonal neurite elaboration by neuroblastoma cells. *J. Neuroscience Res.* 32:363-374.

SHEFFIELD, L. G. (1991). Oligonucleotides antisense to catalytic subunit of cyclin AMP-dependent protein kinase inhibit mouse mammary epithelial cell DNA synthesis. *Exp. Cell Res.* 192:307-310.

SHOJI, Y., AKHTAR, S., PERIASAMY, A., HERMAN, B., and JULIANO, R. L. (1991). Mechanism of cellular uptake of modified oligodeoxynucleotides containing methylphosphonate linkages. *Nucleic Acids Res.* 19:5543-5550.

SIEGRIST, C-A. and MACH, B. (1993). Antisense oligonucleotides specific for regulatory factor RFX-1 inhibit inducible but not constitutive expression of all major histocompatibility complex class II genes. *Eur. J. Immunol.* 23:2903-2908.

SIMONS, M. and ROSENBERG, R. D. (1992). Antisense nonmuscle myosin heavy chain and c-myb oligonucleotides suppress smooth muscle cell proliferation *in vitro*. *Circulation Res.* 70:835-843.

SIMONS, M., EDELMAN, E. R., DeKEYSER, J-L., LANGER, R., and ROSENBERG, R. D. (1992). Antisense c-myb oligonucleotides inhibit intimal arterial smooth muscle cell accumulation *in vivo*. *Nature (London)* 359:67-70.

SIZELAND, A. M. and BURGESS, A. W. (1991). The proliferative and morphologic responses of a colon carcinoma cell line (LIM 1215) require the production of two autocrine factors. *Mol. Cell. Biol.* 11:4005-4014.

SIZELAND, A. M. and BURGESS, A. W. (1992) Anti-sense transforming growth factor- α oligonucleotides inhibit autocrine stimulated proliferation of a colon carcinoma cell line. *Molecular Biology of the Cell* 3:1235-1243.

SKORSKI, T., SZCZYLIK, C., RATAJCZAK, M. Z., MALAGUARNERA, L., GEWITZ, A. M., and CALABRETTA, B. Growth factor-dependent inhibition of normal hematopoiesis by N-ras antisense oligodeoxynucleotides. *J. Exp. Med.* 175:743-750.

SOOD, A., SHAW, B. R., and SPIELVOGEL, B. F. (1990). Boron-containing nucleic acids. 2. Synthesis of oligodeoxynucleoside boranophosphates. *J. Amer. Chem. Soc.* 112:9000-9001.

SORSCHER, E. J., KIRK, K. L., WEAVER, M. L., JILLING, T., BLALOCK, J. E., and LeBOEUF, R. D. (1991). Antisense oligonucleotide to the cystic fibrosis gene inhibits anion transport in normal cultured sweat duct cells. *Proc. Natl. Acad. Sci. (USA)* 88:7759-7762.

SPEIR, E. and EPSTEIN, S. E. (1992). Inhibition of smooth muscle cell proliferation by an antisense oligodeoxynucleotide targeting the messenger RNA encoding proliferating cell nuclear antigen. *Circulation* 86: 538-547.

SPROAT, B. S., LAMOND, A. I., BEIJER, B., NEUNER, P., and RYDER, U. (1989). Highly efficient chemical synthesis of 2'-O-methyloligoribonucleotides and tetrabiotinylated derivative: Novel probes that are resistant to degradation by RNA or DNA specific nucleases. *Nucleic Acids Res.* 17:3373-3386.

STEIN, C. A., SUBASINGHE, C., SHINOZUKA, K., and COHEN, J. S. (1988a). Physicochemical properties of phosphorothioate oligodeoxynucleotides. *Nucleic Acids Res.* 16:3209-3221.

STEIN, C. A., MORI, K., LOKE, S. L., SUBASINGHE, C., SHINOZUKA, K., COHEN, J. S., and NECKERS, L. M. (1988b). Phosphorothioate and normal oligodeoxyribonucleotides with 5'-linked acridine: Characterization and preliminary kinetics of cellular uptake. *Gene* 72:333-341.

STEPKOWSKI, S. M., TU, Y., CONDON, T. P., and BENNETT, C. F. (1994). Blocking of heart allograft rejection by intracellular adhesion molecule-1 antisense oligonucleotides alone or in combination with other immunosuppressive modalities. *J. Immunol.* 153:5336-5346.

STEVENSON, M. and IVERSEN, P. (1989). Inhibition of human immunodeficiency virus type-1 mediated cytopathic effects by poly(L-lysine)-conjugated synthetic antisense oligodeoxyribonucleotides. *J. Gen. Virol.* 70:2673-2682.

STRAUSS, M., HERING, S., LIEBER, A., HERRMANN, G., GRIFFIN, B. E., and ARNOLD, W. (1992). Stimulation of cell division and fibroblast focus formation by antisense repression of retinoblastoma protein synthesis. *Oncogene* 7:769-773.

STULL, R. A., TAYLOR, L. A., and SZOKA, F. C. Jr. (1992). Predicting antisense oligonucleotide inhibitory efficacy: A computational approach using histograms and thermodynamic indices. *Nucleic Acids Res.* 20:3501-3508.

1. The first part of the document discusses the importance of maintaining accurate records of all transactions. It emphasizes that proper record-keeping is essential for the integrity of the financial system and for the ability to detect and prevent fraud.

2. The second part of the document outlines the specific requirements for record-keeping, including the need to maintain original documents and to keep copies of all transactions. It also discusses the importance of regular audits and the need to report any discrepancies immediately.

3. The third part of the document discusses the consequences of failing to maintain accurate records, including the potential for fines and penalties. It also discusses the importance of training staff on proper record-keeping procedures and the need to establish a strong internal control system.

4. The fourth part of the document discusses the importance of maintaining accurate records of all transactions, including the need to maintain original documents and to keep copies of all transactions. It also discusses the importance of regular audits and the need to report any discrepancies immediately.

5. The fifth part of the document discusses the consequences of failing to maintain accurate records, including the potential for fines and penalties. It also discusses the importance of training staff on proper record-keeping procedures and the need to establish a strong internal control system.

STULL, R. A., ZON, G., and SZOKA, F. C. Jr. (1993). Single-stranded phosphodiester and phosphorothioate oligonucleotides bind actinomycin D and interfere with TNF-induced lysis in the L929 cytotoxicity assay. *Antisense Res. Devel.* 3:295-300.

SUDDATH, F. L., QUIGLEY, G. L., McPHERSON, A., SNEDEN, D., KIM, J. J., KIM, S. H., and RICH, A. (1973). Three-dimensional structure of yeast phenylalanine transfer RNA at 3.0Å resolution. *Nature (London)* 248:20-24.

SUMMERS, M. F., POWELL, C., EGAN, W., BYRD, R. A., WILSON, W. D., and ZON, G. (1986). Alkyl phosphotriester modified oligodeoxyribonucleotides. VI. NMR and UV spectroscopic studies of ethyl phosphotriester (Et) modified R_p - R_p and S_p - S_p duplexes, [d[GGAA(Et)TTCC]]₂ *Nucleic Acids Res.* 14:7421-7436.

SZCZYLIK, C., SKORSKI, T., NCOLAIDES, N. C., MANZELLA, L., MALAGUARNERA, L., VENTURELLI, D., GEWIRTZ, A. M., and CALABRETTA, B. (1991). Selective inhibition of leukemia cell proliferation by BCR-ABL antisense oligonucleotides. *Science* 253:562-565.

TAJ, A. S., MARTIAT, P., DHUT, S., CHAPLIN, T. J., DOWDING, C., TN'NG, K. H., GOLDSTEIN, I., DALEY, G. Q., YOUNG, B. D., and GOLDMAN, J. M. (1990). Inhibition of P210^{bcr/abl} expression in K562 cells by electroporation with an antisense oligonucleotide. *Leukemia and Lymphoma* 3:201-208.

TAKESHITA, K., BOLLEKENS, J. A., HIJIYA, N., RATAJCZAK, M., RUDDLE, F. H., and GEWIRTZ, A. M. (1993). A homeobox gene of the *Antennapedia* class is required for human adult erythropoiesis. *Proc. Natl. Acad. Sci. (USA)* 90:3535-3538.

TANG, J. Y., TEMSAMANI, J., and AGRAWAL, S. (1993). Self-stabilized antisense oligodeoxynucleotide phosphorothioates: properties and anti-HIV activity. *Nucleic Acids Res.* 21:2729-2735.

TEICHMAN-WEINBERG, A., LITTAUER, U.Z., and GINZBERG, I. (1988). The inhibition of neurite outgrowth in PC12 cells by tubulin antisense oligodeoxyribonucleotides. *Gene* 72:297-307.

THIERRY, A. R., RAHMAN, A., and DRITSCHILO, A. (1992). "Liposomal delivery as a new approach to transport antisense oligonucleotides". In *Gene Regulation: Biology of Antisense RNA and DNA*. Erickson, R. P., and Izant, J. G., eds. (Raven Press, New York) pp. 147-161.

THINAKARAN, G. and BAG J. (1990). Alterations in the expression of muscle-specific genes mediated by troponin C antisense oligodeoxynucleotide. *Exp. Cell Res.* 192:227-235.

THUONG, N. T., ASSELINE, U., ROIG, V., TAKASUGI, M., and HÉLÈNE, C. (1987). Oligo(α -deoxynucleotide)s covalently linked to intercalating agents: Differential binding to ribo- and deoxyribopolynucleotides and stability towards nuclease degradation. *Proc. Natl. Acad. Sci. (USA)* 84:5129-5133.

TINOCO, I., UHLENBECK, O. C., and LEVINE, M. D. (1971). Estimation of secondary structure in ribonucleic acids. *Nature (London)* 230:362-367.

TINOCO, I., BORER, P. N., DENGLER, B., LEVINE, M. D., UHLENBECK, O. C., CROTHERS, D. M., and GRALLA, J. (1973). Improved estimation of secondary structure in ribonucleic acids. *Nature (London)* 246:40-41.

TOMASSINI, J.E., GRAHAM, D., DEWITT, C. M., LINEBERGER, D. W., RODKEY, J. A., and COLONNO, R. J. (1989). cDNA cloning reveals that the major group rhinovirus receptor on HeLa cells is intracellular adhesion molecule 1. *Proc. Natl. Acad. Sci. (USA)* 86:4907-4911.

TORTOLA, G. and CHO-CHUNG, Y. S. (1990). Type II regulatory subunit of protein kinase restores cAMP-dependent transcription in a cAMP-unresponsive cell line. *J. Biol. Chem.* 265:18067-18070.

TOULMÉ, J. J., KRISCH, H. M., LOREAU, N., THUONG, N. T., and HÉLÈNE, C. (1986). Specific inhibition of mRNA translation by complementary oligonucleotides covalently linked to intercalating agents. *Proc. Natl. Acad. Sci. (USA)* 83:1227-1231.

TROY, C. M., GREENE, L. A. and SHELANSKI, M. L. (1992). Neurite outgrowth in peripherin-depleted PC12 cells. *J. Cell. Biol.* 117:1085-1092.

UHLENBECK, O. C., BALLER, J., and DOTY, P. (1970). Complementary binding to the anticodon loop of fMet-transfer RNA. *Nature (London)* 225:508-510.

UHLENBECK, O. C. (1971). Complementary oligonucleotide binding to transfer RNA. *J. Mol. Biol.* 65:25-41.

UHLMANN, E. and PEYMAN, A. (1990). Antisense oligonucleotides: A new therapeutic principle. *Chemical Reviews* 90:544-584.

ULLOA, L., DÍAZ-NIDO, J., and AVILA, J. (1993). Depletion of casein kinase II by antisense oligonucleotide prevents neurogenesis in neuroblastoma cells. *EMBO J.* 12:1633-1640.

VALTERI, M., VENTURELLI, D., CARÉ, A., FOSSATI, C., PELOSI, E., LABBAYE, C., MATTIA, G., GEWITZ, A. M., CALABRETTA, B., and PESCHLE. (1990). Antisense *myb* inhibition of purified erythroid progenitors in development and differentiation is linked to cyclin activity and expression of DNA polymerase α . *Blood* 77:1181-1190.

VANDERKLISH, P., NEVE, R., BAHR, B. A., ARAI, A., HENNEGRIFF, M., LARSON, J., and LYNCH, G. (1992). Translational suppression of a glutamate receptor subunit impairs long-term potentiation. *Synapse* 12:333-337.

VENTURELLI, D., TRAVALI, S., and CALABRETTA, B. (1990). Inhibition of T-cell proliferation by a MYB antisense oligomer is accompanied by selective down regulation of DNA polymerase alpha expression. *Proc. Natl. Acad. Sci. (USA)* 87:5963-5967.

VICKERS, T., BAKER, B. F., COOK, P. D., ZOUNES, M., BUCKHEIT, R. W. Jr., GERMANY, J., and ECKER, D. J. (1991). Inhibition of HIV-LTR gene expression by oligonucleotides targeted to the TAR element. *Nucleic Acids Res.* 19:3359-3368.

VIGNOVICH, J., and BECKER, D. (1993). Expression of bFGF and differential expression of FGF receptors in normal myoblasts and rhabdomyosarcomas. *Internat. J. of Oncology* 2:637-642.

von HIPPEL, P. H. (1979). "On the molecular bases [sic] of the specificity of interaction of transcriptional proteins with genome DNA". In *Biological Regulation and Development*, Goldberger, R. F., ed. (Plenum, New York), Vol. 1 pp. 279-347.

1. The first part of the document discusses the importance of maintaining accurate records of all transactions. It emphasizes that proper record-keeping is essential for ensuring the integrity and reliability of financial data. This section also highlights the role of internal controls in preventing errors and fraud.

2. The second part of the document focuses on the implementation of effective internal control systems. It provides a detailed overview of the various components of such systems, including segregation of duties, authorization procedures, and regular monitoring and reporting. The text stresses the need for a strong control environment to support these systems.

- WADKINS, R. M. and JOVIN, T. M. (1991). Actinomycin D and 7-aminoactinomycin D binding to single-stranded DNA. *Biochemistry* 30:9469-9478.
- WAGNER, R. W., MATTEUCCI, M. D., LEWIS, J. G., GUTIERREZ, A. J., MOULDS, C., and FROEHLER, B. C. (1993). Antisense gene inhibition by oligonucleotides containing C-5 propyne pyrimidines. *Science* 260:1510-1513.
- WALDER, R.Y., and WALDER, J.A. (1988) Role of RNase-H in hybrid-arrested translation by antisense oligonucleotides. *Proc. Natl. Acad. Sci. (USA)* 85:5011-5015.
- WANG, A. H.-J., FUJI, S., van BOOM, J. H., van der MAREL, G. A., van BOECKEL, S. A. A., and RICH, A. (1982), Molecular structure of r(GCG)d(TATACGC): a DNA-RNA hybrid helix joined to double helical DNA. *Nature (London)* 299:601-604,
- WANG, J. C. and DAVIDSON, N. (1966). On the probability of ring closure of lambda DNA. *J. Mol. Biol.* 19:469-482.
- WATSON, J. D. and CRICK, F. H. C. (1953). Molecular structure of nucleic acids: A structure for deoxyribose nucleic acid. *Nature (London)* 171:737-738.
- WATSON, P. H., PON, R. T., and SHIU, R. P. C. (1991). Inhibition of *c-myc* expression by phosphorothioate antisense oligonucleotide identifies a critical role for *c-myc* in the growth of human breast cancer. *Cancer Res.* 51:3996-4000.
- WETMUR, J. G. and DAVIDSON, N. (1968). Kinetics of renaturation of DNA. *J. Mol. Biol.* 31:349-370.
- WEIGENT, D. A., BLALOCK, J. E., and LeBOEUF, R. D. (1991). An antisense oligodeoxynucleotide to growth hormone messenger ribonucleic acid inhibits lymphocyte proliferation. *Endocrinology* 128:2053-2057.
- WEST, A. P. and COOKE, B. A. (1991) A novel method to modulate desensitization and truncation of lutenizing hormone receptors using antisense oligodeoxynucleotides. *Mol. Cell. Endocrinol.* 79:R9-R14.
- WICKSTROM, E. (1986). Oligodeoxynucleotide stability in subcellular extracts and culture media. *J. Biochem. Biophys. Methods.* 13:97-102.
- WICKSTROM, E. L., BACON, T. A., GONZALEZ, A., FREEMAN, D. L., LYMAN, G., and WICKSTROM, E. (1988). Human promyelocytic leukemia HL-60 cell proliferation and *c-myc* protein expression are inhibited by an antisense pentadecadeoxynucleotide targeted against *c-myc* RNA. *Proc. Natl. Acad. Sci. (USA)* 85:1028-1032.
- WICKSTROM, E. L., BACON, T. A., GONZALEZ, A., LYMAN, G., and WICKSTROM, E. (1989). Anti-*c myc* DNA increases differentiation and decreases colony formation by HL-60 cells. *In vitro Cell. & Develop. Biol.* 24:297-302
- WITSELL, A. L. and SCHOOK, L. B. (1992). Tumor necrosis factor α is an autocrine growth regulator during macrophage differentiation. *Proc. Natl. Acad. Sci. (USA)* 89:4754-4758.
- WOOLF, T., MELTON, D. A., and JENNINGS, C. G. B. (1992). Specificity of antisense oligonucleotides *in vivo*. *Proc. Natl. Acad. Sci. (USA)* 89:7305-7309.

THE UNIVERSITY OF CHICAGO
DIVISION OF THE PHYSICAL SCIENCES
DEPARTMENT OF CHEMISTRY
5708 SOUTH ELLIS AVENUE
CHICAGO, ILLINOIS 60637
TEL: 773-936-3700
FAX: 773-936-3701
WWW: WWW.CHEM.UCHICAGO.EDU

OFFICE OF THE DEAN OF THE PHYSICAL SCIENCES

PHYSICAL SCIENCE CENTER
5708 SOUTH ELLIS AVENUE
CHICAGO, ILLINOIS 60637
TEL: 773-936-3700
FAX: 773-936-3701
WWW: WWW.CHEM.UCHICAGO.EDU

- WU, G. Y. and WU, C. H. (1992) Specific inhibition of Hepatitis B viral gene expression *in vitro* by targeted antisense oligonucleotides. *J. Biol. Chem.* 267:12436-12439.
- WU, J., ZHU, J-Q., ZHU, D-X, SCHARFMAN, A., LAMBIN, G., HAN, K-K. (1992). Selective inhibition of normal murine myelopoiesis *in vitro* by a HOX 2.3 antisense oligodeoxynucleotide. *Cellular and Molecular Biol.* 38:367-376.
- WYATT, J. R., PUGLISI, J. D., and TINOCO, I. Jr. (1990). RNA pseudoknots: Stability and loop size requirements. *J. Mol. Biol.* 214:455-470.
- YAGER, T. D. and von HIPPEL, P. H. (1991). A thermodynamic analysis of RNA transcript elongation and termination in *Escherichia coli*. *Biochemistry* 30:1097-1118.
- YANG, J.K., MASTERS, J.N., and ATTARDI, G. (1984). Human dihydrofolate reductase gene organization: Extensive conservation of the G+C rich 5' non-coding sequence and strong intron size divergence from homologous mammalian genes. *J. Mol. Biol.* 176:169-187.
- YAKUBOV, L. A., DEEVA, E. A., ZARYTOVA, V. F., IVANOVA, E. M., RYTE, A. S., YIRCHENKO, L. V., and VLASSOV, V. V. (1989). Mechanism of oligonucleotide uptake by cells: Involvement of specific receptors? *Proc. Natl. Acad. Sci. (USA)*. 86:6454-6458.
- YEVICH, R. AND OLSON, W. K. (1979). The spatial distributions of randomly coiling polynucleotides. *Biopolymers* 18:113-145.
- YOUNG, S. and WAGNER, R. W. (1991). Hybridization and dissociation rates of phosphodiester or modified oligodeoxynucleotides with RNA at near-physiological conditions. *Nucleic Acids Res.* 19:2463-2470.
- YU, A. C. H., LEE, Y. L., and ENG, L. F. (1993). Astrogliosis in culture: I. the model and the effect of antisense oligonucleotides on glial fibrillary acidic protein synthesis. *J. Neuroscience Res.* 34:295-303.
- ZHENG, H., SAHAI, B. M., KILGANNON, P., FOTEDAR, A., and GREEN, D. R. (1989). Specific inhibition of cell-surface T-cell receptor expression by antisense oligodeoxynucleotides and its effect on the production of an antigen-specific regulatory T-cell factor. *Proc. Natl. Acad. Sci. (USA)* 86:3758-3762.
- ZHOU, N., JAMES, T. L., and SHAFER, R. H. (1989). Binding of actinomycin D to [d(ATCGAT)]₂: NMR evidence of multiple complexes. *Biochemistry* 28:5231-5239.
- ZON, G. (1988). Oligonucleotide analogues as potential chemotherapeutic agents. *Pharmaceut. Res.* 5:539-549.
- ZUBAY, G. (1983). Chapter 18: "Nucleic Acids and Nucleoproteins". In *Biochemistry*, Zubay, G., ed. (Addison-Wesley, Menlo Park, CA) p. 669.
- ZUKER, M. (1989a). On finding all suboptimal foldings of an RNA molecule. *Science* 244:48-52.
- ZUKER, M. (1989b). Computer prediction of RNA structure. *Methods Enzymol* 180:262-288.
- ZUKER, M. AND STEIGLER, P. (1981). Optimal computer folding of large RNA sequences using thermodynamics and auxiliary information. *Nucleic Acids Res.* 9:133-148.

THE UNIVERSITY OF CHICAGO
DIVISION OF THE PHYSICAL SCIENCES
DEPARTMENT OF PHYSICS
530 SOUTH EAST ASIAN AVENUE
CHICAGO, ILLINOIS 60607
TEL: 773-936-3700
FAX: 773-936-3701
WWW: WWW.PHYSICS.UCHICAGO.EDU

PHYSICS 311
LECTURE 1
MAY 1998

1. The first part of the document discusses the importance of maintaining accurate records of all transactions and activities. It emphasizes the need for transparency and accountability in financial reporting.

2. The second part of the document outlines the various methods and techniques used to collect and analyze data. It highlights the importance of using reliable sources and ensuring the accuracy of the information gathered.

3. The third part of the document focuses on the interpretation and analysis of the collected data. It discusses the various statistical and analytical tools used to identify trends and patterns in the data.

4. The fourth part of the document provides a detailed overview of the findings and conclusions drawn from the analysis. It discusses the implications of the results and offers recommendations for future research and action.

5. The fifth part of the document discusses the challenges and limitations of the research. It identifies the areas where further research is needed and offers suggestions for addressing these challenges.

6. The sixth part of the document provides a summary of the key findings and conclusions. It emphasizes the importance of the research and offers a final recommendation for future research and action.

APPENDIX ONE: A Simple Thermodynamic Model of ASO Selectivity (from Monia *et al.*, 1992)

NOTE: The following derivation assumes that the ASO is in molar excess over the target RNA.

The association constant, K_{assoc} , of an ASO is defined

$$K_{assoc} = \frac{CR}{C \cdot R} \quad (\text{AI-1})$$

where C is the concentration of the ASO and R is the concentration of the perfectly matched RNA target site.

Rearranging equation AI-1 provides the ratio of bound RNA to free RNA

$$K_{assoc} C = \frac{CR}{R} \quad (\text{AI-2})$$

Therefore, the fraction of the target hybridized is given by

$$f = \frac{CR}{CR + R} = \frac{\frac{CR}{R}}{\frac{CR}{R} + \frac{R}{R}} = \frac{K_{assoc} C}{K_{assoc} C + 1} \quad (\text{AI-3})$$

Plotting f versus $(K_{assoc} \cdot C)$ affords curve A in figure A1-1.

1. The first part of the document is a list of names and addresses of the members of the committee. The names are listed in alphabetical order, and the addresses are given in full. The list includes the names of the members of the committee, the names of the members of the sub-committee, and the names of the members of the advisory committee. The addresses are given in full, including the street, city, and state.

2. The second part of the document is a list of the names and addresses of the members of the committee. The names are listed in alphabetical order, and the addresses are given in full. The list includes the names of the members of the committee, the names of the members of the sub-committee, and the names of the members of the advisory committee. The addresses are given in full, including the street, city, and state.

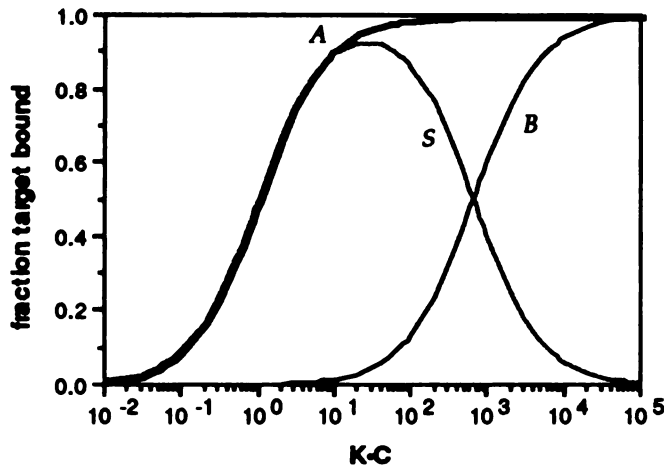


Figure A1-1: Theoretical binding curves for an ASO to its matched target (curve A) and mismatched target site (curve B) as a function of the product $K \cdot C$, where K is the ASO affinity constant and C is the ASO concentration. The difference in binding, or selectivity, is plotted as curve S.

The affinity of the ASO for a mismatched site can be defined as

$$K_{mis} = K_{assoc} e^{\left(\frac{-\Delta\Delta G^\circ}{RT}\right)} \quad (\text{AI-4})$$

where $\Delta\Delta G^\circ$ is the free energy penalty associated with the mismatch site(s). In analogy to equation AI-3, the binding of the ASO to the mismatch site (curve B in figure AI-1) is described by

$$f = \frac{K_{assoc} C e^{\left(\frac{-\Delta\Delta G^\circ}{RT}\right)}}{\left(1 + K_{assoc} C e^{\left(\frac{-\Delta\Delta G^\circ}{RT}\right)}\right)} \quad (\text{AI-5})$$

Curve S represents the selectivity of the ASO for the matched target versus the mismatched target, which is simply the difference between curve A and B. The equation for the curve S is defined

1. The first part of the document is a list of names and addresses of the members of the committee. The names are listed in alphabetical order, and the addresses are listed below each name. The list includes names such as Mr. J. H. Smith, Mr. J. B. Jones, and Mr. W. C. Brown.

2. The second part of the document is a list of names and addresses of the members of the committee. The names are listed in alphabetical order, and the addresses are listed below each name. The list includes names such as Mr. J. H. Smith, Mr. J. B. Jones, and Mr. W. C. Brown.

$$\text{selectivity } (S) = \frac{K_{\text{assoc}} C}{(1 + K_{\text{assoc}} C)} - \frac{K_{\text{assoc}} C e^{\left(\frac{-\Delta\Delta G^\circ}{RT}\right)}}{\left(1 + K_{\text{assoc}} C e^{\left(\frac{-\Delta\Delta G^\circ}{RT}\right)}\right)} \quad (\text{AI-6})$$

Differentiating equation AI-6 affords calculation of the value of maximum discrimination

$$\frac{dS}{d(KC)} = \frac{1}{(1 + K_{\text{assoc}} C)^2} - \frac{e^{\left(\frac{-\Delta\Delta G^\circ}{RT}\right)}}{\left(1 + K_{\text{assoc}} C e^{\left(\frac{-\Delta\Delta G^\circ}{RT}\right)}\right)^2} \quad (\text{AI-7})$$

The maximum will occur when equation AI-7 is set to zero

$$0 = \frac{1}{(1 + K_{\text{assoc}} C)^2} - \frac{e^{\left(\frac{-\Delta\Delta G^\circ}{RT}\right)}}{\left(1 + K_{\text{assoc}} C e^{\left(\frac{-\Delta\Delta G^\circ}{RT}\right)}\right)^2} \quad (\text{AI-8})$$

Rearranging terms provides

$$\left(1 + K_{\text{assoc}} C e^{\left(\frac{-\Delta\Delta G^\circ}{RT}\right)}\right)^2 = e^{\left(\frac{-\Delta\Delta G^\circ}{RT}\right)} (1 + K_{\text{assoc}} C)^2 \quad (\text{AI-9})$$

Which upon expansion of terms, rearrangement, and elimination of common terms, can be further simplified to

1. The first part of the document is a list of names and addresses of the members of the committee. The names are listed in alphabetical order, and the addresses are listed below each name. The list includes the names of the members of the committee, the names of the members of the sub-committee, and the names of the members of the advisory committee.

2. The second part of the document is a list of the names of the members of the committee who have been appointed to the sub-committee. The names are listed in alphabetical order, and the addresses are listed below each name. The list includes the names of the members of the sub-committee, the names of the members of the advisory committee, and the names of the members of the committee.

$$e^{\left(\frac{-\Delta\Delta G^\circ}{RT}\right)} = \frac{1}{K_{assoc}^2 C^2} \quad (\text{AI-10})$$

Taking the \ln of each side then provides

$$\frac{\Delta\Delta G^\circ}{RT} = \ln [(K_{assoc} C)^2] \quad (\text{AI-11})$$

which then affords equation 1-4

$$\Delta\Delta G^\circ = 2RT \ln(K_{assoc} C) \quad (1-4)$$

THE UNIVERSITY OF CHICAGO
DIVISION OF THE PHYSICAL SCIENCES
DEPARTMENT OF CHEMISTRY
5708 S. UNIVERSITY AVENUE
CHICAGO, ILLINOIS 60637
TEL: 773-936-3700
FAX: 773-936-3701
WWW: WWW.CHEM.UCHICAGO.EDU

THE UNIVERSITY OF CHICAGO
DIVISION OF THE PHYSICAL SCIENCES
DEPARTMENT OF CHEMISTRY
5708 S. UNIVERSITY AVENUE
CHICAGO, ILLINOIS 60637
TEL: 773-936-3700
FAX: 773-936-3701
WWW: WWW.CHEM.UCHICAGO.EDU

APPENDIX TWO: DSCORES Program (in "C")

This appendix contains the complete code in ANSI C for the MacIntosh compatible DSCORES program. The program was written using Symantec Corp's Think LightspeedC software, which is an ANSI standard version of C compatible with the MacIntosh.

AII.1 Functionality of DSCORES

The overall strategy of the DSCORES program is outlined as follows:

- I. Define two global structure arrays (in **preprocessor** command lines) which will hold:
 - 1- The RNA sequence to be analyzed. Each element of the RNA sequence array (called **excel_data**) holds a character (RNA nucleotide) and a number corresponding to the nucleotide position in the RNA sequence.
 - 2- The Dscores for each window across the RNA sequence. Each element of the Dscores array (called **INDEX**) holds both the Dscore, and the position in the RNA sequence corresponding to the nucleotide to which the Dscore is attached.
- II. Obtain, from the user, pertinent parameters concerning the sequence to be analyzed and the size of the window over which the Dscores will be computed (in the **main** function)
- III. Open and read the RNA sequence information into the **excel_data** structure array (in the **main** function).
- IV. Open two output files to which the Dscores computations are written:
 - 1- **.dscores** file listing Dscores arranged sequentially across the RNA

1
2
3
4
5
6
7
8
9
10
11
12
13
14
15
16
17
18
19
20
21
22
23
24
25
26
27
28
29
30
31
32
33
34
35
36
37
38
39
40
41
42
43
44
45
46
47
48
49
50
51
52
53
54
55
56
57
58
59
60
61
62
63
64
65
66
67
68
69
70
71
72
73
74
75
76
77
78
79
80
81
82
83
84
85
86
87
88
89
90
91
92
93
94
95
96
97
98
99
100

101
102
103
104
105
106
107
108
109
110
111
112
113
114
115
116
117
118
119
120
121
122
123
124
125
126
127
128
129
130
131
132
133
134
135
136
137
138
139
140
141
142
143
144
145
146
147
148
149
150

sequence.

2- .sort file listing the Dscores arranged from best to worst.

Both open commands are performed within the `main` function.

V. Write headers to each output file (`write_table_header` and `write_sort_header` functions).

VI. Calculate the Dscore for each window (`calc_scores` function) and write the results to the `INDEX` array.

VII. Write the `INDEX` array to the .dscores file (`write_to_output` function).

VIII. Sort the `INDEX` array elements from best to worst (`sort_index`, `cmp_fxn` functions).

IX. Write the sorted `INDEX` array to the .sort file (`write_sorted_list` function)

X. Close all files and terminate the program (`close_file` function)

AII.2 Commentary on the code

This section contains the continuous code lines for the entire `DSCORES` program (*bold italic* font on grey background), followed by a general commentary on the program flow in the function.

Preprocessor commands, global variable declarations, structure definitions

```
#include <ctype.h>  
#include <stdio.h>  
#include <storage.h>  
#include <strings.h>  
#include <unix.h>
```

MEMPHIS
TENN
4/4/68

```

#define INIT                3.4
#define PAD                 0.0
#define MAXWIND            100
#define SEQ_NAME_LEN      100
#define SEQ_FILENAME_LEN  50

typedef    struct data_element
{
    int    pos;
    char   base;
}    DE_TP;
DE_TP    *excel_data;

typedef    struct indices
{
    float  score;
    int    pos;
}    INDEX;
INDEX    *index_data;

float bp_energy_37 [4][4] =    { /* Table to calc eng of duplex at 37 *
                                * 5' nt down, 3' nt across *
                                A    C    G    T */
    /* A */ {    0.9,    2.1,    1.7,    0.9},
    /* C */ {    1.8,    2.9,    2.0,    1.7 },
    /* G */ {    2.3,    3.4,    2.9,    2.1 },
    /* T */ {    1.1,    2.3,    1.8,    0.9 }
};

FILE *sequence_file = (FILE *) 0;
FILE *output_file = (FILE *) 0;
FILE *sorted_output_file = (FILE *) 0;

```

This part of the code contains the preprocessor commands to **#include** standard libraries of predefined functions, **#define** directives to associate a constant numeric value with a variable names, and declarations of global structures, arrays and pointers.

Main function.

```
main()
{
    void                write_table_header();
    void                write_sort_header();
    void                calc_score();
    void                sort_index();
    void                write_sorted_list();
    void                close_file();

    int    seqlen, value, window_size = -1, j = 0;
    char    seqname[SEQ_NAME_LEN], seqfile[SEQ_FILENAME_LEN];
    char    outfile[(SEQ_FILENAME_LEN + 8)], sortfile[(SEQ_FILENAME_LEN + 5)];
    char    window_size_str[3];
    char    base;
    DE_TP    *loc_dtp;

    printf("**** DSCORES ****\n\n\n");
    printf("First select the size of the oligo window for DSCORE computation\n");

    while ((window_size >= 100) || (window_size < 0))
    {
        printf("The window size should be positive and less than 100\n\n");
        printf("Window size? ");
        cgets(window_size_str);
        window_size = atoi(window_size_str);
    }

    printf("\n\nNow enter sequence filename: ");
    cgets(seqfile);

    while ((sequence_file = fopen(seqfile, "r")) == NULL)
    {
        fprintf(stderr, "Failed to open %s file\n", seqfile);
        exit(0);
    }

    fscanff(sequence_file, "# %d, %s", &seqlen, &seqname);

    stpcpy(outfile, seqfile);
    strcat(outfile, ".dscores");

    while ((output_file = fopen(outfile, "w+")) == NULL)
    {
        fprintf(stderr, "Failed to open %s file\n", outfile);
        exit(0);
    }

    stpcpy(sortfile, seqfile);
```

```

strcat( sortfile, ".sort");

while ( (sorted_output_file = fopen( sortfile, "w+")) == NULL)
{
    fprintf( stderr, "Failed to open %s file\n", sortfile);
    exit(0);
}

while ( (excel_data = (DE_TP *) malloc( seqlen * sizeof(DE_TP))) ==
NULL)
{
    fprintf( stderr, "The sequence is too long to be handled in memory\n");
    fprintf( stderr, "Subdivide it and retry again");
    exit(0);
}

loc_dtp = excel_data;

while (fscanf( sequence_file, "%c", &base) != EOF)
{
    if (base != '\n')
    {
        if (isalnum( base))
        {
            loc_dtp->pos = j;
            loc_dtp->base = base;

            j++;
            loc_dtp++;
        }
        else{
            continue;
        }
    }
    else{
        continue;
    }
}

while ( (index_data = (INDEX *) malloc( seqlen * sizeof(INDEX))) ==
NULL)
{
    fprintf( stderr, "Memory failure in allocating for sort file");
    exit(0);
}

write_table_header( window_size, seqname);
write_sort_header( window_size, seqname);

calc_score(window_size, excel_data, index_data, seqlen);

sort_index( index_data, window_size, seqlen);

```

```

write_sorted_list( index_data, seqlen, window_size, excel_data);

close_file( output_file);
close_file( sequence_file);
close_file( sorted_output_file);

printf("\n\n\nThe sequence has been analyzed. A sequential listing of each\n");
printf("window appears in the file appended '.dscores'. The window scores\n");
printf("have also been listed from best to worst in the '.sort' file\n");

exit();

}

```

This is the **main** function, or body, of the program. From it, all the other functions are called, and the program initiated and terminated.

Write table header function.

```

void write_table_header( size, name)
int size;
char name[];
{
    fprintf( output_file, "# Sequence: %s\n", name);
    fprintf( output_file, "# Window Size: %d\n",size);
    fprintf( output_file, "#\n");
    fprintf( output_file, "# \tDscore\t\tmRNA target sequence (5' -> 3')\n");

    return;
}

```

The **write_table_header** function writes a header at the top of the output **.dscores** file.

Write sort header function.

```

void write_sort_header( size, name)

```



```

int size;
char name[];
{
    fprintf(sorted_output_file, "# Sequence: %s\n", name);
    fprintf(sorted_output_file, "# Window Size: %d\n", size);
    fprintf(sorted_output_file, "#\n");
    fprintf(sorted_output_file, "# \t\t\tStart\t mRNA target sequence (5'->3')
caps\n");
    fprintf(sorted_output_file, "# \tDscore\tPos\t\tcomplementary oligo (5' -> 3')
lower case\n");

    return;
}

```

The `write_sort_header` function writes a header at the top of the output .sort file.

Calc score function.

```

void calc_score(size, datap, indexp, seqlen)
int size, seqlen;
DE_TP *datap;
INDEX *indexp;
{
    int switch_it 0;
    void write_to_output();

    int j = 0, k, n, fiveprime, threeprime;
    char sequence[MAXWIND];
    float score;
    DE_TP *startptr, *windowptr, *nextwindptr;
    INDEX *loc_indexp;

    score = 0.;

    startptr = datap;
    loc_indexp = indexp;

    /* Make sure do not read off end of array */
    while( j < seqlen)
    {
        for( n = 0; n < MAXWIND; n++)
            sequence[n] = '\0';
    }
}

```

```

    if( (j + size) <= seqlen)
    {
        windowptr = nxtwindowptr = startptr;
        nxtwindowptr++;

        for( k = 0; k < size; k++, windowptr++, nxtwindowptr++)
        {
            if ( isupper(windowptr->base))
                sequence[k] = windowptr->base;
            else
                sequence[k] = toupper( windowptr->base);

            if( k < (size - 1))
            {
                fiveprime    =    switch_nt( windowptr-
>base);
                threeprime   =    switch_nt( nxtwindowptr-
>base);

                score -= bp_energy_37 [fiveprime] [threeprime];
            }
        }

        score = (score + INIT) / 2; /* Correct for initiation and
strandedness of complex */

        loc_indexp->score    =    score;
        loc_indexp->pos      =    (j+1);
    }

    write_to_output( sequence, score, j);

    score = PAD;
    j++;
    startptr++;
    loc_indexp++;
}

return;
}

```

The `calc_score` function reads the RNA sequence over the specified window size and computes a Dscore for the given sequence.

Switch nt function.

```
int      switch_nt ( base)
char base;
{
    switch( base)
    {
        case 'A':
        case 'a':    return 0;
        case 'C':
        case 'c':    return 1;
        case 'G':
        case 'g':    return 2;
        case 'T':
        case 't':
        case 'U':
        case 'u':    return 3;
        default     return -1;
    }
}
```

The `switch_nt` function, called by the `calc_score` function, converts a single letter base code to an integer, which the function returns to `calc_score`.

Write to output function.

```
void write_to_output( sequence, score, j)
int      j;
char sequence[];
float    score;
{
    fprintf( output_file, "%d\t%.2f\t  %s\n", (j+1), score, sequence);
    return;
}
```

The `write_to_output` function writes the contents of the `INDEX` structure array to the `.dscores` file, producing output which is listed

sequentially as the window "moves" across the RNA sequence from 5' to 3'.

Sort index function.

```
void sort_index( indexp, size, len)
INDEX      *indexp;
int        size, len;
{
    static int      cmp_fxn();

    qsort( indexp, (len-size+1), sizeof(INDEX), cmp_fxn);

    return;
}
```

The `sort_index` function calls upon a standard library quick sort (`qsort`) function to sort the `INDEX` structure array of Dscores (and their associated position fields) from best to worst. Note that this function actually rearranges the elements of the `INDEX` structure array.

Cmp fxn function.

```
static int cmp_fxn( p, q)
INDEX      *p, *q;
{
    if (p->score < q->score)
        return (-1);
    else if (p->score > q->score)
        return (1);
    else
        return (0);
}
```

The `cmp_fxn` function is required by the standard `qsort` function in order to make comparisons between specific fields (`score` field) within the two specific elements of the `INDEX` structure array during the sorting process.

Write sorted list function.

```
void write_sorted_list( indexp, len, size, datap)
INDEX      *indexp;
int        len, size;
DE_TP     *datap;
{
    char    comp_nt();

    int      j, k, m, n, p;
    char sseq[MAXWIND], cseq[MAXWIND];
    INDEX    *loc_indexp;
    DE_TP    *loc_datap;

    loc_indexp = indexp;

    for ( m = 0; m < MAXWIND; m++)
    {
        sseq[m] = '^0';
        cseq[m] = '^0';
    }

    for ( j = 0; j < (len - size + 1); j++)
    {
        fprintf (sorted_output_file, "\t%.2f\t\t%d", loc_indexp->score,
                loc_indexp->pos);

        loc_datap = datap + ((loc_indexp->pos) - 1);

        for ( k = 0; k < size; k++)
        {
            if ( isupper(loc_datap->base))
                sseq[k] = loc_datap->base;
            else
                sseq[k] = toupper( loc_datap->base);

            loc_datap++;
        }
    }
}
```


This function returns the complementary base to the supplied argument. It is called by the **write_sorted_list** function during the process of writing the complementary oligonucleotide sequence to the supplied RNA "window" sequence.

Close file function.

```
void      close_file(arg_file)
FILE *arg_file;
{
    fclose( arg_file);
    return;
}
```

This function simply closes the input/output stream (file) supplied in the argument.

1. The first part of the document is a list of names and addresses, which appears to be a directory or a list of contacts. The names are written in a cursive hand, and the addresses are listed below them. The list includes names such as "John Doe" and "Jane Smith", and addresses such as "123 Main Street" and "456 Elm Street".

2. The second part of the document is a list of names and addresses, which appears to be a directory or a list of contacts. The names are written in a cursive hand, and the addresses are listed below them. The list includes names such as "John Doe" and "Jane Smith", and addresses such as "123 Main Street" and "456 Elm Street".

APPENDIX THREE: Thermodynamic Values for Base-Stacking Interactions

Nearest Neighbor Stacking Energies for Base Pair Duples
(values in kcal/mol)

		3'Base Pair					
		AU	UA	CG	GC	GU	UG
	AU	-0.9 (-1.6) [-0.4]	-0.9 (-1.2) [-1.3]	-2.1 (-1.1) [-1.7]	-1.7 (-1.4) [-1.7]	-0.5*	-0.7
	UA	-1.1 (-0.7) [-1.3]	-0.9 (-1.6) [-0.4]	-2.3 (-1.4) [-1.7]	-1.8 (-1.7) [-1.7]	-0.7	-0.5*
5' Base	CG	-1.8 (-1.7) [-1.7]	-1.7 (-1.4) [-1.7]	-2.9 (-2.9) [-2.9]	-2.0 (-3.3) [-2.9]	-1.5	-1.5
	GC	-2.3 (-1.4) [-1.7]	-2.1 (-1.1) [-1.7]	-3.4 (-2.8) [-2.9]	-2.9 (-2.9) [-2.9]	-1.3	-1.9
Pair	GU	-0.5*	-0.7	-1.9	-1.5	-0.5*	-0.5*
	UG	-0.7	-0.5*	-1.3	-1.5	-0.6	-0.5*

All values reported as RNA:RNA; (DNA-DNA); and [RNA-DNA]

*Indicates particularly uncertain value

References: RNA-RNA (Freier *et al.*, 1986)

DNA-DNA and RNA-DNA (Yager and von Hippel, 1991).

APPENDIX FOUR: Extending the thermodynamic analysis of ASO binding to include concentration terms

AIV.1 INTRODUCTION

A completely rigorous thermodynamic analysis of ASO binding requires accurate thermodynamic parameters for hybrid formation, accurate structural information for both the RNA prior to and after ASO complex formation, and accurate concentration terms for each of the reactants and products involved in the hybridization reaction. Currently, experiments in complex biological systems (*i. e.* cells) do not afford data concerning concentrations of reactants and products. In the absence of mapping studies, knowledge of RNA structure relies upon the accuracy of RNA secondary structure prediction programs. Therefore, it is not surprising that the Sscore and Cscore thermodynamic indices developed in Chapter 2 do not display significant correlations with observed ASO efficacy, since these studies were performed under conditions where concentration terms and exact RNA structure are ill-defined variables.

Lima and colleagues (1992) have studied the effect of target RNA secondary structure upon the binding of RNA oligonucleotides in a cell-free assay. Their study provides important information on the relative concentrations of ASO and structured target RNA for the binding of several RNA oligonucleotides, affording a more rigorous thermodynamic analysis of ASO hybridization than experiments performed within intact cells.

The goals of the computations performed in this appendix are several fold: First, a model for the competition between ASO binding and RNA secondary structure formation at an ASO target site is developed. This model, in which the ASO binding and RNA folding reactions are each mod-

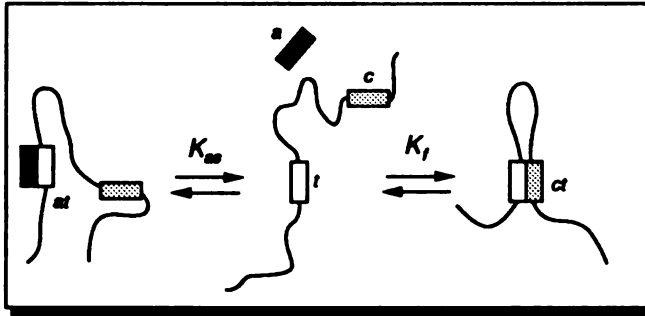


Figure A4-1: Representation of competing RNA folding and ASO binding. An ASO, *a*, is targeted to a region of the mRNA, *t*, which also can form a secondary structure with a complementary region of the mRNA, *c*. Binding of the ASO to its target results in formation of the complex *at*; formation of secondary structure results in creation of complex *ct*.

eled as bimolecular processes (Figure A4-1), allows concentration terms to be derived for each of the reactants and products participating in the ASO hybridization reaction. A direct expression between reactant and product concentrations and the free energy of the process at equilibrium is achieved.

Second, models of RNA chain behavior are developed. Since the RNA folding process is modeled as a bimolecular reaction between the ASO target site, *t*, and a complementary region of the RNA strand, *c* (see Figure A4-1), an effective concentration term for the *c* strand is required for the thermodynamic calculations. Exact solutions for the RNA polymer chain behavior, particularly the spatial distributions of each monomer nucleotide, are complex and not easily specified by simple mathematical functions. As an alternative to an exact solution for effective concentration, boundary values are developed based upon two simple models of RNA chain behavior which provide maximum and minimum competitor strand concentration values. Two additional refinements of these approximations are also presented.

Third, simplification of the equations describing the relationship between free energies of binding and reactant/product concentrations also

afford analysis of the thermodynamic parameters used both to predict RNA secondary structure and to compute Dscores, Sscores and Cscores. The free energy parameters for various base-pair duplex formation (from Freier *et al.*, 1986; Table 2-1) were derived from studies performed using small RNA oligonucleotides. The information supplied by Lima and coworkers allows an independent test of the accuracy of these parameters.

Finally, analysis of the predictions of ASO binding behavior obtained from thermodynamic calculations versus the observed experimental results provides additional insight into both the thermodynamic and kinetic factors which govern ASO binding in more complex biological systems.

In order to assist the reader in deciphering all of the symbols and variables introduced in this appendix, a glossary of variables is presented on the following page.

GLOSSARY OF VARIABLES

Reactant / Product Variables

A or <i>a</i>	the ASO molecule
R	the RNA molecule
<i>t</i>	the ASO target site on the RNA molecule
<i>at</i>	the complex formed by the binding of the ASO to its target
<i>c</i>	a competitor region of the RNA strand which can bind <i>t</i>
<i>ct</i>	the complex formed by the binding of <i>c</i> to <i>t</i> .

Concentration variables

[<i>x</i>]	the concentration of the molecule <i>x</i>
[<i>x</i>₀]	the input concentration of molecule <i>x</i> in any reaction at equilibrium
[<i>x</i>₀]_{50%}	the input conc. of molecule <i>x</i> required to cause 50% binding
[<i>c'</i>]	the effective concentration of the competitor strand

RNA chain behavior models

<i>n</i>	the separation distance, in nucleotides, between two monomers in the polyribonucleotide chain
<i>l</i>	the effective length of an individual monomer unit.
$\rho(n)$	a probability density function used to correct the equilibrium constant for bimolecular association to an equilibrium constant for a loop closure reaction. Essentially a correction for the effective concentration of the loop closing monomers

Thermodynamic Variables

ΔG	Gibbs free energy
ΔG°	Gibbs free energy of a reaction at standard state (1M reactants, products; 1M NaCl, reaction at 37°C)
ΔG_{AR}	Gibbs free-energy of formation for the entire structure containing the bound ASO
ΔG_f	Gibbs free-energy of formation of secondary structure in an entire RNA molecule
$\Delta\Delta G_{local}$	The change in the Gibbs free energy for the system produced by ASO-binding induced changes in secondary structure at the ASO target site
$\Delta\Delta G_{nonlocal}$	The change in the Gibbs free energy for the system produced by ASO binding-induced changes in the conformation of the RNA outside of the target site.
ΔG°_d	The standard state Gibbs free energy of duplex formation between the ASO and its target site. Also denoted ΔG°_{duplex} or ΔG°_{at}
ΔG°_c	The standard state Gibbs free energy due to coaxial stacking of the <i>at</i> duplex and stems in the structure of the RNA outside the duplex site.

AIV.2 METHODS

AIV.2.1 Thermodynamics of ASO binding: generalized descriptive equations

AIV.2.1a Global binding reaction Schematically, the binding of an ASO to an RNA can be depicted



where A is the ASO molecule and R is the RNA molecule. Similarly, the RNA folding process can be represented as



The free energies associated with each reaction can be defined as ΔG_{AR} for the binding reaction, and ΔG_f for the RNA folding reaction. The change in free-energy for the system during the ASO binding process ($\Delta\Delta G$) can be defined as

$$\Delta\Delta G = \Delta G_{AR} - \Delta G_f \quad (\text{IV-3})$$

AIV.2.1b Treating ASO binding on a local level. Figure A4-1 schematically depicts the binding process of an ASO at a local level (i.e. ASO-RNA duplex formation versus the formation of local secondary structure). The ASO, a , binds its target site, t , to form the antisense duplex, at . Symbolically represented



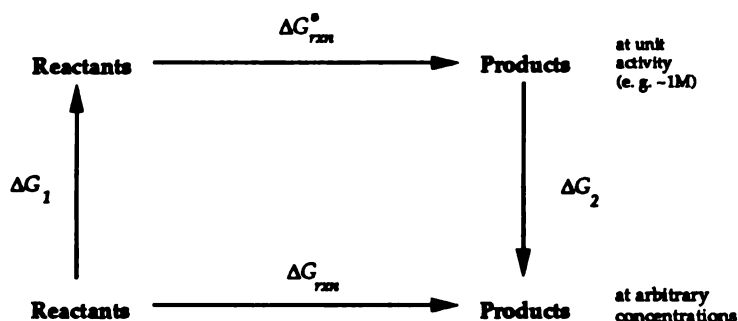


Figure A 4-2: Thermodynamic cycle applicable to correcting for reactions not at standard state. As the free energy is a state function (independent of path), the free energy of a reaction not at standard state (ΔG_{rxn}) is simply the sum of the free energies for each of the steps around the cycle (*i. e.* see equation IV-6)

Similarly, if the ASO target site, t , is capable of forming a helix with some complementary portion of the RNA chain, c , a local secondary structure ct may be formed.



A free energy is associated with each reaction-- defined as ΔG_{ct} for equation IV-4 and ΔG_{ct} for equation IV-5. Figure A4-2 shows a thermodynamic cycle which can be used to relate the free energies of any reaction at standard state (*i. e.* unit activity; ΔG°_{rxn}) to the free energies of the same reaction not at standard state (ΔG_{rxn}). Since G is a state function, ΔG is independent of path. Therefore,

$$\Delta G_{rxn} = \Delta G_1 + \Delta G^{\circ}_{rxn} + \Delta G_2 \quad \text{(IV-6)}$$

For the ASO binding reaction depicted in equation IV-5*,

$$\Delta G_1 = RT \ln \left(\frac{1}{[c][t]} \right) \quad \text{(IV-7)}$$

*Complete thermodynamic rigor requires noting that \ln term is actually the ratio of product activities over reactant activities. We will assume that the reactants and products display ideal behavior ($\gamma = 1$) so that their activities can be approximated by concentration terms.

and

$$\Delta G_2 = RT \ln([at]) \quad (\text{IV-8})$$

Substitution of equations IV-7 and IV-8 into equation IV-6 provides the relation (the Lewis equation)

$$\Delta G_{at} = \Delta G_{at}^{\circ} + RT \ln\left(\frac{[at]}{[a][t]}\right) \quad (\text{IV-9})$$

By similar manipulations, for the RNA folding reaction (equation IV-6) one obtains

$$\Delta G_{ct} = \Delta G_{ct}^{\circ} + RT \ln\left(\frac{[ct]}{[c][t]}\right) \quad (\text{IV-10})$$

The thermodynamic competition between the two local reactions is defined by

$$\Delta\Delta G_{local} = \Delta G_{at} - \Delta G_{ct} \quad (\text{IV-11})$$

Substitution of equations IV-9 and IV-10 into IV-11 affords

$$\Delta\Delta G_{local} = \Delta G_{at}^{\circ} + RT \ln\left(\frac{[at]}{[a][t]}\right) - \Delta G_{ct}^{\circ} - RT \ln\left(\frac{[ct]}{[c][t]}\right) \quad (\text{IV-12})$$

The properties of logarithms allow equation IV-12 to be condensed to

$$\Delta\Delta G_{local} = \Delta G_{at}^{\circ} - \Delta G_{ct}^{\circ} + RT \ln \left(\frac{[at][c]}{[a][ct]} \right) \quad (IV-13)$$

A IV.2.1c A general comment about the local model. Since we have modeled the unimolecular RNA folding reaction as a bimolecular process, it must be noted that c in equation IV-5 represents an "effective" concentration of competitor strand, denoted $[c']$, since the solution volume in which t and c appear is determined by the length of the polymer chain joining them, x . Mathematically, this is equivalent to an adjustment to the equilibrium constant for an intermolecular reaction between c and t . This adjustment can be expressed

$$K_f = K_{inter} \rho(x) \quad (IV-14)$$

where K_f is the equilibrium constant for the formation of the local secondary structure, $\rho(x)$ is a probability density function for a chain of length x that corrects K_{inter} (an intermolecular reaction equilibrium constant) due to the effective concentration of c . A generalized form for the function $\rho(x)$ with regard to hairpin loop closure has been advanced by Flory and colleagues (1976) and by Markey and Olson (1982) and takes the form

$$\rho(x) = W_x(s) \Gamma(\gamma) \quad (IV-15)$$

where $W_x(s)$ is the spatial probability function describing the fraction of chains of length x with end-to-end distances less than a defined loop closure distance, s , and $\Gamma(\gamma)$ is an angular correlation factor describing the fraction of

1. The first part of the document is a list of names and addresses, including "Mr. J. H. Smith, 123 Main St., New York, N.Y.", "Mr. J. D. Jones, 456 Elm St., Chicago, Ill.", and "Mr. W. E. Brown, 789 Oak St., Boston, Mass." The list continues with several other names and addresses, some of which are partially obscured by the scanning process.

2. The second part of the document is a list of names and addresses, including "Mr. R. L. Green, 101 Pine St., Philadelphia, Pa.", "Mr. S. K. White, 202 Cedar St., San Francisco, Cal.", and "Mr. T. M. Black, 303 Birch St., Los Angeles, Cal." The list continues with several other names and addresses, some of which are partially obscured by the scanning process.

chains with the specified separation distance s that also have the proper angular orientation required for base pairing.

AIV.2.2 Effect of $[c']$ upon the binding of an ASO to its target

The importance of $[c']$ upon the binding behavior of an ASO can be discerned from manipulation of equation IV-13. Recalling that at equilibrium $\Delta\Delta G_{rxn} = 0$, and noting that at 50% occupancy of the ASO target site, $[at] = [ct]$, equation IV-13 rearranges to give

$$\Delta G^{\circ}_{at} - \Delta G^{\circ}_{ct} = -RT \ln\left(\frac{[c']}{[a]}\right) \quad (\text{at 50\% binding}) \quad (\text{IV-16})$$

Note that $\Delta G^{\circ}_{at} - \Delta G^{\circ}_{ct}$ is essentially the definition of a Cscore (equation 2-5), when one considers ΔG°_{at} to represent hybrid duplex formation ($\Delta G^{\circ}_{duplex\ formation}$) and ΔG°_{ct} to represent the formation of a local secondary structure (ΔG°_{stem}). A graph of $\ln([c']/[a])$ versus $(\Delta G^{\circ}_{at} - \Delta G^{\circ}_{ct})$ then allows the influence of $[c']$ to be examined (Figure A4-3). Strong secondary structures in

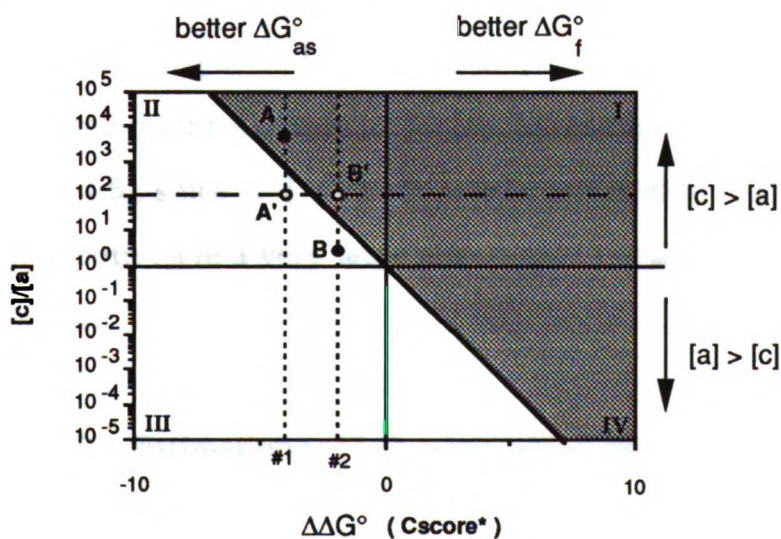


Figure A4-3: The influence of $[c']$ upon ASO binding. The solid sloping black line is the graph of equation IV-16. Gray regions represent conditions which favor secondary structure formation; white regions, conditions that favor formation of an ASO-RNA complex

THE UNIVERSITY OF CHICAGO
DIVISION OF THE PHYSICAL SCIENCES
DEPARTMENT OF CHEMISTRY
5708 SOUTH ELLIS AVENUE
CHICAGO, ILLINOIS 60637
TEL: 773-936-3700
FAX: 773-936-3701
WWW: WWW.CHEM.UCHICAGO.EDU

1
2
3
4
5
6
7
8
9
10
11
12
13
14
15
16
17
18
19
20
21
22
23
24
25
26
27
28
29
30
31
32
33
34
35
36
37
38
39
40
41
42
43
44
45
46
47
48
49
50
51
52
53
54
55
56
57
58
59
60
61
62
63
64
65
66
67
68
69
70
71
72
73
74
75
76
77
78
79
80
81
82
83
84
85
86
87
88
89
90
91
92
93
94
95
96
97
98
99
100

molar excess of ASO favor secondary structure formation (quadrant I), while strong ASO binders in molar excess of weak secondary structures favor ASO binding (quadrant III). However, when the secondary structures and ASO binding thermodynamics are of the same order, the concentration ratio of the reactants becomes important in determining which structure is favored (quadrants II and IV).

When Cscores are computed by comparing multiple ASO at a single concentration $[a]$ while neglecting to account for $[c']$, the ratio $[c']/[a]$ is assumed to be constant. Therefore, analysis of the thermodynamics of the system is restricted to an arbitrary horizontal line in Figure A4-3 (dashed line), despite the fact that the thermodynamic parameters for the different ASO and target sites actually may lie elsewhere in the plane. Consider two ASO at the same concentration, $[a]$, targeted to different secondary structures. The resulting $(\Delta G^{\circ}_{at} - \Delta G^{\circ}_{ct})$ values for each ASO are depicted at positions 1 and 2 (vertical dotted lines, figure A4-3). Ignoring $[c']$ (or assuming $[c']/[a]$ to be constant), we would predict that the equilibrium binding of ASO 1 would be favored (point A'), while the binding of ASO 2 would not (point B'). Incorporating considerations of $[c']$ reveals that the binding of ASO 1 is not favored (point A), since $[c'] > [a]$. Likewise, the binding of ASO 2 is favored (point B), since $[c'] < [a]$. It now becomes clear that $(\Delta G^{\circ}_{at} - \Delta G^{\circ}_{ct})$ and $[c']$ will both have a very large effect upon the ability of the ASO to bind to its target.

AIV.2.3 Estimations of $[c']$: establishing boundaries

In order to apply equations IV-12 and IV-13, values for $[c']$ need to be estimated. As the interchain distance between c and t increases, the volume subtended by c will increase, so that the effective concentration of c will

44-38861-100
ALL INFORMATION CONTAINED
HEREIN IS UNCLASSIFIED
DATE 08-14-2001 BY 60322
UCBAW/BJS
DATE 08-14-2001 BY 60322
UCBAW/BJS

1-1-1
S
S

decrease. Therefore, $[c']$ will be inversely proportional to the chain distance x separating c from t .

An exact solution for $[c']$ requires a probability density function for the polymer chain of length x , which in turn requires both a spatial distribution function and an angular correlation factor (equation IV-14) for the RNA polymer chain. If c and t are separated by greater than 128 ribonucleotides, the spatial distribution function for a real polyribonucleotide chain can be approximated by a spherical Gaussian distribution function (Yevich and Olson, 1979). For chains under 128 ribonucleotides, however, the exact spatial distribution functions are not symmetric and are not easily specified by a simple mathematical expression. Similarly, the angular correlation factor is best described by a summation of Legendre polynomials (Flory *et al.*, 1976) requiring solution of numerous coefficients.

A first approach to estimating $[c']$ would be to assume one of two boundary conditions-- (1) the maximal possible separation of c from t in the case of a fully extended linear polyribonucleotide chain (linear extended model or "l.e.m"; Figure A4-4, and (2) a mean separation distance of c from t when the polyribonucleotide chain is considered to be a random-walk polymer without excluded volume effects, so that the symmetric Gaussian distribution function can be applied (Gaussian random-walk model or "g.r.w."; Figure A4-6). The l.e.m. values will represent the maximal volume element containing c and t (and therefore a minimum effective concentration) while the g.r.w values will represent the average volume element in which c and t appear (and therefore a statistically average effective concentration).

AIV.2.3a An extreme case based upon a maximally extended molecule.

Assuming that each nucleotide in the polyribonucleotide chain is maximally

1

1
2
3
4
5
6
7
8
9
10
11
12
13
14
15
16
17
18
19
20
21
22
23
24
25
26
27
28
29
30
31
32
33
34
35
36
37
38
39
40
41
42
43
44
45
46
47
48
49
50
51
52
53
54
55
56
57
58
59
60
61
62
63
64
65
66
67
68
69
70
71
72
73
74
75
76
77
78
79
80
81
82
83
84
85
86
87
88
89
90
91
92
93
94
95
96
97
98
99
100

1
2
3
4
5
6
7
8
9
10
11
12
13
14
15
16
17
18
19
20
21
22
23
24
25
26
27
28
29
30
31
32
33
34
35
36
37
38
39
40
41
42
43
44
45
46
47
48
49
50
51
52
53
54
55
56
57
58
59
60
61
62
63
64
65
66
67
68
69
70
71
72
73
74
75
76
77
78
79
80
81
82
83
84
85
86
87
88
89
90
91
92
93
94
95
96
97
98
99
100

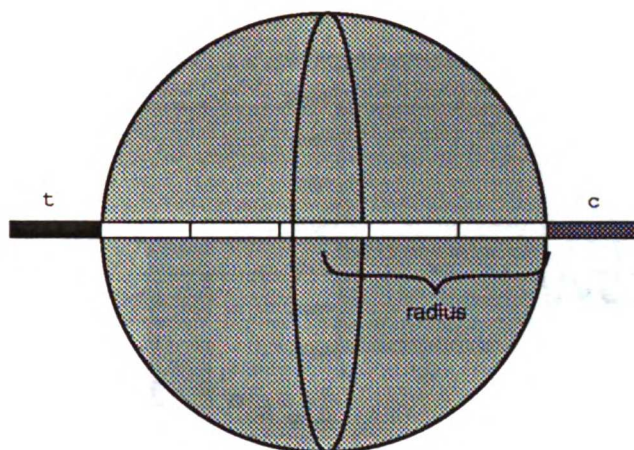


Figure A4-4: The linear extended model of an RNA chain. This model assumes the RNA chain to be rigid rod composed of m nucleotide monomers (rectangular boxes). The final nucleotide in the ASO target site, t (black box), is then separated from its complementary base, c (gray box) by n nucleotides. An effective concentration, $[c]$, of competitor nucleotide can be computed by calculating the separation distance between t and c , using this distance to determine the volume of a sphere which then contains one c molecule

separated from its neighbors, the volume of solution containing a single c molecule can be determined when c is separated from t by n nucleotide monomers (Figure A4-4). Noting that 1\AA^3 is equivalent to 10^{-27} L, two complementary nucleotides (t and c) separated by n nucleotide monomers of length l , define a sphere with volume

$$\left(\frac{nl}{2}\right)^3 \times \frac{4}{3}\pi \times \frac{1}{10^{27}} = \text{volume}(L) \quad (\text{IV-17})$$

The effective molar concentration of the complement can then be calculated as

$$[c'] = \left(\frac{6 \times 10^{27}}{\pi N_A}\right) n^{-3} l^{-3} = 3170 n^{-3} l^{-3} \quad (\text{IV-18})$$

where N_A is Avagadro's number, and l is provided in angstroms. The results of this calculation for maximally extended ribonucleotides with $l = 7\text{\AA}$ (Zubay, 1983) are depicted by closed squares in Figure A4-5.

1. The first part of the document is a list of names and addresses of the members of the committee. The names are listed in alphabetical order, and the addresses are listed below each name. The list includes the names of the members of the committee, the names of the members of the sub-committee, and the names of the members of the advisory committee. The addresses are listed in the same order as the names.

2. The second part of the document is a list of the names and addresses of the members of the committee. The names are listed in alphabetical order, and the addresses are listed below each name. The list includes the names of the members of the committee, the names of the members of the sub-committee, and the names of the members of the advisory committee. The addresses are listed in the same order as the names.

Calculated $[c]$ versus separation distance, n

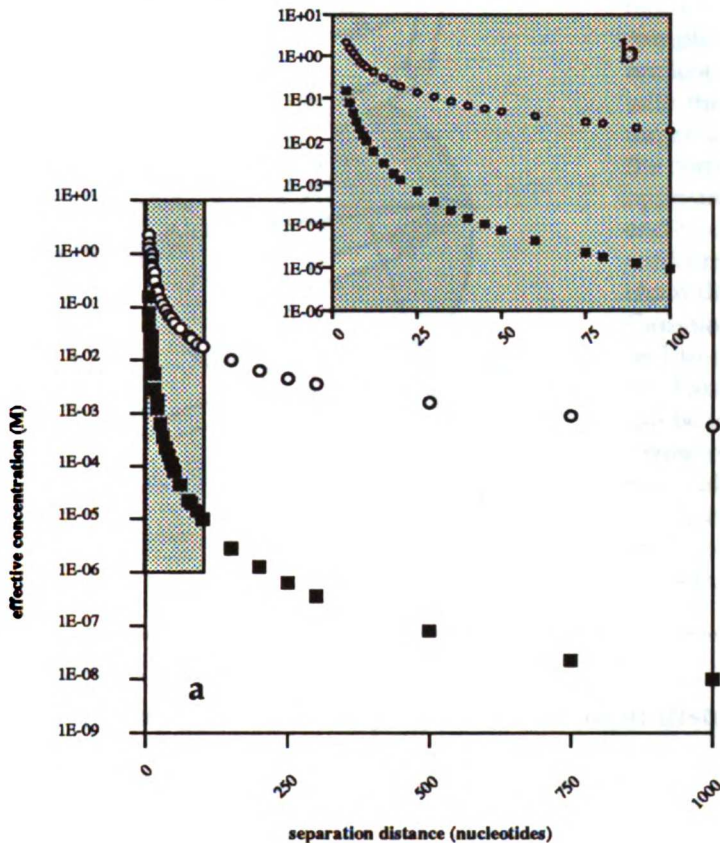


Figure A4-5:
Relationship between separation distance and effective concentration. (a) The separation distance, n , is defined as the number of nucleotides between the ASO target region of the mRNA, t , and a region of complementarity, c . By means of the linear extended model of RNA conformation, a relationship between the effective concentration c and the distance n can be derived (closed squares, see text for details). Likewise, a similar relationship can be derived for a Gaussian random-walk model of RNA conformation (open circles). Note that these models establish the boundary values for the relationship between effective concentration and separation distance. (b) Inset of shaded region in panel a.

AIV.2.3b Gaussian type behavior in a random-walk chain. The second boundary condition assumes that the polyribonucleotide chain behaves as an ideal or random-walk polymer. This model places no restrictions upon the bond angles and dihedral angles between the ribonucleotide monomer units of the chain, and therefore does not prevent two monomer units from occupying the same region of space (*i. e.* no excluded volume effects). As such, it is unrealistic, but offers the advantage of mathematical manipulation of a simple Gaussian radial distribution function.

1. The first part of the document is a list of names and addresses of the members of the committee. The names are listed in alphabetical order, and the addresses are given in full. The list includes the names of the members of the committee, the names of the members of the sub-committee, and the names of the members of the advisory committee. The addresses are given in full, including the street name, the city, the state, and the zip code.

2. The second part of the document is a list of the names and addresses of the members of the committee. The names are listed in alphabetical order, and the addresses are given in full. The list includes the names of the members of the committee, the names of the members of the sub-committee, and the names of the members of the advisory committee. The addresses are given in full, including the street name, the city, the state, and the zip code.

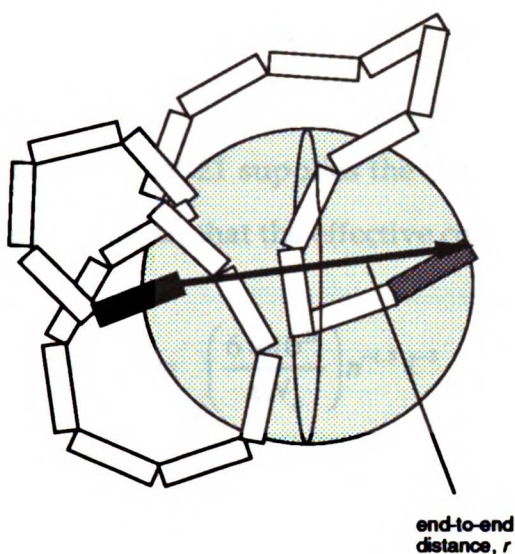


Figure A4-6: The Gaussian random-walk model of an RNA chain. This model assumes the RNA chain to be a completely random flight polymer of m nucleotide monomers (white boxes), with the final nucleotide in the ASO target site, t , and the first nucleotide in the complementary site, c , lying at opposite ends of the chain (separated by end-to-end distance, r). Analysis of the conformational statistics of polymer chain distributions then provides a Gaussian shaped function for possible end-to-end distances between r and $r + dr$. This distribution function, in turn, can be used to arrive at an r value, or the diameter of a sphere containing 1 c molecule. The sphere depicted in this figure is roughly to scale, assuming c and t to be separated by 21 nucleotide monomers.

For a random-walk polymer, the radial distribution function for a chain with an end-to-end distance (Figure A4-6) between r and $r + dr$ is

$$W(r)dr = \left(\frac{\beta}{\sqrt{\pi}} \right)^3 e^{-\beta^2 r^2} 4\pi r^2 dr \quad (\text{IV-19})$$

where $\beta = \sqrt{3/2nl^2}$ and n is the number of monomer units in the ribonucleotide chain, each with length l .

Normalizing equation IV-19 allows computation of a root-mean-square end-to-end distance, $\langle r^2 \rangle_0$,

$$\langle r^2 \rangle_0 = \frac{\int_0^\infty r^2 W(r) dr}{\int_0^\infty W(r) dr} = nl^2 \quad (\text{IV-20})$$

so that

$$\sqrt{\langle r^2 \rangle_0} = \sqrt{nl^2} \quad (\text{IV-21})$$

Equation IV-21 supplies the diameter of a sphere containing one t and one c molecule, so that the effective concentration of c is given by

$$[c'] = \left(\frac{6 \times 10^{27}}{\pi N_A} \right) n^{-1.5} l^{-3} = 3170 n^{-1.5} l^{-3} \quad (\text{IV-22})$$

with l in angstroms. Substitution of $l = 7\text{\AA}$ provides the series of with open circles in Figure A4-5.

AIV.2.4 Estimations of $[c']$: a trial spatial distribution function

AIV.2.4a Gaussian distribution for a random-walk polymer: The Jacobson-Stockmayer derivation. The assumption of a Gaussian distribution as exact description of the polymer chain distributions, while admitted incorrect for small n (see Flory *et al.*, 1976), allows calculation of an exact probability density function, $\rho(n)$ (*i. e.* $\rho(x)$ expressed as a function of monomer units rather than total chain length $x = nl$) for the fraction of chain conformations permitting loop closure. Supposing that the two ends of the chain must be within a distance s in order to permit loop closure, $\rho(n)$ is given by (Jacobson and Stockmayer, 1950)

$$\rho(n) = \int_0^s \left(\frac{\beta}{\sqrt{n}} \right)^3 e^{-\beta^2 r^2} 4\pi r^2 dr \quad (\text{IV-23})$$

Where as before, $\beta = \sqrt[3]{3/2nl^2}$. For cases where $\beta s \ll 1$, the exponential term ~ 1 , so that equation IV-23 can be evaluated as

$$\rho(n) = \left(\frac{3}{2\pi n l^2} \right)^{\frac{3}{2}} \left(\frac{4\pi s^3}{3} \right) = \left(\frac{3}{2\pi n l^2} \right)^{\frac{3}{2}} dV \quad (\text{IV-24})$$

where dV is the volume element defined by s . The effective molarity of the complement is then given by

$$[c'] = \left(\frac{3}{2\pi n l^2} \right)^{1.5} \left(\frac{10^{27}}{N_A} \right) = 548 n^{-1.5} l^{-3} \quad (\text{IV-25})$$

The $(3/2\pi n l^2)$ term in equations IV-24 and IV-25 is known as the Jacobson-Stockmayer factor. Thus equation IV-25 can be used to approximate $[c']$ for an exact, simple mathematical spatial distribution function.

AIV.2.4b Correction for self-avoiding random walk polymers: The Fisher approximation to Jacobson-Stockmayer. Equation IV-25 was derived by allowing the polymer chain to self-intersect. Fisher's (1966) approximation of a Gaussian distribution of chain conformations for a self-avoiding, random-walk polymer on a cubic lattice suggests that $\rho(n)$ is more closely related to $n^{-1.75}$. Simply replacing the exponent in equation IV-25 affords

$$[c'] = \left(\frac{3}{2\pi n l^2} \right)^{1.75} \left(\frac{10^{27}}{N_A} \right) = 455 n^{-1.75} l^{-3} \quad (\text{IV-26})$$

AIV.2.4c Values of l . In section AIV.2.3, values of l were set a 7\AA , to reflect the maximal length for individual monomer units (ribonucleotides).

11
12
13
14
15
16
17
18
19
20
21
22
23
24
25
26
27
28
29
30
31
32
33
34
35
36
37
38
39
40
41
42
43
44
45
46
47
48
49
50
51
52
53
54
55
56
57
58
59
60
61
62
63
64
65
66
67
68
69
70
71
72
73
74
75
76
77
78
79
80
81
82
83
84
85
86
87
88
89
90
91
92
93
94
95
96
97
98
99
100

101
102
103
104
105
106
107
108
109
110
111
112
113
114
115
116
117
118
119
120
121
122
123
124
125
126
127
128
129
130
131
132
133
134
135
136
137
138
139
140
141
142
143
144
145
146
147
148
149
150
151
152
153
154
155
156
157
158
159
160
161
162
163
164
165
166
167
168
169
170
171
172
173
174
175
176
177
178
179
180
181
182
183
184
185
186
187
188
189
190
191
192
193
194
195
196
197
198
199
200

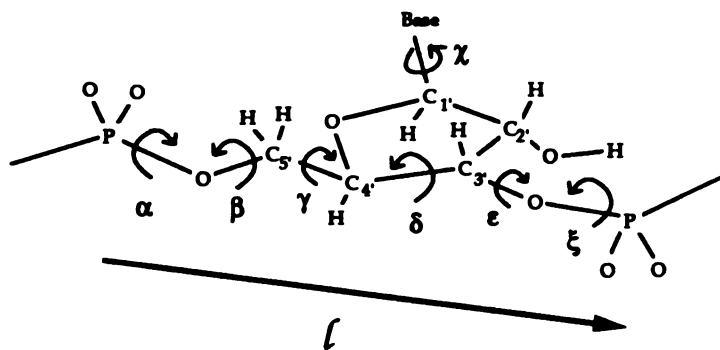


Figure A4-7: Single virtual bond representation of RNA backbone atoms (Olson, 1975). The six individual atomic bonds (α , β , γ , δ , ϵ , ξ) in a single nucleotide can be represented by a single virtual bond, from phosphate to phosphate, of length l . Depending upon the sugar pucker, l will vary between 5.6 and 6.6 Å (see Table A4-1).

Olson (1975) presents a simplified virtual bond scheme for ribonucleotide chains, where the six chemical bonds in the backbone of each ribonucleotide monomer are represented by a single virtual bond (Figure A4-7). The length of this virtual bond varies, depending upon the conformation ("pucker") of the sugar ring in the ribonucleotide monomers (Table A4-1). Use of Olson's values for l and equations IV-25 and IV-26 affords the relationships between $[c']$ and n shown in Table A4-1. The curves defined by these relationships are plotted in Figure A4-8.

TABLE A4-1: $[c']$ as a function of n , in nucleotides and l , in angstroms

	l (Å) ^b	relationship		$(\rho(n)10^{27}/N_A)^a$	
		l. e. m.	g. r. w.	j. s.	j. s. f.
extended form ^c	7	$9.25 n^{-3}$	$9.25 n^{-1.5}$	-	-
C'3 endo (B form) ^d	6.6	-	$11.0 n^{-1.5}$	$1.90 n^{-1.5}$	$0.62 n^{-1.75}$
average	6.1	-	$14.7 n^{-1.5}$	$2.42 n^{-1.5}$	$0.81 n^{-1.75}$
C'3 endo (A form) ^d	5.6	-	$18.1 n^{-1.5}$	$3.12 n^{-1.5}$	$1.10 n^{-1.75}$

^aSupplies $[c_0]$ in M units; l. e. m. = linear extended model; g. r. w. = Gaussian random-walk; j. s. = Jacobson-Stockmayer approximation; j. s. f. = Jacobson-Stockmayer-Fisher approximation.

^bLength of virtual bond

^cZubay (1983)

^dOlson (1975)

1. The first part of the document is a list of names and addresses of the members of the committee. The names are listed in alphabetical order, and the addresses are listed below each name. The list includes names such as Mr. J. H. Smith, Mr. J. D. Jones, and Mr. W. E. Brown, among others.

2. The second part of the document is a list of names and addresses of the members of the committee. The names are listed in alphabetical order, and the addresses are listed below each name. The list includes names such as Mr. J. H. Smith, Mr. J. D. Jones, and Mr. W. E. Brown, among others.

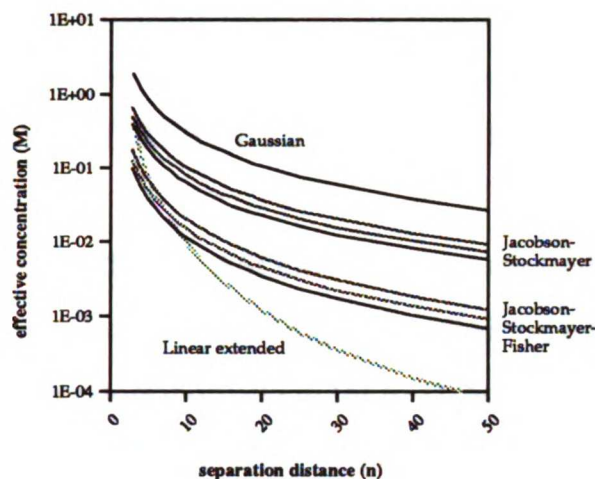


Figure A4-8. Relationship between separation distance and effective concentration. Two trial spatial distribution functions, one derived from Jacobson-Stockmayer polymer loop closure theory (Jacobson-Stockmayer) and a modified version designed to eliminate polymer self-intersection (Jacobson-Stockmayer-Fisher) supply the relationships between effective concentration and separation distance depicted at the left. In both cases, the curves fall between the previously developed Gaussian random walk and Linear extended models of RNA chain behavior.

AIV.2.5 Summary of methods

The mathematical framework for a more rigorous thermodynamic analysis of ASO binding has now been established. A set of competing bimolecular reactions has been developed to describe ASO binding and formation of local RNA secondary structure. Equations IV-12 and IV-13 link free energy changes for each of these processes to equilibrium concentrations of reactants and products. The last requirement for the reaction scheme depicted in Figure A4-1 is a numerical value for $[c']$. Two models of RNA chain behavior were developed to establish the boundary values for $[c']$ as a function of the separation distance, n , between the ASO target region on the RNA and any potential complementary region on the same RNA strand. Well established theoretical models were used to estimate values of $[c']$. The experimental results presented by Lima and coworkers can now be analyzed on a thermodynamic basis, and the predictive utility of Dscores, Cscores, and

1. The first part of the document is a list of names and addresses of the members of the committee. The names are listed in alphabetical order, and the addresses are listed below each name. The list includes names such as Mr. J. H. Smith, Mr. J. D. Jones, and Mr. W. E. Brown, among others.

2. The second part of the document is a list of names and addresses of the members of the committee. The names are listed in alphabetical order, and the addresses are listed below each name. The list includes names such as Mr. J. H. Smith, Mr. J. D. Jones, and Mr. W. E. Brown, among others.

Score be tested and possibly refined for a case where structure and concentration variables are well defined.

AIV.3 RESULTS AND DISCUSSION

AIV.3.1 The ASO:RNA system studied

Lima and colleagues studied the equilibrium solution binding of six 10-mer oligoribonucleotides to 1) their 10-mer oligoribonucleotide complements and 2) a structured 47-mer RNA target (Table A4-2). The 47-mer sequence was derived from the *c-Ha-ras* mRNA sequence, nucleotides +18 to +64, around the region of a point mutation in codon 12 responsible for activating the oncogene (Reddy, 1983). Enzymatic mapping suggests the 47-mer RNA folds upon itself to form a stem/hairpin loop structure (Figure A4-9). The binding sites for each of the six 10-mers are shown.

TABLE A4-2: Oligoribonucleotides used by Lima and colleagues (1992)

Oligo designation (Lima)	Oligo designation (this chapter)	Sequence (5' → 3')	Observed [a ₀]50% binding to 10-mer complement (nM)	Observed [a ₀]50% binding to 47-mer complement (nM)
3270	S1	CCACCACCACC	0.020	10,000
3271	S2	GGCGCCACCA	0.007	200
3292	S3	CGACGGCGCC	0.017	5,000
3291	L1	CACACCGACG	0.050	0.033
3283	L2	UUGCCCACAC	0.030	0.500
3284	L3	ACUCUUUGCC	0.050	> 10,000
target	(16/12) or (19/11)	GGUGGUGGUGGGCGCCGUCGGUGUGGGCAAGAG UGCGCUGACCAUCC		

Handwritten text, possibly a list or notes, appearing as a vertical column of illegible characters.

Handwritten text, possibly a signature or name, appearing as a vertical column of illegible characters.

and 33 (at arrow, Figure A4-9a). Three of the 10-mer ASO bind to sites within the hairpin loop (e.g. ASO 3291, 3283, and 3284; hereafter termed L1, L2 and L3, respectively), while three of the ASO bind to sites along the hairpin stem (e.g. ASO 3270, 3271, and 3292; hereafter termed S1, S2 and S3, respectively).

AIV.3.2 Binding of 10-mer RNA ASO to their 10-mer RNA complements

As part of their study on ASO binding, Lima and coworkers examined the apparent binding of 10-mer RNA ASO to their corresponding 10-mer complements. Analysis of their equilibrium binding data for each ASO affords a chance to test both the computational approach developed above and to test the validity of the thermodynamic parameters (Table 2-1) used to guide RNA folding algorithms and to calculate Dscores.

AIV.3.2a Derivation of suitable concentration-based equations. When considering the binding of an ASO to a single-stranded complementary oligonucleotide, the last two terms of equation IV-12 equal zero, so that the free energy change during the binding process is defined by

$$\Delta\Delta G_{duplex\ formation} = \Delta G_{at}^{\circ} + RT \ln \frac{[at]}{[a][t]} \quad (IV-27)$$

Equilibrium binding resulting in 50% occupancy of the ASO target site will occur when $\Delta\Delta G_{duplex\ formation} = 0$ and $[at] = [t]$. Simplification of equation IV-27, followed by rearranging terms and conversion to base 10 provides

$$[a]_{50\%} = \frac{1}{10^{\left(\frac{-\Delta G_{at}^{\circ}}{2.303RT}\right)}} \quad (IV-28)$$

ALL INFORMATION CONTAINED
HEREIN IS UNCLASSIFIED
DATE 08-14-2001 BY 60322 UCBAW/STP
REASON: EXECUTIVE ORDER 11652

1
2
3
4
5
6
7
8
9
10
11
12
13
14
15
16
17
18
19
20
21
22
23
24
25
26
27
28
29
30
31
32
33
34
35
36
37
38
39
40
41
42
43
44
45
46
47
48
49
50
51
52
53
54
55
56
57
58
59
60
61
62
63
64
65
66
67
68
69
70
71
72
73
74
75
76
77
78
79
80
81
82
83
84
85
86
87
88
89
90
91
92
93
94
95
96
97
98
99
100

Note that $[a]_{50\%}$ is the equilibrium concentration of free ASO at 50% occupancy. The input concentration of ASO necessary to produce 50% occupancy of the target site can be denoted $[a_o]_{50\%}$. By conservation of mass

$$[a_o]_{50\%} = [a]_{50\%} + [at]_{50\%} \quad (\text{IV-29})$$

Substituting equation IV-28 into equation IV-29, and noting that $[at]_{50\%}$ is equivalent to one-half the starting concentration of target molecule, t_o , provides

$$[a_o]_{50\%} = \frac{1}{10^{\left(\frac{-\Delta G_{\#}^{\circ}}{2.303RT}\right)}} + \frac{1}{2}t_o \quad (\text{IV-30})$$

AIV.3.2b Comparison of theory to experimental results. The results of the equilibrium solution binding of the six 10-mer RNA oligonucleotides to their single-stranded 10-mer RNA complements reported by Lima and coworkers are presented in Table A4-3. In these experiments the input con-

TABLE A4-3: Binding of 10-mer ASO to 10-mer complements (Lima *et al.*, 1992)

Oligo	$\Delta G^{\circ}_{\text{duplex}}$ (kcal/mol)	Dscore	Rank by Dscores	Predicted $[a_o]_{50\%}$ (pM)	Rank by predicted binding	Observed $[a_o]_{50\%}$ (pM)	Rank by observed binding
S1	-17.0	-8.50	3	5	3	20	3
S2	-19.8	-9.90	1	4	1	7	1
S3	-19.6	-9.80	2	4	1	17	2
L1	-15.7	-7.85	5	13	5	50	5
L2	-16.3	-8.15	4	7	4	30	4
L3	-15.2	-7.60	6	24	6	50	5

centration of target strand, $[t_0]$, was 8 pM, while the input concentration of ASO, $[a_0]$, varied from 1 pM to 10 μ M.

Table A4-3 reveals good agreement between predicted $[a_0]_{50\%}$ values and experimentally observed $[a_0]_{50\%}$ values ($r^2 = 0.747$ ($P < 0.05$)), suggesting that the mathematical framework derived in the Methods section is valid. The correlation between the Dscore and observed $[a_0]_{50\%}$ ($r^2 = 0.824$ ($P < 0.01$)) also supports the validity of the thermodynamic values used to compute ΔG°_{at} .

AIV.3.3 Binding of ASO to the 47-mer RNA hairpin: predictions from the thermodynamic indices (Dscore, Sscore, Cscore).

AIV.3.3a Calculation of ΔG°_f for the hairpin structures In order to compute the thermodynamic indices developed in Chapter 2, or to apply equations IV-3 or IV-13, values for the free energy of formation of the RNA hairpin must be estimated. These values can be obtained using the Zuker suboptimal algorithm. Constraining the nucleotides mapped to the loop to remain single-stranded provides the following free energies of formation for the mapped structures:

s16/12 structure (Figure A4-9a)	$\Delta G^{\circ}_{stem} = \Delta G^{\circ}_f = -13.1$ kcal/mol
s19/11 structure (Figure A4-9b)	$\Delta G^{\circ}_{stem} = \Delta G^{\circ}_f = -12.8$ kcal/mol

The difference in energies between the two structures (0.3 kcal/mol) corresponds to a $K_{eq} = 1.6$, supporting the notion of a substantial amount of both forms of the hairpin present in the solutions subjected to enzymatic mapping. Interestingly, the Zuker algorithm predicts a different optimal structure possessing a $\Delta G^{\circ}_f = -14.7$ kcal/mol. This predicted structure is illustrated in Figure A4-9c.

AIV.3.3b Failure of the thermodynamic indices as predictors of binding behavior towards a structured target site. To examine the methodology used to calculate Sscores and Cscores, the ΔG°_f value for the hairpin structures was distributed back among the base-paired nucleotides according to equation 2-2. For the (s16/12) structure, $\Delta G^\circ_f = -13.1$ kcal/mol. According to equation 2-2:

$$E_N = \frac{\Delta G^\circ_{stem}}{B} = \frac{-13.1}{(2 \times 12)} = -0.546 \text{ kcal mol}^{-1} \text{ base}^{-1} \quad (\text{IV-31})$$

Therefore, an Sscore for each 10-mer ASO target site on the (s16/12) structure is computed by

$$Sscore = \sum_{N=1}^{10} b_N (E_N) \quad (\text{IV-32})$$

where $b_N = 0$ if the base is single-stranded, or 1 if the base is base-paired.

This is equivalent to

$$Sscore = mE_N \quad (\text{IV-33})$$

where m = the number of base-paired nucleotides in the target site. Dscores for each ASO were computed according to equation (2-4), while Cscores were computed according to equation (2-5).

$$Dscore = \frac{\Delta G^\circ_{stem}}{2} \quad (2-4)$$

1. The first part of the document is a list of names and addresses of the members of the committee. The names are listed in alphabetical order, and the addresses are given in full. The list includes the names of the members of the committee, the names of the members of the sub-committee, and the names of the members of the advisory committee. The addresses are given in full, including the street, city, and state.

2. The second part of the document is a list of the names and addresses of the members of the committee. The names are listed in alphabetical order, and the addresses are given in full. The list includes the names of the members of the committee, the names of the members of the sub-committee, and the names of the members of the advisory committee. The addresses are given in full, including the street, city, and state.

TABLE A4-4: Analysis of 10-mer ASO binding to 47-mer target (16/12 structure) using thermodynamic indices

Oligo	ΔG°_{st}	Dscore	Dscore ordinal	ΔG°_f	m	Sscore	Cscore	Cscore ordinal	$[a_o]_{50\%}^{obs}$ (nM)	binding ordinal
S1	-17.0	-8.5	3	-13.1	6	-3.3	-5.2	5	10,000	5
S2	-19.8	-9.9	1	-13.1	9	-4.9	-5.0	6	200	3
S3	-19.6	-9.8	2	-13.1	6	-3.3	-6.5	3	5000	4
L1	-15.7	-7.9	5	-13.1	0	0	-7.9	2	0.033	1
L2	-16.3	-8.2	4	-13.1	0	0	-8.2	1	0.5	2
L3	-15.2	-7.6	6	-13.1	2	-1.1	-6.5	3	> 10,000	6

Statistics:	Dscore vs. $[a_o]_{50\%}^{obs}$	$r^2 = 0.027$	(N. S.)
	Sscore vs. $[a_o]_{50\%}^{obs}$	$r^2 = 0.318$	(N. S.)
	Cscore vs. $[a_o]_{50\%}^{obs}$	$r^2 = 0.552$	(N. S.)

^aFor the (s16/12) hairpin structure

^bComputed by $Sscore = m \cdot E_n = m \cdot -0.546$ (equation IV-33)

$$Cscore = Dscore - Sscore = \left(\Delta G^{\circ}_{stem} / 2 \right) - (mE_N) \quad (2-5)$$

The results of these computations are shown in Table A4-4. No significant correlations were obtained between any of the thermodynamic indices (Dscore, Sscore and Cscore) and the $[a_o]_{50\%}^{obs}$ values, nor did any of the indices correctly rank the ASO with respect to $[a_o]_{50\%}^{obs}$ (compare the ordinal values).

AIV.3.4 Analysis of ASO binding to the structured RNA target: $\Delta\Delta G^{\circ}_{rxn}$ computations.

The thermodynamics of an ASO binding reaction is best described by a $\Delta\Delta G$ value defined as the difference in the free energy of ASO binding versus

RNA secondary structure formation (Equation IV-3). With the knowledge of pseudo half-knot formation introduced in Chapter 1, the ΔG_{AR} value of equation IV-3 can be decomposed into the following components

$$\Delta G_{AR} = \Delta G_{at} + \Delta G_{f'} + \Delta G_c \quad (\text{IV-34})$$

where ΔG_{at} is the Gibbs free energy of formation of the ASO-RNA duplex, $\Delta G_{f'}$ is the Gibbs free energy of formation for the RNA structure outside of the ASO-RNA duplex region, and ΔG_c is the free energy of any possible coaxial stacking between the ASO-RNA duplex and stems in the new RNA structure. Each of these free energy values can be computed at standard state to afford a standard state approximation to equation IV-3:

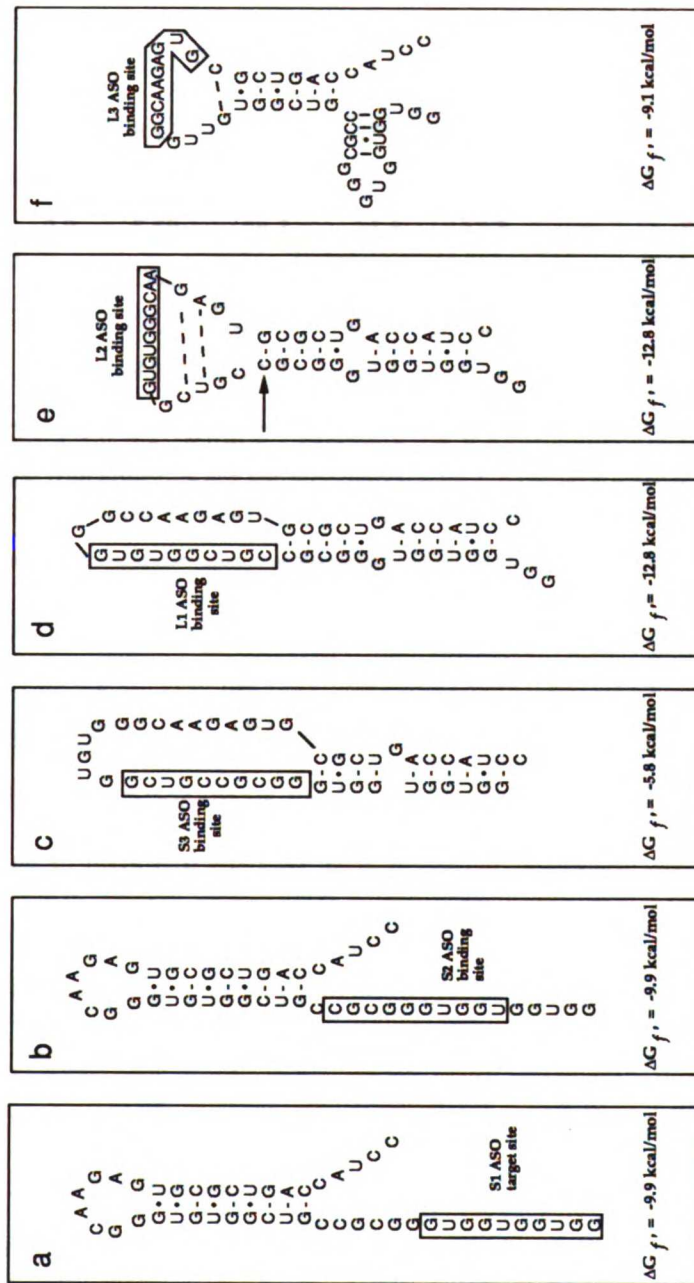
$$\Delta \Delta G^\circ = \Delta G^\circ_{AR} - \Delta G^\circ_f = \Delta G^\circ_{at} + \Delta G^\circ_{f'} + \Delta G^\circ_c - \Delta G^\circ_f \quad (\text{IV-35})$$

Values for $\Delta G^\circ_{f'}$ and ΔG°_c can be supplied by the Zuker FOLD algorithm for foldings of the 47-mer hairpin sequence where the target sites of the various ASO are forced to remain single stranded. The structures predicted for the constrained foldings are shown in Figure A4-10. Note that Lima and coworkers supply mapping data for the complexes formed by the binding of L1 and L2. The predicted structure for the L1 bound complex agrees with the experimentally mapped structure; the predicted structure for the L2 bound complex also agrees with the mapped structure once pseudo half-knot loop formation distances are considered (see caption to Figure A4-10). Mapped structures were not presented for any of the other bound complexes (L3, S1, S2, or S3)— therefore the validity of the predicted structures is not known.

1
2
3
4
5
6
7
8
9
10
11
12
13
14
15
16
17
18
19
20
21
22
23
24
25
26
27
28
29
30
31
32
33
34
35
36
37
38
39
40
41
42
43
44
45
46
47
48
49
50
51
52
53
54
55
56
57
58
59
60
61
62
63
64
65
66
67
68
69
70
71
72
73
74
75
76
77
78
79
80
81
82
83
84
85
86
87
88
89
90
91
92
93
94
95
96
97
98
99
100

1
2
3
4
5
6
7
8
9
10
11
12
13
14
15
16
17
18
19
20
21
22
23
24
25
26
27
28
29
30
31
32
33
34
35
36
37
38
39
40
41
42
43
44
45
46
47
48
49
50
51
52
53
54
55
56
57
58
59
60
61
62
63
64
65
66
67
68
69
70
71
72
73
74
75
76
77
78
79
80
81
82
83
84
85
86
87
88
89
90
91
92
93
94
95
96
97
98
99
100

Figure A4-10: Predicted RNA structures adopted upon ASO binding to the target 47-mer hairpin, and their calculated free energies of formation



The Zuker FOLD algorithm supplied the above six predicted structures and the free energies of their formation when constraining the ASO target sites (shown within boxes) to remain single-stranded. Base-paired nucleotides are shown connected by dashes; G-U matches are shown connected by dots. The dashed lines appearing in panels e and f indicate base-pairs predicted to occur according to the Zuker algorithm, but which are sterically impossible according to the theory of pseudo half-knot formation (Chapter 1). Free energies for these structures containing sterically impossible base pairs were adjusted accordingly (adjusted values shown). Mapping data was presented by Lima and coworkers for the bound complexes formed between L1-RNA and L2-RNA. The predicted structure shown in panel d for L1-RNA is identical to the experimentally mapped structure; the adjusted predicted structure shown in panel e for the binding of L2-RNA also agrees with the experimentally mapped structure. Lima and coworkers suggest the base pair denoted by the arrow is transiently opening and closing due to steric effects produced by the binding of L2. The free energy of formation for the L2 bound structure assumes this base pair to be closed.

Table A4-5: Computed $\Delta\Delta G^\circ$ values as rank predictors of ASO binding

ASO	ΔG°_d	ΔG°_c	ΔG°_f	ΔG°_{AR}	ΔG°_f	$\Delta\Delta G^\circ$	Rank by $\Delta\Delta G^\circ$	obs [a ₀]50% (nM)	obs $\Delta\Delta G^a$	Rank by bind
S1	-17.0	0	-9.9 ^b	-26.9	-13.1	-13.8	5	10000	-7.1	5
S2	-19.8	0	-9.9 ^b	-29.7	-13.1	-16.6	2	200	-9.5	3
S3	-19.6	-2.9	-5.8 ^b	-28.3	-13.1	-15.2	4	5000	-7.5	4
L1	-15.7	-2.9	-12.8	-31.4	-13.1	-18.3	1	0.033	-14.9	1
L2	-16.3	0	-12.8	-29.1	-13.1	-16.0	3	0.5	-13.2	2
L3	-15.2	0	-9.1 ^b	-24.3	-13.1	-11.2	6	> 10000	> -7.1	6

^aComputed from $\Delta\Delta G^\circ = -RT \ln K_a'$ (where K_a' is the experimentally measured K_a)

^bDenotes these free energies are for structures which represent a complete reorganization of the hairpin structure, rather than simply displacement of the competitor strand at the ASO target site.

Use of the previously determined values of ΔG°_{at} and ΔG°_f , combined with values of ΔG°_f and ΔG°_c thus computed, afford the values presented in Table A4-5. The Spearman rank correlation coefficient for the calculated $\Delta\Delta G^\circ$ values versus the ranked 50% binding concentrations is $r_s = 0.928$ ($P < 0.01$). However, it can be seen that the calculated $\Delta\Delta G^\circ$ values differ significantly from the observed $\Delta\Delta G$ values. For the stem binding ASO, the difference varies between 6.7 and 7.7 kcal, while for the loop binding ASO, the difference varies between 2.8 and 4.1 kcal. Note that for each of the stem binding ASO, and for ASO L3, the ΔG°_f is computed for a structure which differs significantly from the starting (s16/12) structure (Figure A4-10)— the hairpin stem has been completely reorganized rather than simply displaced at the ASO target site.

1
2
3
4
5
6
7
8
9
10
11
12
13
14
15
16
17
18
19
20
21
22
23
24
25
26
27
28
29
30
31
32
33
34
35
36
37
38
39
40
41
42
43
44
45
46
47
48
49
50
51
52
53
54
55
56
57
58
59
60
61
62
63
64
65
66
67
68
69
70
71
72
73
74
75
76
77
78
79
80
81
82
83
84
85
86
87
88
89
90
91
92
93
94
95
96
97
98
99
100

1
2
3
4
5
6
7
8
9
10
11
12
13
14
15
16
17
18
19
20
21
22
23
24
25
26
27
28
29
30
31
32
33
34
35
36
37
38
39
40
41
42
43
44
45
46
47
48
49
50
51
52
53
54
55
56
57
58
59
60
61
62
63
64
65
66
67
68
69
70
71
72
73
74
75
76
77
78
79
80
81
82
83
84
85
86
87
88
89
90
91
92
93
94
95
96
97
98
99
100

AIV.3.5 Binding of ASO to the 47-mer RNA hairpin: Estimating the effective concentration of competitor strand, [c'].

The reaction scheme presented in Figure A4-1 is predicated upon the assumption that the ASO binding reactions can be modeled as a competition between two "ligands" for the same binding site. Binding of the ASO (ligand *a*) is in competition with the binding of the complementary strand (ligand *c*). The observed binding properties of the ASO will then depend upon the affinity constants for each "ligand", and the relative concentrations of each ligand in the system. The affinity of ligand *a* will be $\Delta G^{\circ}_{duplex\ formation}$; the affinity for ligand *c* in this simple hairpin system will be ΔG°_f for the secondary structure.

AIV.3.5a Estimations for [c'] from RNA chain behavior models. Using the mapped (s16/12) and (s19/11) structures, effective [c'] values for the input amount of competitor, [c], can be computed from the RNA chain behavior models, once an appropriate separation distance, *n*, has been selected. What value of *n* should be selected?

Studies of nucleic acid hybridizations suggest that nucleation events are the rate limiting step in helix formation (Wetmur and Davidson, 1968). Nucleation is dependent upon probabilities of molecular collisions, which are in turn dependent upon reactant concentrations. *N* values should be selected that reflect the complementary bases most likely to nucleate (*i.e.* have the highest effective concentrations or smallest separation distances). In the case of hairpin formation by a single polynucleotide strand, the nucleotides most likely to nucleate are those which close the hairpin loop. Thus, *n* = 16 for the (s16/12) structure and *n* = 19 for the (s19/11) structure. Table A4-6 lists the

TABLE A4-6: Values of [c'] from models; comparison of theoretical [c'] to observed [c']

l (Å)	[c'] mM ^a								observed	
	l. e. m.		g. r. w.		j. s.		j. s. f.		Oligo	
	n = 16	n = 19	n = 16	n = 19	n = 16	n = 19	n = 16	n = 19		
7	2.3	1.3	-	-	-	-	-	-	S1	5.6
6.6	-	-	170	130	30	23	4.8	3.6	S2	10.4
6.1	-	-	230	180	39	29	6.4	4.7	S3	113
5.6	-	-	280	220	48	38	8.6	6.3		

^aValues for various models obtained from equations in Table A4-1; Observed [c'_o] from equation IV-36.

calculated [c'_o] values derived from each of the various models of RNA chain behavior.

AIV.3.5b Checking the theoretical [c'] values versus a [c'] value computed from the experimental data. Equation IV-13 can be rearranged to solve for observed [c'] values. Equilibrium binding resulting in 50% occupancy of the ASO target site will occur when $\Delta\Delta G_{process} = 0$ and $[at] = [ct]$. Simplification of equation IV-13, followed by rearranging terms, and converting to base 10 provides

$$[c'] = [a]10^{\left(\frac{-(\Delta G_{at}^{\circ} - \Delta G_{ct}^{\circ})}{2.303RT}\right)} \quad (IV-36)$$

The [c'] and [a] values in equation IV-36 are free concentrations at equilibrium, and must be corrected to input values by conservation of mass.

The input concentration of t for these experiments was 25 pM, so that $[at]_{50\%} = 12.5$ pM. These corrections then afford

$$[c'_o] = ([a_o]_{50\%} - 12.5 \text{ pM}) 10^{\left(\frac{-(\Delta G_{at}^\circ - \Delta G_{ct}^\circ)}{2.303 RT} \right)} \quad (\text{IV-37})$$

Substitution of the $[a_o]_{50\%}^{obs}$ values for oligos S1, S2, and S3, (from Table A4-2) as well as their computed ΔG_{at}° values (from Table A4-3) and the computed structure energy ($\Delta G_{ct}^\circ = \Delta G_{\beta}^\circ$) into equation IV-37 affords $[c']$ estimates (Table A4-6). It can be seen that the estimated $[c']$ values agree most closely with the Jacobson-Stockmayer-Fisher approximations of RNA chain behavior.

AIV.3.6 Computing $[a_o]_{50\%}$ values for each of the ASO.

AIV.3.6a Predictions for loop binding ASO. In the case of ASO binding to single-stranded regions of the hairpin loop, no competing ligand is present at the binding site. Therefore, the ASO binding process can be treated as approximately equivalent to 10-mer ASO binding to a complementary 10-mer; equation IV-30 can be used to calculate $[a_o]_{50\%}$ for the binding reactions in these cases. These calculated values appear in Table A4-7. It can

Table A4-7: Predicted $[a_o]_{50\%}$ values for loop binding ASO

Oligo	ΔG_{at}°	calculated $[a_o]_{50\%}$ (nM)	observed $[a_o]_{50\%}$ (nM)
L1	-15.6	0.021	0.033
L2	-16.3	0.016	0.500
L3	-15.2	0.032	> 10000

be seen that the agreement between $[a_o]_{50\%}^{calc}$ and $[a_o]_{50\%}^{obs}$ is quite good for ASO L1, moderate for L2, and quite poor for L3. Interestingly, treatment of L3 as a stem binder produces much better agreement with its observed binding properties (see section AIV.3.7 and Discussion, below).

AIV.3.6b Predictions for stem binding ASO. For the general case of an oligonucleotide binding to a region of the target RNA possessing secondary structure, equation IV-13 applies. Considering equilibrium binding resulting in 50% target site occupancy, equation IV-13 can be rearranged to give

$$\frac{[c]_{50\%}}{[a]_{50\%}} = 10^{\left(\frac{-(\Delta G_{st}^{\circ} - \Delta G_f^{\circ})}{2.303 RT}\right)} \quad (IV-38)$$

Further rearrangement and accounting for conservation of mass affords

$$[a_o]_{50\%} = \frac{[c]_{50\%}}{10^{\left(\frac{-(\Delta G_{st}^{\circ} - \Delta G_f^{\circ})}{2.303 RT}\right)}} + [at]_{50\%} \quad (IV-39)$$

Table A4-8 shows the results of the equation IV-39 when applied to the thermodynamic data for ASO S1, S2 and S3. It can be seen for all three ASO that the $[a_o]_{50\%}^{obs}$ values lie between the $[a_o]_{50\%}^{calc}$ values set by the two boundary models (i. e. linear extended model and Gaussian random walk). The overall best agreement occurs when using the $[c']$ values from the Jacobson-Stockmayer-Fisher approximation; however, the agreement ranges from quite good for S1 to moderate for S3. Note also that ASO L3 is treated as a stem binder on this chart, resulting in a much better prediction of its binding behavior (see Discussion, below).

TABLE A4-8: Calculation of $[a_0]_{50\%}$ for stem-binding oligonucleotides

Oligo	ΔG°_{at} (kcal/mol)	n (nts)	ΔG°_{ct} (kcal/mol)	$\Delta \Delta G^{\circ}$ (kcal/mol)	l (Å)	calculated $[a_0]_{50\%}$				obs $[a_0]_{50}$ %
						lem	grw	js	jsf	
S1	-17.0	16	-13.1	-3.9	7.0	4.1 μ M	300 μ M	53 μ M	8.6 μ M	10 μ M
						6.6	410 μ M	68 μ M	11 μ M	
						6.1	500 μ M	86 μ M	15 μ M	
S2	-19.8	16	-13.1	-6.7	7.0	44 nM	3.2 μ M	570 nM	91 nM	200 nM
						6.6	4.4 μ M	720 nM	121 nM	
						6.1	5.3 μ M	910 nM	163 nM	
S3	-19.6	16	-13.1	-6.5	7.0	60 nM	4.5 μ M	790 nM	130 nM	5 μ M
						6.6	6.0 μ M	1 μ M	170 nM	
						6.1	7.3 μ M	1.3 μ M	230 nM	
L3	-15.2	16	-13.1	-2.1	7.0	7.6 μ M	5.6 mM	990 μ M	160 μ M	>10 μ M
						6.6	7.6 mM	1.3 mM	210 μ M	
						6.1	9.3 μ M	1.6 mM	290 μ M	

AIV.4 DISCUSSION

The hairpin system reported on by Lima and colleagues is well characterized with respect to structure of the target RNA prior to ASO binding. Theoretical models concerning the formation of pseudo half-knots and the minimal distances for loop formation in pseudo knots (Chapter 1) were used to guide interpretation of the structure predictions for ASO-RNA complexes (Figure A4-10). Additional information supplied by mapping of two ASO-RNA complexes suggests these predicted structures are reasonable.

AIV.4.1 Dscores and ASO binding to 10-mer complements.

The correlation between the Dscores and the observed binding of the 10-mer ASO to their 10-mer complements is not surprising since the thermodynamic values used to compute Dscores were derived from studies of the melting of various small RNA oligonucleotide helices. This correlation reaffirms that these values are applicable as predictors of the physical behavior of an oligonucleotide. Manipulation of the calculated $\Delta\Delta G^\circ$ values for duplex formation also produces reasonable agreement with the observed oligonucleotide concentrations required to produce 50% binding to their 10-mer complements. The confidence which can then be placed in the Dscore and $\Delta G^\circ_{duplex\ formation}$ computations for simple duplex formation then allows a detailed examination of the effects of target site RNA structure upon ASO binding, since differences between the computed free energies of complex formation and the observed ASO binding free energies are likely due to concentration effects, target RNA secondary structure formation and disruption, and ionic strength effects.

1
2
3
4
5
6
7
8
9
10
11
12
13
14
15
16
17
18
19
20
21
22
23
24
25
26
27
28
29
30
31
32
33
34
35
36
37
38
39
40
41
42
43
44
45
46
47
48
49
50
51
52
53
54
55
56
57
58
59
60
61
62
63
64
65
66
67
68
69
70
71
72
73
74
75
76
77
78
79
80
81
82
83
84
85
86
87
88
89
90
91
92
93
94
95
96
97
98
99
100

101
102
103
104
105
106
107
108
109
110
111
112
113
114
115
116
117
118
119
120
121
122
123
124
125
126
127
128
129
130
131
132
133
134
135
136
137
138
139
140
141
142
143
144
145
146
147
148
149
150

AIV.4.2 Caveats about RNA structure prediction.

Figure A4-9 reveals that RNA folding algorithms may have difficulty predicting even simple RNA structures. This is particularly disturbing since the algorithm utilized to obtain the structure free energies is considered to be among the best predictive algorithms available. While the Zuker folding algorithm is guaranteed to produce structures with the absolute global free energy minimum for a given RNA sequence, the discrepancy between predicted and mapped structures only serves to reiterate that folding algorithms may not predict biologically relevant structures. This may in some degree, be attributable to differences in structures formed at physiological ionic strength and those predicted to form using thermodynamic values determined at 1M NaCl.

AIV.4.3 Failure of the thermodynamic indices as predictors of ASO binding to structured targets.

The absence of a statistically significant correlation between Dscores and $[a_o]_{50\%}^{obs}$ for the binding of the 10-mer ASO to the hairpin structure is not surprising since the Dscores index does not account for target secondary structure, while the secondary structure of the 47-nucleotide RNA clearly has an effect upon the binding of the ASO. Table A4-4 also reveals the Sscores and Cscores are also poor indicators of ASO binding. It should be noted that the 47-mer hairpin system is simple in the fact that each of the ASO is binding the same RNA secondary structure, and therefore $[c_o]/[a_o]$ is constant (e.g. all the ASO are targeted to the same secondary structure) an assumption inherent to the Sscores and Cscores indices as defined in Chapter 2. Therefore, the inability of these indices to correctly rank the ASO with respect to binding affinity is most likely is due to an inaccuracy of these indices in representing the thermodynamics of this ASO-RNA system.

Although the ΔG_f° for the entire local secondary structure is considered when computing an Sscore, the redistribution function (equation 2-2) only considers a fraction of the total $\Delta G_{f,stem}^\circ$ (*i. e.* only those bases in the secondary structure which appear in the target site *t*). Therefore, ASO binding is considered to disrupt the local RNA secondary structure only at the target site. The binding of the ASO is not presumed to be affected by changes in the RNA secondary structure outside of the target site. This assumption is clearly erroneous, particularly when one examines the better rankings of ASO binding supplied by the $\Delta\Delta G^\circ$ calculations (Table A4-5), which accommodate alterations in RNA secondary structure outside the ASO target site.

AIV.4.4 Comments about the ASO binding model, $\Delta\Delta G^\circ$ calculations, and predicted ASO concentrations required to produce 50% binding.

The models developed in this appendix reflect a second level of refinement over the simple thermodynamic indices introduced in Chapter 2. The binding of the ASO to the RNA target was examined both at the global level (consideration of RNA structure changes both at and outside of the target site; equations IV-3 and IV-35) and at the local level (equations IV-13, IV-30 and IV-39). Each approach has afforded insights into important target site structural effects upon ASO binding, yet each approach also is limited in its utility for correctly predicting ASO binding behavior for this system.

AIV.4.4a $\Delta\Delta G^\circ$ calculations. Equation IV-35 allows calculation of an estimated $\Delta\Delta G^\circ$ for the ASO-RNA binding reactions. In this equation, ΔG_{at}° and ΔG_f° values are computed for known RNA structures; thus the uncertainty in these values is primarily the uncertainty associated with the thermodynamic data set determined at 1M NaCl versus experiments conducted at 0.1M Na⁺. The major uncertainty associated with equation IV-

35 applied to the Lima study is due to the ΔG°_f and ΔG°_c terms— these values are strongly dependent upon the accuracy of the predicted RNA structures. Use of the Zuker FOLD algorithm for prediction of constrained RNA structures produces structures consistent with those mapped for the bound complexes of L1-RNA and L2-RNA. However, the validity of the remaining predicted structures is unknown.

The $\Delta\Delta G^{\circ}$ values computed by equation IV-35 correctly predict the observed rank order of binding for the ASO set (Table A4-5). However, the computed $\Delta\Delta G^{\circ}$ values differ significantly from the apparent $\Delta\Delta G$ supplied using the actual binding constants for the ASO set; a difference of about 3-4 kcal/mol for the loop binding ASO, and about 7 kcal/mol for the stem binding ASO. The sources of these deviations may be ionic strength effects and/or competitor strand effects, since the global reaction scheme does not weight the effective concentration of competitor strand leading to secondary structure formation. If a uniform difference of ~4 kcal/mol is attributed to ionic strength effects (the average deviation observed for loop binding ASO which are not in competition with any RNA strands), the discrepancy between the calculated $\Delta\Delta G^{\circ}$ and observed $\Delta\Delta G$ values for the stem binding ASO (S1, S2, S3) reduces to ~ 3 kcal/mol, equivalent to a 8 mM effective concentration value. This is well within the boundary concentrations computed using the linear extended model or Gaussian random walk model of RNA chain behavior for this particular hairpin loop (Table A4-6).

AIV.4.4b Results for each of the local binding reactions. Tables A4-7 and A4-8 estimate the concentration of ASO required to produce 50% binding to the target RNA. The predictions for the stem binding ASO S1 and S2 (using the Jacobson-Stockmayer-Fisher approximation) and for the loop binding ASO L1 agree quite well with the observed binding behavior of these

1
2
3
4
5
6
7
8
9
10
11
12
13
14
15
16
17
18
19
20
21
22
23
24
25
26
27
28
29
30
31
32
33
34
35
36
37
38
39
40
41
42
43
44
45
46
47
48
49
50
51
52
53
54
55
56
57
58
59
60
61
62
63
64
65
66
67
68
69
70
71
72
73
74
75
76
77
78
79
80
81
82
83
84
85
86
87
88
89
90
91
92
93
94
95
96
97
98
99
100

101
102
103
104
105
106
107
108
109
110
111
112
113
114
115
116
117
118
119
120
121
122
123
124
125
126
127
128
129
130
131
132
133
134
135
136
137
138
139
140
141
142
143
144
145
146
147
148
149
150

ASO. The observed binding of ASO S3 is about an order of magnitude weaker than predicted by the Jacobson-Stockmayer-Fisher treatment. Note that each of the stem binding ASO does bind within the limits proscribed by the linear extended model and Gaussian random-walk models of RNA chain behavior.

The binding behavior of ASO L2 is not adequately described by an analysis of the local reaction free energies for loop binders (equation IV-11, from which equations IV-13 and IV-38 were subsequently derived). It is predicted to display 50% binding at lower concentrations than ASO L1, and at concentrations about an order of magnitude lower than what was experimentally observed (Table A4-7). Yet examination of the results from the global $\Delta\Delta G^\circ$ calculations (Table A4-5) shows that when computing the global thermodynamics of ASO binding, L2 should bind less well than L1. This discrepancy in predicted binding behavior can be reconciled to some degree by inspection of the mapped L2-ASO complex presented in Figure A4-10. Binding of L2 to the hairpin loop slightly destabilizes the top of the hairpin stem, which amounts to a free energy penalty to ASO binding. Thus a "loop binding" ASO actually influences the structure of stem regions of the target RNA hairpin. This type of interaction, which thermodynamically can be considered to be a nonlocal free energy penalty, is not included in equation IV-30 when modeling the local binding reaction of loop targeted ASO. The global $\Delta\Delta G^\circ$ computations account for both local and nonlocal changes in RNA structure; hence the better predictions supplied by the $\Delta\Delta G^\circ$ computations for L2. This type of nonlocal effect, however, could not be predicted *a priori* from current models of loop structure, nor does any theory currently address the minimum length of single stranded regions required to connect a helix within a loop to the loop closing stem.

1
2
3
4
5
6
7
8
9
10
11
12
13
14
15
16
17
18
19
20
21
22
23
24
25
26
27
28
29
30
31
32
33
34
35
36
37
38
39
40
41
42
43
44
45
46
47
48
49
50
51
52
53
54
55
56
57
58
59
60
61
62
63
64
65
66
67
68
69
70
71
72
73
74
75
76
77
78
79
80
81
82
83
84
85
86
87
88
89
90
91
92
93
94
95
96
97
98
99
100

1
2
3
4
5
6
7
8
9
10
11
12
13
14
15
16
17
18
19
20
21
22
23
24
25
26
27
28
29
30
31
32
33
34
35
36
37
38
39
40
41
42
43
44
45
46
47
48
49
50
51
52
53
54
55
56
57
58
59
60
61
62
63
64
65
66
67
68
69
70
71
72
73
74
75
76
77
78
79
80
81
82
83
84
85
86
87
88
89
90
91
92
93
94
95
96
97
98
99
100

The binding behavior of ASO L3 is the most problematic to predict. Again treatment of L3 as a loop binder (equation IV-30) does not predict the observed binding behavior; in fact such a treatment is woefully inadequate (predicted $K_d \sim 32$ pM versus an apparent $K_d > 10$ μ M). Lima and coworkers were not able to directly measure the K_d for L3— however they estimate it to be on the order of hundreds of micromolar from extrapolated binding curves. They also note that for each of the bound ASO-RNA complexes, the migrational retardation observed in their gel shift binding assay correlates with the K_d values measured for each ASO (weaker binders show larger migrational retardation; L3 shows the greatest migrational retardation of the entire ASO set). This observation was explained by suggesting ASO whose binding produces major conformational changes in the RNA target will necessarily display weaker binding affinities than ASO that can bind with minimum perturbation to the preexisting RNA structure (e.g. ASO L1). Lima and coworkers suggest that the binding of ASO L3 forces the target RNA through a radical conformational change, hence the apparent weak binding. Interestingly, the constrained folding of the RNA supplied by the Zuker algorithm for this ASO (Figure A4-10) also suggests a radical conformational change produced upon ASO binding. Treatment of the local reaction of L3 as a stem binding ASO (i.e. one which must compete with and disrupt the target RNA structure in order to bind) allows much better predictions of the binding behavior of this ASO (Table A4-8). But as was the case for ASO L2, this apparent stem-binding behavior of L3 could not be predicted *a priori* simply by looking at its intended loop binding target site.

AIV.5 CONCLUSIONS

The data presented by Lima and colleagues clearly demonstrates the effect of RNA secondary structure upon the binding of small ASO. Therefore, it is not surprising that the Dscore index does not accurately predict the relative binding affinities of the 10-mer ASO for the structured 47-mer target, since the Dscores do not account for target secondary structure. The inability of the Sscore and Cscore indices to predict the relative binding affinities of the small ASO suggests that these indices do not accurately represent the thermodynamics of the system. The Sscore and Cscore indices are computed on the assumption that ASO binding disrupts RNA secondary structure only at the ASO target site, while the data presented by Lima and coworkers suggest the stem-binding ASO and some loop binding ASO may produce conformational changes in regions of the target RNA outside the ASO binding site. The Sscores and Cscores also assume that single-stranded regions of target RNAs possess no structure of their own, an assumption clearly in conflict with the widely divergent binding affinities found for the three loop-binding ASO.

Of the various models of RNA chain behavior used to estimate effective concentrations of strands in competition with the ASO for binding at the target site, the Jacobson-Stockmayer-Fisher approximation produces concentration terms which agree best with the published results. However, the surprisingly weak binding displayed by oligomer L3 could not be predicted by any thermodynamic equation when it was considered to be a loop-binder. This clearly demonstrates that the current models of loop thermodynamics and structure are incomplete.

In summary, the development of thermodynamic indices to predict ASO efficacy is limited by a knowledge of RNA structure, kinetics and thermodynamics. Even in this well defined model system, several variables exist for which we have not accounted in our analysis, evidenced by the inability to consistently predict appropriate binding behavior of the six 10-mer ASO to their structured RNA target sites. Thus for cases where the structure of the target RNA is unknown (e.g. all of the studies examined in Chapter 2), an additional level of uncertainty is added by the reliability of the RNA structure prediction algorithms. Figure A4-9 illustrates that even for the case of a simple RNA hairpin, the folding algorithms do not predict biologically relevant structures on the first attempt (although presumably, the suboptimal folding set for this RNA would include the biologically relevant structures among a host of irrelevant structures). Some experts suggest that the improvements which can be expected in RNA secondary structure prediction algorithms are minimal (M. Zuker, personal communication). Additionally, RNA structures are likely to possess tertiary structure, an issue not even addressed by the thermodynamic approaches in Chapter 2 or in this appendix. Therefore, the use of the Dscore index and thermodynamic calculations developed in Chapter 2 and this appendix appear to be useful tools in narrowing the empirical search for ASO with biological effects, but clearly do not obviate empirical testing for ASO binding and efficacy.



For reference

Not to be taken
from the room.

6354586



3 1378 00635 4586

